1960

The development of a corpuscular radiation experiment for an earth satellite

George H. Ludwig
State University of Iowa

THE DEVELOPMENT OF A CORPUSCULAR RADIATION EXPERIMENT FOR AN EARTH SATELLITE *

by

George H. Ludwig **

A dissertation submitted in partial fulfillment of the requirements for the degree of Doctor of Philosophy in the Department of Electrical Engineering in the Graduate College of the State University of Iowa

August 1960

Co-Chairmen: Professor Lawrence A. Ware
Professor James A. Van Allen

* Assisted by National Aeronautics and Space Administration (Contract NASw-17) and joint program of Office of Naval Research and Atomic Energy Commission (Contract N9 onr 93803)

** Research Fellow of the U.S. Steel Foundation

ABSTRACT

The satellite S-46 payload system was developed to study the belts of high intensity radiation surrounding the earth. In particular, it was designed to monitor the spatial and temporal intensity structure to a radial distance of about seven earth radii and for a one year period, to permit a crude study of particle composition and energy spectra, and to provide the first exploratory study of the very low energy component of the trapped radiation. The payload consisted of five detectors and their high voltage power supplies, electronic circuits to count and encode their outputs, a telemetry system, and a solar and chemical battery power system. The factors influencing the selection of the payload configuration and the satellite orbit are discussed, and a detailed description of the instrumentation is included.

The satellite launch attempt on 23 March 1960 failed due to improper functioning of the second,

third, and fourth stage rocket assembly. Operation of the instrumentation during the nine minute launch trajectory was, however, completely satisfactory. The detectors and electronics system are still believed capable of fulfilling the initial objectives, and a new set of instruments utilizing similar detectors is being prepared for flight in another satellite-launch vehicle configuration in 1961.

ACKNOWLEDGMENTS

The author wishes to express his sincere appreciation to Professor James A. Van Allen for making this investigation possible and for his suggestions and guidance throughout the work.

The successful completion of the satellite S-46 program was made possible by the efforts of a large number of individuals both at SUI and in other laboratories. The goals of the experiment were formulated during frequent discussions among Messrs. Van Allen, C. E. McIlwain, E. C. Ray, J. W. Freeman, C. D. Laughlin and the author. Messrs. Freeman, G. Pizzella, J. Thissell, and McIlwain were responsible for the development of the CdS detectors, Mr. Laughlin developed the electron spectrometer assembly, and Mr. L. Frank assisted in the calibration of the G.M. counters. The assistance of Mr. W. A. Whelpley in the construction and testing of the prototype SUI instruments

and of Mr. D. C. Enemark in supervising the production of the flight instruments is gratefully acknowledged. The operation of the SUI instruments during the environmental testing program at ABMA was monitored by Mr. H. K. McCune, who also assisted during the launch operation at Cape Canaveral. The structural components of the SUI assembly were machined in the Physics Department instrument shop by Messrs. J. G. Sentinella, supervisor, and E. D. Freund, R. Markee, R. C. Russell, E. McLachlan, and M. McLaughlin. The excellent drawings which appear in this paper and from which the instrument shop worked are the work of Messrs. R. Trachta, G. G. Lippisch, A. M. Hubbard, and B. W. Fry. The typing of this paper was done by Mrs. E. Robison and Mrs. A. Steege.

The working relationship between SUI and the personnel of the Army Ballistic Missile Agency at Huntsville, Alabama, throughout the Juno program has been outstandingly pleasant and rewarding. The services performed in the accomplishment of this

program by Messrs. Wernher Von Braun, E. Stuhlinger, A. Thompson, G. Heller, B. Greever, H. Kampmeier, J. Boehm, C. Chambers, and H. Burke, with whom frequent personal contact was maintained, were greatly appreciated. In addition, Messrs. W. Haeussermann, H. Fichtner, Speer, O. B. King, G. Cagle, A. Fisher, P. Youngblood, H. Pfaff, H. Wagner, and S. Stevens were responsible for the development of various parts of the S-46 payloads. The contributions of the many other ABMA individuals who assisted in this program are gratefully acknowledged.

This program was assisted by the National Aeronautics and Space Administration (Contract NASw-17) and the joint program of the Office of Naval Research and Atomic Energy Commission (Contract N9 onr 93803). Mr. L. H. Meredith was very helpful in his role as the NASA payload supervisor.

TABLE OF CONTENTS

TABLE OF CONTENTS (continued)

TABLE OF CONTENTS (continued)

TABLE OF TABLES

TABLE OF FIGURES

TABLE OF FIGURES (continued)

TABLE OF FIGURES (continued)

TABLE OF FIGURES (continued)

TABLE OF FIGURES (continued)

TABLE OF FIGURES (continued)

I. INTRODUCTION

During a large part of the past decade the State University of Iowa (SUI) cosmic ray group has been engaged in a program of study of the corpuscular radiation in the vicinity of the earth and in extra-terrestrial space. The most important single finding of this program has been the discovery in 1958 of belts of radiation consisting of reservoirs of charged particles trapped by the earth's magnetic field. The study of these trapped particles and the associated phenomena by the use of earth satellite and space probe borne instrumentation has occupied an increasingly large fraction of the laboratory's effort.

This paper describes one of the most recent instrumentation projects, the preparation of the experiments for satellite S-46.* It is hoped, in spite of the fact that this payload failed to orbit following the launch attempt on 23 March 1960, that the complete description of this project will serve as a valuable reference for those engaged in similar projects.

---

* The designation S-46 is a NASA project number.

II. HISTORICAL BACKGROUND

The work of this laboratory began in 1952 with the use of balloon and rockoon borne experiments to investigate the lower energy end of the primary cosmic-ray spectrum.[1] An unexpected result was observed in 1953 in the vicinity of the northern auroral zone when the counting rates of G.M. counters were observed to rise to very high rates at altitudes above about 40 km.[2] During the following five years the effect was observed repeatedly, and was interpreted as being due to the bremsstrahlung from low energy (< 100 kev.) electrons incident on the high atmosphere and on the material of the rocket instrumentation. It was believed that this was a direct detection of the particles which produced

---

1. J. A. Van Allen, "The Cosmic Ray Intensity Above the Atmosphere Near the Geomagnetic Pole", Il Nuovo cimento 10, 630 (1953).
2. L. H. Meredith, M. B. Gottlieb, and J. A. Van Allen, "Direct Detection of Soft Radiation Above 50 Kilometers in the Auroral Zone", Phys. Rev. 97, 201 (1955).

the visible aurorae.[3,4,5,6]

In 1956, after it was realized that this country had advanced technologically to the point where satellites could be launched, instruments for the investigation of the primary cosmic rays were designed to take advantage of their ability to gather data for long periods of time over large fractions of the earth's surface. The first instruments used in the SUI program were contained in satellite 1958 Alpha (Explorer I),[7] launched on 1 February 1958 (universal time). The first data from this satellite, obtained from receiving

---

3. F. B. McDonald, R. A. Ellis, and M. B. Gottlieb, "Rocket Observations on Soft Radiation at Northern Latitudes", Phys. Rev. 99, 609 (1955) (abstr.).

4. J. A. Van Allen, "Direct Detection of Auroral Radiation with Rocket Equipment", Proc. Natl. Acad. Sci. U.S., 43, 57 (1957).

5. C. E. McIlwain, "Direct Measurement of Radiation Associated with Visible Aurorae", IGY Rocket Report Series No. 1, National Academy of Sciences, 164 (July 1958).

6. C. E. McIlwain, "Direct Measurement of Particles Producing Visible Aurorae", J. Geophys. Research, in press, (1960).

7. G. H. Ludwig, "Cosmic Ray Instrumentation in the First U. S. Earth Satellite", Rev. Sci. Instr. 30, 223 (1959).

stations located in the United States, and therefore transmitted while the satellite was near perigee height, indicated that the instrumentation was operating as planned. The G.M. counter rate was plotted as a function of height in the vicinity of California, and this curve, when extrapolated down to altitudes previously investigated by rockets, agreed with the earlier data. During the second week in March the first tapes from stations in South America were reduced. These data were obtained while the satellite was at a greater height and near the equator, and showed an immediately unexplainable apparent counting rate of zero. This phenomenon was still being investigated at the time satellite 1958 Gamma (Explorer III)[8] was successfully launched on 26 March 1958. The first recording of the internal storage mechanism in the satellite was received at SUI on 3 April 1958, and almost immediately the conclusion was reached that the zero apparent rate was due to counter

---

8. G. H. Ludwig, "The Instrumentation in Earth Satellite 1958 Gamma", M.S. Thesis, State University of Iowa research report 59-3, (February 1959).

saturation and that the earth was therefore surrounded by a region of intense radiation. The later recordings from this satellite yielded the first crude survey of the spatial extent of this region of radiation.[9]

These two early satellites had originally been instrumented to investigate the cosmic ray and cosmic ray albedo corpuscular radiation, and the high intensity trapped radiation had been quite unexpected. As soon as the general characteristics of the belt became known from the Explorer I and III data, it was decided to instrument another payload with detectors having a much greater dynamic range and able to provide some information about the radiation belt particle type and energy spectrum. As a result satellite 1958 Epsilon (Explorer IV) was launched on 26 July 1958.[10] This satellite provided:

---

9. J. A. Van Allen, G. H. Ludwig, E. C. Ray, and C. E. McIlwain, "Observation of High Intensity Radiation by Satellites 1958 Alpha and Gamma", IGY Bulletin, Trans. Am. Geophys. Union 39, 767 (1958). Also Jet Propulsion 28, 588 (1958).

10. J. A. Van Allen, C. E. McIlwain, and G. H. Ludwig, "Radiation Observations with Satellite 1958 Epsilon", J. of Geophys. Research 64, 271 (1959).

(a) A more complete survey of the spatial distribution of the radiation at heights up to 2220 km, and to a latitude of ± 51° geographic. (The earlier U.S. satellites had inclinations of 33°.)

(b) A measure of the radiation intensity by detectors having several different characteristics and under various amounts of absorber.

(c) Some information on particle identification.

(d) Several points on the particle energy spectrum curve for a wide range of positions.

(e) A rough indication of the angular distribution of the trapped particles.

(f) Important information about the trapping mechanism obtained as a result of project Argus.[11]

The USSR satellite 1957 Beta (Sputnik II), launched 3 November 1957, had carried a G.M. counter for the study of cosmic rays, but because its orbit was so low over the USSR, and because their ground receiver

---

11. J. A. Van Allen, C. E. McIlwain, and G. H. Ludwig, "Satellite Observations of Electrons Artificially Injected into the Geomagnetic Field", J. Geophys. Research 64, 877 (1959).

network was confined almost entirely to the USSR, only a very small counting rate increase at the latitude corresponding to the lower extreme of the outer belt was detected, and the proper significance was not attached to it.[12,13] Upon learning of the Explorer I and III results, they included equipment on satellite 1958 Delta (Sputnik III, launched on 15 May 1958) to study the high intensity radiation. The results obtained from this experiment confirmed, in general, our earlier findings and those obtained from Explorer IV.[14]

---

12. S. N. Vernov, N. I. Grigorov, Yu. I. Logachev, and A. Ye. Chudakov, "Artificial Satellite Measurements of Cosmic Radiation", Doklady Akad. Nauk S.S.S.R. 125, 1231 (1958).

13. "Soviet Artificial Earth Satellites - Some of the Results of Scientific Researches on the First Two Artificial Earth Satellites", Report of IGY Committee of USSR (May 1958).

14. "Annals of the International Geophysical Year", Vol. X, now in preparation, will contain the following papers: V. I. Krassovsky, Y. M. Kushnir, G. A. Bordovsky, G. F. Zakharov, and E. M. Svetlitsky, "A Discovery of Corpuscular Fluxes by Means of the Third Sputnik"; S. N. Vernov, A. Ye. Chudakov, E. V. Gorchakov, Yu. I. Logachev and P.V. Vakulov, "Study of Cosmic-Ray Soft Component by the Third Soviet Earth Satellite"; A. Ye. Chudakov, "A Photon Study on the Third Sputnik".

The experiments described above were carried in satellites having apogee heights of less than 2500 km. As a result, the configuration of the higher altitude regions of the belt structure was not known. The existence of two separate belts had not been unambiguously indicated by the low altitude data, although its possibility was realized.*

The importance of extending the spatial survey to greater radial distances was evident. As a result, radiation detectors were prepared for the Pioneer series of space probes. The data received from Pioneer I, which was launched on 11 October 1958, and which traveled to a radial distance of about 110,000 km., indicated that the high intensity radiation was confined to the region near the earth and did not extend into extraterrestrial space. It did not, however, show the existence of the two distinct belts due to gaps in telemetry coverage and failure of the probe equipment.[15] Pioneer III, launched

---

* C. E. McIlwain, Private communications (October 1958).

15. P. J. Coleman, Jr., C. P. Sonett, and A. Rosen, "Ionizing Radiation at Altitudes of 3500 to 36,000 km., Pioneer I", Bull. Am. Phys. Soc., Series II 4, 223 (1959).

on 6 December 1958 to a comparable radial distance, made two cuts through the trapping region and revealed the existence of the two great belts.[16] The USSR solar orbiting vehicle Mechta launched 2 January 1959 confirmed the findings of Pioneer III.[17] They were further confirmed following the launching of Pioneer IV on 3 March 1959 into a solar orbit. More importantly, the Pioneer IV data, by comparison with the earlier data, showed that the position, intensity, and composition of the outer belt were variable and apparently related to solar activity, thus indicating the high probability of the solar origin of the particles responsible for the outer belt.[18]

---

16. J. A. Van Allen and L. A. Frank, "Radiation Around the Earth to a Radial Distance of 107,400 Kilometers", Nature 183, 430 (February 1959).

17. S. N. Vernov, A. Ye. Chudakov, P. V. Vakulov, and Yu. I. Logachev, "Study of Terrestrial Corpuscular Radiation and Cosmic Rays During Flight of the Cosmic Rocket", Doklady Akad. Nauk S.S.S.R. 125, 304 (April 1959). (Translation available from U.S. Dept. of Commerce, "Information on Soviet Bloc International Geophysical Cooperation - 1959", PB131632-64 of May 1, 1959, also Soviet Phys. JETP 4, 338 (1959)).

18. J. A. Van Allen and L. A. Frank, "Radiation Measurements to 648,300 km. with Pioneer IV", Nature 184, 219 (1959).

Plans were begun as early as March, 1958, for a satellite having a high orbital inclination (51^{o}) and long lifetime to serve as a temporal monitor for the corpuscular radiations above the atmosphere. With the discovery of the high intensity belts it was realized that such an experiment would be extremely valuable as an aid to the study of the injection and storage mechanisms for the trapped particles. This program was temporarily delayed by the Explorer IV program and other projects, but finally became a reality on 13 October 1959 when satellite 1959 Iota (Explorer VII) was launched into orbit.[19] This experiment has produced a wealth of data during the months since its launching, and is expected to continue to do so until October, 1960, when it is scheduled to be turned off. It has already yielded information about variations in the intensity, structure, and nature of the outer belt and their correlations with solar storms and flares, magnetic

---

19. G. H. Ludwig and W. A. Whelpley, "Corpuscular Radiation Experiment of Satellite 1959 Iota (Explorer VII)", J. Geophys. Research 65, 1119 (1960).

field variations, aurorae, and radio noise. The relative stability of the inner belt has been shown, and the instruments have shown the arrival of solar protons at high latitudes on several occasions.[20] Comparison of results with those of the contemporary experiments in satellite 1959 Delta (Explorer VI) and space probe Pioneer V have been particularly interesting.[21,22,23,24]

---

20. B. J. O'Brien and G. H. Ludwig, "Development of Multiple Radiation Zones on 18 October 1959", J. Geophys. Research, in press (1960).

21. R. L. Arnoldy, R. A. Hoffman, and J. R. Winckler, "Observations of the Van Allen Radiation Regions during August and September 1959, Part 1", J. Geophys. Research 65, 1361 (1960).

22. J. A. Van Allen and W. C. Lin, "Outer Radiation Belt and Solar Proton Observations with Explorer VII during March-April 1960", J. Geophys. Research (in press).

23. R. L. Arnoldy, R. A. Hoffman, and J. R. Winckler, "Solar Cosmic Rays and Soft Radiation Observed at 5,000,000 km. from Earth", J. Geophys. Research (in press).

24. C. Y. Fan, P. Meyer, and J. A. Simpson, "Preliminary Results from the Space Probe Pioneer V", J. Geophys. Research 65, 1862 (1960) (ltr.).

The experiments outlined above have produced a great deal of information about the charged particles which make up the radiation belts.[25] As in the case of most major physical discoveries, these simple early experiments indicated the need for further experiments of a progressively more discriminating nature, in order that the new phenomenon can be completely understood. The ultimate goal of the program of investigation of the corpuscular radiation near the earth is to understand in detail the nature of the radiation (its composition), its origin, how the particles travel to the vicinity of the earth, the trapping mechanism, and the mechanisms by which they are lost from the trapping region. With this understanding it should then be possible to gain a greater understanding of a large number of geophysical and heliophysical phenomena such as aurorae, high atmospheric heating, magnetic storms, nuclear processes on the sun, etc. In order to gain this knowledge, an understanding of at least some of the following aspects

---

25. For a brief survey of our knowledge of the trapped radiation as of June 1959 see J. A. Van Allen, "The Geomagnetically-Trapped Corpuscular Radiation", J. Geophys. Research 64, 1683 (1959).

in some detail is essential:

(a) Identification of the particle types in the various regions.

(b) The number-energy spectrum of each of the particle types as a function of position in space.

(c) The integrated energy flux as a function of position in space.

(d) The angular distribution of the various components of the radiation as a function of position along the trapping lines.

(e) Details of the variations of the whole trapped particle-solar proton complex in time and the relationships between these variations and geo- and heliophysical phenomena.

(f) The vector magnetic field as a function of position in space and time.

In early 1959 a program was begun to develop an experiment to further this line of investigation. This culminated in the attempt to launch satellite payload S-46 into orbit on 23 March 1960. Unfortunately this

launch attempt failed due to the improper functioning of the high-speed rocket stages. No backup rocket was immediately available, and the instrumentation is being rebuilt, with updating of the detectors and instrumentation, for a new attempt in a different payload-rocket configuration into a similar orbit in the first half of 1961.

III. THE S-46 SYSTEM DESIGN

A. General Considerations.

A satellite program almost always passes through a number of phases, usually in the order listed below, and with varying amounts of overlap of the steps.

1. Development of the goals of the program and initial design of the system.

2. Development of the detectors, electronic circuitry, telemetry system, power system, and payload structure.

3. Construction of one or more prototype payloads.

4. Electrical, mechanical, and thermal testing of these prototype units under the conditions dictated by the vehicle characteristics and orbital environment.

5. Evaluation of these test results and modification of the satellite design if shown to be necessary.

6. Production of the flight and spare payload units.

7. Testing of these payloads under somewhat less severe test specifications than for the prototype units in order to discover mistakes in assembly and weaknesses and potential failures in assembly and components.

8. Calibration of the payload detectors and instrumentation, usually accomplished partially before assembly of the flight units, partially after assembly of the flight unit instrumentation subassemblies but before complete assembly of the payload, partially following complete assembly of the payload, and finally, at the launch site as late in the launch operation as possible.

9. The payload launching.

10. Receipt and recording of the data, and reduction of these data to a useable form.

11. Analysis of the data and the publication of results.

The time scale for these steps may vary considerably from project to project. The shortest time required for any space payload program thus far was for the 1958 Epsilon (Explorer IV) payload, where

77 days elapsed from the meeting at which the major working arrangements between contributing agencies were worked out to the time of launching. The time taken for the S-46 program was considerably greater due to its greater complexity, its lower priority, and the overlap of this and the Explorer VII programs. The first meeting between SUI personnel to decide on the objectives of the project after advice by the National Aeronautics and Space Agency (NASA) that a rocket would be made available occurred on 15 January 1959. By 25 March 1959 much of the system design had been completed and detailed block diagrams for the experiment were in existence. The program was delayed somewhat during the summer by the two 1959 Iota (Explorer VII) launch operations. The first prototype SUI instrument package was delivered to the Army Ballistic Missile Agency (ABMA)* on 21 October 1959, and the ABMA prototype testing program began soon after that.

---

* Now the George C. Marshall Space Flight Center (MSFC).

The first SUI flight unit instrument package was delivered to ABMA on 25 January 1960, and the launching attempt occurred on 23 March 1960, slightly more than one year after the beginning of the project.

The S-46 system design problem was undertaken jointly by SUI and ABMA. Such a problem is always a complex one involving the careful weighing of such factors as rocket capability, objectives, and telemetry and data reduction capabilities. The goal of the optimizing process is to arrive at the most valuable experiment possible in terms of its potential yield of new and useful data, within the framework of the imposed limitations. The usual procedure, and the one followed for this project, is to assume a properly chosen set of experiment requirements, develop a satellite system, modify the requirements as necessary to fit the rocket and support system capabilities, review the resulting potential usefulness of the experiment, and remodify the requirements as necessary. This procedure is usually repeated many times as new considerations become important, in some cases as late as just prior to completion of the flight

payload units.

The conclusions of this design procedure as applied to the development of the S-46 system, with a discussion of some of the factors leading to these conclusions, will occupy the bulk of this section. For the sake of simplicity, the various aspects are discussed separately, but it is to be understood that each one depends directly on most of the others.

B. Rocket Availability.

In early 1959 NASA made available for the S-46 program an ABMA - Jet Propulsion Laboratory (JPL) Juno II rocket system, which consists of a Jupiter booster rocket and a cluster of scaled Sergeant rocket motors arranged to form the second, third, and fourth stages. The booster rocket lifts the rocket instrumentation section, the high speed cluster, and the payload to injection height, and the second, third, and fourth stages impart the necessary orbital velocity to the payload. The attitude of the booster rocket is controlled during its powered flight by a programed inertial platform. This platform then controls the attitude of the high speed cluster during

the period that the assembly coasts to the peak of its trajectory. The cluster of rockets is spin stabilized (at a spin rate of 600 rev/min) for attitude control during injection into orbit. The entire sequence of operation following lift-off is controlled internally. The booster rocket takes off vertically but soon begins to tilt into a launch trajectory. Soon after booster burnout the rocket instrument section is released from the booster, and retro-rockets on the booster fire to insure positive separation. The rocket guidance system then begins to tilt the high speed assembly by the use of a set of auxiliary jets so that its axis is parallel to a line tangent to the earth at the point of injection. While the tilt program is being accomplished the shroud, which protects the payload during ascent through the dense atmosphere, is ejected forward, and a lateral-thrust rocket carries it aside. The tilt program is completed soon after shroud ejection, and the cluster assembly continues on its elliptical path until it reaches the peak of its trajectory, at which time the high speed stages fire in rapid succession to impart the necessary orbital

velocity to the payload assembly. For a more detailed description of the rocket system the reader is referred to the literature.[26,27]

This rocket configuration has a capability for launching a 41.5 kgm. payload into an orbit having an apogee of 1080 km. (558 km. perigee, 50° inclination; Explorer VII), a 10.0 kgm. payload into an orbit having an apogee of 44,000 km. (340 km. perigee, 28° inclination; satellite S-46 final computation), or a 6.1 kgm. payload to escape velocity (Pioneer IV).

C. Objectives of the Experiment.

Accomplishment of all the measurements listed in the last section would require a large number of complex instruments. Furthermore, an approximate value for the quantities to be measured would have to be known in advance in order to adjust the scaling

---

26. B. B. Greever, "General Description and Design of the Configuration of the Juno I and II Launching Vehicles", IRE Trans. on Military Electronics, (April-July 1960) (in press).

27. "Structures and Mechanics Laboratory Model Description of Juno AM-19C", Army Ballistic Missile Agency, Structures and Mechanics Laboratory, (19 February 1959), unpublished (secret).

factors for the proper range of operation, or the dynamic range of the instruments would have to be very large. Since it is not possible at the present time to perform a single "grand experiment" which will accomplish all the listed objectives because of various limitations in rocket and instrumentation capability, it is necessary to continue the investigation on a logical step-by-step basis. After careful consideration of the various factors it was decided that the following program was possible and that it would be the most valuable in terms of its ability to answer the greatest possible number of the most pressing questions about the trapped radiation.*

1. "Monitoring of the intensity structure of the two principal zones of geomagnetically trapped radiation over an extended period of time with the broad objective of conclusive establishment of the origins and gross dynamics (i.e., build-up and decay

---

* From a letter to L. H. Meredith from J. A. Van Allen (20 October 1959), unpublished.

times and mechanisms, local acceleration of particles, long term and short term temporal fluctuations, etc.) of the respective zones and the more specific objective of detailed correlation with solar activity and with geophysical phenomena (aurorae, magnetic storms, heating of the atmosphere and airglow).

2. "Crude study of the particle composition and the energy spectra of the respective components as a function of position in space and as a function of time.

3. "Exploratory study of energy flux of very low energy trapped particles (protons and electrons separately) by use of zero-wall-thickness detectors."

D. Orbit Parameters.

The weight which can be placed in orbit with a given rocket depends most directly on three of the orbit parameters; perigee height, apogee height, and inclination. The figures decided upon for these parameters and the considerations affecting their selection were:

1. Perigee. The basic requirement was that the perigee height should be the lowest value which would

ensure a one year lifetime. The perigee height is the same as the satellite injection height only if there is no elevation angle error at the time of injection (and, of course, if the injection velocity is sufficiently high). The final injection height depends strongly on booster rocket performance. Therefore, the selection of a program injection height must allow for possible guidance angle errors and variations from standard rocket performance, in order that the perigee will have a high probability of being equal to or greater than the minimum acceptable height.

On the other hand, the perigee height should be sufficiently below the radiation belts so that an approximate calibration of the detectors can be obtained periodically in the relatively stable cosmic ray and albedo flux found between about 50 and 600 km., in order that failure of any part of the instrumentation can be immediately detected. An injection height of 340 km. above the earth's surface was chosen.

2. Apogee. Ideally the apogee height should be sufficiently great so that the detectors would be carried well outside the radiation belts and into

interplanetary space, perhaps to a radial distance of 20 earth radii from the earth's center. Such an orbit would provide frequent passes through the entire belt structure, and would also permit the detection of solar protons and other particles well outside the influence of the magnetic field of the earth. The main disadvantages of such an orbit are the fact that the period would be so long (48 hours) that important changes might occur within the belt system and be missed entirely while the detectors were outside that system, and that the payload weight would have to be so small (due to the limitations in capability of the Juno II rocket) that the overall value of the experiment in the program adopted would be seriously reduced. It was decided that the apogee should be sufficiently high that the detectors would pass beyond the peak of the outer belt in the equatorial plane when that peak intensity was at its maximum distance from the earth. Figure 1 shows the counting rate as a function of radial distance as obtained by Pioneers III and IV on 6 December 1958 and 3 March 1959 respectively. The Pioneer IV data were obtained

following a period of high solar activity when the peak intensity of the outer belt was at a much greater distance from the earth than at any other recorded time. It was considered likely that the peak intensity will occur at a greater distance only very rarely.

On this basis, a minimum apogee height of six earth radii (38,200 km.) from the earth's center was specified, and the payload weight was determined accordingly. A final calculation of the launch trajectory by ABMA, using more accurate rocket performance data and the actual final payload weight, indicated that the apogee height should have been about 44,000 km.

3. Inclination. In order to simplify the analysis of the data and to insure the maximum number of sweeps through the central belt structure (rather than in the slot between the belts or outside the outer belt) a minimum inclination orbit was selected. This also produces the greatest apogee height, since the greatest advantage can be taken of the earth's rotational motion. The minimum inclination obtainable from a launching at Cape Canaveral, Florida, is 28.3°,

the geographic latitude of the launch site. This requires a launch azimuth of 90^{o} (due east).

4. Summary of Orbit Parameters. The orbit parameters decided upon, then, were:[28]

a. Perigee height, 1.0534 r_e from the earth's center (r_e = 6371 km.).

b. Apogee height, 6.906 r_e or greater.

c. Semi-major axis, a = 3.980 r_e.

d. Semi-minor axis, b = 2.699 r_e.

e. Eccentricity, e = 0.735.

f. Period, P = 40,200 sec. = 11.2 hours.

g. Inclination, i = 28.3 degrees.

h. Motion of longitude of ascending node, $\dot{\Omega}$ = -0.51 deg./day.

i. Motion of argument of perigee, $\dot{\omega}$ = +0.47 deg./day.

---

28. R. J. Davis, F. L. Whipple, and J. B. Zirker, "The Orbit of a Small Earth Satellite," Chapter 1 of "Scientific Uses of Earth Satellites" (University of Michigan Press, Ann Arbor, 1958), 2nd ed.

E. Motion of the Satellite About Its Center of Mass.

Several of the detectors have defining apertures which make them directional. It was decided that the payload should spin in such a manner that the detectors viewed a wide range of angles, rather than a direction which was fixed in space or changing in a completely unknown way. The superposition of two rotations so that the detectors looked at every point on a full sphere was not considered desirable, since the CdS detectors are light sensitive over the solid angle defined by the aperture, and periodic rotation through the sun and earth would make the measurements very difficult to use. Thus simple rotation of the detectors about a line perpendicular to the line of detector directivity was decided upon.

This motion can be obtained in either of two ways. Preferably the satellite can be made to spin initially about its axis of greatest moment of inertia with the detectors directed perpendicularly to the axis. The simple spin would be maintained until the spin rate decreased to a very low value. Explorer VII is an example of a satellite which was so

stabilized, and its spin damping time constant is of the order of two years. The direction of its angular momentum vector has remained very nearly constant.[29]

Alternatively, the satellite can be made to spin initially about its axis of least moment of inertia (its longitudinal axis), with the detector axes directed parallel to the longitudinal axis. Then as the spin rate $\dot{\psi}$ decreases, the satellite will undergo a transition to a complex spin with the longitudinal axis of the payload moving on the surface of a cone of half angle α at an angular rate $\dot{\varphi}$ where α will change from zero to $\pi/2$.[30] Figure 2 illustrates this transition, where (a) is a sketch of the satellite immediately after injection before

---

29. R. J. Naumann, "Orientation of Explorer VII (AM 19-A)," ABMA report number DV-TN-13-60 (20 June 1960).

30. R. J. Naumann, "Recent Information Gained from Satellite Orientation Measurement," paper presented at the 4th Symposium on Ballistic Missiles and Space Technology at UCLA, Los Angeles, Calif., 24-27 August 1959, mimeograph copies available from author.

the tumble has begun, and (b) shows it later as the opening angle α is increasing. In (c) α has opened up completely and the satellite is in a flat spin. Explorer IV is an example of this configuration, in which the ratio of the moments about the longitudinal and transverse axes was 84. Figures 3 and 4 show, respectively, the spin rate ($\dot{\psi}$) of Explorer IV as a function of time after launch, and the opening angle (α) of Explorer IV as a function of time.[31] Explorer VII was spun initially about its axis of greatest moment of inertia. However, if the satellite had not separated from the fourth stage rocket as planned, then this initial spin axis would have been the axis of least moment, and the payload would have made a transition to a flat spin approximately as indicated in Figure 5.[32]

---

31. R. J. Naumann, "Attitude Determination of Explorer IV," ABMA internal report number DV-TN-19-59 (12 June 1959).

32. R. J. Naumann, "Tumble Rate Investigation for AM-19A," ABMA report number DV-TN-28-59 (30 October 1959).

The latter alternative was chosen so that the basic Explorer I, III and IV configuration could be retained, since it could be fabricated with only slight modification of the previous design. In addition, the weight was not available to allow modification of the structure to produce a configuration in which the axis of greatest moment was coincident with the initial spin axis.

Prediction of the opening angle (α) as a function of time is very difficult and a complete analysis was not performed. It depends on the ratio of the moments about the final and initial spin axes, atmospheric damping, magnetic damping, and energy losses due to flexing of parts of the structure (such as antennae in the case of Explorers I and VII). The ratio of the moments was $\frac{I_{trans.}}{I_{long.}} = 30$ in the case of the S-46 satellite. The effects of the atmospheric and magnetic damping were expected to be less than for Explorers I, III, and IV due to the greater apogee height. And the energy losses due to flexing of structure were expected to be comparable with, or slightly greater than, those of Explorers III and IV. It was believed that the

opening angle would follow approximately the curve of Figure 4 for Explorer IV, with a possible error by a factor of two in either direction in the time scale.*

F. Lifetime

The satellite was designed to operate for a period of one year to provide a high probability for the occurrence of interesting solar phenomena and to permit the accumulation of a reasonably complete set of data. The satellite orbit was chosen to insure this orbital lifetime, and a solar battery system was employed to provide electrical power to all instrumentation for this period. An extensive reliability program was followed to reduce the probability of premature failure of the equipment (see chapter V).

A timer was included in the payload to turn off the instruments at the end of the one year period in conformity with NASA policy, in order that the frequency would become available for later experiments.

---

* G. Heller, ABMA, private communication (14 March 1959).

G. Launch Time.

The launch time was determined after considering:

1. The percentage of time in sunlight. This parameter affects both the temperature control problem and the design of the solar battery. It was computed for the one year lifetime for a number of possible launch times. Figure 6 shows the result of the computation for local sun times at the point of injection (H_o) of 0800 and 1000 (1212:57 and 1412:57 U.T.). The local sun time at the point of actual injection was 0922:24.

2. The initial angle between the satellite axis and the satellite-sun line. This parameter affects the temperature control problem and the design of the solar battery, and must be chosen to minimize the lengths of the periods of time during which the light sensitive particle detectors sweep across the sun or earth.

3. Temperature requirements. It was desired that the temperature remain within the limits 0° C to $+50^{\circ}$ C. Minus 20° C and $+75^{\circ}$ C were established as absolute limits.

4. The effects of orbit perturbations by the sun and moon on the perigee altitude.[33]

In cases where all conditions could not be met simultaneously for the entire one year period, emphasis was placed on the first two months of operation, since the probability of successful operation of the instrumentation diminishes with time. Less weight was attached to those considerations which might have resulted in temporary cessation of proper operation (such as those which lead to an abnormal but not damaging temperature) than to those which could have resulted in premature permanent failure (such as those which cause the perigee height to be markedly reduced).

Consideration of items 1, 3, and 4 indicated a launching time between 0800 and 1200 for the epoch beginning 23 March 1960. Consideration of item 2 placed a more severe limitation on the launch time because of the necessity that the detectors not point toward the

---

33. R. J. Naumann, "The Effect of Lunar and Solar Perturbations on the Perigee Height of a High Eccentricity Satellite (AM-19C)", ABMA internal report number DV-TN-5-60 (4 March 1960).

sun either initially, or after conversion of the satellite motion to a flat spin. The factors bearing on the selection of the exact time were:

1. The detectors were somewhat light sensitive within a cone of half angle 20°, with the cone axis coincident with the longitudinal axis of the payload.

2. An initial angle error of ten degrees between the detector axes and the intended direction of injection was considered possible because of possible misalignment of rocket thrust with respect to the longitudinal axis, and guidance angle errors at the time of final stage ignition.

3. The detectors should not "see" the sun for a minimum initial period of twenty hours to permit the collection of meaningful data from at least several orbits very early in the satellite's lifetime.

Figure 7 shows a projection of the initial satellite motion onto the plane of the ecliptic. The arrow at the position of injection points in the initial direction of the spin axis. The initial angle to the sun from the payload (β) is indicated in figure 2 as well as in figure 7. The launching time (on 23 March

1960) was chosen so that β would be between 50° (0834 EST) and 59° (0907 EST). Figure 8 shows how the angle β changes during the one year period for local sun times at injection of 0800 and 1000. Assuming that the direction of the angular momentum vector remains fixed in space and that $\beta = 50^{\circ}$ initially, the satellite alignment would follow the following pattern: During the first few orbits the sun would remain outside the cone of detector light sensitivity. The earth would fall within this cone on the portion of the orbit marked A in figure 7. As the satellite transforms from a simple spin to a flat spin, the sun would fall within the cone while α was in the approximate range 30° to 65°. The angle β would change at the rate of about one degree per day due to the earth's rotation about the sun. After α became equal to 90°, the sun would fall within the cone of sensitivity again about 110 days after launch, and would continue to do so for about 50 days. The earth would fall within this cone whenever the satellite is within the shaded regions in figure 7.

The launch time interval agreed upon was 0834 to 0907 EST on 23 March 1960. A postponement of the firing

date by as many as three days would have required no change in the launch time. The vehicle was actually launched at 0835:11 on 23 March 1960.

H. Payload Weight.

The permissible payload weight based on the above considerations was computed by ABMA to be 10.19 kgm. The final payload weight for the unit launched on 23 March 1960 was 10.22 kgm.

I. The Payload Instrumentation.

Figure 9 is a block diagram of the S-46 payload. Five detectors were used. Detectors A and B are cadmium sulfide semi-conductor crystals, whose resistances are known functions of the rate of energy loss for charged particles in the crystals. No material is located between the active volumes of the crystals and the outside of the satellite. Therefore the crystals are capable of measuring the energy loss of electrons and protons having energies of less than 100 electron volts. The two detectors are identical except that detector A employs a magnet to curve the paths of all electrons having energies below about 500 kev. away from the crystal so that it acts almost exclusively as

a proton detector. Thus the two detectors permit the simultaneous separate determination of low energy electron and proton fluxes.

The currents through the crystals produced by a regulated power supply are converted into pulse rates by charging capacitor-neon bulb relaxation oscillator circuits. The pulses are counted by binary scalers.

Detector C is an electron energy spectrometer having an energy "window" of approximately 45 kev. to 55 kev. It consists of defining apertures, a magnetic field, another aperture, and a thin window G.M. counter. Only those electrons having energies within the desired range are deflected through the proper angle by the magnetic field so that they are counted by the counter. The G.M. counter is surrounded by a lead and stainless steel absorber to reduce the counting rate contribution from high energy particles which pass through the structure and from x-rays (bremsstrahlung) produced by the inelastic scattering of particles in the structure.

Detector D is identical to the G.M. counter assembly in detector C except that no entrance opening is provided in the absorber. Thus it counts only the

radiation which penetrates the absorber. It is used to allow subtraction of the component counted by detector C which does not enter through its opening. It is also used in conjunction with detector E to obtain information about the radiation absorption spectrum.

Detector E is a G.M. counter surrounded by a moderately thin absorber and located outside the shell in order to obtain as clean an environment as possible. Different counter types were used in different payloads. The prototype payloads and flight unit number one used Anton type 302 counters, which are similar to the ones used in Explorers IV, VI, and VII and Pioneers III, IV, and V. In flight unit two a change was made to a smaller Anton type 213 counter for two reasons. First, because of the smaller size the counter would be able to measure a larger particle intensity (the outer belt intensity measured by the type 302 counter in Pioneer IV was high enough to cause partial counter saturation); and second, because the supply of fully calibrated type 302 counters was low at the time of payload assembly, and the best available counters had somewhat undesirable characteristics.

The pulses obtained from the G.M. counters in detectors C, D, and E were also scaled by binary scalers.

Since the detectors would have been penetrating regions in which the pulse rates would have been extremely low, as well as the centers of the belts, a large dynamic range was required. This is provided by the telemetering of three different scaling factors for each detector. The outputs of three stages in each binary scaler are combined in logic circuits to provide a completely unambiguous eight level code for each channel. This combination is done in such a manner that the required information bandwidth is minimized. In addition, RC integrating circuits with time constants of 5 seconds are included to further reduce the information bandwidth. The outputs of the logic circuits are passed through amplifiers to provide low output impedances.

The outputs of the five detector channels frequency modulate individual voltage controlled subcarrier oscillators, directly, in the case of all except the detector D channel, and through an electronic commutator in that channel. This commutator is provided to permit the sampling of several slowly changing temperature and

voltage measurements with a sufficiently low sampling duty cycle so that the value of the data from the primary experiment is not significantly reduced. The analog auxiliary measurements sampled by the commutator are:

1. The detector assembly temperature, made by a thermistor located on the electron spectrometer housing and in thermal contact with all radiation detectors;

2. The temperature of an isolated Tabor surface in order to investigate the thermal properties of a potential new satellite surface coating;

3. The voltage of one of the solar power supplies; and

4. Two channel calibration voltages.

The commutator first samples the radiation detector output for about 649 seconds, then the auxiliary measurements for eleven seconds each. Thus the duty cycle for the detector D radiation measurement is 649 seconds on and 55 seconds off.

The outputs of the five subcarrier oscillators are combined in a simple arithmetic summing circuit.

J. Data Transmission.

A transmitter frequency of 108.03 mc./sec. was selected to permit the use of the extensive network of tracking and receiving stations which are equipped for that frequency.

The transmitter power requirement was determined by a conventional signal-to-noise ratio computation.[34,35] The signal power received at the input to a receiver (P_r) for a transmission path through free space is

$$P_r = P_t \frac{G_t G_r \lambda^2}{(4\pi r)^2}$$

where P_t is the radiated power,

G_t is the transmitting antenna gain referred to isotropic radiation,

G_r is the receiving antenna gain, with the same reference,

λ is the wavelength, and

---

34. "Reference Data for Radio Engineers" edited by H. P. Westman (American Book Stratford Press, Inc., New York, 1956) 4th ed., pp. 750-769.

35. H. J. Peake, "Some Basic Considerations of Telemetry System Design", NASA Technical Note D-355 (June, 1960).

r is the distance from transmitter to receiver antenna.

The total noise power (P_n) is the sum of the sky noise (P_{ns}), which depends on the beam width of the receiver antenna and on the region of the sky to which the receiver antenna is directed, and the noise generated in the receiver (P_{nr}). The sky noise consists of cosmic and solar, atmospheric, and man-made noise. The cosmic and solar noise levels are graphed on page 764 of reference 34. A value of +10 db (referred to ideal-receiver noise) was used for all computations. Atmospheric and man-made noise are negligible at this frequency at the isolated receiver locations.

The ideal-receiver input circuit Johnson noise power is given by $P_{nj} = kTB$ where k is Boltzmans constant, T is the absolute temperature, and B is the receiver bandwidth. The value of kT for T = 290 is -204 dbw or -174 dbm. The receiver total noise power (P_{nr}) is

$$P_{nr} = P_{nj}F$$

where F is the noise figure of the receiver. Thus, the total noise power (P_n) is

$$P_n = kTBFP_{ns}$$

and the signal-to-noise power ratio is

$$\left(\frac{S}{N}\right)_P = \frac{P_r}{P_n} = \frac{P_t G_t G_r \lambda^2}{(4\pi r)^2 kTBFP_{ns}}$$

Values of some of the parameters for the S-46 system are:

G_t = -7.8 db above isotropic (10 db below that at the lobe peak and for parallel transmitting and receiving antenna polarization vectors).

G_r = 23 db for the Minitrack antenna.

λ = 2.78 meters (λ^2 = 8.9 db (meter)).

$(4\pi)^2$ = 158 (= 22 db).

r = 44,000 km. (r^2 = 153 db (meter)).

kT = -174 dbm.

F = 4 db (with reference to ideal-receiver noise).

N_s = 10 db (with reference to ideal-receiver noise).

Thus the signal-to-noise power ratio in db is

$$\left(\frac{S}{N}\right)_P = P_t \text{ (dbm)} - B \text{ (db)} + 9 \text{ db}$$

The Minitrack receivers have an input bandwidth for this signal of about 3 kc./sec., or 34.8 db above

one cycle/sec. However, the audio phase lock filters used as subcarrier discriminators can be adjusted as low as 2 cycles/sec. for the form of telemetry encoding employed. If the receiver has good linearity and if the discriminators are not overloaded, then the receiver system bandwidth (B) is equal to the post-detection bandwidth.* Figure 10 is a plot of signal-to-noise power ratio as a function of transmitter power (P_t), with the receiver bandwidth (B) as a parameter, for the S-46 system under the most unfavorable conditions. It was decided that the minimum signal-to-noise voltage ratio should be 4:1, that is $\left(\frac{S}{N}\right)_P = 12$ db. An additional 8 db was allowed for system degradation. This indicated, for B = 2, a transmitter power output of 200 mw., requiring, on the basis of the transmitters in existence at the time of the original computation, a transmitter input power of 800 mw. After the transmitter and power supply designs were completed, the higher efficiency of the new design resulted in an increased output of about 300 mw., which should have resulted,

---

* A. Hamilton, Collins Radio Co., private communication (16 June 1960).

under the worst conditions in $\left(\frac{S}{N}\right)_P$ = 23 db.

The computations were experimentally checked by using a payload and a receiver with a variable attenuator at its input. This test showed that the telemetry threshold power (received signal power for $\frac{S}{N}$ = 1) with B = 20 cycles/sec., was -140 dbm, in good agreement with the predicted result.

The transmitter is phase modulated by the composite signal with a maximum phase deviation of $\pm$ 1.5 radians. It drives an antenna in which the active elements of an asymetrical dipole are the payload shell and the fourth stage rocket motor. These are insulated at the driving point by a fiberglass gap. The antenna impedance is matched to the transmitter output impedance by an L section transformer.

K. The Power Supply.

Electrical power for all circuits was obtained from a solar cell-secondary battery system. The solar cells are silicon p-n junction cells capable of a solar energy to electrical energy conversion efficiency of 9 per cent.

It was considered possible that the particle

fluxes in the radiation zones might be high enough to cause a marked reduction in solar cell output (by, say, 25 per cent) in a period of the order of weeks or months if the cells were directly exposed.[36*] Therefore, the flight unit solar cells were covered by thin (0.15 mm) plates of radiation resistant glass. These plates were fastened over individual cells with cement placed only on the ends of the plates.

Six separate solar batteries were provided, one on each side of the mounting structure, to allow for all possible satellite orientations. Excess capacity of each of the six solar batteries was provided to allow for:

1. 25 per cent battery losses;
2. Operation 20 per cent of the time in the earth's shadow;

---

* J. A. Van Allen, J. W. Freeman, C. E. McIlwain, (SUI); L. H. Meredith, (NASA); R. D. Shelton, (ABMA); private communications.

36. J. J. Loferski and P. Rappaport, "The Effect of Radiation on Silicon Solar-Energy Converters", R.C.A. Review XIX, 536-554 (1958).

3. 12 per cent solar energy transmission loss in the glass covers; and
4. Derating by 24 per cent to allow for additional unknown and unforeseen losses.

The solar cell power capacity for the S-46 payload is listed in Table I.

Nickel-cadmium secondary batteries were included to regulate the voltage furnished to the instruments as the solar battery voltage fluctuates, and to furnish electrical power during the periods when the satellite would pass through the earth's shadow. Sufficient chemical battery capacity was provided so that they would be cycled over only the top 10 per cent of their charge-discharge curves. This was considered necessary in order to insure long cycle lifetime. It also provided the capability of operating the payload for from eight to ten hours from the chemical battery system alone in the event of early solar battery failure.

L. Physical Configuration.

The determination of a payload physical configuration for S-46 was an evolutionary process accomplished jointly by SUI and ABMA. Figure 11 is an outline

Table I

S-46 Solar Battery Power Capacity

Supply System	Payload Requirements (mw.)	Side Plate Capacity (each)(mw.)	End Plate Capacity (each)(mw.)
Transmitter, 15.6 volts	967	1750	1750
Commutator and Subcarrier Oscillators, 10.4 volts	107	245	500
SUI Instruments, 6.5 volts	192	517	735

drawing of the final overall satellite configuration, figure 12 is a drawing of the payload column assembly, and figure 13 is a photograph of the payload assembly.

The payload is generally similar to that of Explorers I, III, and IV, [7,8] the most obvious difference being the addition of the box-like structure to support the solar cells. The 1.067 meter long fourth stage rocket is attached to the payload assembly by the fibre-glass antenna insulator ring. The payload itself is 0.587 meter long and consists of a 15.88 cm. diameter thin wall cylinder on which the solar cell frame is attached, and within which the instrument column is located. The radiation detectors are located at the top of the payload, with all directional detectors pointing upward. The channel E G.M. counter is located in a detector assembly thimble protruding from the top of the payload.

Located below the detector assembly, in order, are the SUI scaling and encoding circuitry and the ABMA transmitter, commutator, subcarrier oscillators, and chemical battery pack. The SUI instrumentation and the ABMA telemetry system are contained in separate

assemblies, connected by several screws and a single electrical cable, thus simplifying fabrication, testing, and definition of areas of responsibility.

The solar cells are mounted on flat plates attached to a box-like supporting framework, as seen in figure 13.

M. Telemetry Reception and Tracking

Telemetry data acquisition and satellite tracking facilities were to have been provided by NASA in the event of a successful launching.[37] Satellite tracking was to have been done by the established network of Minitrack stations located primarily along the west 75th meridian for the lifetime of the satellite. A satellite ephemeris based on their observations was to have been provided by the Space Computing Center located in Washington, D. C.

Most of these Minitrack stations do not, however, possess the necessary equipment for the recovery of the telemetered data. For this purpose, several networks

---

37. D. A. Premo, "Request for Data Acquisition Service Project S-46", NASA internal memorandum, (15 February 1960).

of stations were evaluated with regard to the percentage of time the satellite would have been within range of at least one of the stations. The stations considered, with a brief description of the equipment and station availability at the time of the S-46 launching, are:

1. Fort Monmouth, New Jersey; U. S. Army; 15 and 18 meter diameter parabolic antennae; necessary receivers and recording equipment; time code generator to be furnished by NASA; in operation except for the time code generator.

2. Singapore, BCC; Space Technology Labs (STL); quad-helix antenna with 18 db gain; all necessary equipment being installed; availability for first week or two somewhat questionable.

3. South Point, Hawaii; Same as 2.

4. Jodrell Bank, England; Same as 2 except early availability somewhat more questionable.

5. Goldstone, California; Jet Propulsion Lab (JPL); 26 meter diameter parabolic antenna; all necessary equipment on hand; availability contingent on schedule and success of several other projects.

6. Monterey, California; D. S. Kennedy and Co.; 18 meter diameter dish antenna; all receiving, recording,

and timing equipment to be provided by NASA.

7. Blossom Point, Maryland; NASA; 16 Yagi array with 23 db gain; equipment being installed but not tested for reception of phase modulation; availability expected shortly after scheduled launching.

8. Johannesburg, South Africa; Same as 7.

9. Woomera, Australia; Same as 7.

It was proposed that a network consisting of stations 1, 2, 3, and 4 be used initially, until the network consisting of stations 7, 8, and 9 was completed and operating properly, at which time the latter would become the primary network. Either of these networks is capable of providing more than 90 per cent horizon to horizon data acquisition of which more than 70 per cent is above a 10^{o} elevation angle for the satellite S-46 orbit. The other stations listed above were considered alternate stations.

All stations were to have recorded the demodulated signal on one of two tracks of a 1/4 inch magnetic recording tape. The other track was to have contained either a direct recording of a suitable standard time station such as WWV, or an accurate pulse coded time

signal. The tapes were to have been sent to NASA for editing and rerecording, and these recordings were to have been forwarded to SUI for data reduction and analysis.

IV. DETAILED DESCRIPTION OF THE INSTRUMENTATION

A. General Discussion.

This section contains a detailed description of those elements of the payload assembly which were furnished by SUI, and an abbreviated description of those elements supplied by ABMA. The physical location in the payload of the modules containing the various circuits can be seen in the drawings of figures 11 and 12, and their functions can be seen in the block diagram of figure 9. The block diagram also indicates the division of responsibility between SUI and ABMA for the development and production of the various circuits. The Army Ballistic Missile Agency was also responsible for the power system and most of the payload structure.

Five S-46 payloads were fabricated in this program, three prototype test units, and two flight units. Table II indicates the payload designations and the manner in which each was used. There were a number of differences between the payloads, especially between the prototype units and flight units. These differences are summarized in Table III.

Table II

Table of Satellite S-46 Payloads

ABMA Payload Number	SUI Package Number	Name	Function in Program
PL-1	PT-3	Thermal Test	Measurement of thermal characteristics; antenna impedance measurements and matching; vibration and spin on cluster.
PL-2	PT-2	Electrical Test	Payload electrical tests; temperature-vacuum soak; RF radiation tests; flight acceptance vibration tests.
PL-3	PT-1	Environmental Test	Shock; vibration; spin; acceleration with spin; RF radiation tests; temperature calibration.
PL-4	FU-2	Flight Unit	Primary flight unit. PL-4 with SUI FU-1 given all flight acceptance tests. PL-4 and FU-2 mated on 18 March and launched 23 March 1960. Note: 213 G.M. counter in detector E.
PL-5	FU-1	Flight Unit	Spare flight unit. PL-5 with SUI FU-2 given all flight acceptance tests. PL-5 and FU-1 mated on 18 March 1960. Note: 302 G.M. counter in detector E.

Table III

Tabulation of Payload Differences

Item	Reference Figures	Remarks
1. Glass solar cell cover plates.	13	Not present on prototype units. Prototype testing accomplished on test panel and flight units.
2. Commutated solar cell voltage measurement.	52	Was a solar cell temperature measurement on PT units.
3. CdS detectors. Detectors A, B.	16, 17	Detectors in SUI PT-3 fixed in place rather than plug in. Lead absorber in aperture system not used in PT units. Thinner magnetic shielding used in PT units. Clairex Cl-2P CdS crystals used in PT-2, PT-3.
4. Electron spectrometer. Detectors C, D.	21	Different magnet pole shape used in PT units. Different aperture system used in PT units. Lead baffle and shield in line with detector opening not used in PT units.
5. G.M. counter. Detector E.	18	Type 302 G.M. counter used in PT units and FU-1, type 213 counter in FU-2. Container for 302 counter had 0.020 inch Al. wall, that for 213 counter had 0.093 inch Al. wall. Flight cover for 302 counter had 0.125 inch Al. wall, that for 213 counter had 0.032 Al. wall.

Table III (continued)

Item	Reference Figures	Remarks
6. Thermistor network.	22	14 K ohm shunt resistor was 30 K ohm in PT units.
7. 160 volt power supply.	22	(2) 6.2 M ohm resistors at output of supply were 10 M ohm in PT units. IN 1327 zener diode in regulator circuit was Victoreen type RCA-125 trigger tube in PT units.
8. 700 volt power supply.	22	Transformer was Rayco type 0-5263 in PT units. 390 K ohm secondary circuit current limiting resistor was 100 K ohm in PT units. 4.7 M ohm regulator resistor was 2.7 M ohm in PT units. (4) 5.6 M ohm resistors at output of supply not in PT units.
9. Step Limiting MV No. 1.	39, 40, 41	Input circuit contained unnecessary components in PT units. Initializing RC network not used in PT units.
10. Step Limiting MV No. 2.	39, 40, 41	Initializing RC network not used in PT units.
11. Antenna matching network.	55	Shunt 0.47 μh choke not used in PT units. 1 M ohm resistor in parallel with capacitor in PT units.

B. Detectors.

1. Detector B.

Detector B is a low energy particle detector developed at SUI by Messrs. J. W. Freeman, G. Pizzella, and J. Thissell following earlier work of C. E. McIlwain. An introductory description is presented here; a more complete description is being prepared by Mr. Freeman.

The basic detector element is a doped single semiconducting crystal of cadmium sulfide of a type which is in general use as a photoelectric detector. The absorption of charged particles in the body of the crystal by inelastic collision results in the creation of electron-hole pairs. Until these carriers are lost by recombination, the conductivity of the crystal is increased. The recombination time of the electrons is relatively long; therefore they act as the majority carriers. The minimum particle energy which can be detected is the sum of the energy required to create an electron-hole pair and the work function of the surface

(a total of about 2.5 ev.).[38] The number of electron-hole pairs created per unit energy lost in the crystal per unit time rises from zero for incident electrons with energies of a few ev. to a nearly constant value for particle energies above about 50 ev.* Above this energy the conduction current through the crystal from a constant potential supply is nearly proportional to the time rate of loss of particle energy by absorption within the crystal.

The conductivity is also related to T, the absolute temperature. For low incident fluxes, where the conductivity is primarily the intrinsic conductivity of the bulk material, the conductivity is proportional to $T^{-3/2}$ in the neighborhood of room temperature. For high incident fluxes the amount of the decrease in conductivity with increasing temperature is somewhat less. The temperature coefficient

---

* G. Pizzella, private communication.

38. Li Chih-Tsien, Physics Abstracts 63, No. 745, p. 605 (Abstr).

varies from crystal to crystal, but is typically of the order of -0.3 per cent per degree centigrade.

When a change in energy flux occurs, the adjustment of the conductivity to its new value occurs quite slowly, the speed of response depending on the final value of the conductivity. This is illustrated in figure 14 in which the pulse rate of the relaxation oscillator (proportional to current) is plotted as a function of time, as the intensity of a light source illuminating the crystal is changed in discontinuous steps.

The Clairex type Cl-2 CdS crystals used in the S-46 payloads have a typical area of 3 mm^2 and thickness of 0.5 mm. This thickness corresponds to the range of approximately 700 kev. electrons or 13 Mev. protons.

The detector conductivity is also increased by incident light due to the creation of electron-hole pairs by the photoelectric effect. For this reason a series of light baffles is provided to eliminate its light sensitivity except over a solid angle of about 10^{-3} steradian (see the assembly drawing of

figure 17). These baffles and a lead aperture act also as the geometry determining collimator for all particles not sufficiently energetic to penetrate the material of the assembly. In addition, the detector is mounted in a lead and stainless steel cylindrical absorber to further reduce the contribution from the X-rays (bremsstrahlung) produced in the payload structure and from energetic particles arriving from outside the angle of collimator acceptance.

In order to reduce the effects of external magnetic fields on the arrival of low energy electrons at the detector, it is surrounded by a sheet of 0.51 mm. thick Perfection Mica Co. type NETIC S-3 high permeability magnetic shielding material.

The conductivity of the crystal is measured, in practice, by measuring the current through the crystal from a regulated 160 volt power supply (see figure 18). This current charges a capacitor in a relaxation oscillator until the ionizing potential of a neon bulb (NE-76 or NE-81) is reached, at which time the capacitor is discharged through the bulb. The discharge pulse obtained across a resistor in the

discharge path is shaped and used to drive a scalar (see section IV D below). The pulse rate from the relaxation oscillator is proportional to crystal current over a large range of current. Figure 19 shows the relationship between the crystal current and pulse period for the FU-2 circuit at room temperature. The variation in pulse rate with changes in temperature for an input current in the range from 10^{-5} to 10^{-9} ampere can be made less than 2.5 per cent over a temperature range from -25° to $+75^{\circ}$ C. by proper selection of the neon bulb.

2. Detector A.

This detector is identical to detector B except for the addition of a permanent magnet with a field strength of about 500 gauss in the aperture system to sweep aside low energy electrons (see figure 16). With this field strength electrons having energies less than 500 ± 100 kev. are deflected from the crystal. Thus, the simultaneous measurements of detectors A and B yield independently the flux of all particles with $E > \approx 50$ ev., and the flux of all of these particles except for electrons with $E < \approx 500$ kev.

3. Detector C.

Detectors C and D are contained in the spectrometer assembly, designed at SUI by Mr. C. D. Laughlin. The spectrometer assembly is described in more detail in a paper being prepared by the designer. Figures 20 and 21 are, respectively, a photograph and an assembly drawing of the unit.

The spectrometer proper (detector C) consists of a stainless steel aperture system having a known geometric configuration to admit the particles, a magnet to deflect them through a 90° angle, another aperture to further define the geometry, and a thin window G.M. counter to detect the particles. The magnet field strength (1050 $\pm$ 25 gauss) is adjusted to deflect electrons in the desired energy range through the proper angle so that they will enter the G.M. counter. The spectrometer unit in FU-2 had an electron energy "window" from about 47 kev. to 56 kev. measured at the half height of the response curve.

The counter is heavily shielded by lead and stainless steel absorbers to reduce the contribution from particles traversing the payload structure and from X-rays produced by inelastic collisions of electrons in

the payload structure. The lead thickness is 0.442 cm. (5.0 gm./cm.^{2}) corresponding to the ranges of approximately 10 Mev. electrons and 50 Mev. protons. The stainless steel absorber thickness is 0.40 gm./cm.^{2}.

The G.M. counter used as the spectrometer detector is an Anton type 223 halogen quenched counter having a mica window with a thickness of 1.2 $\pm$ 0.2 mg./cm.^{2} (27 kev. energy loss for electrons). The designation of this counter has recently been changed from "223" to "213 without ceramic button" by its manufacturer. The practice adopted in this paper is to refer to the counters used in detectors C and D as 223 counters and the counter with the ceramic button over the mica used as detector E in FU-1 as a 213 counter. The effective omnidirectional factor (ϵG_o) of both types is typically

$$\epsilon G_o = 0.12 \text{ cm.}^2$$

The effective geometric factor (ϵg_c) of the complete spectrometer assembly for electrons incident within a cone of angles about the initial aperture system axis, assuming an idealized rectangular counting rate vs. electron energy curve with upper and lower edges at the half height energies of the actual curve,

is:

$$\epsilon g_c = 1.7 \times 10^{-5} \text{ cm.}^2 \text{ ster.}$$

for the unit in FU-2. Hence, the unidirectional intensity (j_c) of electrons in this range of energy is:

$$j_c = \frac{R_c}{\epsilon g_c} = (5.9 \times 10^4)\, R_c \text{ cm.}^{-2} \text{ sec.}^{-1} \text{ ster.}^{-1}$$

where R_c is the true counting rate of the G.M. counter, if the counting rate contributions from all other sources are zero.

4. Detector D.

This detector is identical to the cylindrical counter and absorber assembly in the electron spectrometer in every respect except that no window is provided in the lead and stainless steel absorbers, so that all low energy charged particles and almost all locally produced bremsstrahlung are excluded from the counter. This counter was included to permit a correction of the electron spectrometer rates for the counting rate contribution from particles not entering through its opening, and to give additional information about the particle absorption spectrum.

5. Detector E.

Detector E protrudes from the top of the payload, and employs a G.M. counter surrounded by a relatively thin absorber. Both Anton types 302 and 213 halogen quenched G.M. counters were used as indicated in Table III. Typical values of their most important characteristics are listed in Table IV.

C. High Voltage Power Supplies

Two high voltages are required in the S-46 instrumentation, 700 volts for the G.M. counters and 160 volts for the CdS detectors. They are provided by independent transistor saturating core converters, voltage multipliers, and voltage regulators. The schematic diagrams of the supplies are contained in figure 22; figures 23 and 24 show, respectively, top and bottom views of a completed power supply assembly.

The basic high voltage power supply circuit was originally developed by the Power Sources Division of the Signal Corps Engineering Laboratories for Explorer I.[7] The present supplies are modifications of this design.

1. 700 volt supply.

The 700 volt supply utilizes two transistors in

Table IV

Detector E Characteristics (Typical Values)

	213 counter	302 counter
Effective omnidirectional geometric factor, ϵG_o	0.12 $cm.^2$	0.59 $cm.^2$
Omnidirectional intensity of energetic charged particles, J_o	8.7 R_{213}	1.7 R_{302}
Counter wall thickness (stainless steel)	0.4 gm/cm^2	0.40 gm/cm^2
Thickness of mounting thimble plus flight cover (aluminum)	0.86 gm/cm^2	0.99 gm/cm^2

a conventional transformer feedback oscillator circuit in which core saturation is employed to stabilize the operating conditions and to obtain high power supply efficiency.

The type 0-3767A transformer was designed and wound by the Rayco Electronic Manufacturing Company of North Hollywood, California. It employs an Arnold Engineering Company Supermalloy type 4168-S1 tape wound core, and is wound with 532 turns (center tapped) for the primary winding, 80 turns (center tapped) for the feedback winding, and 13,500 turns for the secondary winding. The secondary winding is both bank wound and split wound to minimize distributed capacitance.

The frequency of oscillation is about 900 cycles per second for an input voltage of 6.50 volts, and the peak-to-peak amplitude of the collector square waveform is 12.0 volts. This is transformed to an approximate peak-to-peak square wave amplitude of 475 volts at the secondary. A voltage quadrupler is used to multiply and rectify this square waveform. The D. C. voltage produced at the output of the quadrupler, based on the

assumption of perfect diodes and capacitors, is:[39,40]

$$V_{mult.} = nE - \frac{i\left(\frac{2n^3}{3} + \frac{n^2}{2} + \frac{n}{6}\right)}{fC}$$

where n is the number of doubler stages,

E is the peak-to-peak input voltage,

i is the output current in amperes,

f is the operating frequency in cycles per second, and

C is the value of the multiplier capacitors in farads.

In the present case $n = 2$, $E = 475$, $f = 900$, and $c = 10^{-8}$, so that

$$V_{mult.} = 950 - 0.78\ i$$

where i is now in microamperes. Thus, for $i = 45$ microamperes, $V_{mult.} = 915$.

A corona discharge voltage regulator tube is used

---

39. W. R. Arnold, "A 500-Kilovolt Linear Accelerator Using Selenium Rectifiers," Rev. Sci. Instr. 21, 796 (1950).

40. Von A Bouwers and A. Kuntke, "Ein Generator fur drei Millionen Volt Gleichspannung", Z. technische Physik 8, 27 (1937).

in a conventional shunt regulator circuit to regulate the output voltage at approximately 700 volts. Capacitance is placed across the regulator (in series with the 100 K ohm resistors) to stabilize the regulation at low regulator currents. The tube employed is a Victoreen type GV3B-690, and the flight unit tubes are carefully selected to give the best possible regulation characteristics. Figure 25 shows these characteristics for the tube used in FU-1. The circuit was designed to produce a quiescent current I_{ss} through the regulator tube under no-load conditions of 45 μA. at room temperature and with a nominal primary supply voltage. The regulator tube current, which is the current that can be drawn by the load before regulation is lost, is plotted in figure 26 as a function of temperature and supply voltage V_{cc2} (FU-1).

The G.M. counter series resistors were chosen so that the total current drawn by the counters under the saturated condition would not exceed the regulator current. The current requirements for the saturated counters when operating from a 700 volt supply are approximately 6.7 μA. for a 223 counter with 19.4 megohms

series resistance, 29 μA. for a 213 counter with 5.6 megohms series resistance, and 18.5 μA. for a 302 counter with a 1.8 megohm series resistance. The design was finalized on the basis of the requirements of two type 223 and one type 302 counters as used in FU-1, which require a total of 31.9 μA. if all three counters are saturated at the same time. This is available under all operating conditions for $V_{cc2} \geq 5.62$ volts. This is acceptable because the supply voltage is not expected to fall below 5.85 volts in practice. When the decision was made to substitute a type 213 counter in FU-2, it was done with the knowledge that the supply could not have delivered the 42.4 μA. required if all counters were saturated simultaneously, if the supply voltage became less than 6.5 volts. This was not considered a serious limitation, however, because the probability of simultaneously saturating all three counters, with their assorted absorber thicknesses and different geometric factors, at the same time is very small. Furthermore, the overloading of the supply does not cause the supply to cease operating. It simply

reduces the voltage below the regulated value, and a new operating point is established. The fact that the counter calibrations are no longer valid is obvious from the data by the fact that the channel C, D, and E rates are all very high.

2. 160 volt supply.

The 160 volt supply is, in general, similar to the 700 volt supply. The transformer is a Rayco type 0-3753 transformer with 532 (center tapped) primary turns, 80 (center tapped) feedback turns, and 5500 secondary turns wound on the same core type as that in the 700 volt supply. Since the output voltage is relatively low, a voltage doubler circuit is used rather than the quadrupler. And since 160 volts is below the range for which satisfactory corona discharge regulators are available, zener diodes are used for voltage regulation. The zener diode regulation characteristics are shown in figure 27 for the regulator in FU-1. The large variation in the regulated voltage with changes in temperature is not considered serious due to the fact that high accuracy is not

required for the CdS detectors in this experiment, and that the temperature of the detector assembly, within which the power supplies are located, is measured by one of the thermistors.

The diode current, which is the available load current, is plotted in figure 28 as a function of temperature and primary supply voltage (FU-1). This figure indicates that a minimum of 64 μA. is available under all possible operating conditions. Thus, regulation is maintained even if the terminals on the load side of the series resistors are grounded, in which case the current would be 52 μA. Actually, the maximum current drawn from this supply when both detectors are saturated by a strong light source is only 32 μA. due to the manner of operating of the relaxation oscillator circuit.

D. Pulse Shaping Circuits.

The function of the pulse shaping circuit is to furnish a stabilized optimum shaped pulse to the scaler circuits. Its use is particularly necessary with the G.M. counters to minimize the effects of changes in temperature and supply voltage on the counting rates when these rates are very high. They are also used with the CdS detectors to prevent the load from influencing the operation of the relaxation oscillators.

Figure 29c shows the envelope of the G.M. counter pulses following an initial pulse, and figure 29a shows an oscilloscope recording of the pulses which form this envelope. Whenever a pulse occurs at time t_o and another occurs at time t_1, as in figure 29c, then the amplitude of the second pulse is as indicated by the envelope. The pulses drive a scaling circuit where the threshold voltage of the combined shaping circuit and scaler is V_t. When the particle flux is sufficiently great so that there is a high probability that some pulses will be separated by less than the dead time $t_1 - t_o$, then the counting

rate varies with changes in the dead time, the threshold voltage, and the G.M. counter pulse amplitude. The pulse shaping circuit used in satellite S-46 establishes a set of operating conditions such that variations in the values of these parameters combine to reduce the overall variation in maximum counting rate to a low value.

The pulse shaping circuit uses a two stage bootstrap amplifier. In order to simplify the discussion of its operation, the basic single stage amplifier, as shown in figure 30a, is described first. A Z-parameter equivalent circuit of the amplifier is shown in figure 30b. It has been simplified by omitting the components which introduce the effects of the open circuit reverse transfer impedances Z_{12} and Z'_{12}, since they are small for the transistors used. The calculations are further simplified by ignoring I_3 in all calculations, since for the transistors and resistors used $\frac{I_4}{I_3} > 10$ over the complete range of operating conditions. With these assumptions, $V_1 = \frac{R_2}{R_1 + R_2} V_{out}$. The quantity V_{be} is the input transistor base-emitter junction

D.C. voltage, and Z_{11} is the transistor open circuit input impedance. Since Z_{11} is less than 2000 ohms, V_{be} is of the order of 0.5 volt for these transistors, and I_1 is less than 10 microamperes under all operating conditions, the voltage drop across Z_{11} is negligible compared with V_{be}. Thus the D.C. input-output relationship is

$$V_{out} = \frac{R_1 + R_2}{R_2} (V_{in} - V_{be})$$

and the dynamic gain is

$$\Delta V_{out} = \frac{R_1 + R_2}{R_2} \Delta V_{in}$$

Both the D.C. and A.C. voltage gains, in this approximation, are independent of all circuit parameters except the ratio $\frac{R_1 + R_2}{R_2}$. The D.C. relationship is, however, dependent on temperature, since V_{be} is temperature dependent. A family of D.C. output voltage vs. input voltage curves are given in figure 31, where temperature is the parameter. The linearity of response over a large fraction of the supply voltage and the constancy of the dynamic gain (the slopes of the curves) can be seen. The x-axis

intercepts of the lower extensions of the straight line sections are the values of V_{be} at the temperatures plotted.

Figure 32 shows the independence of the output voltage for fixed input voltages as the supply voltage V_{cc} is varied. The slopes of the linear portions of the curves are less than 0.002.

The D.C. input impedance of the circuit $Z_{in} = \frac{V_{in}}{I_1}$, which is a function of V_{in} and temperature, is shown in figure 33. The effect of output loading on the circuit can be seen in figure 34, where the output voltage is plotted as a function of the output load resistance R_L, and V_{in} is the parameter. Adding the load causes less than a one per cent change in V_{out} (with V_{in} constant) if $R_L \geq 6000$ ohms, and less than a ten percent change if $R_L \geq 1000$ ohms. The output impedance Z_{out}, found from the data used for this plot, is approximately 100 ohms. Thus the impedance ratio $\frac{Z_{in}}{Z_{out}}$ for the circuit is of the order of 10,000. The current ratio $\frac{I_{out}}{I_{in}}$ is about 1300 when the device is terminated in its output impedance of 100 ohms and with $V_{in} = 2.00$, $V_{cc} = 5.00$, and

temp. = 25° C.

This basic circuit has been used in a number of previous experiments as a linear pulse amplifier where its high frequency response was useful,[41] as an emitter follower (with $R_1 = 0$),[41] and as a D.C. voltage amplifier and impedance transformer (see Section IV F of this paper).

The pulse shaping amplifiers employed in the S-46 payloads are shown in schematic form in figure 18, and figure 35 is a photograph of the top of the instrumentation deck containing these five circuits. The pulse shaping circuits for the five channels are identical except for the input circuit resistor values, which are selected to produce the proper input pulse amplitudes.

Two stages of amplification are used in each circuit to provide an overall gain of 3.4. The output transistor of the first stage is used as

---

41. C. E. McIlwain, "Scintillation Counters in Rockets and Satellites", SUI Research Report 60-4 (February, 1960).

the input transistor of the second stage, so that only three transistors are required for the two stages instead of four. The circuit is used as a nonlinear amplifier. A zener diode voltage limiter is used at the output to clip the negative pulses at the 3.3 volt level, producing an optimum pulse amplitude for driving the scaler. This waveform can be seen in the oscilloscope photograph of figure 29b. The threshold effect due to V_{be} is used to establish an input pulse amplitude threshold. The overall effect of the circuit is to produce no output for input pulses just below the threshold, and to provide output pulses having full amplitude for input pulses slightly above threshold. This is illustrated in the graph of figure 36, in which the output pulse height is plotted as a function of input pulse height. The threshold effect can be seen in the oscilloscope photograph of figure 29, in which the upper trace is the amplifier input pulse train at the G.M. counter cathode, and the lower trace is the resultant shaping amplifier output.

It was determined experimentally that a diode

placed in the input circuit as shown in the schematic diagram effectively reduces the high counting rate temperature dependence of the complete configuration. Its primary effect is to partially balance the temperature dependence of V_{be} by generating an equal voltage with a similar junction placed in a position where their variations subtract. The effectiveness of the over-all temperature compensation can be seen in figure 37, in which the counting rate of detector E with a radioactive source positioned to produce a maximum scaler switching rate is plotted as a function of temperature.

E. Binary Scalers.

The binary scalers used in the payload for S-46 are an outgrowth of the circuits designed for Explorers I and III.[7] The major modifications are a change in supply voltage from 2.68 volts to 6.50 volts and appropriate changes in the component values.* The advantages are a decrease in the

---

* These changes were proposed by R. J. Parent and V. E. Suomi, University of Wisconsin, Madison, Wisconsin.

power requirements and the ability to drive one stage directly from the output of a preceding stage without the need of interstage coupling amplifiers.

The basic scaling circuit is the bi-stable multivibrator shown in figure 38. Several departures from conventional techniques are the omission of the usual base to negative potential biasing resistors and the use of unusually large collector resistor values to reduce operating power. The D.C. biasing conditions are as follows:

Assume that T_1 is conducting and that T_2 is cut off. The T_2 collector current is essentially I_{co}, which for the silicon transistors used is negligible (less than one microampere). Then

$$V_{c_2} = V_{cc} - \frac{R_2(V_{cc}-V_{b_1})}{R_2 + R_4} = 3.4 \text{ volts}$$

for the resistance values indicated and for V_{cc} = 6.5 volts, since V_{b_1} = 0.3 volt when T_1 is conducting. The base current of the conducting transistor is

$$I_{b_1} = \frac{V_{cc} - V_{b_1}}{R_2 + R_4} = 30 \ \mu A.$$

which would be great enough to provide $I_{c_1} = 1.5$ ma. (with $\beta_{min} = 50$) if this current could be supplied by V_{cc} through R_1. However, the current is limited by R_1 to $I_{c_1} = \frac{V_{cc}}{R_1} = 65 \ \mu A$. The result is that V_{c_1} is firmly clamped to ground ($V_{c_1} = 0.03$ volt).

With $V_{c_1} = 0.03$ volt the cut-off transistor base voltage (V_{b_2}) is well below the silicon transistor base-emitter junction potential (I_c is only a few microamperes when $V_b = 0.2$ volt). As a result, T_2 is adequately cut off, and I_{c_2} is negligible as was initially assumed.

Thus it is seen that all biasing conditions for stable operation are met, and that the base to negative potential resistors are not required as a result of the low I_{co} and high base-emitter potential of the silicon transistors, and the low current operating conditions of the circuits. The design is sufficiently conservative so that operation over very wide ranges of temperature and supply voltage is possible.

To trigger a change of state, a negative pulse is applied to the base of the conducting transistor by the pulse steering network consisting of C_1, C_2, R_5, R_6, D_1, and D_2. The two resistors R_5 and R_6 bias the diodes to accomplish the steering action. If T_1 is conducting, diode D_2 is reverse biased by a potential of 3.4 volts, while D_1 has essentially zero bias. A negative pulse applied to the input is conducted by D_1 to the base of T_1 and to the collector of T_2 through the speed-up capacitor C_4, but is not conducted by the reverse biased D_2. Thus the circuit begins a transition to the opposite state, and the regenerative action of the circuit completes the transition. The values of the speed-up capacitors C_3 and C_4 are not critical, the primary requirement being that the time constant of the capacitors and their discharging resistors R_2 and R_4 or R_1 and R_3 be of the order of a few microseconds. A value of 33 $\mu\mu$fd. is used, giving RC = 1.6 μ sec.

The values of the steering network components were chosen empirically to produce the best operation over a wide range of operating conditions from the

waveform obtained from the collector of an identical circuit. The time constant of the input circuit consisting of C_1 and R_5 is 470 microseconds. This establishes a maximum frequency of operation of about 16,000 counts per second ($f_{max.} \approx \frac{8}{RC}$). The time constant can be reduced considerably before serious deterioration of performance results. The values shown in the schematic are used whenever high speed of operation is not necessary. In the cases where faster counting is necessary, a modification of the basic circuit is used in which the operating currents are increased by reducing the values of R_1, R_2, R_3, and R_4, and the input time constants are reduced in value. The first stages of the scaler of figure 40 are examples of circuits which count at maximum rates of about 39,000 counts per second (RC = 44 microseconds; $f_{max.} \approx \frac{2}{RC}$). Even higher speeds of operation are possible, although this requires a somewhat more careful selection of transistors, diodes, and resistor values.

The input pulse amplitude must be considerably greater than the silicon diode junction voltage of

the unbiased steering diode (about 0.6 volt). However, if it is made greater than the 3.4 volts by which the other diode is reverse biased, then the performance is deteriorated. The most immediate effect is that the maximum speed of operation decreases. A pulse amplitude of about 3.3 volts is used at all the scaler inputs. The zener diode in the pulse shaping amplifier regulates the first scaler stage input pulse amplitude at this value, and for succeeding stages this amplitude is provided directly by differentiation of the scaler collector waveform.

The output impedance of the scaler circuit is 50 K ohms (with $R_1 = R_2 = 100$ K ohms).

The values of the scaler components are not critical. Resistor value tolerances are $\pm$ 10 per cent, and the transistor forward current gain (β) can be any value greater than about 50. The transistors having the higher values of β are used in the stages which must operate at the higher rates, and an attempt is made to use pairs of transistors in each stage with approximately equal values of β. The capacitor values are also non-

critical, although, of course, the scaler has a dead-time vs. temperature characteristic which is partially determined by the capacitors C_1 and C_2.

In the S-46 payload, 65 scaler stages are used. The scaler module schematic diagrams of figures 39, 40, and 41 show the manner in which they are connected. Figures 42 and 43 are, respectively, photographs of the top and bottom of the detector E seventeen stage scaler (scale of 131,072) and the logic circuit and output amplifier associated with it.

Several of the performance characteristics of the scaler stages are indicated in figures 44, 45, and 46. The data used to plot the curves are average values obtained from a number of individual circuits, as indicated in the figures. The signal source for all tests was a pulse generator furnishing a negative 3.1 volt rectangular pulse having a width of 5 μ sec., a rise time of less than 0.1 μ sec., and a source impedance of 50 ohms. In all cases the output of the stage under test was loaded by an identical scaler stage input impedance.

The scaler stages operate over a wide range of

supply voltage V_{cc}. Figure 44 indicates the minimum value V_{cc} (min.) as a function of temperature for the low speed scaler, with the scaler operating at a rate of 1000 sec^{-1}. The analogous curve for the high speed scaler is similar in character but about 0.3 volts higher. The maximum value (V_{cc} max.) is in every case greater than 8.0 volts, the highest value attempted.

The operating power per low speed scaler stage is nominally about 0.75 milliwatt with V_{cc} = 6.5 volt. A plot of the operating power as a function of supply voltage is shown in figure 45 for temperatures of -50° C. and +100° C.

Figure 46 shows the dependence of the maximum counting rate (of the scaler alone) on temperature and supply voltage V_{cc} for both the high and low speed scalers. The difference in temperature characteristics between the two circuits is due primarily to the difference in the input capacitor (C_1 and C_2) temperature coefficients. The high speed scaler uses Glenco Corp. type TC-220-9 (Code Q) 220 μμfd. capacitors having a negative

temperature coefficient of about 0.2 per cent per degree centigrade, while the low speed scaler uses Glenco Corp. type SSM-001-23 (Code M) 1000 μμfd. capacitors having a positive temperature coefficient of somewhat less than 0.14 per cent per degree centigrade. Thus the difference in capacitor coefficients is a little less than 0.34 per cent per degree centigrade. The difference in the slopes of the maximum counting rate curves for the two scalers is of the order of 0.28 per cent per degree centigrade. It is reasonable to assume, then, that the counting rate temperature coefficient for the scaler circuit, if zero temperature coefficient input capacitors were used, would be about -0.14 per cent per degree centigrade. This is due primarily to changes in transistor characteristics with changes in temperature. The variation can be reduced to a low value by the proper selection of input capacitor characteristics. In this particular scaler application the variation in scaler dead time does not effect the maximum G.M. counter counting rate because the scaler dead time is significantly less

than the counter dead time under all operating conditions (see figure 37).

F. Logic Circuits and Output Amplifiers.

Since a large dynamic range in counting rates is expected for any experiment traversing the high intensity radiation belts, it was considered necessary to telemeter three different scaling factors for each detector. Outputs are obtained from three stages of each scaler. The various scaling factors used in the S-46 instruments are as indicated in the block diagram of figure 9. These outputs are combined in logic circuits in such a way that all three scaling factors can be identified unambiguously in the single output waveform.

This method of telemetering three scaling factors on a single channel was first proposed by the writer in April, 1958. The Jet Propulsion Laboratory designed the first version of the system and used it successfully in the Pioneer III and IV space probes.[42] The present system is an improved

---

42. C. S. Josias, "Radiation Instrumentation Electronics for the Pioneer III and IV Space Probes", Proc. IRE 48, 735 (1960).

design of the JPL system in which the remaining large shifts in SCO frequency are eliminated, less operating power is required, and the operation is more stable.

The operation of the logic circuit can be seen with the aid of the block diagram of figure 47, the schematic diagrams of figures 39, 40, and 41, and the waveforms of figure 48. Inputs from the three scaler stages A, B, and C (which correspond, for example, to stages 1, 5, and 9 respectively of the channel A scaler) operate transistor switches 1, 3, and 5 directly. The collectors of these switches are either at ground potential (0.02 volt) or at 5.0 volts minus the voltage drop across the 100 K ohm collector resistors, depending on whether the switches are off or on. These voltages produce an eight level waveform in the summing circuit as shown in figure 48 by waveform (f).

It was found necessary to keep the telemetry bandwidth as low as possible to reduce the transmitter power requirements (see section III J). This was accomplished by choosing the scaling factors large enough so that the highest anticipated counting rates

were scaled to rates of less than one cycle per 5 seconds, and by limiting the rate of change of the logic circuit output voltages (and therefore sub-carrier oscillator frequencies). This was accomplished by including elements in the logic circuit to prevent all output voltage shifts of greater than one unit, and by passing the output waveform through an RC integrating circuit having a time constant of about five seconds.

The "OR" circuits, step reducing multivibrators, and switches 2 and 4 were added to reduce the large voltage shifts. The step reducing multivibrators produce waveforms which, when used to generate waveforms (b) and (d) of figure 48 at the outputs of switches 2 and 4, produce the logically perfect waveform (g). This waveform is integrated by the RC circuit. The resultant output waveform is shown in figure 70, in which the input pulse rate increases smoothly from 1 to 40,000 pulses per second. Thus it can be seen that the dynamic range provided by this system is greater than 4×10^4.

The operation of step reducing multivibrator number two is as follows: Its normal position is with C_2 (collector number two) at ground potential.

A negative pulse (the waveforms shown occur at the outputs of the switches where the multivibrator waveforms have been reversed) at B_2 (base number two) coincident with the triggering of scaler stage C at time t_1 switches the multivibrator. The subsequent input to B_1 from scaler stage B at time t_2 resets it, and no further action occurs until another pulse appears at B_2 (at time t_4). The operation of step reducing multivibrator number one is similar, except that an extra pulse is inserted at the time (t_2) that step reducing multivibrator number two resets (through input B of "OR" circuit 2), and a pulse is blanked at the time (t_3) that scaler stage C resets (through input B of "OR" circuit 1). Input B to "OR" circuit 1 occurs about 40 microseconds later than input A to "OR" circuit 2 due to switching delays in the scaler stages between stages B and C. Therefore the multivibrator is triggered as usual, but is immediately reset. The integrating circuit removes all traces of the 40 microsecond wide pulse which results.

The step reducing multivibrators are identical to the low speed scaler stages except for several minor modifications. They are used as bi-stable

multivibrators with separate inputs. Therefore the diodes are zero biased rather than collector biased. Additional diode networks are added to step reducing multivibrator number one to form the two "OR" circuits. And an RC network is added to one of the collector circuits in each multivibrator. The capacitors hold those collectors at ground potential momentarily when power is applied to cause them to be initially in the "down" state. If this were not done, there would be a probability that more than three of the summing circuit inputs of some channel might be in the "on" state, which would cause that subcarrier oscillator frequency to be out-of-band. This could not be allowed because, during launch, the internal payload power was finally applied only 5.5 minutes prior to rocket lift-off. With the low counting rates observed near the earth's surface, these SCO's would probably have remained out-of-band throughout the launch trajectory, and no launch data would have been obtained from those channels.

The transistor switches are grounded-emitter amplifiers. The common emitter lead connection is maintained at approximately 0.6 volt by the diode at

the input to the D.C. amplifier. When the multivibrator collector driving a switch is in the "off" state (near ground potential), the switch is reverse biased and essentially zero base current results. The transistor is thus cut off and the collector potential is that established by the current through the summing circuit resistors. When the multivibrator collector is in the "on" state, however, base current in the transistor switch results. Its value is about 13 microamperes (the multivibrator collector voltage with this load is 2.58 volts), resulting in full conduction. Thus the collector is within 0.03 volt of the emitter voltage.

The summing circuit consists of 2.2, 1, and 0.42 megohm input resistors (and a 1.2 megohm resistor used to establish one operating point) and a 0.82 megohm shunt resistor. The exact value of the 0.82 megohm nominal value shunt resistor is selected to produce a D.C. voltage of 1.0 $\pm$ 0.1 at the amplifier output with all transistor switches conducting and at room temperature. The 1.2 megohm nominal value resistor is selected to produce

5.0 ± 0.2 volts at the same point with switches 1, 3, and 5 cut-off and switches 2 and 4 conducting. These voltages establish the SCO frequencies when the amplifier output waveform is in its lowest and highest states, i.e., states one and eight.

The transistor switches and summing circuits are operated from a 5.0 volt supply which is regulated to reduce the output voltage changes with variations in supply voltage. The regulator is shown in the schematic diagram of figure 41. It is a conventional series transistor regulator for which a reference voltage is established by a type 652C3 5.8 volt zener diode. The regulation characteristics of this regulator are shown in figure 49, in which the output voltage is plotted as a function of temperature and supply voltages. This circuit maintains the voltage within ± 4 per cent of 5.0 volts, which is adequate in this application.

Integration of the output amplifier waveform is provided by the 15 microfarad capacitor and the resistors in the summing circuit. One terminal of this capacitor, shown unconnected in the schematic

diagrams, is grounded through the test socket (TS) on top of the payload except during laboratory testing, when the long time constant would result in an unnecessarily long wait to accumulate test data. The capacitor value was chosen to produce a time constant of 5 ± 1 second.

The D.C. output amplifier is a simple, linearly operated bootstrap amplifier having somewhat higher voltage divider resistor values than the input circuits (which are biased off in the steady-state condition) to keep the power requirements low. The resulting higher output impedance is acceptable in view of the high subcarrier oscillator input impedance. The amplifier dynamic gain is 2.5.

A diode is included in the input circuit of this amplifier to partially compensate the amplifier temperature characteristic. As was indicated in section IV D, the shifts in output voltage with changes in temperature is due primarily to the temperature dependence of the first transistor

base-emitter junction voltage. This is balanced by inserting a silicon diode junction having similar characteristics in the input circuit so that the two variations subtract.

Figure 50 shows the variation in the output of this amplifier with changes in temperature and supply voltage with the complete system consisting of the scaler, logic circuit, output amplifier, and voltage regulator operating together. It can be seen that the temperature compensation is not complete. The primary requirement was, however, that the input voltage to the subcarrier oscillators remain between 0.70 and 6.0 volts over the temperature range -20 to +75 degrees centigrade. This condition is adequately met, and more complete compensation was not attempted in order to keep the circuits as simple as possible.

G. Telemetry System.

The entire telemetry system consisting of the electronic commutator, subcarrier oscillators, transmitter, and antenna system was developed and built by ABMA. A qualitative description of its operation and the schematic diagrams are included to give a more complete understanding of the entire system operation. Much of the information in this section was obtained from an ABMA publication* and from the references cited.

1. Electronic Commutator.

The electronic commutator was included to permit the transmission of temperature and primary power supply data by interrupting the transmission of the detector D data periodically. The operation of the commutator can be seen with the aid of the block diagram of figure 51 and the schematic diagram of figure 52. It consists of six analog gates controlled by a ring counter. The ring counter is advanced by pulses derived

---

* "S-46 Satellite Instrumentation" prepared by the Planning and Engineering Section, Guidance and Control Laboratory, ABMA (9 Feb. 1960).

from a multivibrator timing pulse generator having an eleven second period. When the ring counter is in position number one (with the gate for the data from detector E open), then the timing pulses are prevented from advancing the ring counter by the inhibitor circuit until the 64th pulse has been accumulated in the binary counter. The ring counter then advances one step each eleven seconds, sampling inputs two through six in turn. At the completion of this cycle, stage one of the ring counter is again on and remains on until 64 pulses have again been accumulated in the binary counter. Some of the basic elements of this circuit were used in the Explorer VII instrumentation which has been described in the literature.[43]

A number of tests were performed on the gates to ensure the absence of crosstalk and leakage. The specifications for these circuits at room temperature are:

---

43. O. B. King, "Multiplexing Techniques for Satellite Applications", Electronics 32, No. 44, p. 58 (Oct. 1959).

a. Leakage. The base-collector reverse currents of the gate transistors produce a signal level in the commutator output which is termed leakage. With the supply voltages equal to 11.55 and 7.15 volts the voltage at the commutator output is less than 0.010 volt during the time that each of inputs 1, 4, 5, and 6 is sampled, with all inputs except the one being tested at ground potential.

b. Spillover. Spillover is the presence of a signal in the commutator output from an input to a closed gate. The spillover from the calibration channels 2 and 3 into any of the other channels is less than 0.010 volt. For a spillover into channel 1 from channels 4, 5, or 6 of 0.010 volt, the input resistance of the channel is greater than 40 k ohms in the case of channel 4 and greater than 30 K ohms in the cases of channels 5 and 6. For a spillover of channel 1 into channels 4, 5, or 6 of 0.010 volt, the input voltage to channel 1 is greater than 6.0 volts.

c. Voltage drop across the gates. The voltage drop from emitter to collector of the gate transistors when conducting is less than 0.030 volt for

primary supply voltages of 11.55 and 7.15 volts for V_{cc1} and V_{cc2} respectively, and of 9.8 and 5 volts.

The inputs to the six commutator channels are listed in the schematic diagram of figure 52. Channels 2 and 3 are the high calibration (5.5 volts nominally) and the low calibration (1.2 volts nominally) channels respectively, which permit the correction of the analog data sampled in channels 4 and 6 for variations in supply voltage.

The input to channel 4 is a thermistor located in thermal contact with a special surface located on one edge plate of the solar cell assembly (see the photograph of figure 13). This surface is a small disc 3.2 cm. in diameter and 0.13 mm. thick which is thermally isolated from the payload structure. It is mounted on a Kel-F support having a very low thermal conductivity and its back surface is aluminized. This aluminized surface faces a mirror finish gold plated surface to reduce the radiative transfer of heat between the disc and the structure to a low value. The outer surface of the disc is given a Tabor finish. The temperature of the disc is measured by the Fenwall Electronics type GA45J-1 bead

thermistor connected between ground and the channel 4 input. The primary purpose of this disc was to ascertain the potential usefulness of the Tabor surface as a satellite thermal control surface. In addition it was hoped that the low thermal time constant of the disc would permit its use in determining the satellite motion in orbit.

The input to channel 5 is a voltage derived from the 10.4 volt solar battery, which was telemetered to assist in studying the operation of the solar battery system. In particular, it was expected to indicate the occurrence of damage to the cells by particle radiation when and if it occurred.

A thermistor network is located between the channel 6 input and ground. It is a Bourns, Inc. type 11 thermistor located in thermal contact with the detectors in the SUI detector assembly. Its primary purpose was to provide temperature corrections for the telemetered data. In addition, it was expected that the temperature data would indicate whether proper satellite thermal balance had been achieved, and whether temperature was the cause of any malfunction which may have occurred.

2. Subcarrier Oscillators.

Five subcarrier oscillators, tuned to RDB channels 1 through 5 as indicated in the block diagram of figure 9, are used to frequency multiplex the five data channels. They are multivibrator type voltage controlled oscillators (see the schematic diagram of figure 53). The high harmonic content of the output waveforms is removed by LC low pass filters. The oscillators are tuned so that an input of 0.0 volts results in a frequency corresponding to high band edge (center frequency plus 7.5 per cent), and +6.0 volts results in a low band edge frequency (center frequency minus 7.5 per cent). Figure 54 is a plot of the channel 4 oscillator frequency as a function of input voltage at room temperature. The temperature coefficient varies from about 0.0023 per cent per degree centigrade with an input voltage of zero to about 0.0044 per cent per degree centigrade with an input voltage of 5.0 (PL-4). The input circuits for the various channels are nearly identical except for the channel 4 input, which includes an RC network to provide the five second time constant for the commutated channel.

The outputs of the five oscillators are mixed in a ladder type linear adding network and fed into a high input impedance amplifier which provides a high degree of isolation between the terminating resistor of the adding network and the load. The amplifier consists of a two transistor emitter follower with A.C. feedback to obtain very nearly unity gain.

The oscillators are operated from a voltage regulator similar to the one used in the SUI instrumentation except for the addition of temperature compensating networks to improve the regulation.

The input impedances of the oscillators are greater than 100 K ohms, and, therefore, they impose no appreciable loading on the driving circuits. Their normal input voltage ranges are + 1.0 to + 5.0 volts, corresponding to a frequency range of two-third of full bandwidth, or $\pm$ 5 per cent.

3. Transmitter.

The transmitter, shown in the schematic diagram of figure 55, consists of an input audio amplifier, a crystal oscillator, a phase modulator, a driver

amplifier, and a power amplifier.[44] The power levels at the various points in the circuit are: at the output of the oscillator, 4 mw; output of modulator, 2 mw; output of driver amplifier, 38 mw; output of power amplifier, 300 mw.

The input audio amplifier provides gain and pre-emphasis for the composite subcarrier oscillator signal. The gain curve slope is approximately 4 db per octave between 400 and 1300 cycles per second. Its input impedance is of the order of 10 K ohms.

The Colpits crystal oscillator employs a fifth mode crystal oscillating at a frequency of 108.030 mc./sec. $\pm$ 1.5 kc./sec. A voltage controlled diode is used to minimize the effect of frequency pulling caused by changes in collector-base transistor capacitance.

The phase modulator employs a bridged-T network to change the phase of the oscillator signal as the

---

44. A. J. Fisher, W. R. Talbert, and W. R. Chittenden, "Telemetry Transmitter for Radiation Satellite", Electronics 33, No. 19, p. 68 (May, 1960).

amplitude of the modulating signal is varied. Capacitive diodes are used as the variable reactance elements. A nearly linear phase shift vs. diode control voltage is obtained by a suitable combination of non-linear elements. Although the linearity is quite good, it was found that some further improvement is desirable to eliminate cross channel mixing of the subcarrier oscillator frequencies. The peak phase deviation is ± 1.5 radians and the coincident amplitude modulation is less than 6 per cent.

The driver amplifier has a power gain of 12.8 db. It is followed by the power amplifier, which has a gain of from 9 to 10 db and a power output of 300 ± 30 mw. It operates with a power efficiency of about 55 per cent, and the output impedance is 50 ohms.

The entire transmitter module is powered from the 15.6 volt supply and requires a total supply current of 62 ma., or an input power of 967 mw. Thus the overall transmitter power efficiency is about 31 per cent.

4. Antenna.

The antenna is an asymmetrical dipole antenna in

which the conducting elements are the payload shell and the fourth stage rocket casing. These two elements are joined by a fibreglass insulating gap at the driving point. The antenna impedance as seen at the connecting points is transformed to 50 ohms to match the transmitter output impedance by the network shown in figure 56. The L-section transformer composed of the capacitor and the 0.08 microhenry inductor performs the impedance transformation, and the 0.47 microhenry input shunt inductor suppresses low frequency transmitter parasitic oscillations which were found to be possible under certain antenna loading conditions.

Seven conductors are passed through the antenna gap to provide external power to the payload while it was mounted on the rocket vehicle during the countdown, to switch the internal power on and off, and to monitor the switching operation. This was necessary due to the fact that the payload was mounted on the rocket about eight hours prior to launch time, the solar cells were covered by the payload shroud, and it was desired to launch the payload with its chemical batteries fully charged. These conductors are passed

through torroidal inductors mounted in the antenna insulator as indicated in figure 57, so they do not short the antenna input. The location of these chokes in the antenna gap was chosen to assist in dynamically balancing the payload for spin about its longitudinal axis.

H. Power Supply.

The power supply system was designed and built by ABMA. It consists of the solar cells with their diodes, the secondary cells, the timer, and the control relays. The power requirements of the payload are outlined in Table V for nominal supply voltages and at room temperature. In general, the circuits behave as resistive elements, in which the input power increases as the square of the supply voltage. The actual total power required from the 6.5 volt supply by the SUI instrumentation as a function of temperature and supply voltage is plotted in figure 58.

1. Solar Battery

The solar cells are mounted on flat aluminum plates which are fastened to the four sides, top and bottom of the solar battery framework, as seen in the

Table V

S-46 Payload Power Requirements

Module	Current (ma.)			Nominal Power (mw.)		
	6.5 volt Supply	10.4 volt Supply	15.6 volt Supply	6.5 volt Supply	10.4 volt Supply	15.6 volt Supply
SUI Package*				177	9.4	
Detector Assy. deck AB	17.90					
Scaler deck C	1.28					
Scaler deck D	1.28					
Scaler deck E	2.53					
Scaler deck F	1.70	0.9				
Scaler deck G	2.53					
Transmitter**						967
Audio Amplifier			5.0			
Oscillator			10.5			
Driver Amp.			11.5			
Power Amp.			35.0			
Commutator*	0.80	5.4		5	56.2	
S.C. Oscillators*		4.0			41.6	
TOTALS	28.02	10.2	62.0	182	107.2	967

* Average measured values for FU-1, FU-2.
** Obtained from reference 44.

photograph of figure 13. The power available from each solar battery element is listed in Table I.

The silicon p-n junction cells were obtained from the International Rectifier Co., El Sequndo, California. The number and type of cells used are listed in Table VI. The type S-0520-C and S-1020-C cells are 5 x 20 mm. and 10 x 20 mm. in size respectively. They are rated by the manufacturer at 9 per cent energy conversion efficiency.

The cells are cemented to the flat plates by a special cement made of 30 parts by weight of Armstrong C-1 cement, 12 parts of flexible resin, 20 parts of titanium dioxide, 3 parts of celosolve thinner, and 3 parts of activator. The titanium dioxide pigment assists in controlling the temperature of the solar cells by lowering the ratio of absorptivity to emissivity of the exposed cement areas. Electrical connections to the cells are made from behind the mounting plates. They are wired in series-parallel combinations to provide the proper battery charging voltages and capacities. Type 1N697 diodes are inserted between the solar and chemical batteries to prevent reverse currents when the

Table VI

Tabulation of Solar Cells by Type and Location

Plate Location	Number of Plates	Total Number of Cells Type S-0520-C	Type S-1020-C
Bottom	1	68	152
Top	1	68	152
Left Side	4	212	216
Right Side	4	12	304
TOTALS		360	824

solar cells are illuminated at a large angle of incidence, at which time both their terminal voltages and internal resistances are low. The locations of the diodes were chosen to assist in dynamically balancing the payload for spin about its longitudinal axis.

To prevent damage to the cells by high corpuscular radiation fluxes, 0.15 mm. thick plates of glass obtained by SUI from the Optical Coating Laboratory, Santa Rosa, California, were installed over each solar cell. Nine by 22 mm. and 9 x 23 mm. plates cover the larger cells, and 4 x 22 mm. and 4 x 23 mm. plates are installed over the smaller cells. These plates are coated on the outside surface with a magnesium fluoride low reflecting coating to reduce the energy loss by reflection of sunlight, and on the inside with an ultraviolet absorbing (λ = 0.435 to 0.465 micron) coating. The plates absorb about 12 per cent of the sun's energy in the range of wavelengths to which the solar cells are sensitive. The plates are cemented in place over the individual solar cells by applying a small quantity of the cement specified above to the ends of the plates. Considerable care was exercised to prevent

the cement from running between the cells and plates.

2. Chemical Batteries.

The chemical batteries are alkaline nickel-cadmium batteries obtained from the Alkaline Battery Division, Gulton Industries, Inc., Metuchen, New Jersey. The cell configuration is indicated in Table VII. The hermetically sealed cells are assembled into cylindrical batteries by the manufacturer. Three type 4VO-.500 batteries, containing four type VO-.500 cells each, form the transmitter battery. The other two supplies are single 5VO-.500 and 8VO-.180 batteries, consisting of five VO-.500 cells and eight VO-.180 cells respectively.

It can be seen from Tables V and VII that the operating lifetimes for the 6.5, 10.4, and 15.6 batteries in the absence of solar cell recharging are approximately 17.7, 18.0, and 8.1 hours respectively.

3. Power Control System.

Power from the three batteries is applied to the instrumentation through the contacts of two Filtor, Inc., type P26A1P6A 28 volt relays. Seven leads were passed from the payload, across the antenna gap (see

Table VII

S-46 Payload Chemical Battery Configuration

Supply	Cell Type	Cell Capacity (mah.)	Total Number of Cells	Nominal Battery Voltage	
				Discharge	Charge
Transmitter	VO-.500	500	12	14.4	16.8
Telemetry System	VO-.180	180	8	9.6	11.2
SUI Instrumentation	VO-.500	500	5	6.0	7.0

section IV G4), through a rotating commutator in the high speed rocket assembly, through the missile, to the blockhouse during the launch operation to permit the use of external batteries for payload operation and the monitoring of several functions in the payload. The functions of the seven leads were:

a. Payload, battery, and relay coil common connection.

b. Transfer relay actuation. Twenty-eight volts was applied to this lead to actuate the two relays, which transfered the instrumentation from internal to external power.

c. Three leads carry external 6.5, 10.4, and 15.6 volt power.

d. External power "on" indication, obtained from a transfer relay contact.

e. Indication of timer zero.

A cut-off timer was included to turn the power to the transmitter off after an operating lifetime of one year $\pm$ 10 per cent. This timer is a Bulova type 116001 electro-mechanical device which is powered by an internally contained mercury cell. When the preset time interval elapses a timer contact is closed which

actuates the turn-off relay. This relay is a Sigma type 93295 polarized latching relay in which momentary application of coil power from the 15.6 volt supply by the timer contact permanently opens a contact. This contact disconnects the transmitter from its 15.6 volt supply, thereby terminating its operation.

To turn the instrumentation on and off during laboratory testing, a nine pin turn-on socket was provided on the side wall of the antenna gap. Power is applied to the payload instruments from the internal power supply by inserting a jumper plug. Alternatively, a laboratory power supply cable can be connected to this socket to provide external power for payload testing.

I. Physical Structure.

The detailed design of the payload structure with the exception of the SUI instrumentation package was accomplished by ABMA. The basic structure is that of a cylinder which contains the instrumentation column

and on which is mounted the solar cell framework. Figure 12 shows the method of assembly of the instrument column, the antenna gap, and the cylinder.

The antenna gap is made up of laminated fiberglass cloth and phenolic resin (91LD). Strength is obtained by careful molding of the basic shape to avoid the necessity for cutting through the fibers when machining the corners. This material is used because of its high strength and electrical and thermal insulating properties.

The basic payload cylinder is machined from aluminum alloy 6061-J6. The wall thickness is 0.76 mm. thick and the inside diameter is 15.71 cm. The cylinder is lightened by boring a large number of holes in the section which is located inside the solar battery framework.

This solar cell framework which surrounds the lower two-thirds of the main cylinder, consists of various magnesium (grade AZ-31B) structural members and stiffeners to provide a rigid mounting for the solar cell plates. It is designed so that all mechanical resonance frequencies are high to prevent

destructive oscillation of the solar cell plates when excited by the vibration encountered during the rocket launching. The structure is assembled as an integral unit which can be removed from the central cylinder by removing the mounting screws and a single electrical cable connector. The boxlike structure is large enough to serve as a mounting for the necessary aluminum solar battery plates and the aluminum thermal control panels located at the four corners of the box.

The instrument column located inside the main cylinder is supported by the antenna gap at the bottom, a central ring, and another ring at the top. It consists of two main sections, the telemetry and power section at the bottom, and the SUI instrumentation package at the top. The entire column can be removed from the cylinder by removing the upper end plate and the mounting screws and connector plugs at the bottom, and sliding it out the top of the cylinder. The two major instrumentation assemblies can be separated by removing a single electrical connector and six screws. This easy disassembly into major components was found to be highly advantageous because of the resulting

simplification of the working arrangements between the various responsible laboratories. The major units were completely assembled in these laboratories and then brought together for a simple final assembly.

The method of assembly of the battery deck, subcarrier oscillators, electronic commutator, and transmitter within metal stacking rings can be seen in figure 12. All electronic components are mounted on fibreglass circuit boards which are then encapsulated in Emerson and Cumming Company Eccofoam FP to form flat cylindrical modules. These modules are held together by two rods which pass through the stack. They are inter-connected by a wiring harness in the longitudinal wiring channel.

The method of assembly of the SUI instrumentation package can be seen in figures 12, 59, 60, and 61. The electronics components are mounted on fibreglass boards. The completed electronics decks are encapsulated in Eccofoam FP Isocyanate foam mixed in the ratio one cubic centimenter of 12-6 catalyst to ten grams of prepolymer. The detectors are mounted on the top plate of the detector assembly, and are encapsulated in foam in common with the high voltage power supply and pulse shaping

amplifier decks. All high voltage points are coated before encapsulation with epoxy resin in order to provide a seal to prevent arc-over when the completed unit is placed in vacuum. Figure 62 is a photograph of the complete FU-1 detector assembly before encapsulation.

After the modules are encapsulated they are arranged on the stacking rods. Thin (0.3 mm.) insulating disc are placed between modules to eliminate the possibility of shorts between modules. Figure 60 is a photograph of a package (PT-2) which was stacked before encapsulation to show the internal structure of the assembly and to illustrate the rather high component density. Following stacking of the completed modules they are interconnected by a channel wiring harness. The wiring diagram is shown in figure 63, and figure 61 is a photograph of the completed package. The completed SUI instrumentation stack is placed in the thin wall (0.56 mm.) cylindrical aluminum case shown in figure 61. Screwing this case to the base plate places the module stack in compression to minimize mechanical oscillation during vibration.

Mechanical drawings of the parts of the SUI instrumentation package are contained in Appendix I.

A number of practices were adopted to solve the payload thermal control problem. The instrumentation column is thermally isolated as well as possible from the shell so that its temperature remains relatively constant during the occurrence of short term fluctuations in the shell temperature. The instrumentation assumes a temperature somewhat higher than the mean shell temperature due to power dissipation in the instruments. The shell surface temperature, in turn, is determined by the amount of radiant energy incident on it and by the ratio of the mean absorptivity of the satellite surface at visual light wavelengths, to the mean emissivity of the surface at infra-red wavelengths.

To minimize the radiative transfer of heat energy between the instrument column and the main cylinder the facing surfaces are highly polished. Aluminum foil (0.18 mm. thick) is cemented to the bottom section of the main cylinder to prevent radiative transfer between the inside of the solar cell framework and the instrument column through the lightening holes. To minimize the conductive transfer between the column and shell all connecting members are made of materials having low thermal conductivity. The antenna gap on which the

column rests and the central supporting ring are made of fibreglass (91LD and epoxy resin impregnated, respectively), while the upper support ring is made of Kel-F. The time constant for the transfer of heat between the shell and the instrument column was measured by applying a step function temperature change to the shell and measuring the temperature of the instrument column as a function of time.[45] The experiment was performed in vacuum (10^{-5} mm. Hg.) and the temperature step was from -20° C to 80° C. The time constant (time for a rise to within e^{-1} of its final value) was found to be seven hours. The thermal transfer coefficient is therefore 140 calories per hour per degree centigrade.

All externally exposed aluminum surfaces are sandblasted according to specifications developed at ABMA to produce the proper ratio of absorptivity to emissivity. The sandblasted surfaces were protected from contamination until shortly before launching by

---

45. W. C. Snoddy, "Thermal Design and Testing of S-46", ABMA publication DV-TM-15-60 (June 1960).

three coatings of stripable transparent blue liquid envelope number 3253 manufactured by the Better Finishes and Coatings Corp., Newark, New Jersey.

Since the satellite was spun during launch, dynamic balancing of the payload about the longitudinal axis was necessary. This was accomplished in the prototype units by properly locating weights on the top and bottom of the solar battery structure. In the flight units, in order to conserve weight, the solar battery diodes located inside the solar battery framework and the choke coils located in the antenna gap were positioned to balance the payload. The positions of the weights were chosen so that the perpendicular distance from the center of gravity of the payload to the nominal axis of rotation did not exceed 0.5 mm.

Due to the severe limitation on total weight of the payload all parts were made as light as possible. The building of a payload unit having the degree of complexity of the S-46 unit within the weight allowance of only 10.22 kgm. is considered a rather remarkable achievement. A detailed outline of the sub assembly weights is contained in Table VIII.

Table VIII

Breakdown of S-46 Payload Weight (FU-2)

Assembly	Mass (gm.)	Subtotals (kgm.)
A. Instrument Column		
1. SUI Instrument Package		2.895
a. Detector assy, consisting of:	1702.0	
Power supply deck A (153.2 gm)		
Amplifier deck B (53.0 gm)		
CdS detector A (229.0 gm)		
CdS detector B (200.1 gm)		
Spectrometer assy (589.0 gm)		
213 counter assembly, det E (43.1 gm)		
Hardware and structure (138.2 gm)		
Encapsulant, coatings (296.4 gm)		
b. Scaler deck C (49.5 gm. foam)	139.8	
c. Scaler deck D (49.5 gm. foam)	139.1	
d. Scaler deck E (38.5 gm. foam)	169.9	
e. Scaler deck F (44.0 gm. foam)	157.8	
f. Scaler deck G (38.5 gm. foam)	169.9	
g. Case (235), Base plate (128), and Hardware (53.2)	416.2	

Table VIII (continued)

Assembly	Mass (gm.)	Subtotals (kgm.)
2. Telemetry Package		1.232
a. Transmitter deck	484.7	
b. Electronic commutator deck	154.0	
c. Subcarrier oscillator deck A	235.6	
d. Subcarrier oscillator deck B	217.4	
e. Rod assy, Hardware	81.5	
f. Spacers	58.9	
3. Chemical Battery Pack		1.391
B. Solar Battery Assembly, Complete		3.230
C. Main Cylinder, Cover, Spacers		1.373
D. Adapter Ring, Misc.		0.099
Total		10.220

V. TESTING

A comprehensive set of tests was performed on the satellite S-46 payloads to give maximum assurance of a low probability for electrical or mechanical failure during the launch operation and in orbit. In general, the probability of failure of a piece of electronics instrumentation rises exponentially as the number of components increases. There are 255 transistors in the S-46 instrumentation. Thus, the probability for the failure of individual electronic components must be very low. As for the mechanical structure, making the parts unnecessarily large to provide a large strength safety factor was not permissible in this case because of the severe weight limitation. Therefore it was necessary to employ an extensive structural testing program in order to obtain a trustworthy estimate of the probability of failure.

The testing program followed in the S-46 program can be divided into four major divisions:

A. Testing of Individual Components.

Individual electronic components (and structural elements in some cases) were carefully checked both mechanically and electrically before insertion into the circuits. At SUI most components were tested, aged, and retested. The aging process was accelerated by placing them in an oven at a temperature of 120° C for a period of approximately 15 days. It was required that the parameters of the components not change excessively during the aging period. An outline of the component test procedures and specifications is contained in Appendix II A for the SUI instrumentation. A parallel, but not necessarily identical, testing program was also followed at ABMA for the components used in the telemetry and power systems.

B. Testing of Modules Before Encapsulation.

An extensive series of tests was employed at SUI following assembly of the electronics circuits to insure that the electrical design had been sufficiently conservative to allow for changes in component parameters under various operating conditions, to

select critical components where necessary to assure reliable operation, and to discover components which were functioning abnormally. Individual module performance was recorded at this time for future reference and for comparison with later readings. Each solder joint was visually inspected under a microscope to detect improperly soldered connections and the modules were mechanically inspected by an ABMA inspector. Following these tests and inspections, the modules were encapsulated.

As in the previous section, a parallel testing program on the telemetry modules and power supplies was followed at ABMA. The SUI program is outlined in Appendix II B.

C. Subassembly Testing.

Following assembly of the SUI instrumentation package by stacking and wiring the modules, the package was subjected to a series of electrical and mechanical tests and detector calibrations. The primary purpose of the tests was to ascertain that the completed package was a reliable and fully operational unit before it was delivered to ABMA. The calibrations

were made to gain as complete an understanding of the detector characteristics as possible. This was the last complete set of tests performed on the SUI instruments by the builders. Although an SUI representative was present at ABMA during the conduct of the payload assembly and environmental testing program there, freedom to work on the SUI instruments was necessarily curtailed at the time they were delivered to ABMA. Access was, of course, assured in the event of failure or suspicion of abnormality and for final payload calibration at the launch site.

An outline of the SUI package testing program is contained in Appendix II C. In general, an analogous program was not carried out at ABMA at this point in the program, but was accomplished during the payload testing program discussed in the next section. The environmental tests performed at SUI included vibration, temperature, and vacuum, these conditions being by far the most stringent.

Several abnormalities occurred at SUI during this testing program. They were:

1. PT-1, vibration test in thrust direction at 25 g. RMS; channel three counting rate equal to

zero after test; failure of G.M. counter; counter replaced.

2. PT-2, vibration test perpendicular to thrust direction and to spectrometer counter axis at 15 g. RMS; channel four counting rate equal to zero after test; breakage of G.M. counter center wire; counter replaced.

3. PT-3, vibration test; change in channel one rate; dirt particle in detector A aperture; dislodged.

4. PT-3, vacuum test; arc-over of 700 volt power supply; incomplete bonding of foam to circuit components; not repaired since unit was to be used for thermal constant measurement; 700 volt system in all other units coated with epoxy resin to obtain more complete seal.

5. FU-1, vacuum test; arc-over of 700 volt power supply; incomplete bonding of epoxy resin; repaired.

The specifications for these SUI tests were in many cases more severe than the specifications established by ABMA. Although this may have been unnecessary, it is interesting to consider the small number of abnormalities which developed after

the SUI packages left our laboratory. There were no failures of the flight unit packages which required cutting into the foam for repair. The abnormalities are listed in section V D below.

D. Testing of the Complete Payload at ABMA.

The completely assembled payloads were given a series of mechanical, electrical, and R.F. tests at ABMA. These tests fall into two main groups; the prototype approval tests performed on PL-1, PL-2, and PL-3, and the flight acceptance tests performed on the flight units PL-4 and PL-5.

The prototype approval test is designed to assure that the newly developed configuration operates as an integral unit exactly as planned and that it possesses sufficient strength to survive the conditions imposed at the time of launch and in orbit. The test levels are set at a sufficiently high level to encompass variations in the encountered environmental conditions and to allow for variations in the strengths of the individual payloads. On the basis of these tests approval or rejection of the

design and/or the need for modification is decided. After being subjected to this series of tests, a unit is usually considered not suitable for flight because of the possibility that the structure may have been weakened by the tests.

The flight acceptance tests are performed on each potential flight unit to assist in determining the operating characteristics of the completed units and to test for mechanical integrity of the completely assembled payloads. On the basis of these tests a unit is either accepted or rejected for flight. In addition, information gained during these tests often assists in the selection of the preferred flight unit from the group of possible flight payloads.

A complete outline of both sets of payload test specifications is contained in Appendix II D.

It is felt that the SUI reliability program achieved its objectives, as evidenced by the small number of failures incurred during the ABMA testing program, and by the fact that the instrumentation operated properly during its launch trajectory.

A complete list of all abnormalities which developed in the SUI assembly during the ABMA testing is as follows. Several failures also occurred in the ABMA components, but no listing of these failures is included herein.

1. PT-2, preliminary testing; intermittent high channel three switching rate; improper quenching of detector C G.M. counter; new detector C and D G.M. counters installed at SUI.

2. PT-2, temperature-vacuum soak test; change in 700 volt power supply regulator current after six hours at 50° C; failure of transistor in power supply; transistors and bias resistor changed.

3. PT-2, temperature-vacuum soak test; intermittent change by a factor of two in the channel three switching rate after 12 hours at 50° C and 12 hours at 0° C, on way to room temperature; failure of transistor in scaler stage four; transistor changed at SUI after completion of tests.

4. PT-2, temperature-vacuum soak test; slow drift in channel five output voltage after about five days at 50° C; change in characteristics of

2N338 transistor in output amplifier; transistor changed at SUI after completion of tests.

5. PT-2, temperature-vacuum soak test; SUI temperature measurement inoperative; open circuit in thermistor; not changed.

6. FU-1, vibration test; change in channel two rate; dirt particle in detector B aperture; removed.

7. FU-2, vibration test; change in channel one rate; paint chip in detector A aperture; removed.

8. FU-2, temperature-vacuum calibration; inability to ground the channel one integrating circuit capacitor through the TS shorting plug; open circuit between wiring channel and test socket; capacitor grounded by soldered jumper in wiring channel during Cape Canaveral checkout.

VI. PAYLOAD CALIBRATIONS

The detectors and electronic circuits in the SUI flight instrumentation packages were fully calibrated before delivery to ABMA for environmental testing. The critical individual components were calibrated before assembly of the modules, and the packages were calibrated as complete, fully operating systems. Table IX identifies the components selected for the various payloads. The detector A, B, C, and D calibrations were made by their respective designers, and will be published by them. The detector E G.M. counter calibrations were made by Messrs. J. A. Van Allen and L. A. Frank and are outlined as follows:

1. G.M. counter plateau measurement. The counting rate for a fixed Co^{60} source distance as a function of the applied voltage was measured for several temperatures. The results are shown in figures 64 and 65 for the counters used in FU-1 and FU-2 respectively. These curves can be used in conjunction with those of figures 25 and 26 to

Table IX

Identification of Critical Components

Description	PT-1	PT-2	PT-3	FU-1	FU-2
Det. A CdS crystal	CL-2/94	CL-2P/63	CL-2P/65	CL-2/131	CL-2/132
Det. A neon bulb	NE=76/42	NE-76/41	NE-76/35	NE-76/56	NE-81/43
Det. B CdS crystal	CL-2/88	CL-2P/66	CL-2P/71	CL-2/102	CL-2/130
Det. B neon bulb	NE-76/39	NE-76/37	NE-76/36	NE-81/5	NE-81/1
Spectrometer assembly	3	2	1	4	6
Det. C G.M. counter	223/18490	223/18092	223/4491	223/17743	223/18094
Det. D G.M. counter	223/18015	223/18163	223/4635	223/18540	223/15415
Det. E assembly	-	-	-	8	10
Det. E G.M. counter	302/055	302/V316	302/N845	302/X538	213/21013
700 V. regulator tube	GV3B-690S/62	GV3B-690/20	GV3B-690/24	GV3B-690/11-8	VXR-700S/11-6
160 V. regulator diode	RCA-125/14	RCA-125/12	SV-18 and SV-24	1N1327/-	1N1327/6
SUI thermistor	11/004	11/009	11/001	11/006	11/012

determine the counting rate dependence on temperature. To obtain these measurements the counters were operated in electronic circuits identical to those used in the satellite instruments.

2. Apparent vs. true counting rate. When operated in high radiation fluxes, the observed or apparent counting rate in a G.M. counter is no longer proportional to the incident flux. Figure 66 shows the relationships, for the FU-1 and FU-2 counters, between the apparent counting rates and the true counting rates, which are defined as the rates which would be obtained from counters identical to the ones in use in every respect, except that they have zero dead times. The curves were obtained by placing the payloads at various distances from an X-ray source and using the inverse square relationship between X-ray intensity and distance to compute the relative intensities. By making a series of runs with different source intensities it was possible to plot the entire curves shown.

It is interesting to note that, in obtaining the data for the 213 counter in FU-2, such high

X-ray intensities were employed in an effort to extend the curve of figure 66 as high as possible that some radiation damage to the high voltage power supply diodes resulted. It was manifested by a reduction in regulator tube current, signifying an increase in diode reverse leakage current. The power supply made a rapid (overnight) partial recovery and returned to completely normal operation after about two weeks.

3. Determination of absolute geometric factor. The geometric factor of each flight G.M. counter was determined relative to a similar reference counter by a standard source - standard distance (SSSD) Co^{60} gamma measurement. The geometric factor of the reference counter was, in turn, determined relative to a large counter in a cosmic ray telescope. The physical geometry of the large counter was determined by measurements of its effective length and diameter and by determination of its cosmic ray counting efficiency. This indirect approach was necessary because the flight counters were so small that their dimensions and efficiencies could not be directly measured with the necessary accuracy.

Standard source - standard distance measurements were also made periodically during the construction and testing of the payloads to ascertain that no changes occurred in the G.M. counter operation.

4. Determination of angular dependence of the absolute geometric factors. The detailed geometry of the very small counters used for the study of the high intensity radiation is not well defined due to the fact that the shape of the effective volume is not simple. Therefore the angular dependence of the absolute geometric factor was determined experimentally by orienting the counters at different angles to a Co^{60} source (at a fixed distance).

5. Determination of absolute electron sensitivity. When the payload is located in regions in which there are energetic electrons, the electrons are detected primarily by a low efficiency secondary process in which they strike the shell of the satellite, bremsstrahlung is produced in the material of the shell, and these X-rays are detected by the G.M. counters. The similar production of bremsstrahlung at the target of an X-ray tube provides

a means for establishing the relationship between the incident electron flux and the payload counting rates. A complete set of laboratory X-ray runs was made using a large range of accelerating potential to determine the detecting process efficiency as a function of incident electron energy.

Several other elements of the payloads required calibration. The effects of changes in temperature and supply voltage on the operation of the SUI instrumentation have been discussed in Chapter IV. Similar calibrations were made of the telemetry system by ABMA. In particular the characteristics of the temperature measuring telemetry channels were determined. The results of these calibrations are shown in figures 67 and 68, which show the subcarrier oscillator frequency as a function of Tabor surface and SUI thermistor temperature respectively for FU-2. The subcarrier oscillator frequency is a weak function of the temperature of the oscillator circuit. But it is within 0.1 per cent of the room temperature value at all circuit operating temperatures.

VII. OPERATION DURING FLIGHT AND CONCLUSIONS

A. Operation During Flight.

The S-46 payload failed to achieve an orbit due to failure of the high speed rocket cluster. A conclusive determination of the exact reason for failure was not possible in spite of the fact that a complete analysis of all available launch records was made.[46] Booster rocket performance was normal and the instrument section and high speed stages were in the proper position at the time of second stage ignition. There is evidence that the velocity increments of the high speed stages were low and that there were angular deviations of all three stages.

Payload telemetry signals were received at several stations during the launch operation. The best and most complete record was made by the STL

---

46. C. R. Fulmer, H. F. Kurtz, and J. P. Lindberg, "Preliminary Aeroballistics Evaluation of Jupiter Test Flight AM-19C(U)," ABMA publication DA-TM-33-60 (2 May 1960) (confidential).

Microlock receiving station at Cape Canaveral. This record extends from the time of lift off until nearly one minute after programmed injection (total time, 9.3 minutes). Following the firing of the high speed stages, the signal began a slow fade at about 1343:50 (U.T.), a more rapid fade at 1344:15, and was below telemetry threshold at 1344:31. No other stations received the signal after this time. Table X lists the times of occurrence of the various operations in the launch sequence.

The only payload instrumentation abnormality was the loss of the Tabor surface temperature measurement soon after the shroud was installed in place over the payload during the prelaunch countdown, apparently due to an open circuit in the thermistor or its wiring. It was decided to launch the payload without this measurement after it was ascertained that the abnormality was not a symptom of the failure of some other component (for example a commutator gate) which could have resulted in invalidation of a portion of the primary data.

The operation of all radiation measuring

Table X

Launch Sequence

Function	Time (U.T.)
Lift off	1335:11.2
Beginning of cluster tilt program	1338:41
Shroud ejection	1338:45
Completion of cluster tilt program	1339:30
Second stage ignition	1343:09.1
Third stage ignition	1343:18.6
Fourth stage ignition	1343:28.1
Programmed injection	1343:38
Loss of telemetry	1344:15

instrumentation, telemetry, and power supply systems appears to have been satisfactory for as long as the signal was received. The data received during the launch from detectors A and B are contained in figure 69. The counting rates observed in these detectors are believed to be proper responses to various stimuli. It appears likely that the first increase, occurring between 1338:46.7 and 1338:47.3, or about two seconds after shroud separation, was caused by the burning of the shroud lateral-thrust rocket. This rocket motor, used to push the shroud aside after separation, was programmed to ignite about three seconds after shroud separation and to burn for about one second. Its location at the time of ignition was computed to be about five meters in front of the payload and about 2.4 degrees from the detector axes, or well within their cones of sensitivity. It is also possible that there was some reflection of sunlight from the shroud (and/or some direct light from the sun) incident upon the detectors. At the time of shroud ejection the angle from the

detector axes to the sun was thirteen degrees and increasing at the rate of 0.67 degree per second. The detector counting rates at sun angles of 15, 20, and 25 degrees were of the order of 0.1, 0.07, and 0.01 counts per second respectively on the basis of the pre-launch calibrations.

There is no obvious explanation for the small increase occurring at 1339:10.

The large increase beginning at 1339:27.1 was probably caused by light from the earth (reflection of sunlight from the sea and from clouds). The angle between the detector axes and the line to the horizon at that time was about 8 degrees. At the end of the tilt program three seconds later this angle was about 6 degrees, which would have resulted in a high counting rate. As the cluster continued down-range on its trajectory, with its height continually increasing, the angle between the detector axes and the horizon steadily increased until it reached the value of about 19 degrees at the time of second stage ignition. The detector counting rate curve during this period declines as

the angle increases. This data can, in fact, be used to obtain realistic plots of detector counting rates as a function of axis-to-light angle for the case of a rapidly spinning payload. A rough comparison with the values obtained from the calibration before launch shows moderately good agreement.

The CdS detector counting rates began to increase again at about 1342:55. The slow increase from this time until the abrupt increase at about 1343:09 is difficult to explain, since the rocket instrumentation telemetry indicated that the cluster orientation was maintained constant until the instant of second stage ignition. McIlwain* has hypothesized that it may have been due to ionic impact directly on the crystals. At the time the increase in counting rate began, the angle between the detector axes and the line of cluster motion was a little less than two

---

* C. E. McIlwain, private communication.

degrees and decreasing. The angle to the horizon at that time was nearly 19 degrees and very slowly increasing.

The large, abrupt increase between 1343:08.9 and 1343:09.9 occurs nearly concurrently with the ignition of the second stage. Slightly more than 0.1 second was required for the second stage rocket to leave the launcher, by which its lateral motion was restrained. It is suggested by the writer that the second stage rocket was pitched downward by at least 16 degrees for a short time immediately following ignition. The possibility exists that the increase in counting rate may have been caused by increased ionic bombardment of the crystal, due to increased detector velocity, but it is difficult to explain why the rate should have decreased from its peak value while the rocket was still burning and the cluster speed was still increasing, unless a monotonically increasing cluster precession angle was introduced during burning.

The resolution and accuracy of the data are not good enough to permit a discussion of the

motion during the third stage burning, other than to state that there seems to have been a slight increase in counting rate at the time of ignition, followed by a decrease. At the time of fourth stage ignition, however, there is a rapid increase in both counting rates to steady values which were maintained until the signal was lost. The rates in both detectors agree, within the possible error, with the predicted counting rates if the detectors were directed toward some portion of the sunlit earth. It seems highly likely, then, that the fourth stage rocket and payload were pitched downward by at least 22 degrees from the intended direction of travel. This finding is compatible with the findings of ABMA based on a study of the doppler data from a network of receiving stations.

The geometric factors and scaling factors of the G.M. counters which were chosen in order to study the high intensity radiation were such that little geophysically significant data were obtained from them during the short flight. Two swtiches of the detector C scaler output (scale

of 128) occurred at 1339:36 and 1343:51, corresponding to an average rate of 0.25 $\pm$ 0.03 counts per second. One switch of the detector E scaler output (scale of 128) occurred at 1337:01. Thus, its average rate could not have been greater than 0.14 counts per second during the period 1337:01 to 1344:30. A number of switches of the detector D scaler output (scale of 8) occurred during the launch trajectory. During the period from 1336:12 to loss of signal, this average rate was 0.20 $\pm$ 0.02 counts per second. The differences in the rates of the three G.M. counters were probably due to differences in the effective geometric factors. If we consider the average of the detector C and D counting rates as the rate obtained from a counter having a typical geometric factor, then the average omnidirectional cosmic ray intensity in that part of space traversed between shroud ejection (about 150 km. height) and loss of signal (about 350 km. height) was $J_o \approx 2.0$ cm^{-2} sec^{-1}. This agrees with the values obtained in other experiments within the accuracy of these measurements.

B. Conclusion.

From the foregoing discussion it can be concluded that the operation of the detectors and associated instruments during the brief launch trajectory was normal, and that the telemetry system operated as anticipated. The flight was not long enough to determine whether the power system would have operated properly, but there is no reason for believing it would not. Since the payload did not go high enough to enter the region of high intensity radiation, the suitability of the cadmium sulfide detectors and the electron spectrometer for investigation of the objectives listed in Chapter III was not ascertained experimentally. However, no evidence to the contrary has been discovered. Similar detectors are being prepared for use in other satellite and space payloads.

In spite of the fact that the S-46 payload configuration may never be utilized due to the lack of a backup launching vehicle, it is felt that this program has resulted in a significant advance

in the state of the art of the development of instruments for the investigation of our space environment.

REFERENCES

1. J. A. Van Allen, "The Cosmic Ray Intensity Above the Atmosphere Near the Geomagnetic Pole", Il Nuovo cimento 10, 630 (1953).

2. L. H. Meredith, M. B. Gottlieb, and J. A. Van Allen, "Direct Detection of Soft Radiation Above 50 Kilometers in the Auroral Zone", Phys. Rev. 97, 201 (1955).

3. F. B. McDonald, R. A. Ellis, and M. B. Gottlieb, "Rocket Observations on Soft Radiation at Northern Latitudes", Phys. Rev. 99, 609 (1955) (abstr.).

4. J. A. Van Allen, "Direct Detection of Auroral Radiation with Rocket Equipment", Proc. Natl. Acad. Sci. U.S., 43, 57 (1957).

5. C. E. McIlwain, "Direct Measurement of Radiation Associated with Visible Aurorae", IGY Rocket Report Series No. 1, National Academy of Sciences, 164 (July 1958).

6. C. E. McIlwain, "Direct Measurement of Particles Producing Visible Aurorae", J. Geophys. Research, in press, (1960).

7. G. H. Ludwig, "Cosmic-Ray-Instrumentation in the First U. S. Earth Satellite", Rev. Sci. Instr. 30, 223 (1959).

8. G. H. Ludwig, "The Instrumentation in Earth Satellite 1958 Gamma", M.S. Thesis, State University of Iowa research report 59-3, (February 1959).

9. J. A. Van Allen, G. H. Ludwig, E. C. Ray, and C. E. McIlwain, "Observation of High Intensity Radiation by Satellites 1958 Alpha and Gamma", IGY Bulletin, Trans. Am. Geophys. Union 39, 767 (1958). Also Jet Propulsion 28, 588 (1958).

10. J. A. Van Allen, C. E. McIlwain, and G. H. Ludwig, "Radiation Observations with Satellite 1958 Epsilon", J. Geophys. Research 64, 271 (1959).

11. J. A. Van Allen, C. E. McIlwain, and G. H. Ludwig, "Satellite Observations of Electrons Artificially Injected into the Geomagnetic Field", J. Geophys. Research 64, 877 (1959).

12. S. N. Vernov, N. I. Grigorov, Yu. I. Logachev, and A. Ye. Chudakov, "Artificial Satellite Measurements of Cosmic Radiation", Doklady Akad. Nauk S.S.S.R. 125, 1231 (1958).

13. "Soviet Artificial Earth Satellites - Some of the Results of Scientific Researches on the First Two Artificial Earth Satellites ", Report of IGY Committee of USSR (May 1958).

14. "Annals of the International Geophysical Year", Vol. X, now in preparation, will contain the following papers: V. I. Krassovsky, Y. M. Kushnir, G. A. Bordovsky, G. F. Zakharov, and E. M. Svetlitsky, "A Discovery of Corpuscular Fluxes by Means of the Third Sputnik"; S. N. Vernov, A. Ye. Chudakov, E. V. Gorchakov, Yu. I. Logachev and P.V. Vakulov, "Study of Cosmic-Ray Soft Component by the Third Soviet Earth Satellite "; A. Ye. Chudakov, "A Photon Study on the Third Sputnik".

15. P. J. Coleman, Jr., C. P. Sonett, and A. Rosen, "Ionizing Radiation at Altitudes of 3500 to 36,000 km., Pioneer I", Bull. Am. Phys. Soc., Series II 4, 223 (1959).

16. J. A. Van Allen and L. A. Frank, "Radiation Around the Earth to a Radial Distance of 107,400 Kilometers", Nature 183, 430 (February 1959).

17. S. N. Vernov, A. Ye. Chudakov, P. V. Vakulov, and Yu. I. Logachev, "Study of Terrestrial Corpuscular Radiation and Cosmic Rays During Flight of the Cosmic Rocket", Doklady Akad. Nauk S.S.S.R. 125, 304 (April 1959). (Translation available from U.S. Dept. of Commerce, "Information on Soviet Bloc International Geophysical Cooperation - 1959", PB131632-64 of May 1, 1959, also Soviet Phys. JETP 4, 338 (1959)).

18. J. A. Van Allen and L. A. Frank, "Radiation Measurements to 648,300 km. with Pioneer IV", Nature 184, 219 (1959).

19. G. H. Ludwig and W. A. Whelpley, "Corpuscular Radiation Experiment of Satellite 1959 Iota (Explorer VII)", J. Geophys. Research 65, 1119 (1960).

20. B. J. O'Brien and G. H. Ludwig, "Development of Multiple Radiation Zones on 18 October 1959", J. Geophys. Research, in press (1960).

21. R. L. Arnoldy, R. A. Hoffman, and J. R. Winckler "Observations of the Van Allen Radiation Regions during August and September 1959, Part 1", J. Geophys. Research 65, 1361 (1960).

22. J. A. Van Allen and W. C. Lin, "Outer Radiation Belt and Solar Proton Observations with Explorer VII during March-April 1960", J. Geophys. Research (in press).

23. R. L. Arnoldy, R. A. Hoffman, and J. R. Winckler, "Solar Cosmic Rays and Soft Radiation Observed at 5,000,000 km. from Earth", J. Geophys. Research (in press).

24. C. Y. Fan, P. Meyer, and J. A. Simpson, "Preliminary Results from the Space Probe Pioneer V", J. Geophys. Research 65, 1862 (1960) (ltr.).

25. For a brief survey of our knowledge of the trapped radiation as of June 1959 see J. A. Van Allen, "The Geomagnetically-Trapped Corpuscular Radiation", J. Geophys. Research 64, 1683 (1959).

26. B. B. Greever, "General Description and Design of the Configuration of the Juno I and II Launching Vehicles," IRE Trans. on Military Electronics, (April-July 1960) (in press).

27. "Structures and Mechanics Laboratory Model Description of Juno AM-19C," Army Ballistic Missile Agency, Structures and Mechanics Laboratory, (19 February 1959), unpublished (secret).

28. R. J. Davis, F. L. Whipple, and J. B. Zirker, "The Orbit of a Small Earth Satellite," Chapter 1 of "Scientific Uses of Earth Satellites" (University of Michigan Press, Ann Arbor, 1958, 2nd ed.)

29. R. J. Naumann, "Orientation of Explorer VII (AM 19-A)," ABMA report number DV-TN-13-60 (20 June 1960).

30. R. J. Naumann, "Recent Information Gained from Satellite Orientation Measurement," paper presented at the 4th Symposium on Ballistic Missiles and Space Technology at UCLA, Los Angeles, Calif., 24-27 August 1959, mimeograph copies available from author.

31. R. J. Naumann, "Attitude Determination of Explorer IV," ABMA internal report number DV-TN-19-59 (12 June 1959).

32. R. J. Naumann, "Tumble Rate Investigation for AM-19A," ABMA report number DV-TN-28-59 (30 October 1959).

33. R. J. Naumann, "The Effect of Lunar and Solar Perturbations on the Perigee Height of a High Eccentricity Satellite (AM-19C)", ABMA internal report number DV-TN-5-60 (4 March 1960).

34. "Reference Data for Radio Engineers" edited by H. P. Westman (American Book Stratford Press, Inc., New York, 1956) 4th ed., pp. 750-769.

35. H. P. Peake, "Some Basic Considerations of Telemetry System Design", NASA Technical Note D-355 (June, 1960).

36. J. J. Loferski and P. Rappaport, "The Effect of Radiation on Silicon Solar-Energy Converters", R.C.A. Review XIX, 536-554 (1958).

37. D. A. Premo, "Request for Data Acquisition Service Project S-46", NASA internal memorandum, (15 February 1960).

38. Li Chih-Tsien, Physics Abstracts 63, No. 745, p. 605 (Abstr).

39. W. R. Arnold, "A 500-Kilovolt Linear Accelerator Using Selenium Rectifiers", Rev. Sci. Instr. 21, 796 (1950).

40. Von A Bouwers and A. Kuntke, "Ein Generator fur drei Millionen Volt Gleichspannung", Z. technische Physik 8, 27 (1937).

41. C. E. McIlwain, "Scintillation Counters in Rockets and Satellites", SUI Research Report 60-4 (February, 1960).

42. C. S. Josias, "Radiation Instrumentation Electronics for the Pioneer III and IV Space Probes", Proc. IRE 48, 735 (1960).

43. O. B. King, "Multiplexing Techniques for Satellite Applications", Electronics 32, No. 44, p. 58 (Oct. 1959).

44. A. J. Fisher, W. R. Talbert, and W. R. Chittenden, "Telemetry Transmitter for Radiation Satellite", Electronics 33, No. 19, p. 68 (May 1960).

45. W. C. Snoddy, "Thermal Design and Testing of S-46", ABMA publication DV-TM-15-60 (June 1960).

46. C. R. Fulmer, H. F. Kurtz, and J. P. Lindberg, "Preliminary Aeroballistics Evaluation of Jupiter Test Flight AM-19C (U)", ABMA publication DA-TM-33-60 (2 May 1960) (confidential).

FIGURE CAPTIONS

Figure No.

1. A comparative plot of the intensity data of Pioneers III and IV on the same scale of radial distances but ignoring differences of latitude and longitude. (Courtesy of J. A. Van Allen.)

2. Satellite motion about its center of mass for $\frac{I_{init.}}{I_{trans.}} < 1$.

3. The spin decay of Explorer IV. (Courtesy of R. J. Naumann, ABMA.)

4. The opening angle (α) as a function of time for Explorer IV. (Courtesy of R. J. Naumann, ABMA.)

5. Predicted opening angle (α) as a function of time for Explorer VII with fourth stage motor attached. (Courtesy of R. J. Naumann, ABMA.)

6. Predicted percentage of time in sunlight as a function of time for the S-46 payload, computed for launches at 1212:57 and 1412:57 universal time (0800 and 1000 local sun times at the point of injection). (Courtesy of G. Heller, ABMA.)

7. Approximate projection of the initial S-46 orbit onto the plane of the ecliptic, showing the alignment of the spin axis with respect to the satellite-sun line for a launch at 1334 U.T., 23 March 1960.

FIGURE CAPTIONS (continued)

Figure No.

8. Predicted angle between spin axis and earth-sun line (β) as a function of time for the S-46 payload for launch times at 1212:57 and 1412:57 universal time (0800 and 1000 local sun times at the point of injection. (Courtesy of G. Heller, ABMA.)

9. Block diagram of the S-46 instrumentation.

10. Signal-to-noise power ratio for the S-46 system under the most severe conditions as a function of transmitter power for several receiver bandwidths.

11. Satellite S-46 outline drawing.

12. Assembly drawing of the S-46 payload column.

13. Photograph of the satellite S-46 payload assembly. (Courtesy of H. Kampmeier, ABMA.)

14. Cadmium sulfide detector relaxation characteristics for discontinuous changes in light illumination.

15. Photograph of the cadmium sulfide detector assembly.

16. Assembly drawing of cadmium sulfide detector A. (Courtesy of J. W. Freeman.)

FIGURE CAPTIONS (continued)

Figure No.

17. Assembly drawing of cadmium sulfide detector B. (Courtesy of J. W. Freeman.)

18. Schematic diagram of the detector circuits and pulse shaping amplifiers, Deck B.

19. Relaxation oscillator characteristics. Pulse rate as a function of crystal current at room temperature. (Courtesy of J. W. Freeman.)

20. Photograph of the electron spectrometer assembly.

21. Assembly drawing of the electron spectrometer assembly. (Courtesy of C. D. Laughlin.)

22. Schematic diagram of the 160 and 700 volt power supplies, deck A.

23. Top view photograph of the power supply deck.

24. Bottom view photograph of the power supply deck.

25. Type GV3B-690 voltage regulator characteristics.

26. Variation of regulator tube current with changes in temperature and input voltage for the 700 volt power supply under no load conditions.

FIGURE CAPTIONS (continued)

Figure No.

27. Type 1N1327 zener diode voltage regulation characteristics.

28. Variation of zener diode current with changes in temperature and input voltage for the 160 volt power supply under no load conditions.

29. Shaping circuit input and output waveforms. (a) Oscilloscope photograph of the pulse train occurring at the cathode of the G.M. counter using an exposure time long enough to include many oscilloscope sweeps. Temp. = 25° C, horiz. scale = 10 microseconds per major division, vert. scale = 1 volt per major division. (b) Oscilloscope photograph of the same pulses as they occur at the shaping circuit output. All conditions are the same as in (a) except vert. scale = 2 volts per major division (c) The pulse envelope of the input pulses occurring in (a).

30. Basic bootstrap amplifier schematic diagram and simplified equivalent circuit.

31. Basic bootstrap amplifier output vs. input voltage, with temperature as a parameter.

32. Basic bootstrap amplifier voltage output dependence on supply voltage, with a constant input voltage.

33. Basic bootstrap amplifier input impedance as a function of input voltage and temperature.

34. Basic bootstrap amplifier output loading characteristics.

FIGURE CAPTIONS (continued)

Figure No.

35. Photograph of the top of the pulse shaping amplifier deck.

36. Pulse shaping circuit output pulse height as a function of input pulse height at room temperature, with V_{cc} = 5.00 volts.

37. Detector E maximum counting rate as a function of temperature.

38. Basic bi-stable multivibrator scaler circuit.

39. Schematic diagram of the channel A and B scalers, logic circuits, and output amplifiers, decks C and D.

40. Schematic diagram of the channel C and E scalers, logic circuits, and output amplifiers, decks E and G.

41. Schematic diagram of the channel D scaler, logic circuit, and output amplifier, and the 5.0 volt regulator, deck F.

42. Photograph of the top of deck G containing the seventeen stage scaler, logic circuit and output amplifier for detector E.

43. Photograph of the bottom of deck G.

44. Low speed scaler minimum supply voltage V_{cc} (min) for proper operation as a function of temperature.

45. Low speed scaler stage operating power as a function of supply voltage at temperatures of -50° C. and + 100° C.

FIGURE CAPTIONS (continued)

Figure No.

46. Scaler maximum counting rates as a function of temperature and supply voltage.

47. Block diagram of the logic and output amplifier circuits.

48. Logic circuit waveforms.

49. Voltage regulation characteristics for the 5.0 volt regulated supply.

50. Output amplifier state one and eight output voltages as a function of temperature and supply voltage.

51. Block diagram of the electronic commutator. (Courtesy of O. B. King, ABMA.)

52. Schematic diagram of the electronic commutator. (Courtesy of O. B. King, ABMA.)

53. Schematic diagram of the subcarrier oscillators. (Courtesy of O. B. King, ABMA.)

54. Subcarrier oscillator frequency vs. input voltage (FU-2, channel 4). (Courtesy of O. B. King, ABMA.)

55. Schematic diagram of the telemetry transmitter. (Courtesy of A. J. Fisher, ABMA.)

56. Schematic diagram of the antenna impedance matching network. (Courtesy of W. Harper, ABMA.)

FIGURE CAPTIONS (continued)

Figure No.

57. Schematic diagram of the external lead isolating inductors. (Courtesy of W. Harper, ABMA.)

58. Power requirements of the SUI instrumentation from the 6.5 volt supply.

59. Assembly drawing of the SUI instrument package.

60. Photograph of the SUI instrument package before encapsulation of individual modules (PT-2).

61. Photograph of the completed SUI package with case removed (FU-1).

62. Photograph of the detector assembly before encapsulation (FU-1).

63. Wiring diagram of the SUI instrumentation.

64. G.M. counter counting rate vs. applied voltage for the type 302 counter used in FU-1.

65. G.M. counter counting rate vs. applied voltage for the type 213 counter used in FU-2.

66. Apparent G.M. counter rates vs. true rates for the FU-1 and FU-2 counters.

67. Channel four subcarrier oscillator frequency as a function of Tabor surface temperature at nominal supply voltage and with the oscillator circuit at room temperature. (Courtesy of H. Kampmeier, ABMA.)

FIGURE CAPTIONS (continued)

Figure No.

68. Channel four subcarrier oscillator frequency as a function of SUI thermistor temperature at nominal supply voltage and with the oscillator circuit at room temperature. (Courtesy of H. Kampmeier, ABMA.)

69. Detector A and B launch data.

70. Output waveform of the integrator circuit. This is the subcarrier oscillator input, and the output of the ground discriminator in the absence of receiver noise. The waveform is shown for a steadily increasing channel G scaler input pulse rate, beginning at one pulse per second and ending at 40,000 pulses per second.

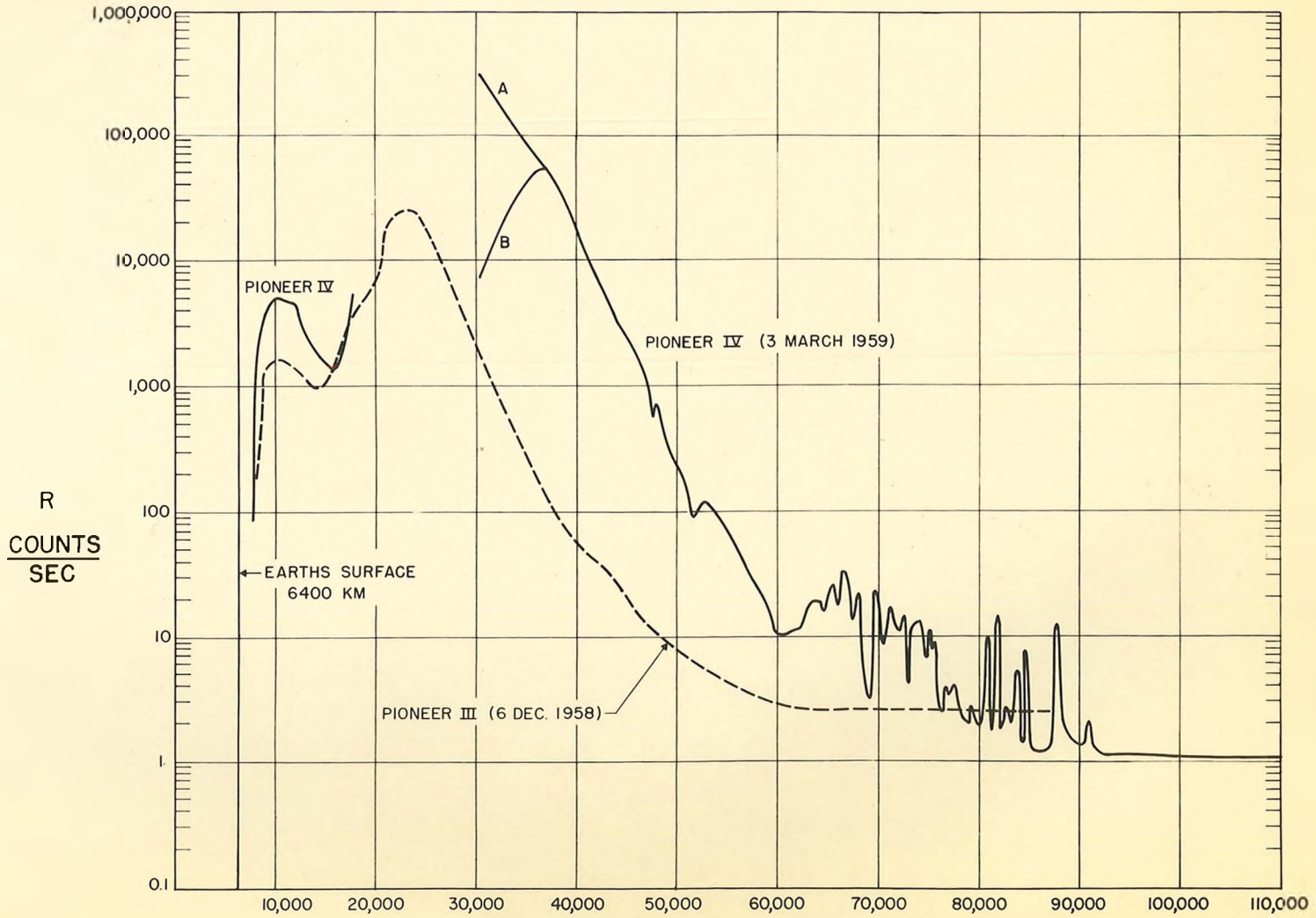
1,000,000
100,000
10,000
1,000
100
10
1
0.1
R
COUNTS
SEC
A
B
PIONEER IV
PIONEER IV (3 MARCH 1959)
EARTHS SURFACE
6400 KM
PIONEER III (6 DEC. 1958)
10,000
20,000
30,000
40,000
50,000
60,000
70,000
80,000
90,000
100,000
110,000
RADIAL DISTANCE FROM CENTER OF EARTH - KM

Fig. 1

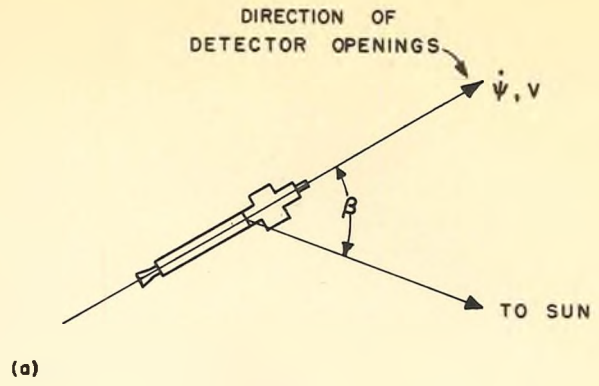

(a)

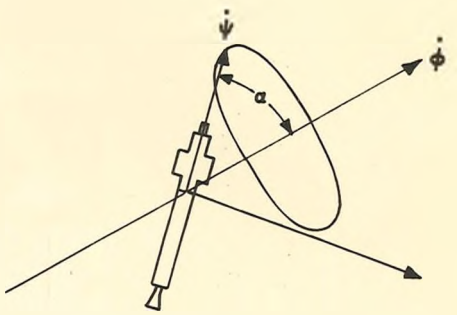

(b)

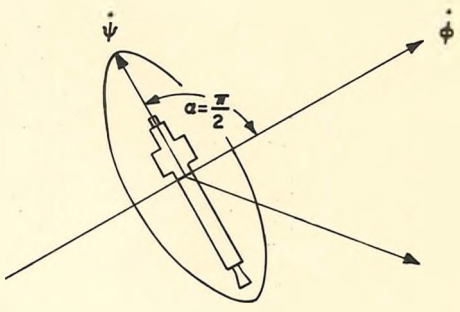

(c)

SATELLITE SPIN MOTION

Fig. 2

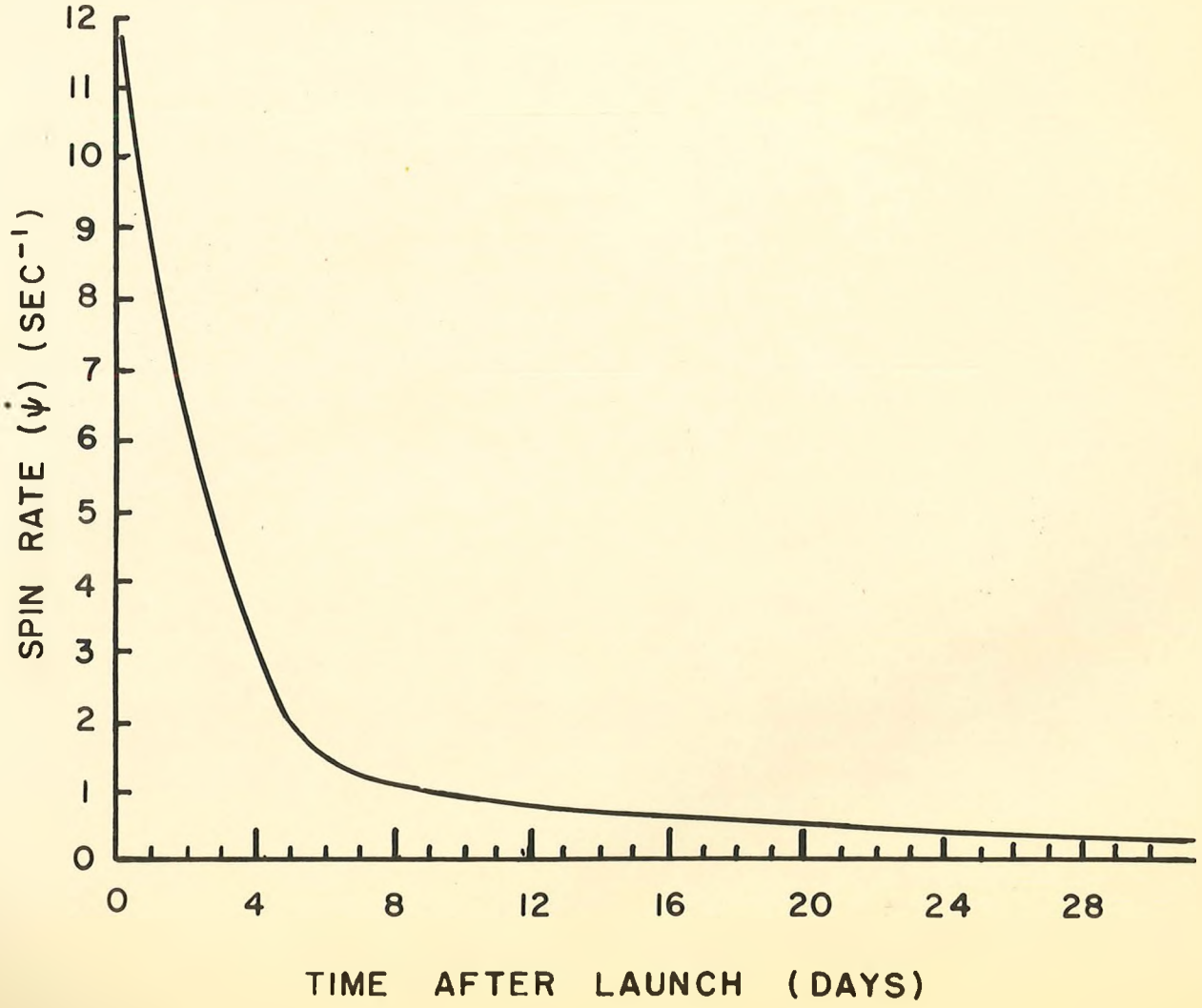

SPIN DECAY OF EXPLORER IV

Fig. 3

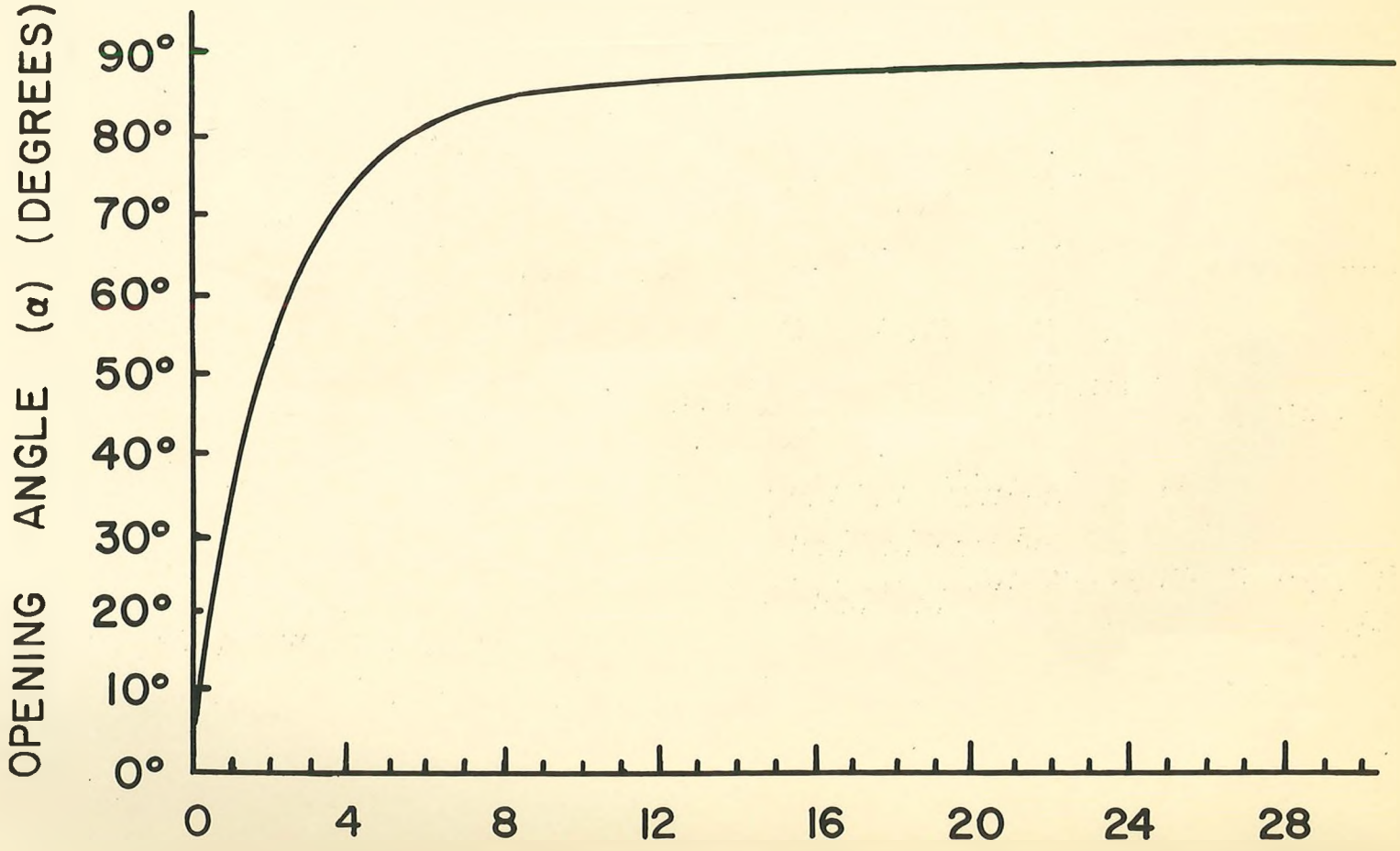

OPENING ANGLE OF EXPLORER IV

Fig. 4

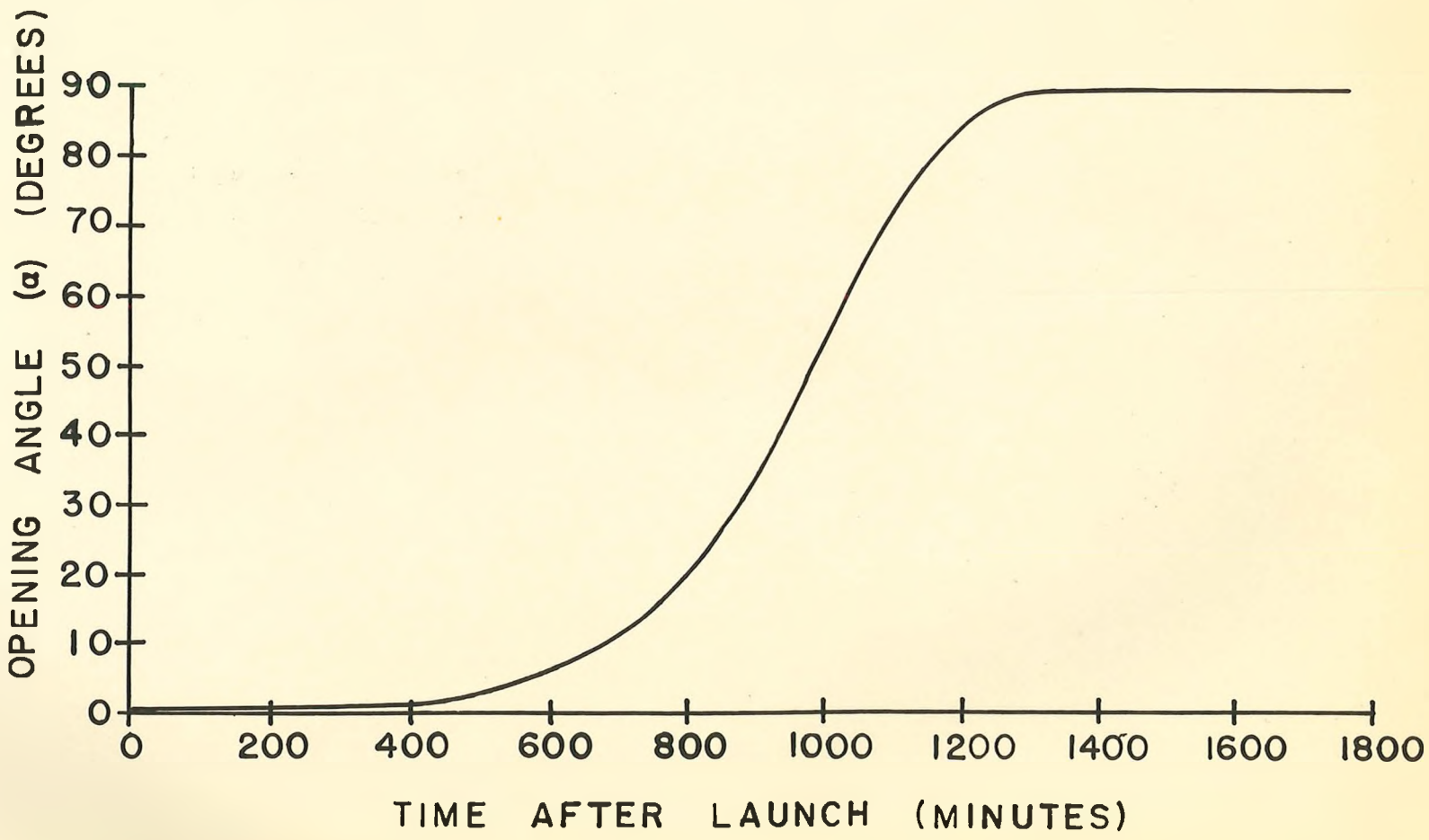

PREDICTED OPENING ANGLE OF EXPLORER VII WITH 4TH STAGE MOTOR ATTACHED

Fig. 5

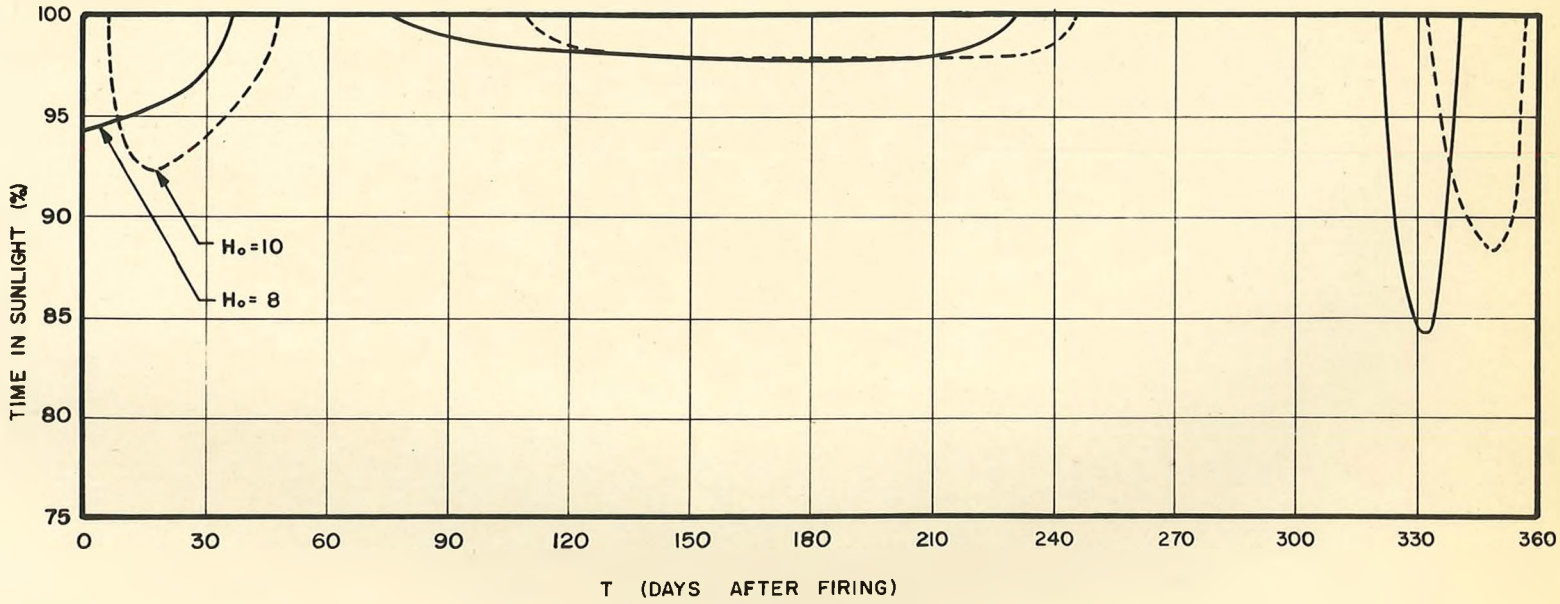

PERCENTAGE OF TIME IN SUNLIGHT

Fig. 6

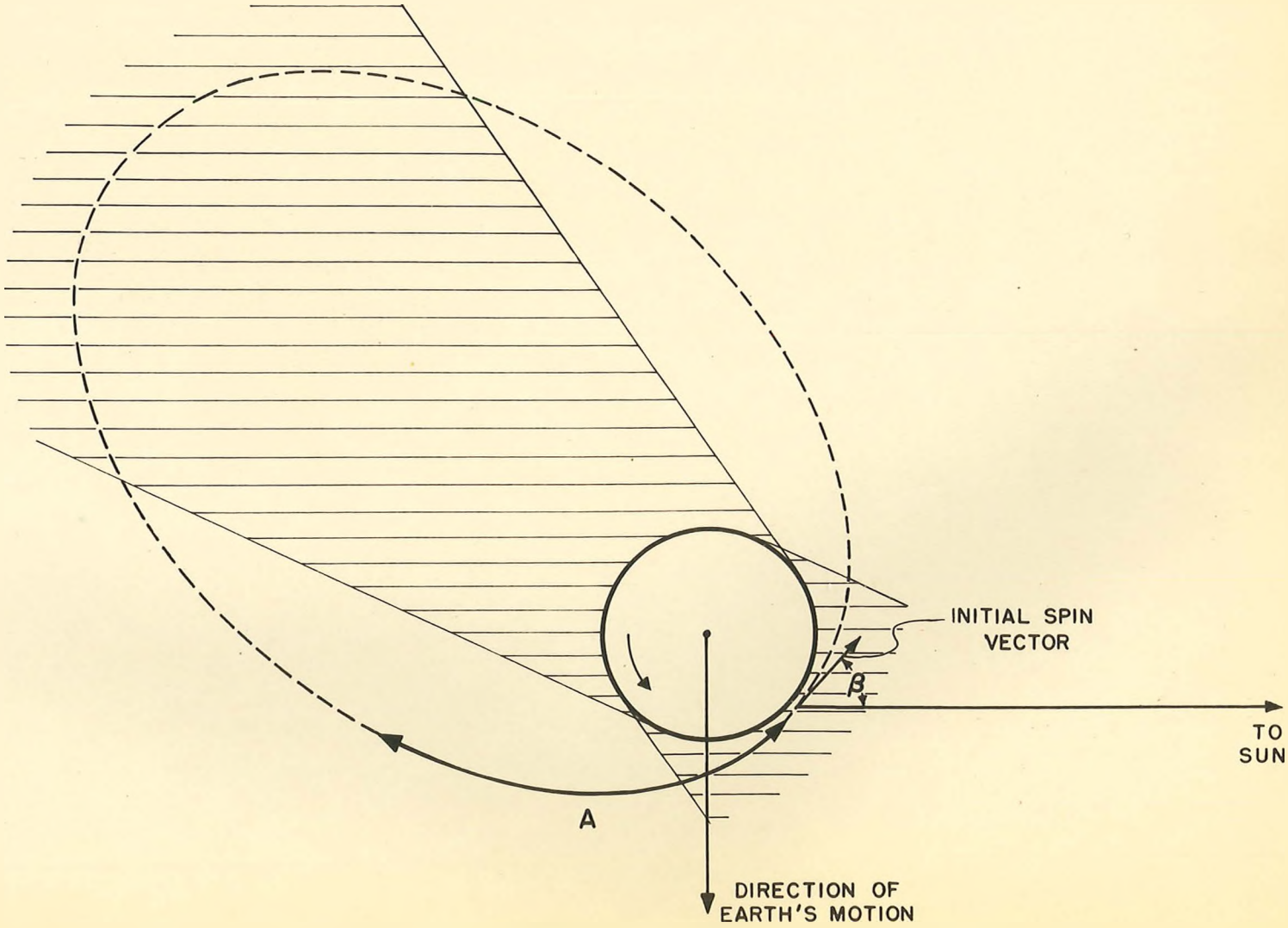

Fig. 7 ALIGNMENT OF SPIN AXIS FOR 1334 U.T. LAUNCH TIME

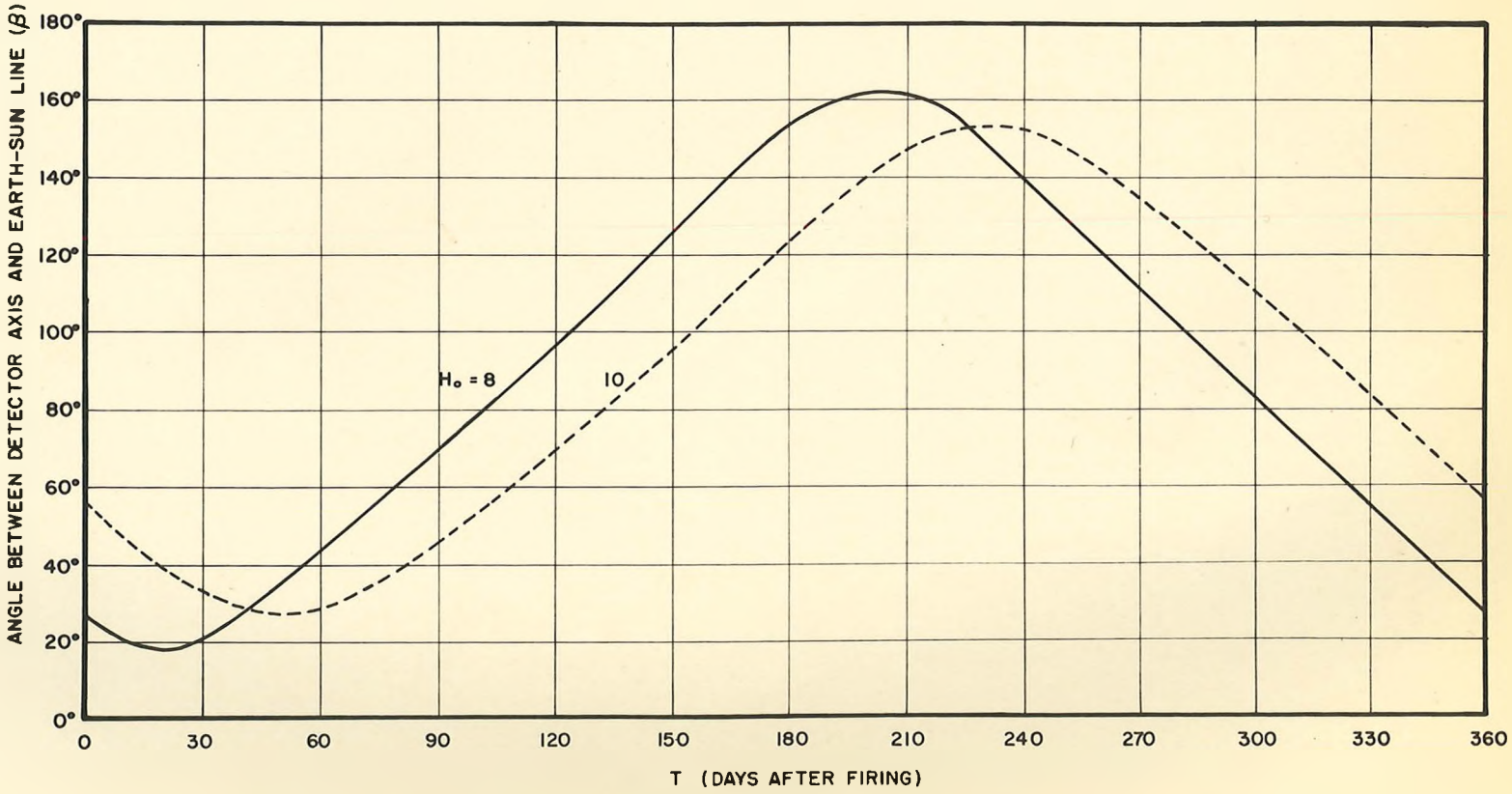

ANGLE BETWEEN DETECTOR AXIS AND EARTH-SUN LINE AS A FUNCTION OF TIME AFTER LAUNCH

Fig. 8

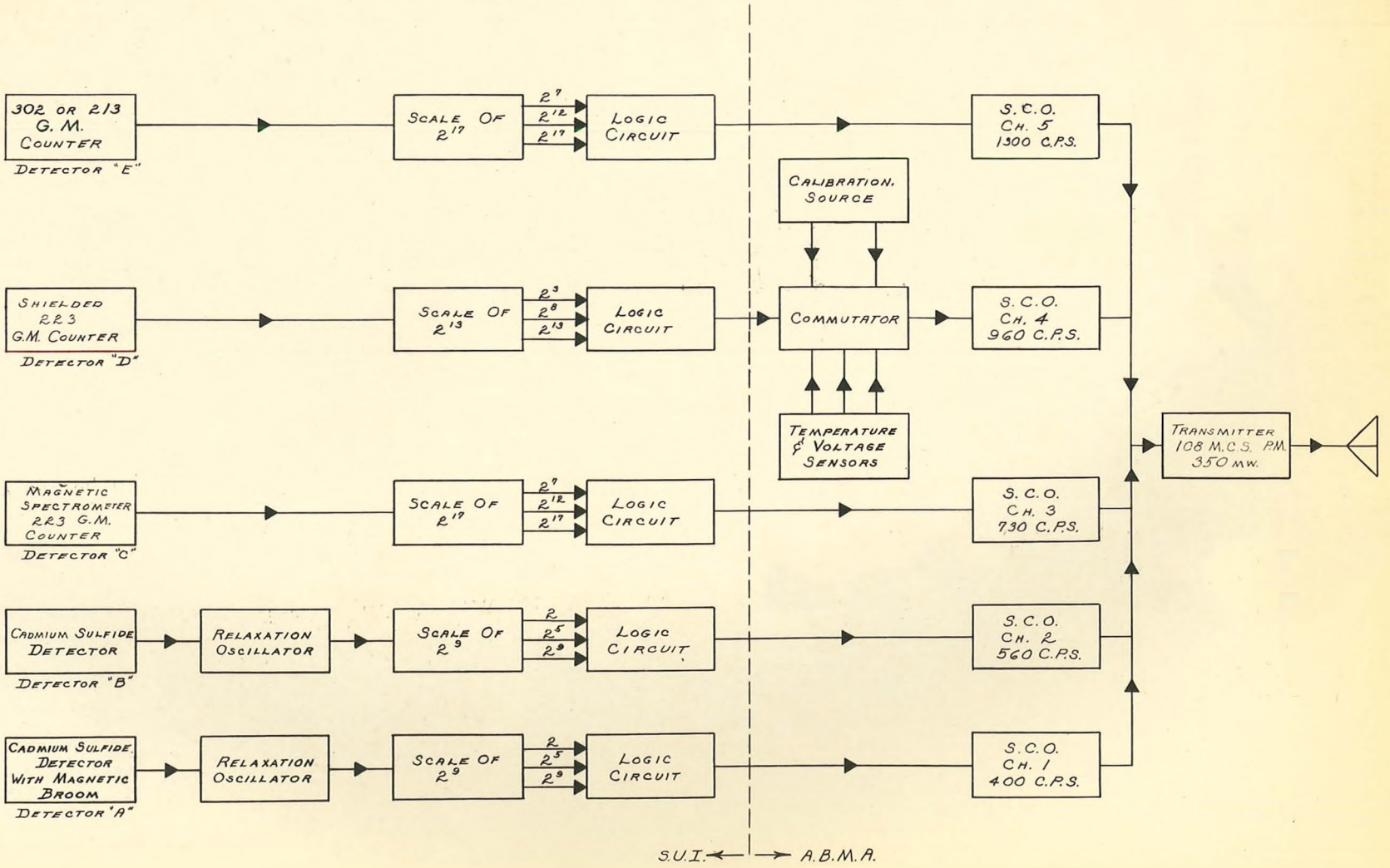

Rev.	Description	Date
B	Notes Corrected	2-12-60
A	Detectors Labled	2-12-60

DESCRIPTION 7-31-59 PL. S-46

BLOCK DIAGRAM PL. 9-46

STOCK SIZE

DEPARTMENT OF PHYSICS

COSMIC RAY LAB

C 11-0301

CLASSIFICATION UNCLASS

REVISION B

Fig. 9

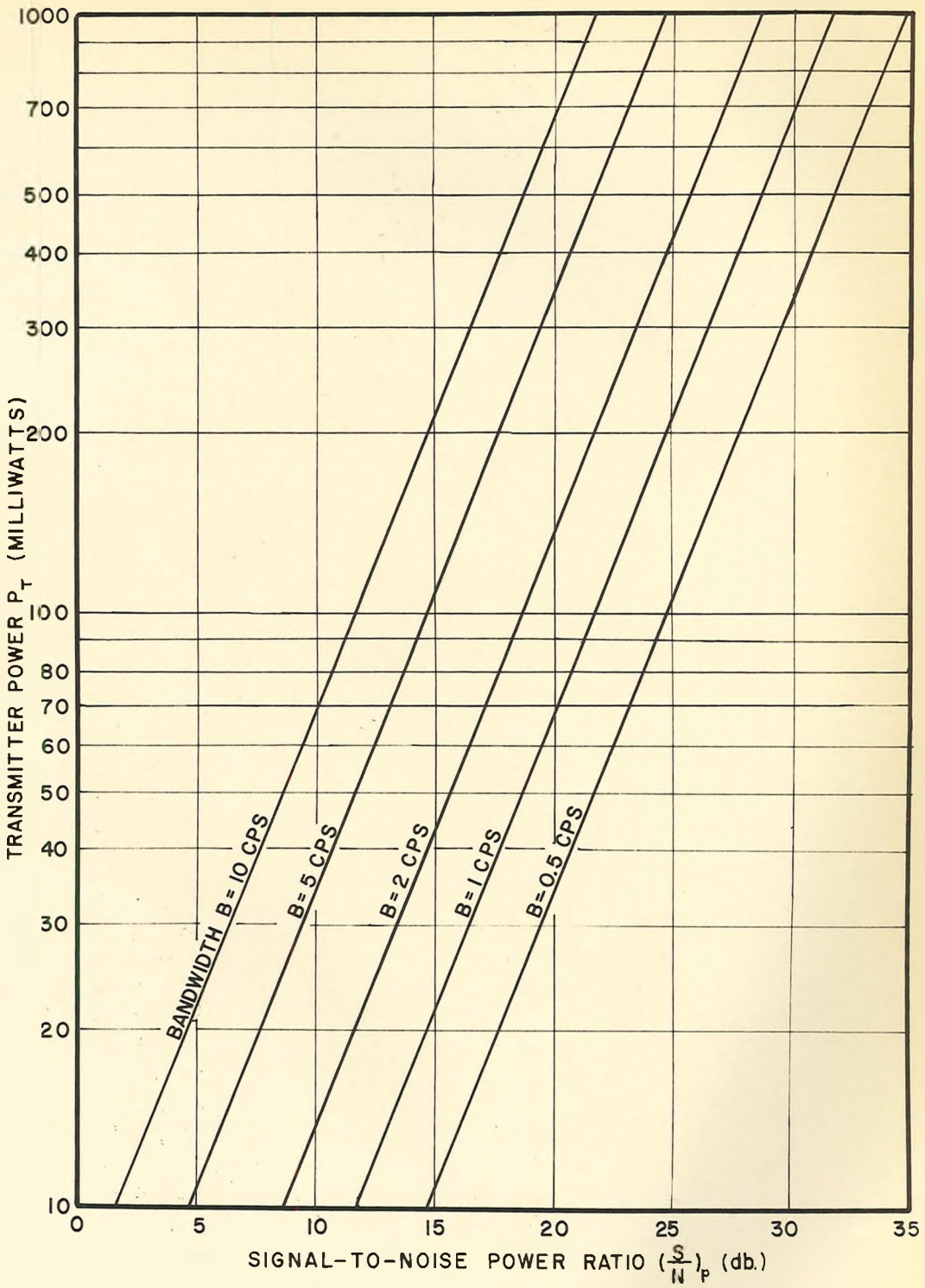

SIGNAL-TO-NOISE RATIO FOR S-46

Fig. 10

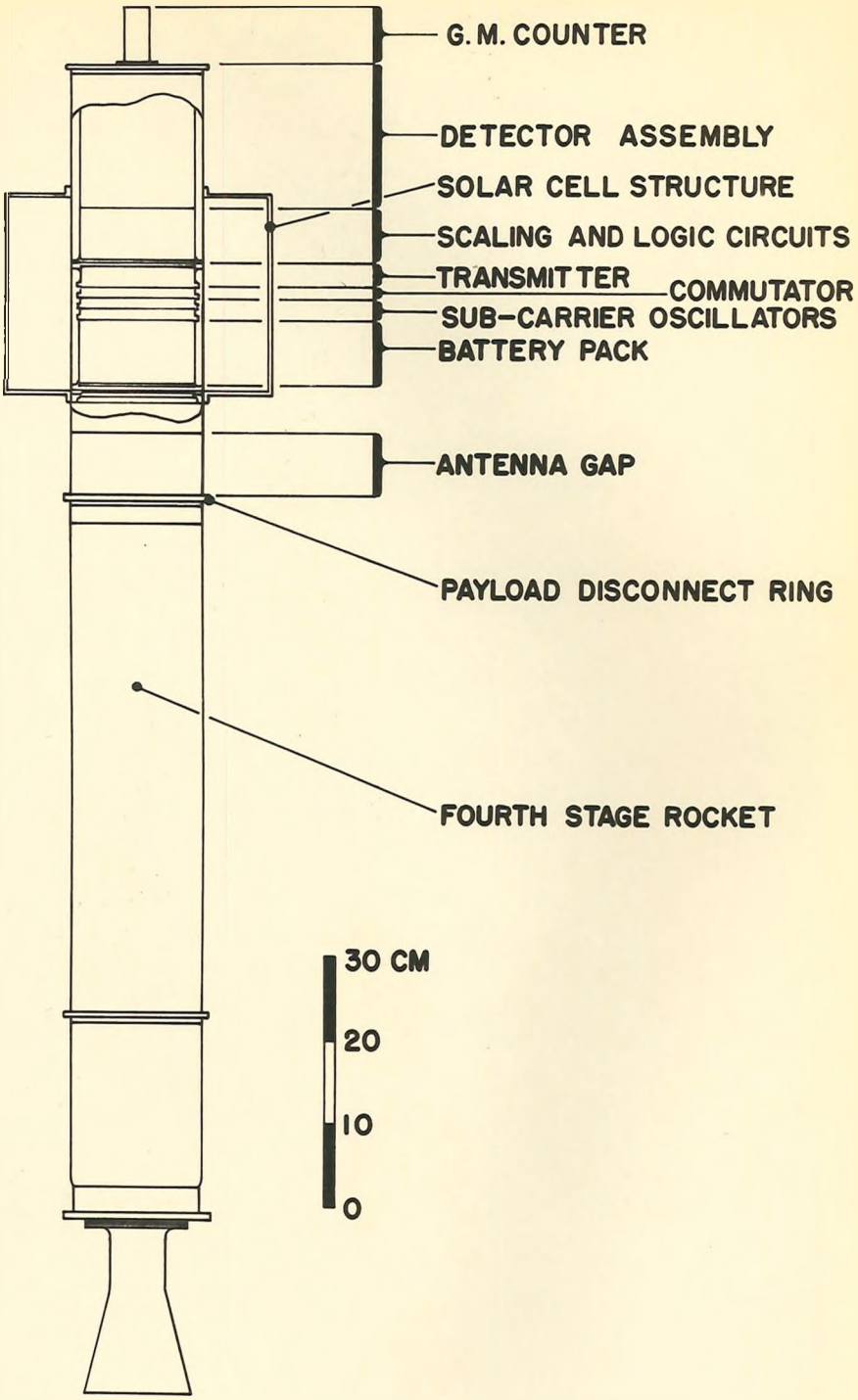

S-46 SATELLITE
Fig. 11

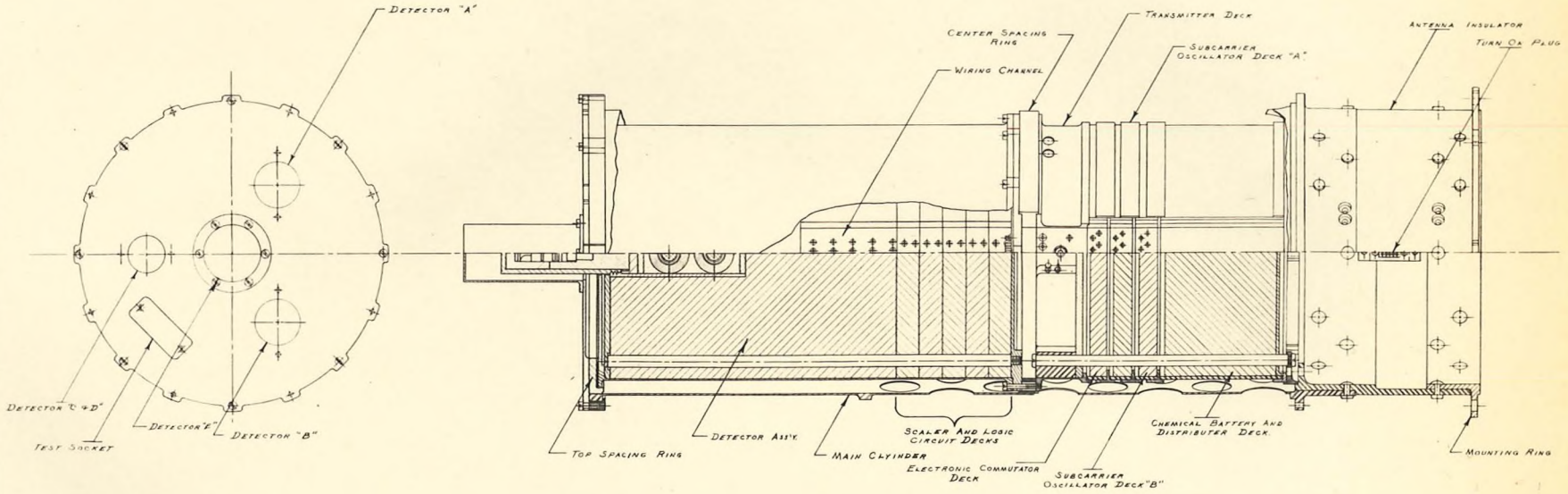
Detector "A"
Center Spacing Ring
Transmitter Deck
Antenna Insulator
Turn On Plug
Subcarrier Oscillator Deck "A"
Wiring Channel
Detector "C" & "D"
Detector "E"
Detector "B"
Test Socket
Top Spacing Ring
Detector Ass'y.
Main Cylinder
Scaler And Logic Circuit Decks
Electronic Commutator Deck
Subcarrier Oscillator Deck "B"
Chemical Battery And Distributer Deck
Mounting Ring

Fig. 12

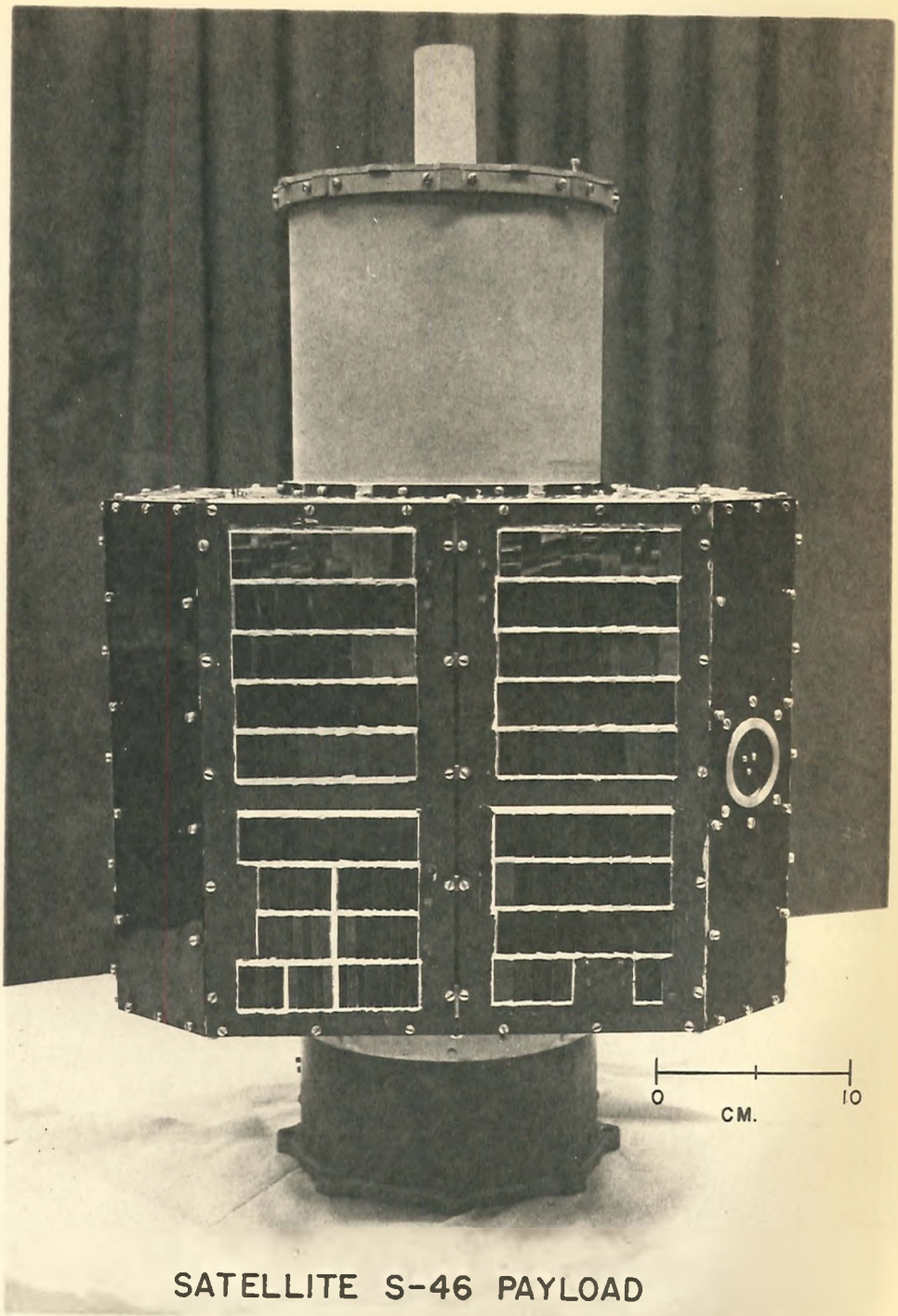

SATELLITE S-46 PAYLOAD

Fig. 13

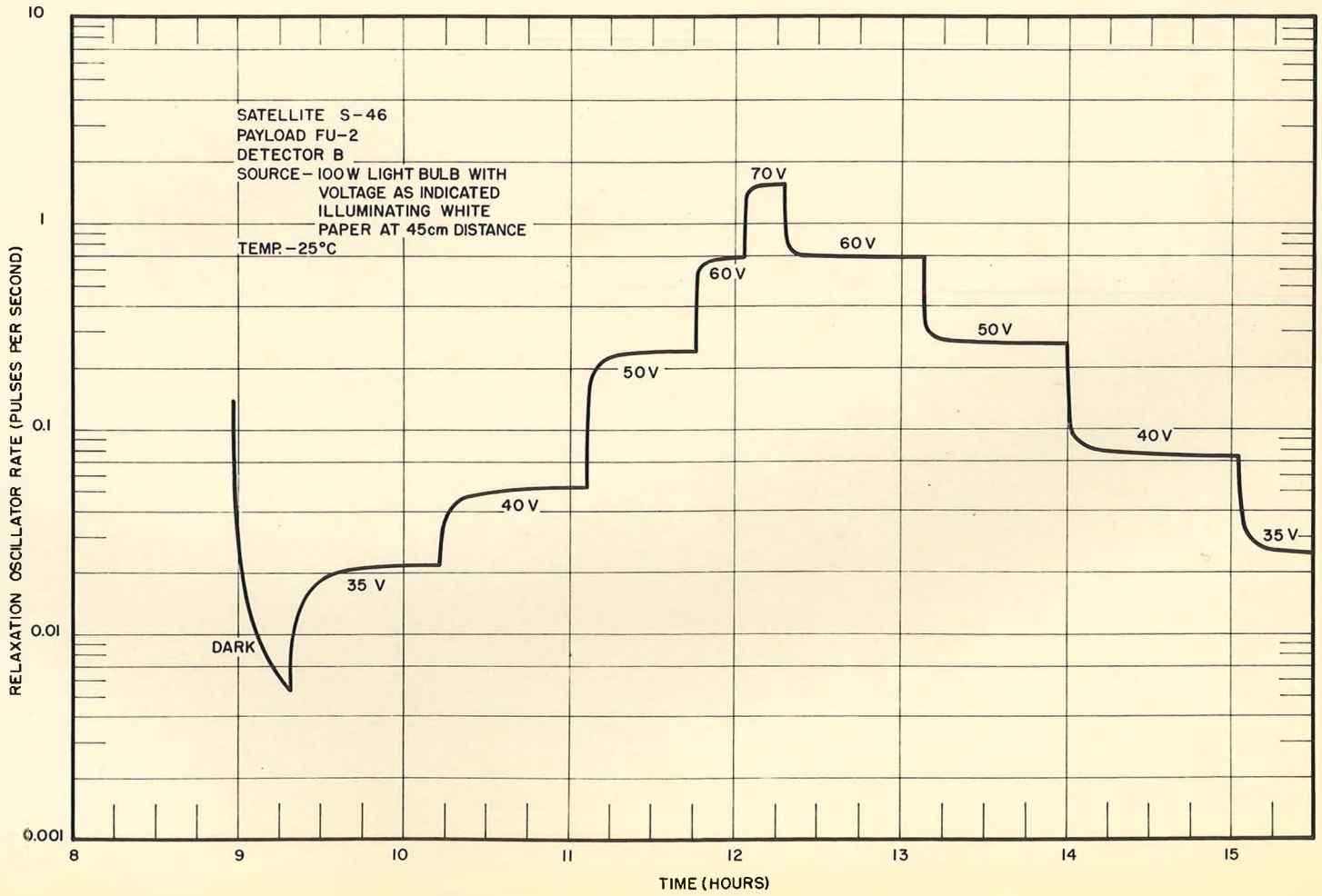

CADMIUM SULFIDE DETECTOR RELAXATION CHARACTERISTICS

Fig. 14

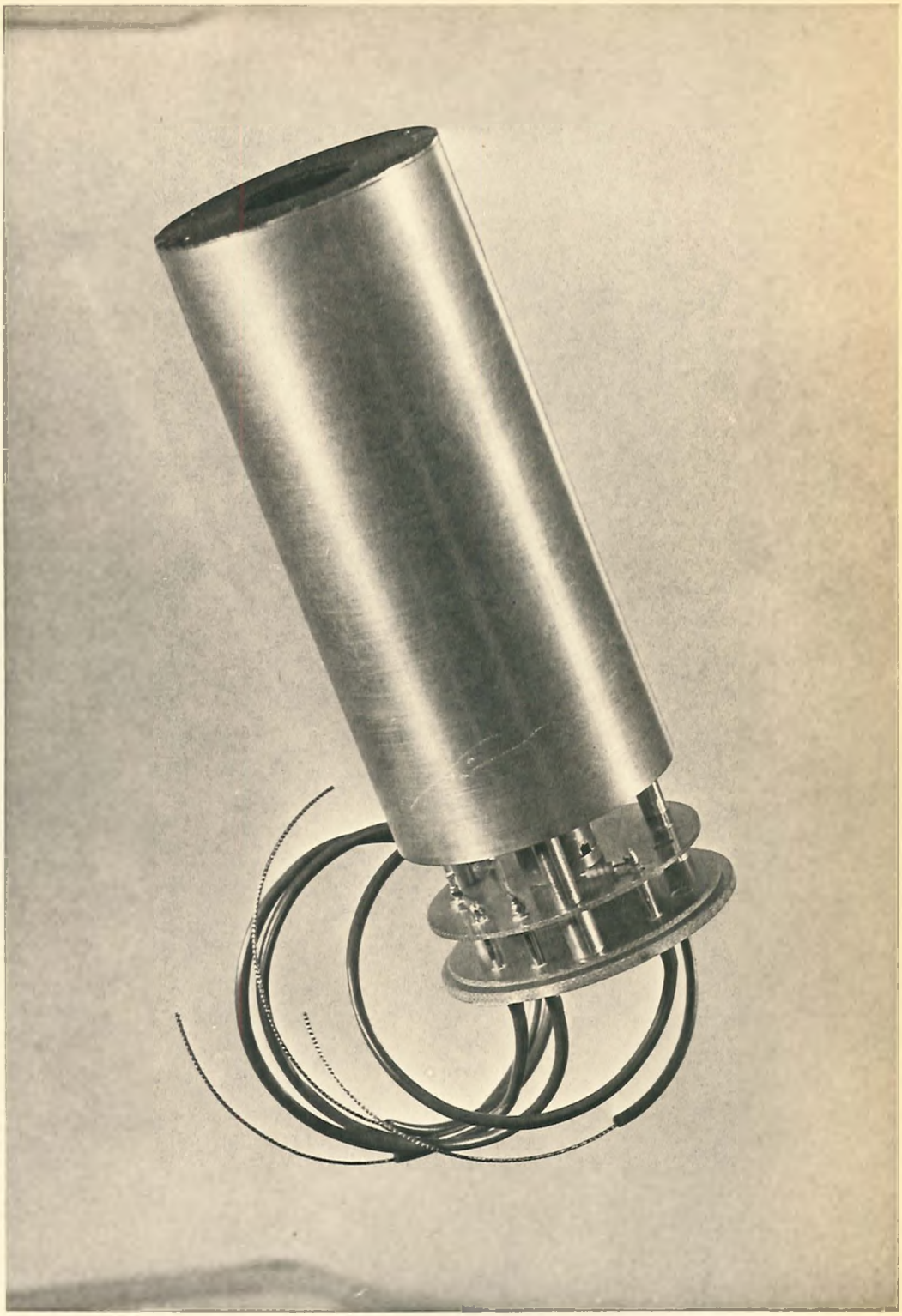

Fig. 15

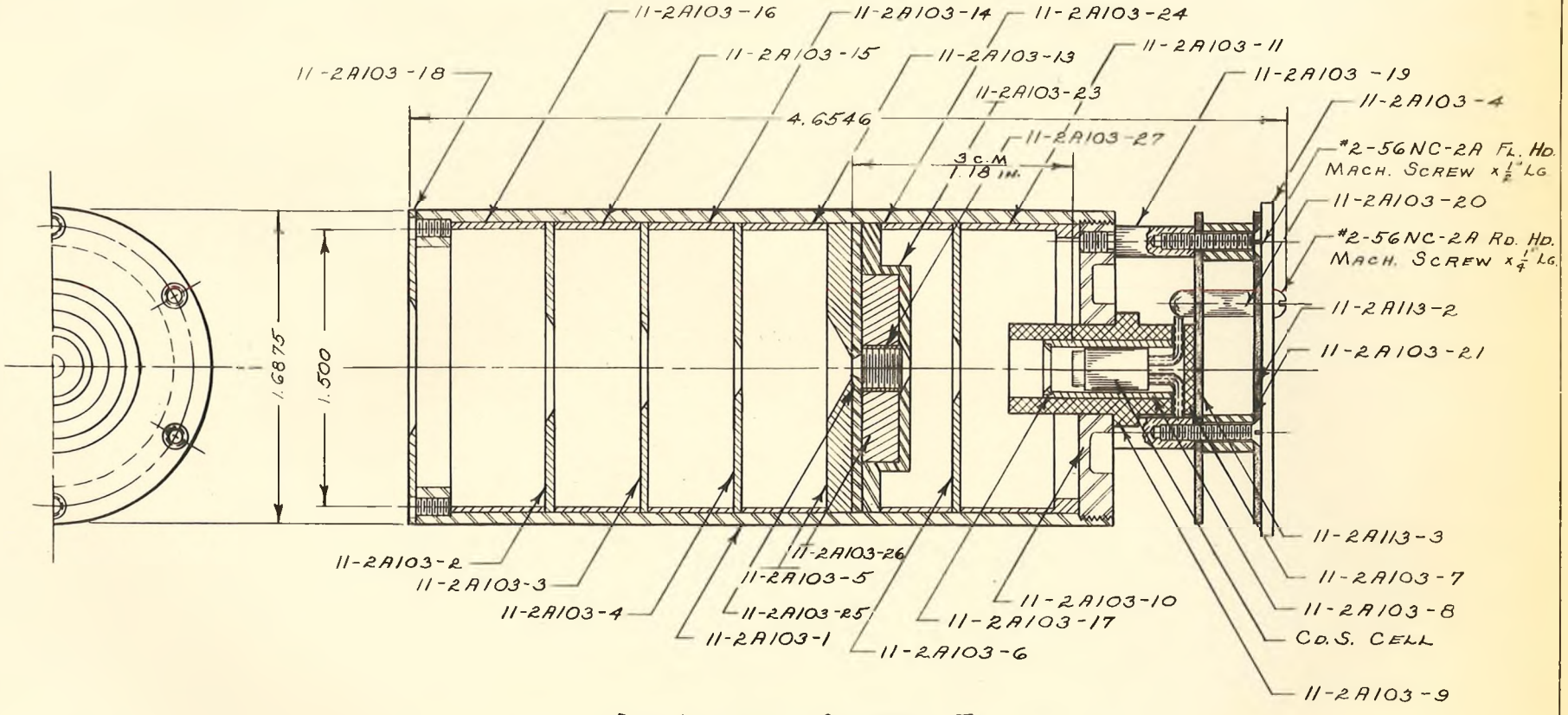

ALL INTERIOR SURFACES TO BE PAINTED FLAT BLACK

NOTE:
SEE DRWG. NO. 11-2A103 & 11-2A113 FOR DETAILS

FIND NO	NO REQD	DESCRIPTION	DWG OR PART NO	MATERIAL	STOCK SIZE
		RELEASE DATE OF DRAWING 12-11-59		Cd.S. DETECTOR ASS'Y. "A."	DEPARTMENT OF PHYSICS STATE UNIVERSITY OF IOWA IOWA CITY IOWA
		SIGNATURES DESIGNER J. Cronin DRAWN			COSMIC RAY LAB
	PL. S-46				DWG SIZE B 11-2A002
NEXT ASSY	USED ON				

UNLESS OTHERWISE SPECIFIED
DIMENSIONS ARE IN INCHES AND APPLY OVER ADDITIVE FINISH EXCEPT ORGANIC COATINGS
TOLERANCES DECIMALS .XX ± .03 .XXX ± .010 ANGLES ± 1/2°

SCALE 2/1 CLASSIFICATION UNCLASS. SHEET 1 OF 1 REVISION

Fig. 16

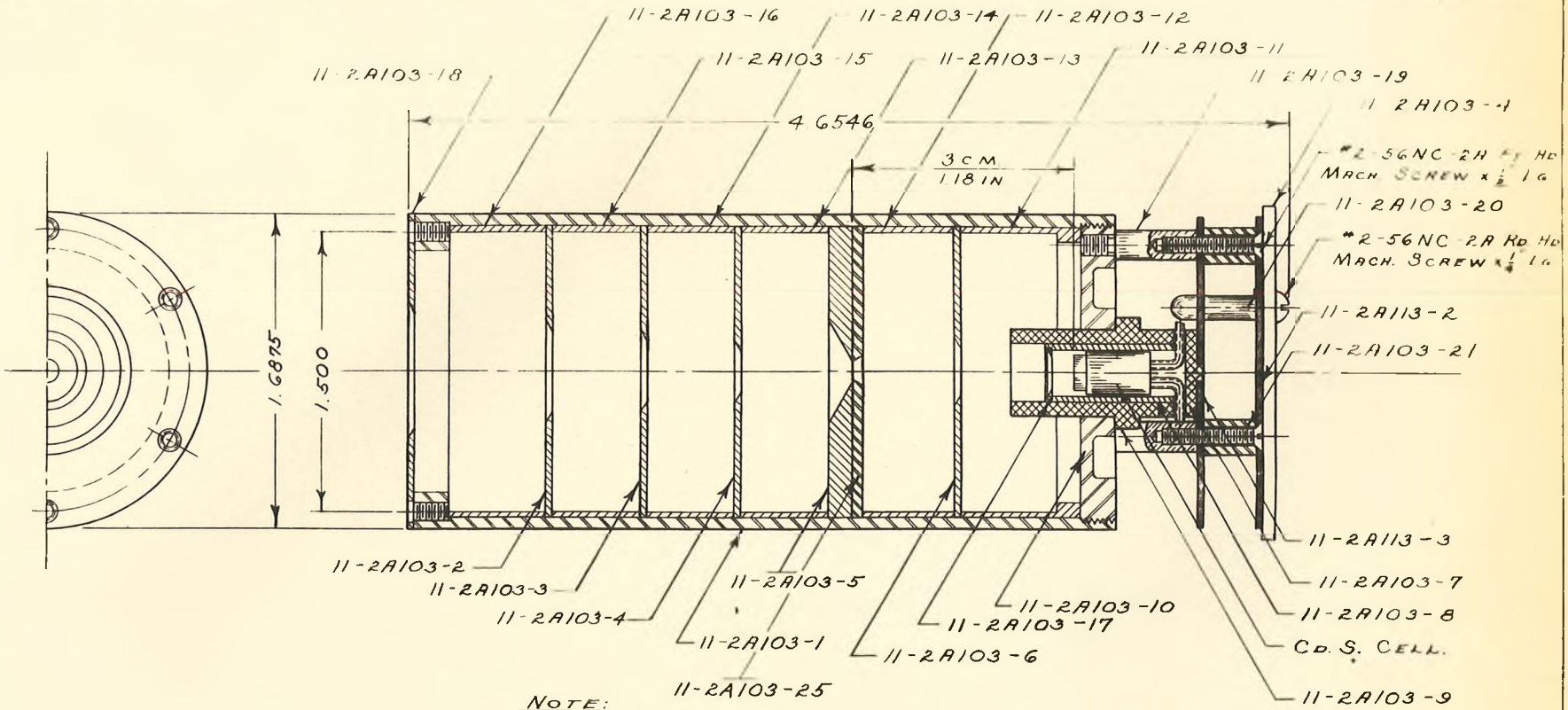

NOTE:
ALL INTERIOR SURFACES TO BE PAINTED FLAT BLACK.

NOTE:
SEE DRAWING NO 11-2A103 & 11-2A113 FOR DETAILS

FIND NO	NO REQD	DESCRIPTION	DWG OR PART NO	MATERIAL	STOCK SIZE
		RELEASE DATE OF DRAWING 12-4-59		Cd. S. Detector Ass'y. "B"	DEPARTMENT OF PHYSICS
		SIGNATURES			STATE UNIVERSITY OF IOWA IOWA CITY IOWA
		DESIGNER John W. Harris / DRAWN			COSMIC RAY LAB
	PL. S-46				DWG SIZE B 11-2A001
NEXT ASSY	USED ON				

UNLESS OTHERWISE SPECIFIED
DIMENSIONS ARE IN INCHES AND APPLY OVER ADDITIVE FINISH EXCEPT ORGANIC COATINGS
TOLERANCES DECIMALS XX ± .03 XXX ± .010 ANGLES ± 1/2°

SCALE 2/1 | CLASSIFICATION | SHEET 1 OF 1 | REVISION B

Fig. 17

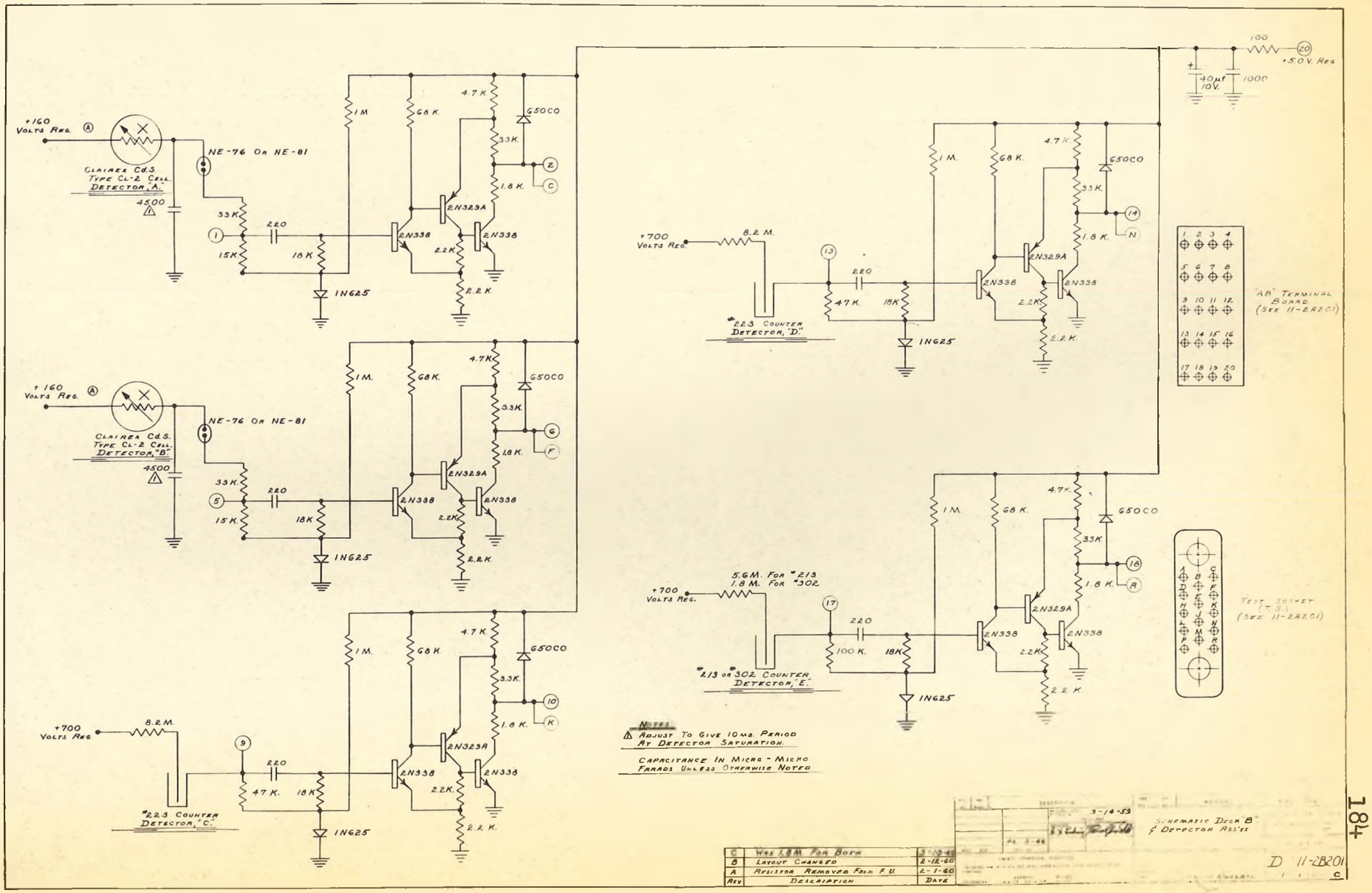
+160 Volts Reg.
Clairex Cd.S. Type CL-2 Cell Detector, "A"
NE-76 Or NE-81
4500
33K
15K
220
18K
1M
68K.
4.7K
650CO
3.3K.
1.8K.
2N329A
2N338
2.2K.
2.2K.
1N625
+160 Volts Reg.
Clairex Cd.S. Type CL-2 Cell Detector, "B"
+700 Volts Reg.
8.2M.
47K.
"223 Counter Detector, "C"
+700 Volts Reg.
8.2 M.
"223 Counter Detector, "D"
+700 Volts Reg.
5.6M. For "213
1.8 M. For "302
100K.
"213 or "302 Counter Detector, "E"
100
+5.0 V. Reg
40 mf 10V.
1000
"AB" Terminal Board (See 11-2B201)
Test Socket T-8 (See 11-2B201)
Notes:
Adjust To Give 10 ms. Period At Detector Saturation.
Capacitance In Micro-Micro Farads Unless Otherwise Noted
C Was 1.8M. For Bore 3-10-59
B Layout Changed 2-12-60
A Resistor Removed From F.U. 2-1-60
Rev Description Date
3-14-59
Schematic Deck B & Detector Ass'ys
D 11-2B201
C

Fig. 18

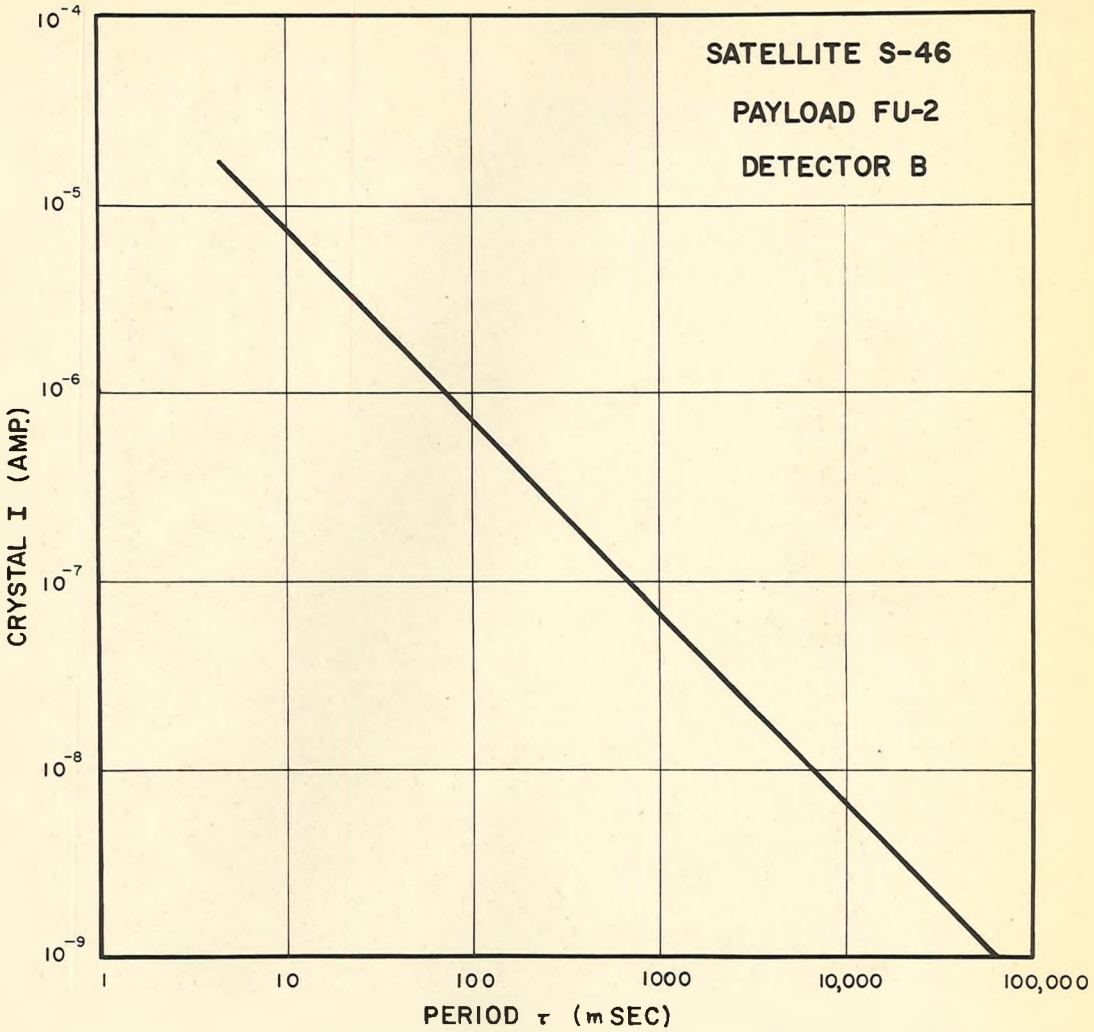

RELAXATION OSCILLATOR CHARACTERISTICS

Fig. 19

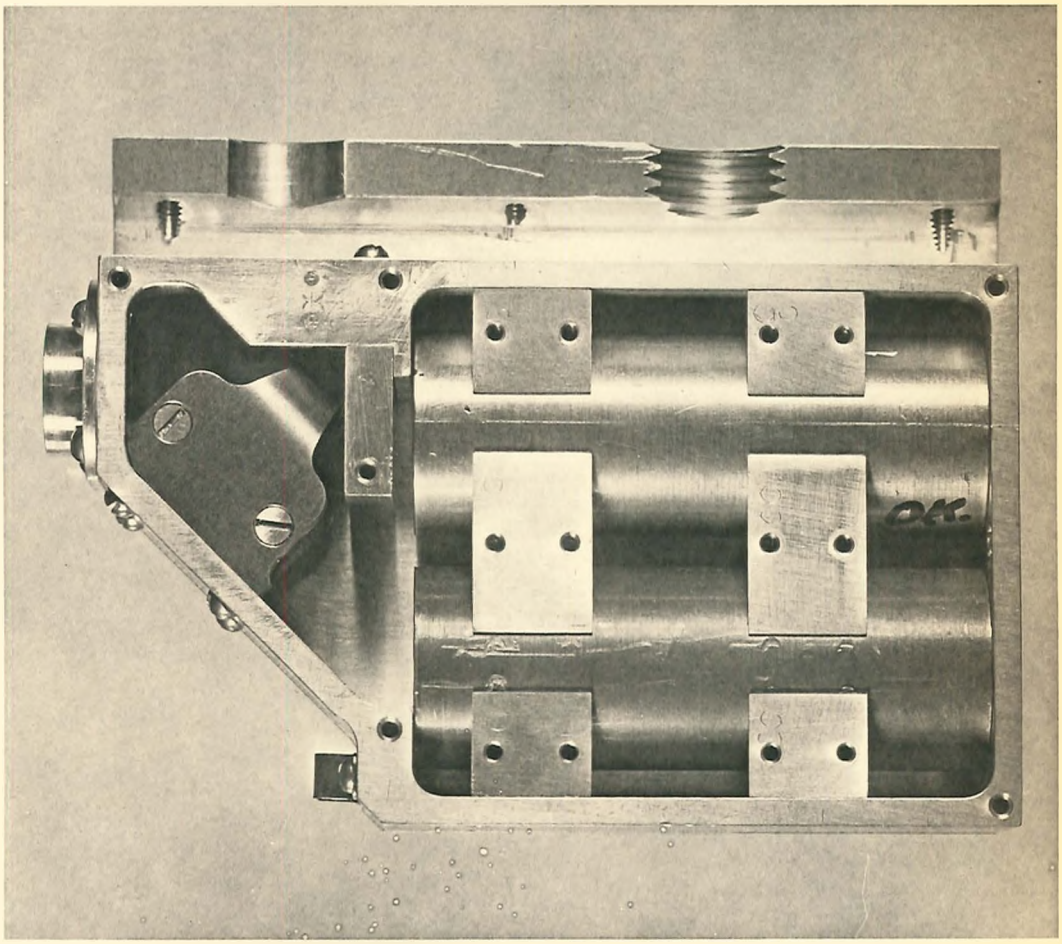

Fig. 20

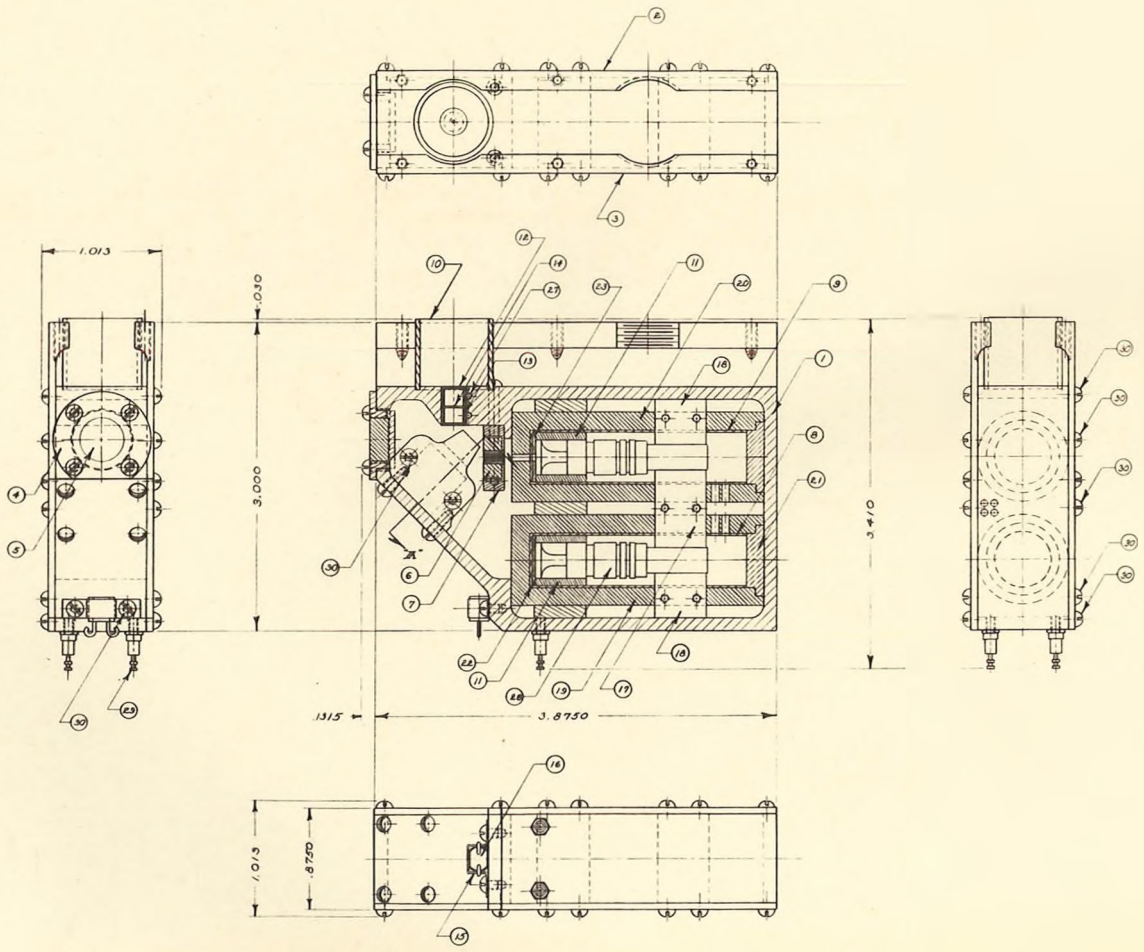

30	1	"E - 56 UNC - 2A RD HD SCREW		PURCHASED	
29	2	INSULATED SPRING FOR "1189		PURCHASED USED	
28	2	"2.23 GEIGER COUNTER TUBE		PURCHASED ANTON	
27	6	PIN		TOOL STEEL	.0625 DIA x .870
26	1	MAGNET	11-2A-16-3	PURCHASED	
25	1	NEG. POLE	11-2A118-2		
24	1	POS. POLE	11-2A120-1		
23	1	SLOTTED RING	11-2A104-5		
22	1	SPACER	11-2A104-4		
21	2	CAP "Pb"	11-2A104-3		
20	1	SLOTTED "Pb" SHIELD	11-2A104-2		
13	1	"Pb" SHIELD	11-2A104-1		
18	4	SINGLE SADDLE	11-2A107-2		
17	2	DOUBLE SADDLE	11-2A107-1		
16	1	THERMISTOR BEADS TYPE II		PROCURED	"834A483
15	1	THERMISTOR CAP	11-2A117-4		
14	1	APERTURE LENS	11-2A117-3		
13	1	APERTURE INNER	11-2A117-2		
12	1	APERTURE OUTER	11-2A117-1		
11	2	ALIGNMENT BLOCK	11-2A112-4		
10	1	APERTURE TUBE	11-2A113-3		
9	1	STEEL SHIELD "SLOTTED"	11-2A112-2		
8	1	STEEL SHIELD	11-2A112-1		
7	1	BAFFLE	11-2A119-4		
6	1	"Pb" FOR BAFFLE	11-2A119-3		
5	1	"Pb" FOR HAT SHIELD	11-2A83-2		
4	1	HAT SHIELD	11-2A118-1		
3	1	LEFT SIDE PLATE	11-2A114-2		
2	1	RIGHT SIDE PLATE	11-2A114-1		
1	1	HOUSING	11-2A106-1		

DESCRIPTION — DATE — BY

MAGNETIC SPECTROMETER ASSY

D 11 2A003

2/1 — UNCLASS — 1 — 1 — A

Fig. 21

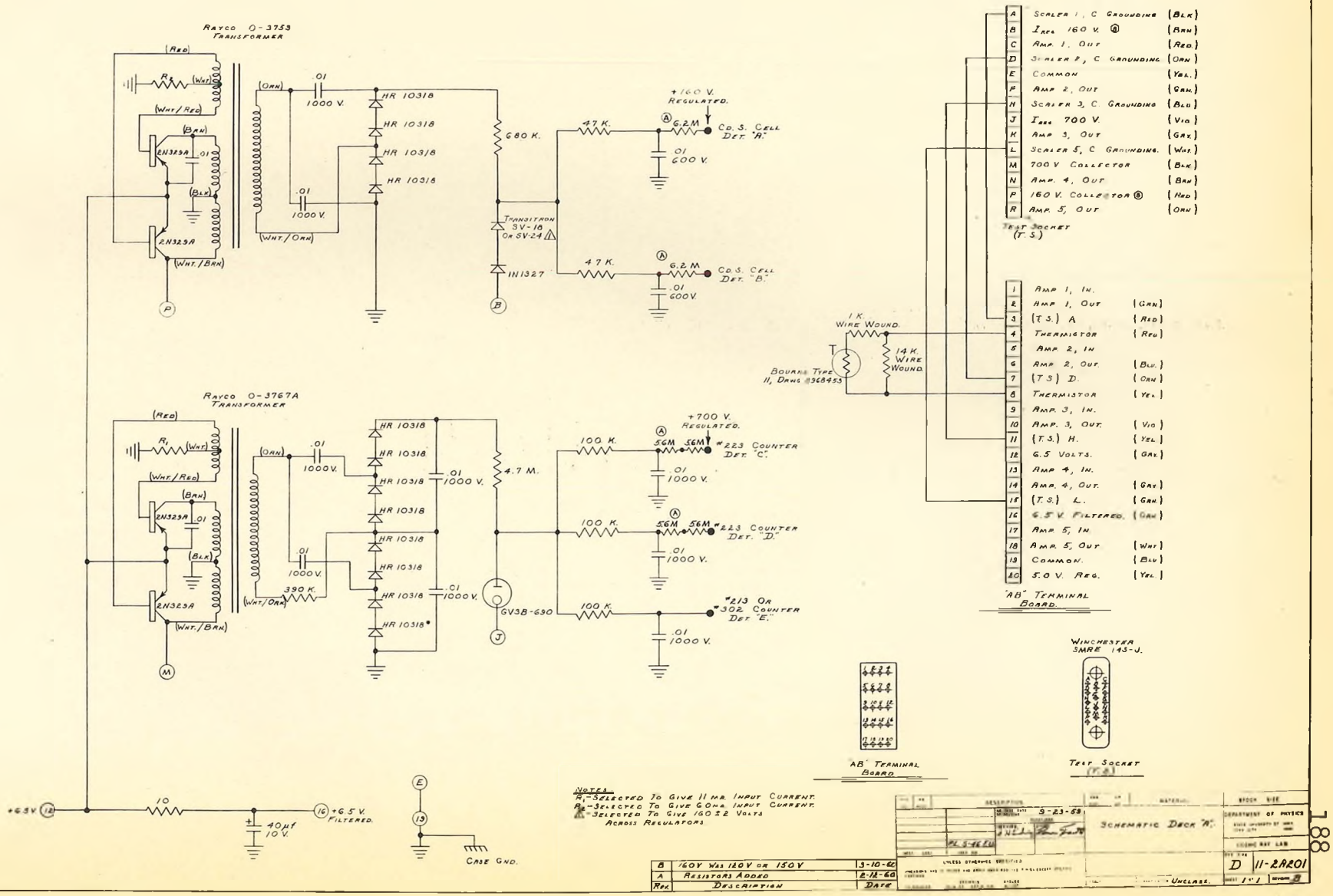
RAYCO O-3753 TRANSFORMER
RAYCO O-3767A TRANSFORMER
2N329A
HR 10318
680 K.
47 K.
6.2 M
CD. S. CELL DET. "A."
CD. S. CELL DET. "B."
+160 V. REGULATED.
TRANSITRON SV-16 OR SV-24
IN1327
1 K. WIRE WOUND.
14 K. WIRE WOUND.
BOURNS TYPE 11, DRWG #3684455
+700 V. REGULATED.
4.7 M.
100 K.
56M
#223 COUNTER DET. "C."
#223 COUNTER DET. "D."
#213 OR #302 COUNTER DET. "E."
GV38-690
390 K.
+6.3 V.
10
40 μf 10 V.
+6.5 V. FILTERED.
CASE GND.
"AB" TERMINAL BOARD.
TEST SOCKET (T.S.)
WINCHESTER SMRE 143-J.
Notes
A - Selected To Give 11 MA. Input Current.
B - Selected To Give 60 MA. Input Current.
C - Selected To Give 160 ± 2 Volts Across Regulators
B 160V Was 120V or 150V 3-10-61
A Resistors Added 2-12-60
Rev. Description Date
SCHEMATIC DECK "A"
D 11-2AR01

Fig. 22

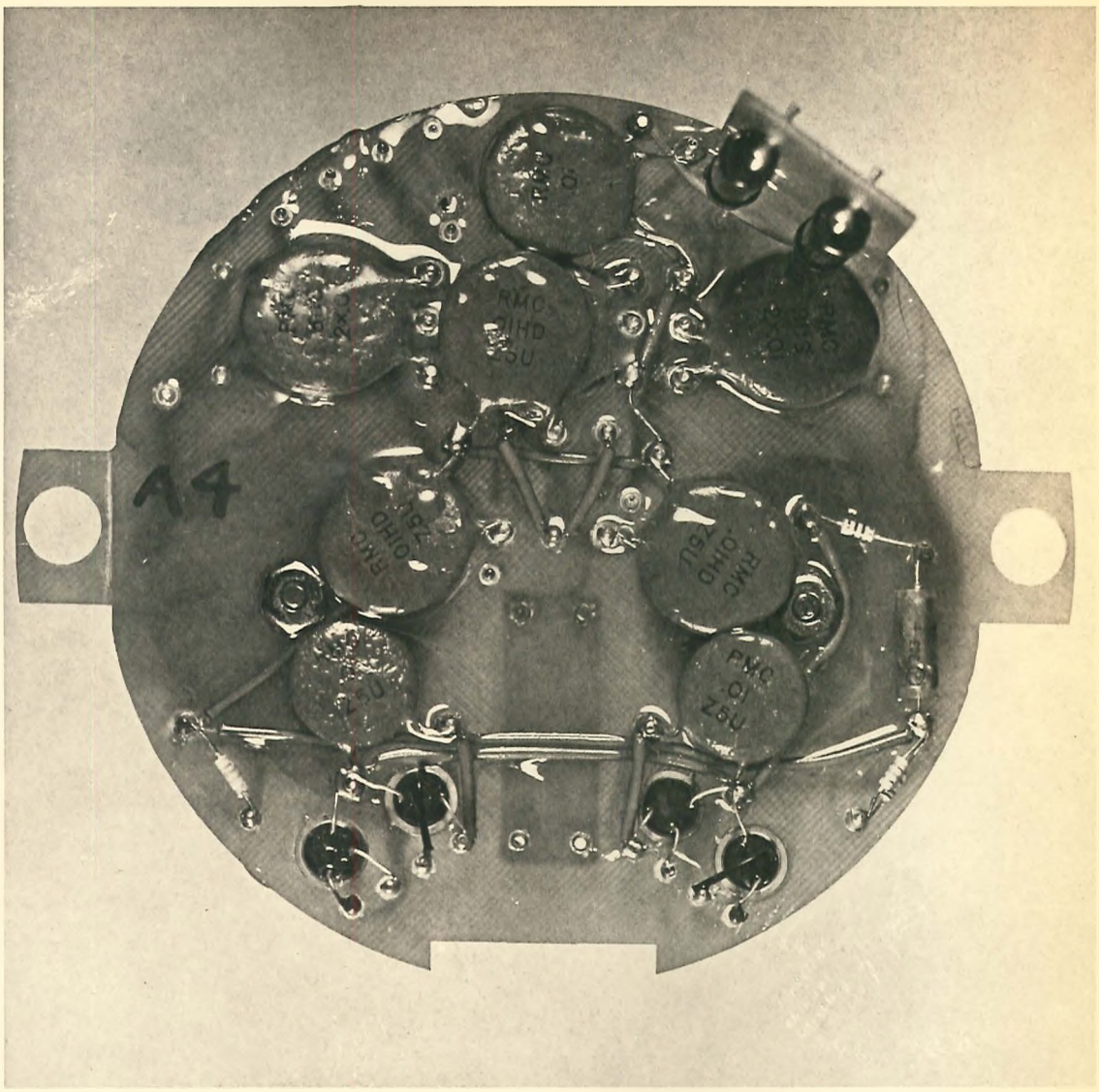

Fig. 23

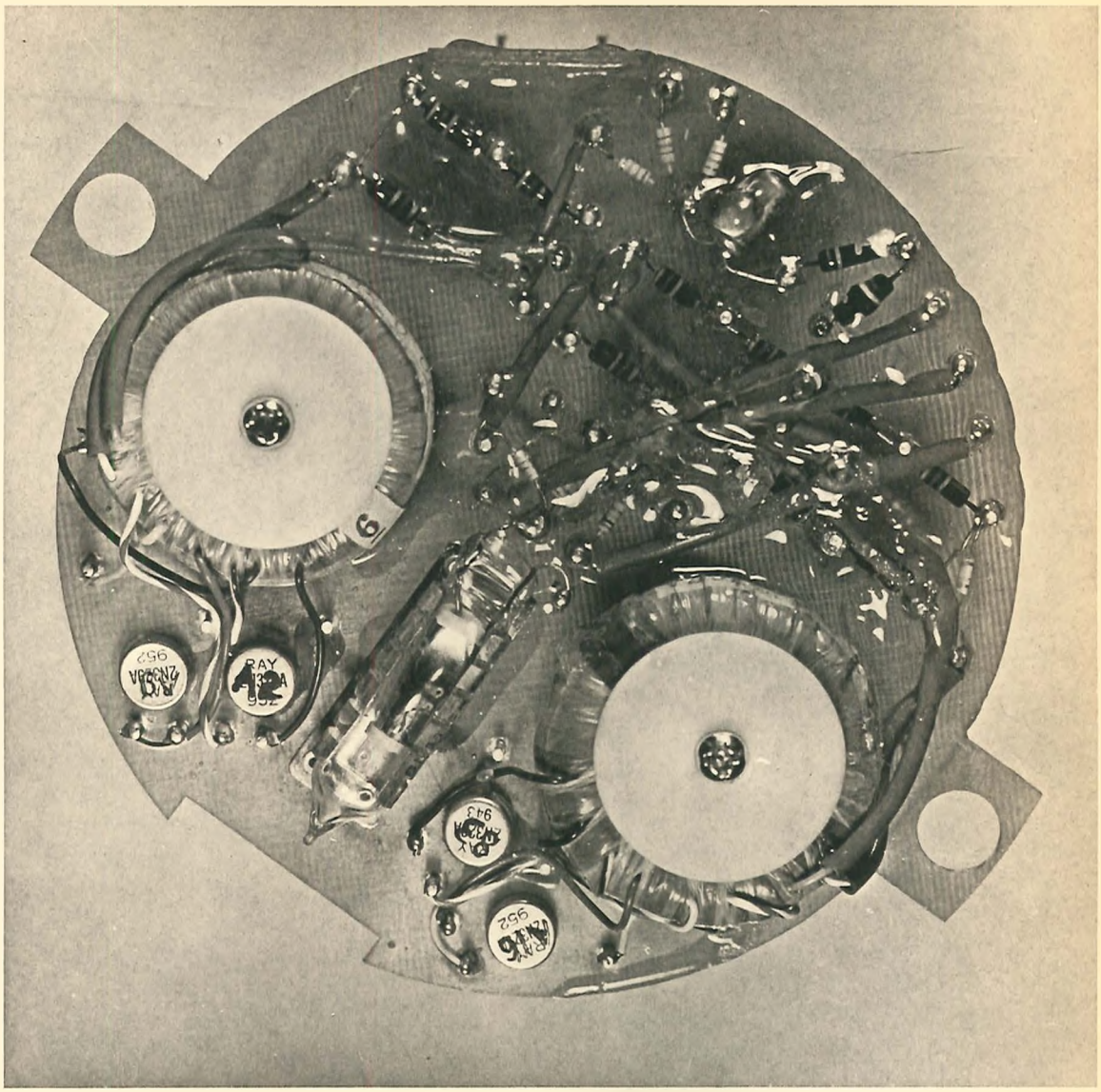

Fig. 24

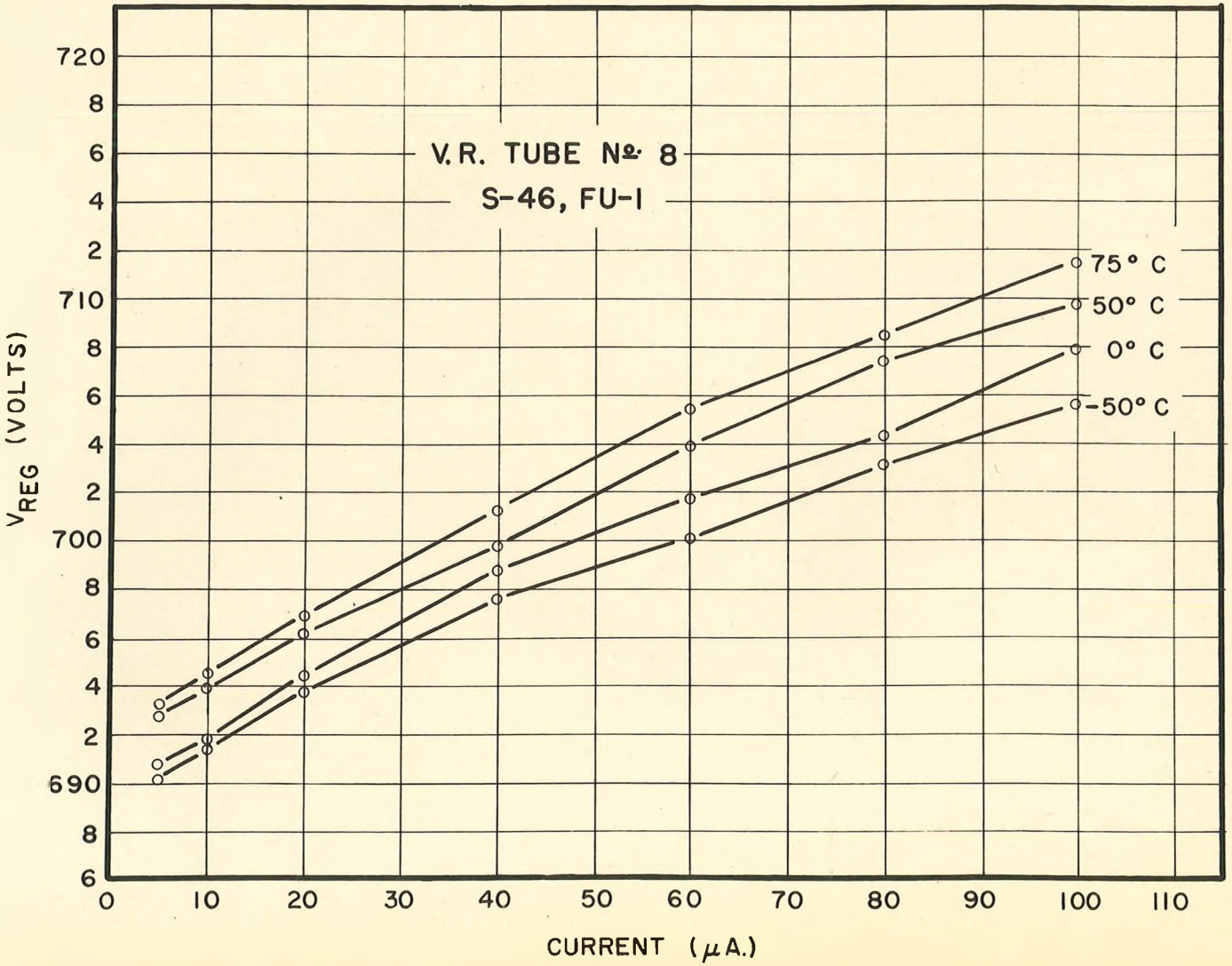

Fig. 25 REGULATOR TUBE CHARACTERISTICS

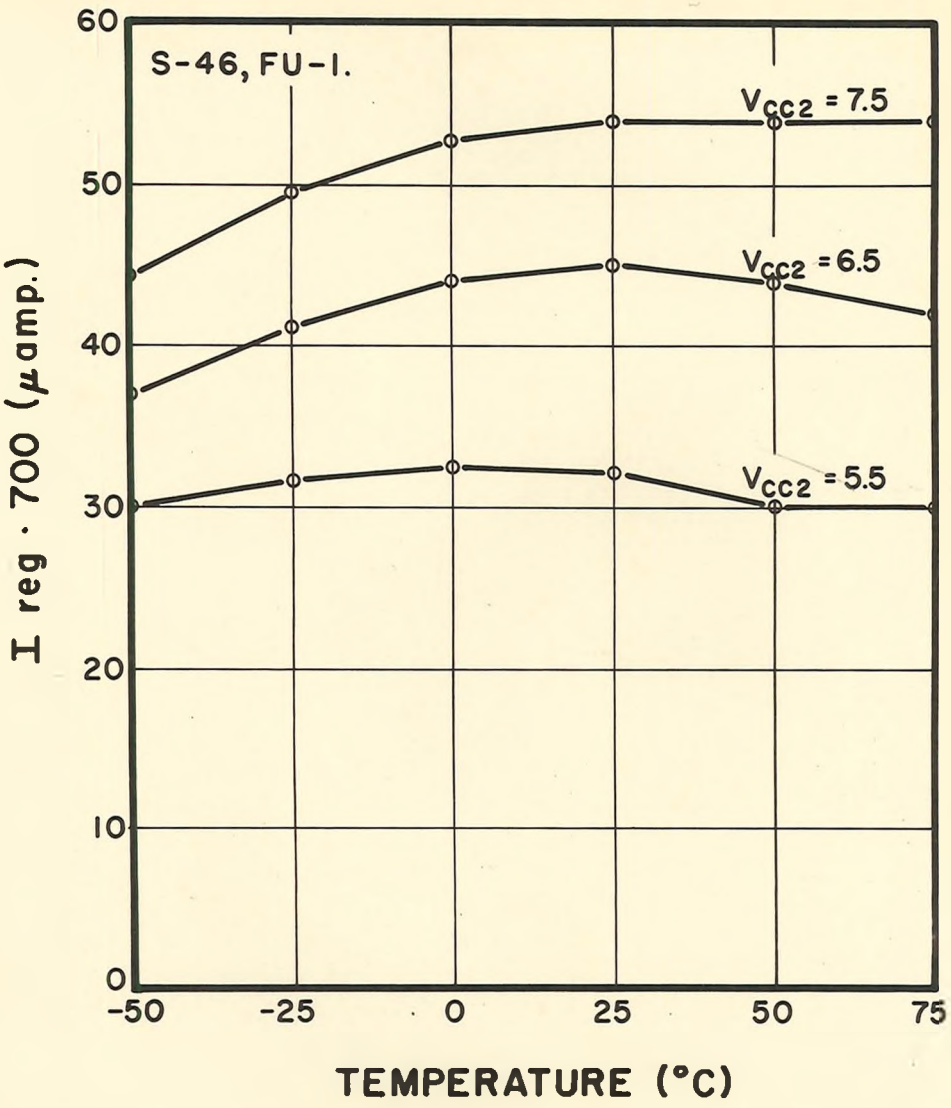

700 VOLT POWER SUPPLY OUTPUT CURRENT

Fig. 26

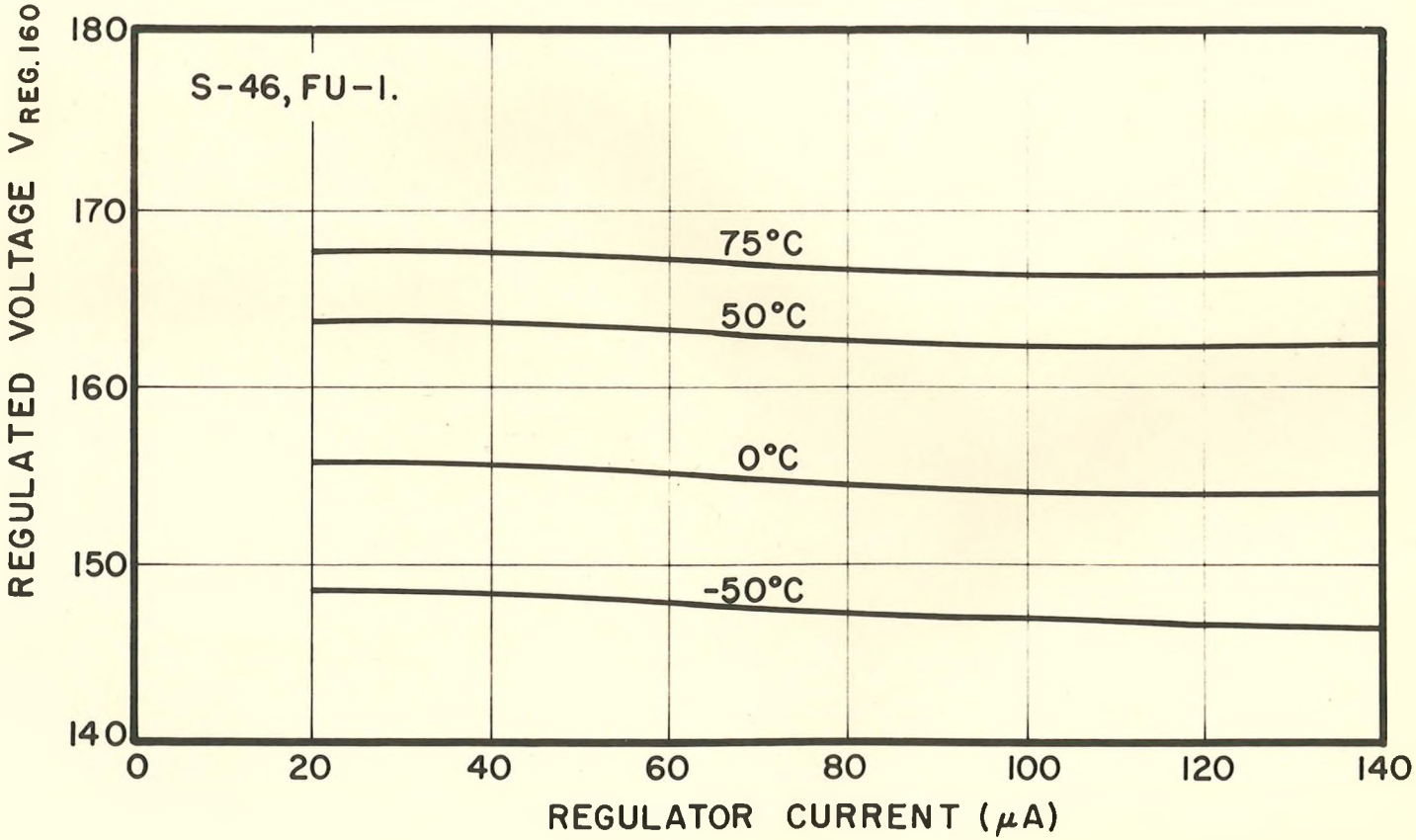

ZENER DIODE REGULATOR CHARACTERISTICS

Fig. 27

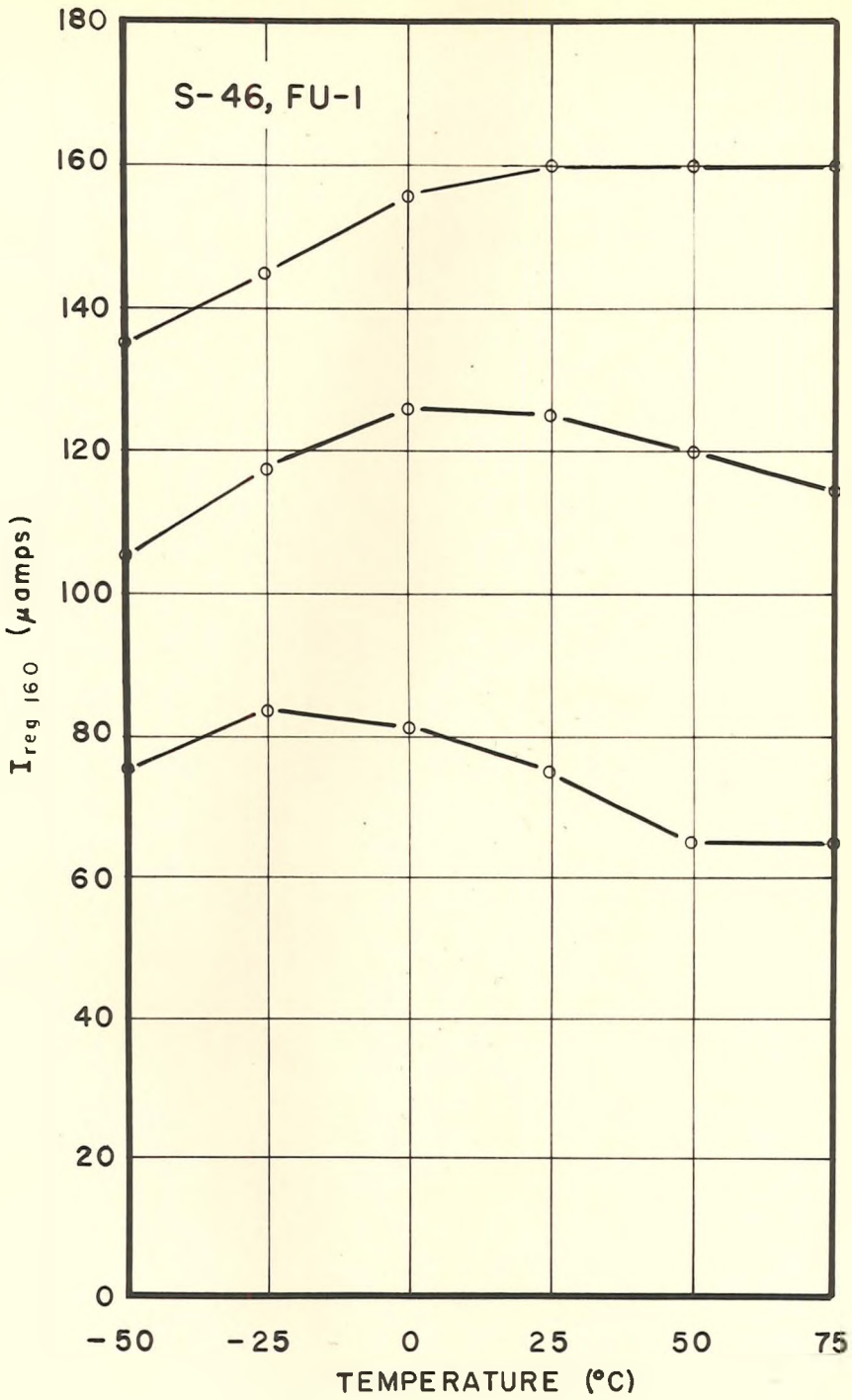

160 VOLT POWER SUPPLY
OUTPUT CURRENT

Fig. 28

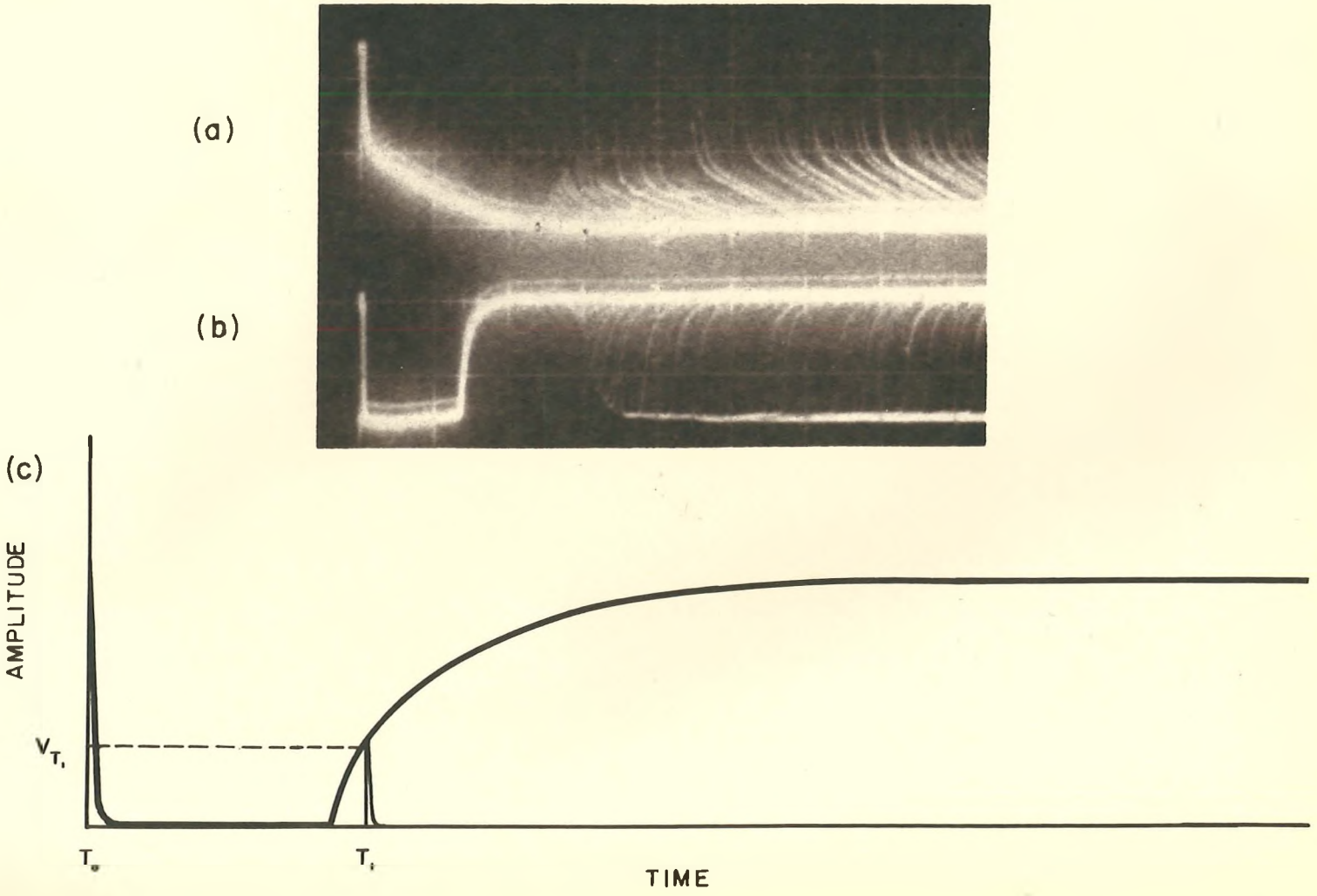

Fig. 29 **G.M. COUNTER PULSE ENVELOPE**

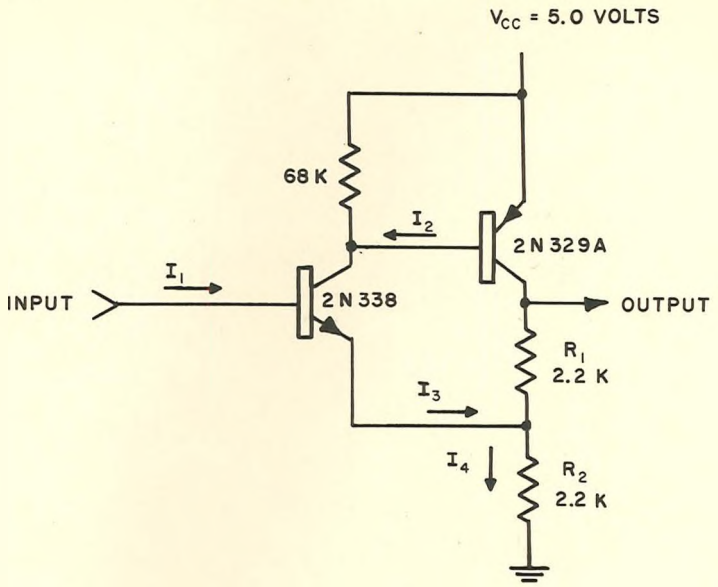

(a) BASIC CIRCUIT

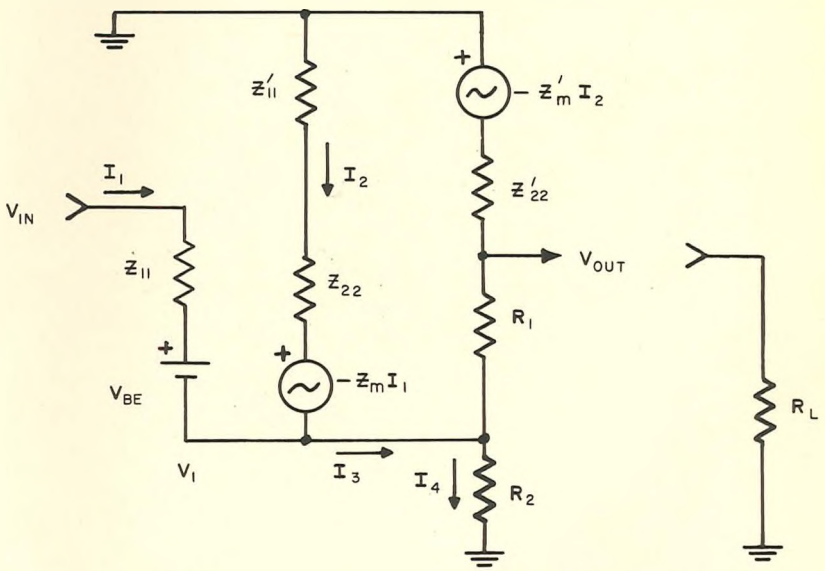

(b) SIMPLIFIED EQUIVALENT CIRCUIT

BASIC BOOTSTRAP AMPLIFIER CIRCUIT

Fig. 30

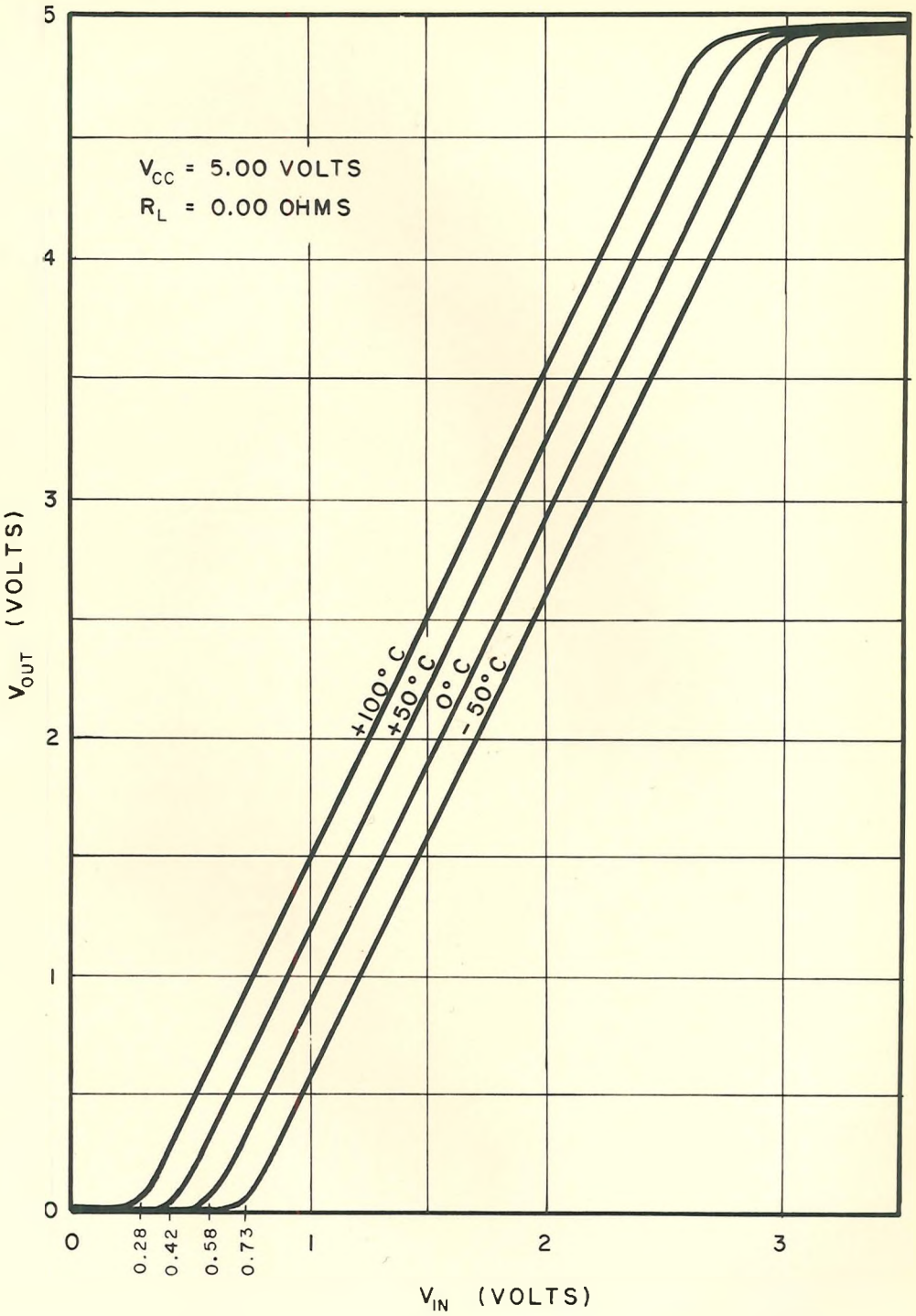

BOOTSTRAP AMPLIFIER VOLTAGE GAIN

Fig. 31

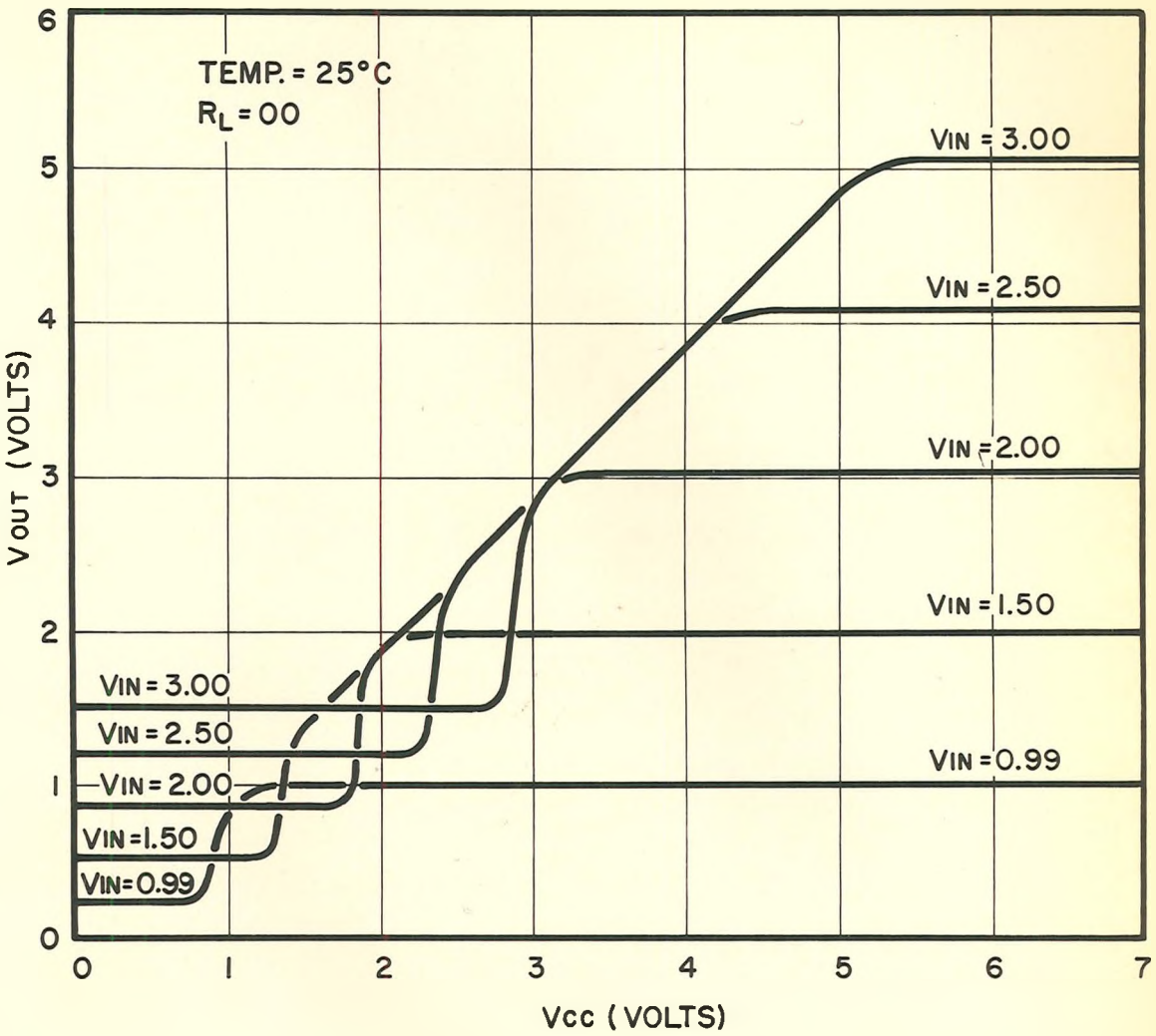

BOOTSTRAP AMPLIFIER PERFORMANCE
WITH CHANGE IN Vcc

Fig. 32

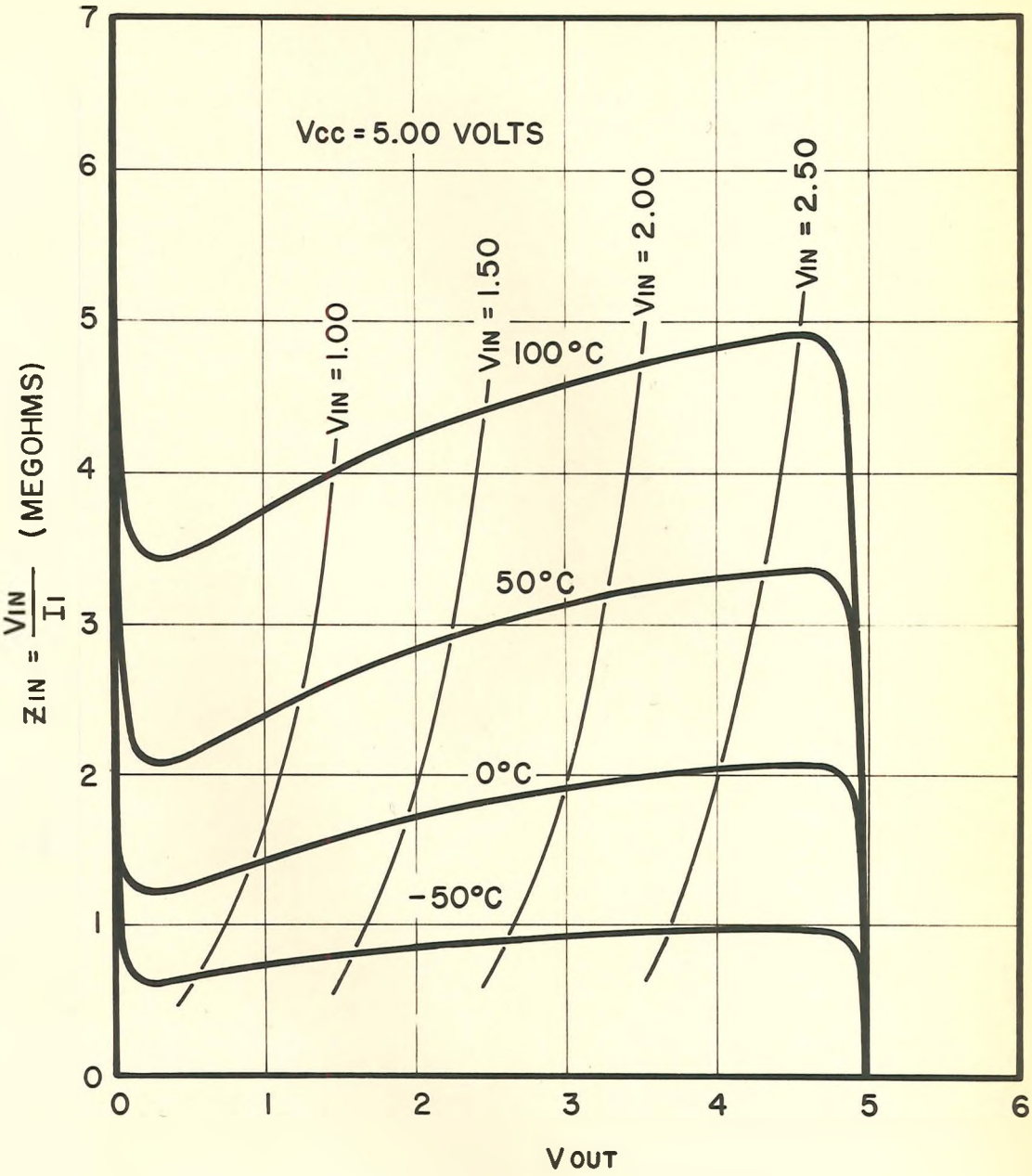

BOOTSTRAP AMPLIFIER
INPUT IMPEDANCE

Fig. 33

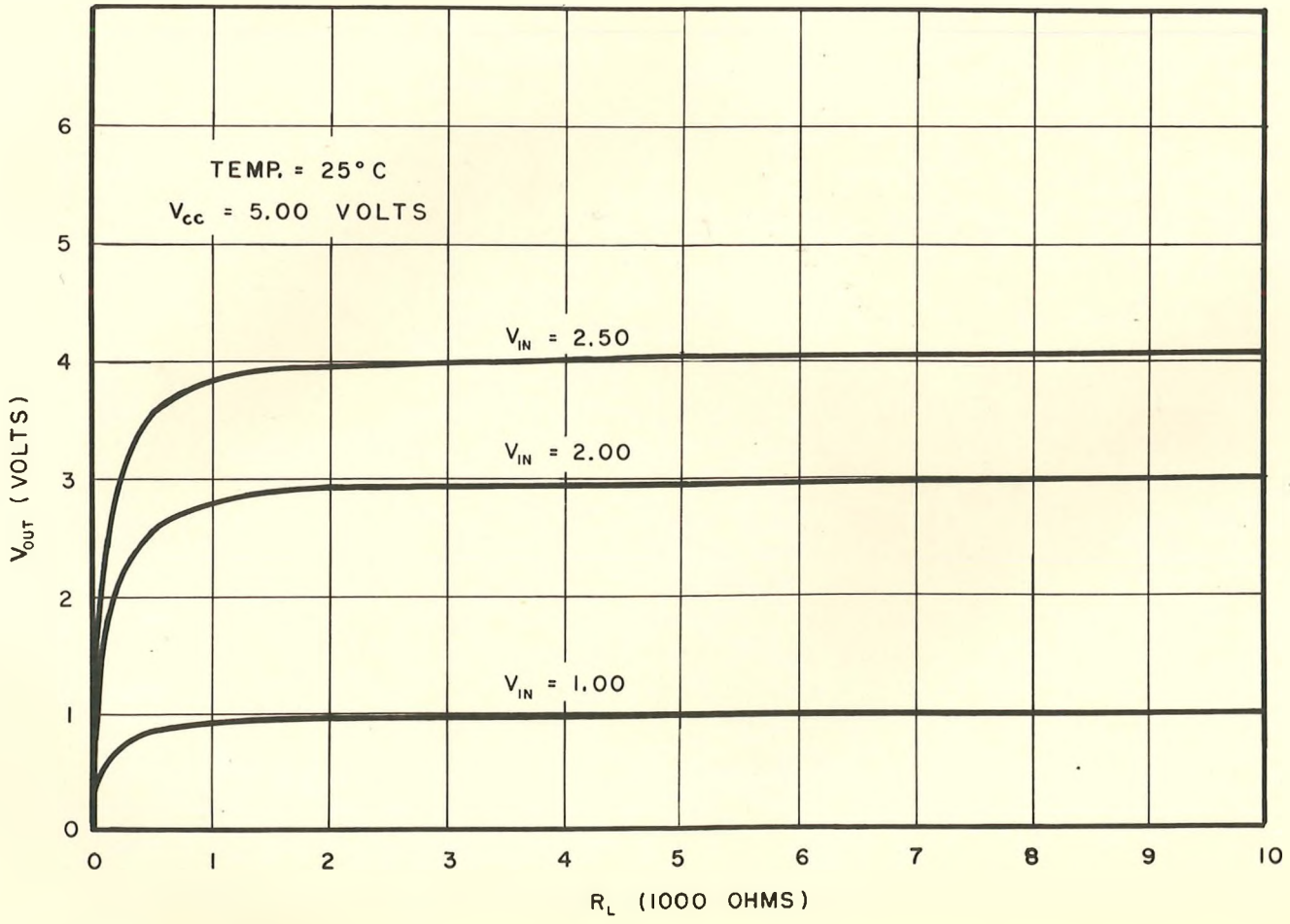

BOOTSTRAP AMPLIFIER PERFORMANCE WITH CHANGE IN R_L

Fig. 34

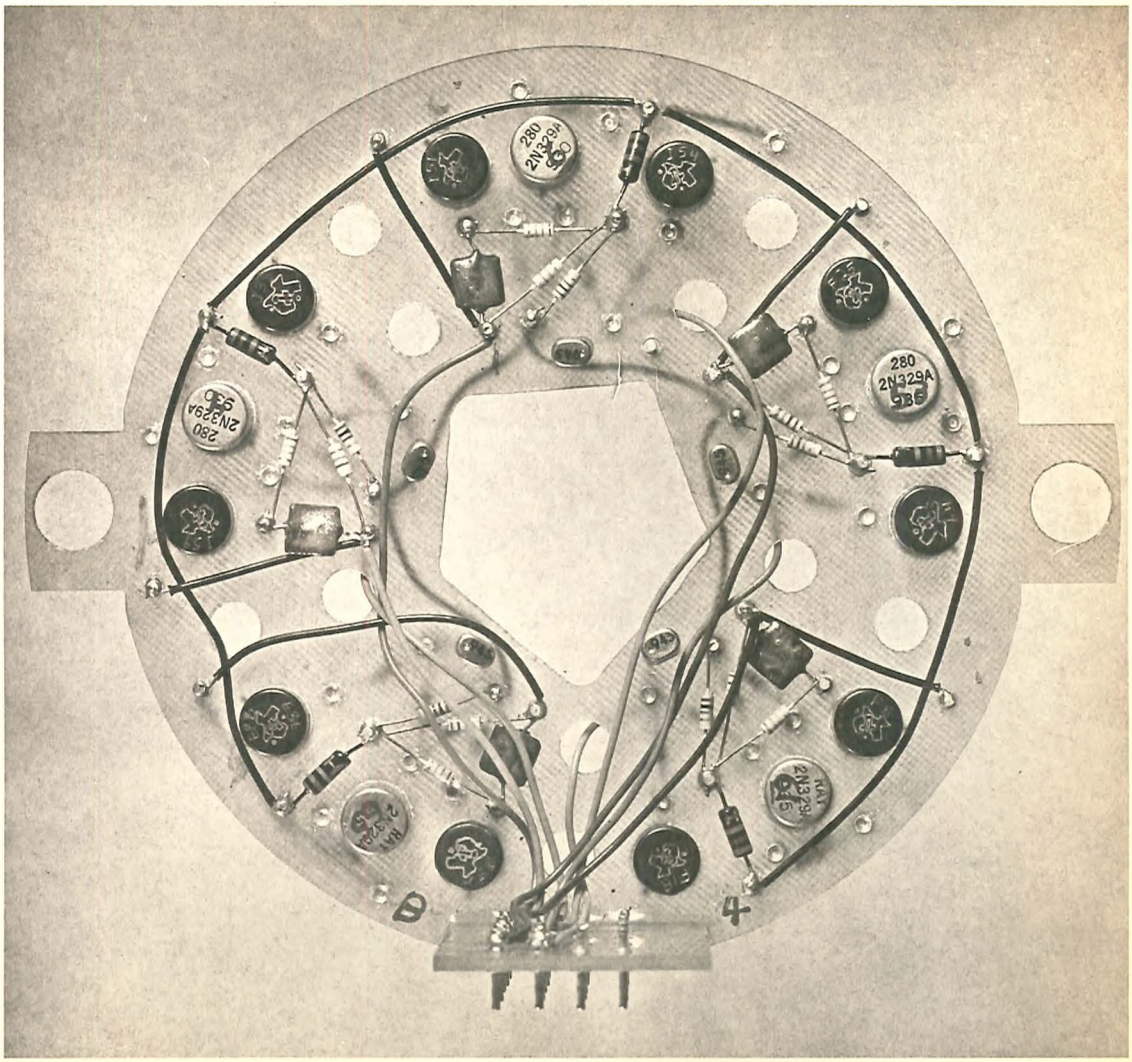

Fig. 35

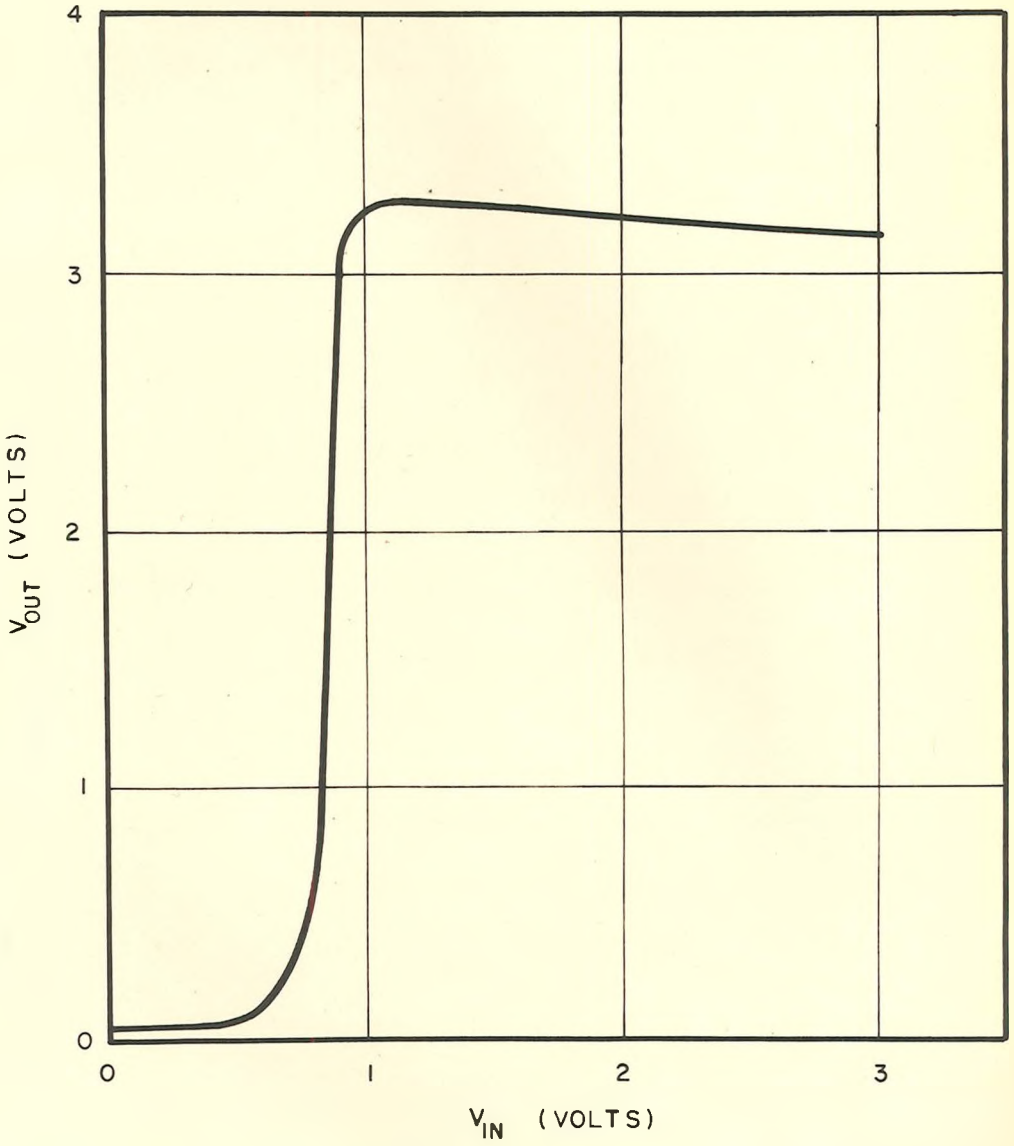

PULSE SHAPING CIRCUIT CHARACTERISTICS

Fig. 36

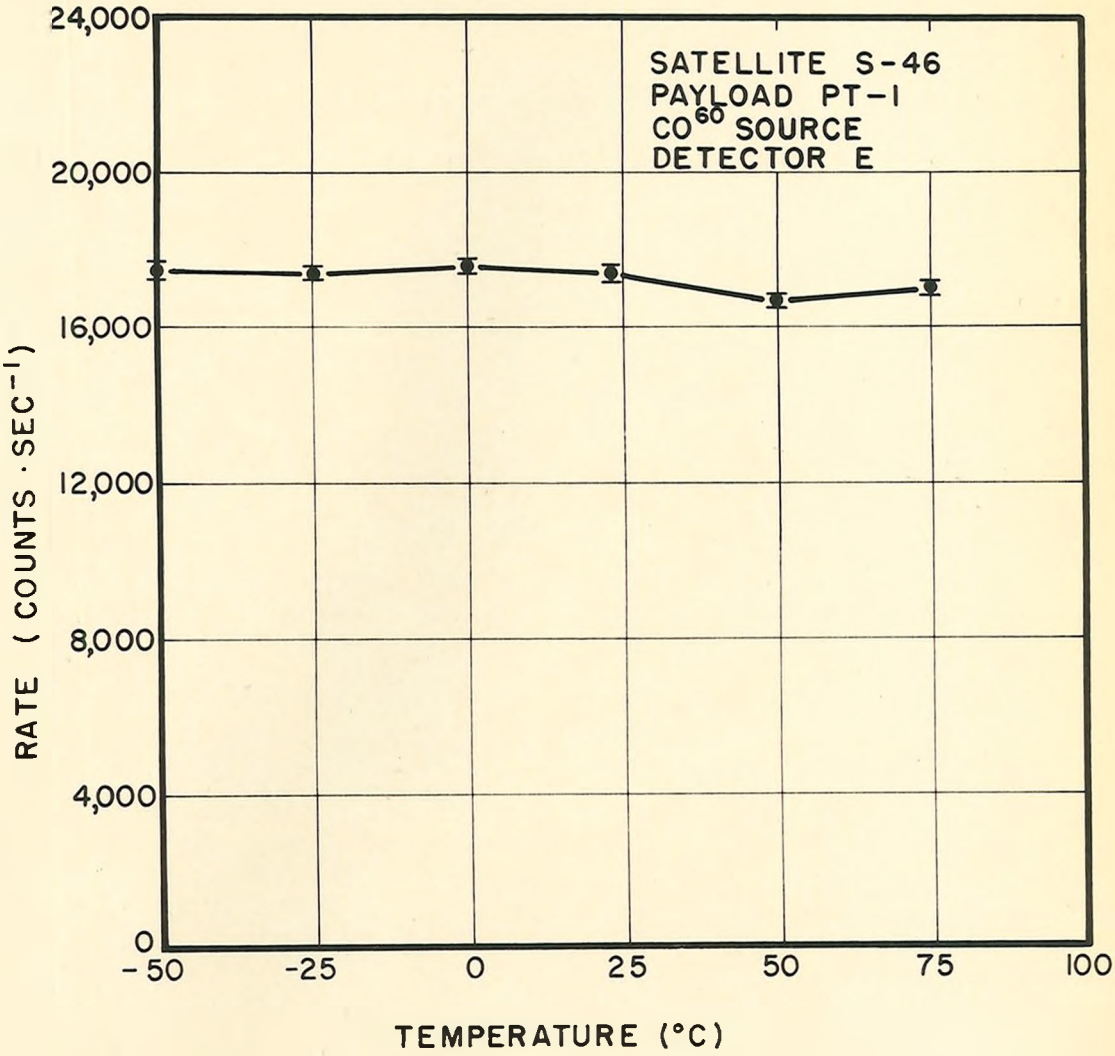

DEPENDENCE OF MAXIMUM COUNTING RATE ON TEMPERATURE

Fig. 37

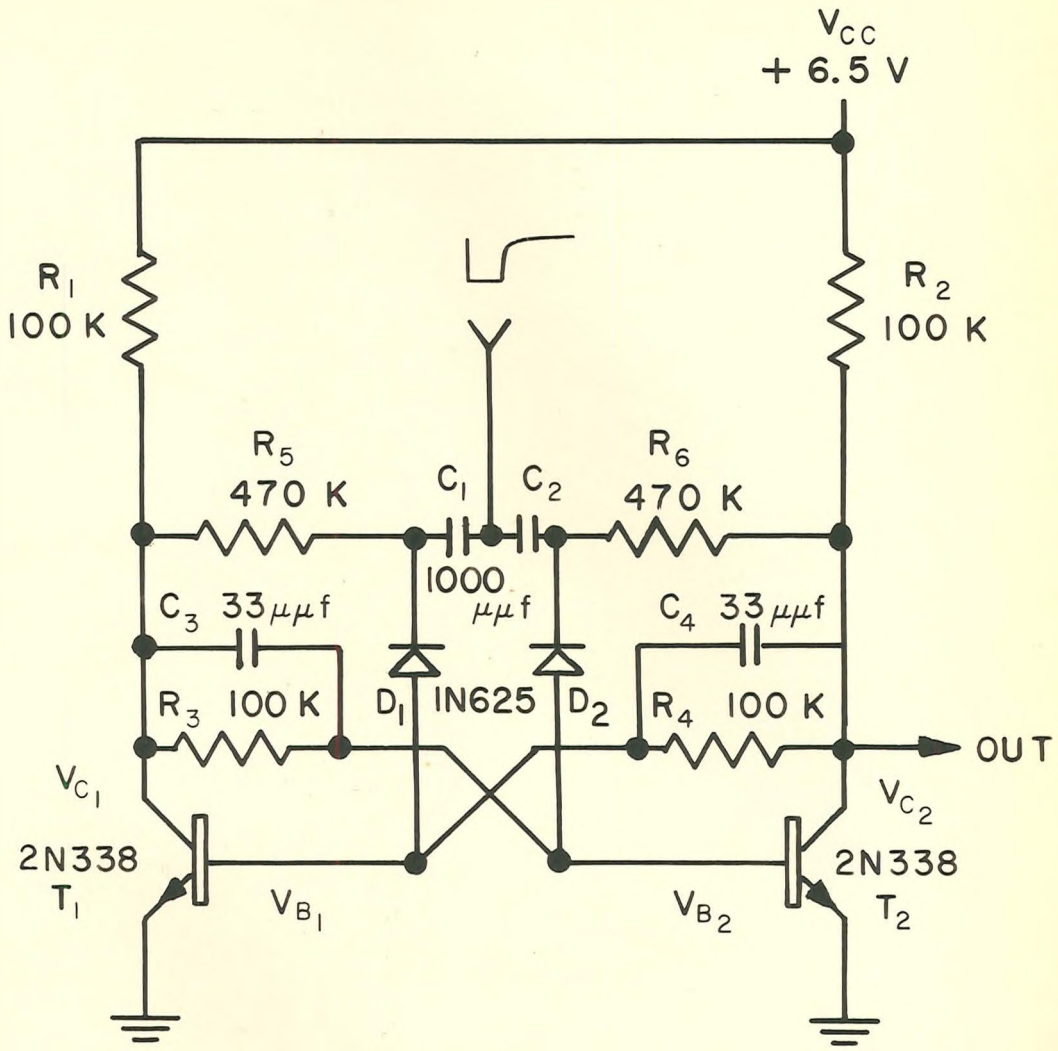

BASIC
BINARY SCALER CIRCUIT

Fig. 38

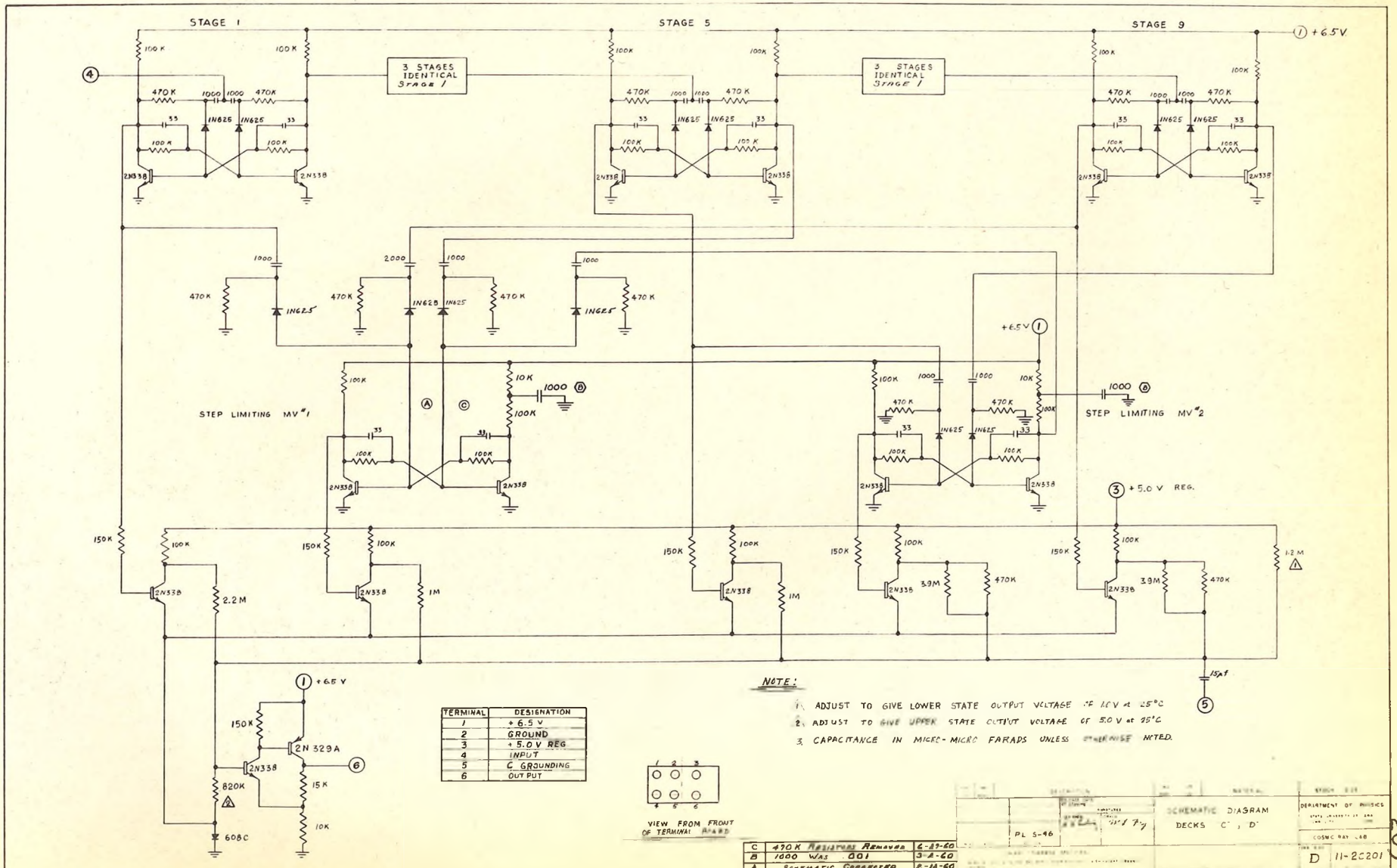

TERMINAL	DESIGNATION
1	+6.5 V
2	GROUND
3	+5.0 V REG
4	INPUT
5	C GROUNDING
6	OUT PUT

VIEW FROM FRONT OF TERMINAL BOARD

Rev.	Description	Date
C	470 K Resistors Removed	6-27-60
B	1000 Was .001	5-2-60
A	Schematic Corrected	2-18-60

SCHEMATIC DIAGRAM DECKS C', D'

DEPARTMENT OF PHYSICS
COSMIC RAY LAB

D 11-20201

205

Fig. 39

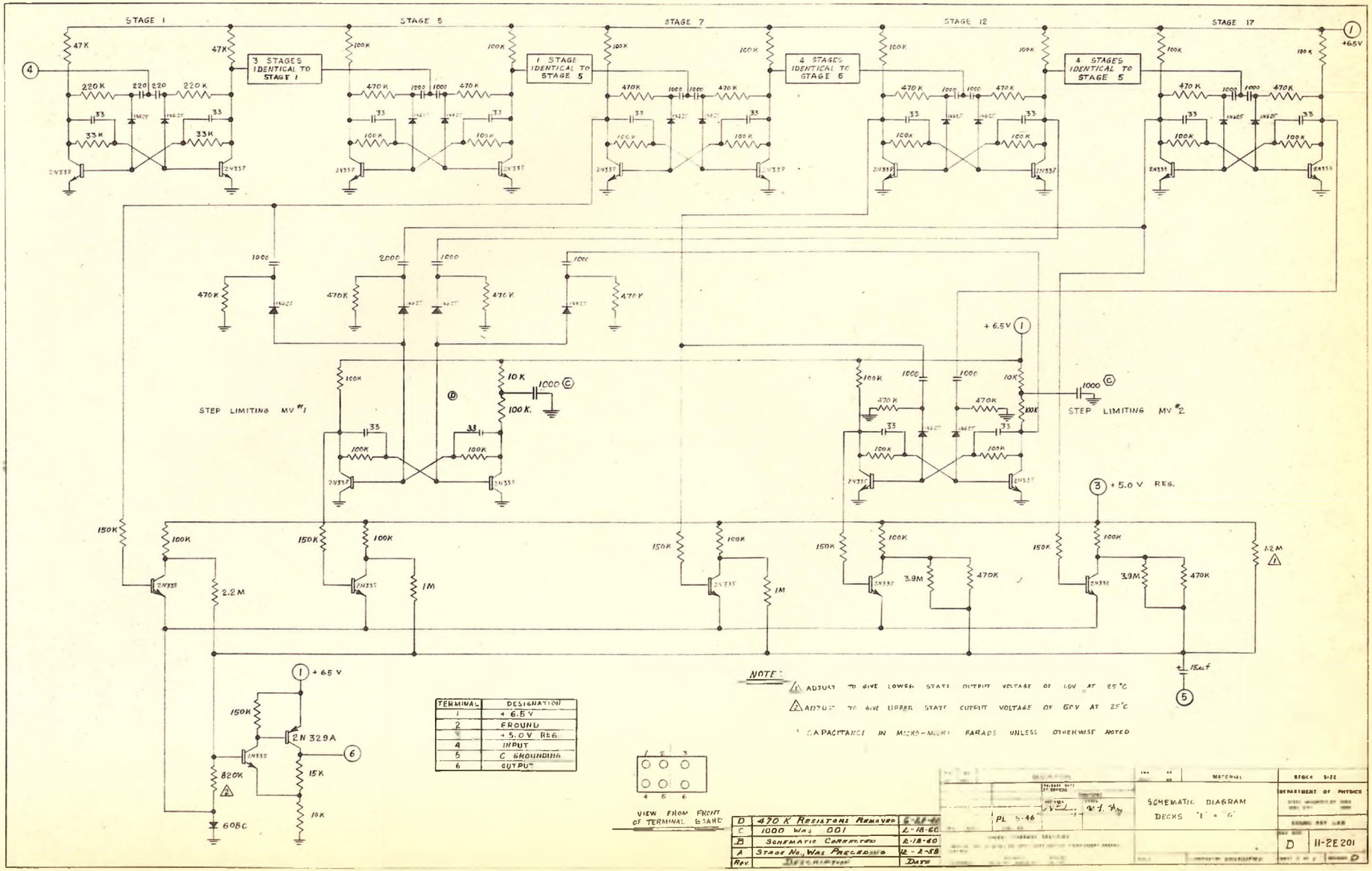

TERMINAL	DESIGNATION
1	+ 6.5 V
2	GROUND
3	+ 5.0 V REG
4	INPUT
5	C GROUNDING
6	OUTPUT

Rev.	Description	Date
D	470 K Resistors Removed	6-22-60
C	1000 Was 001	2-18-60
B	Schematic Corrected	2-18-60
A	Stage No. Was Preceding	12-2-58

Fig. 40

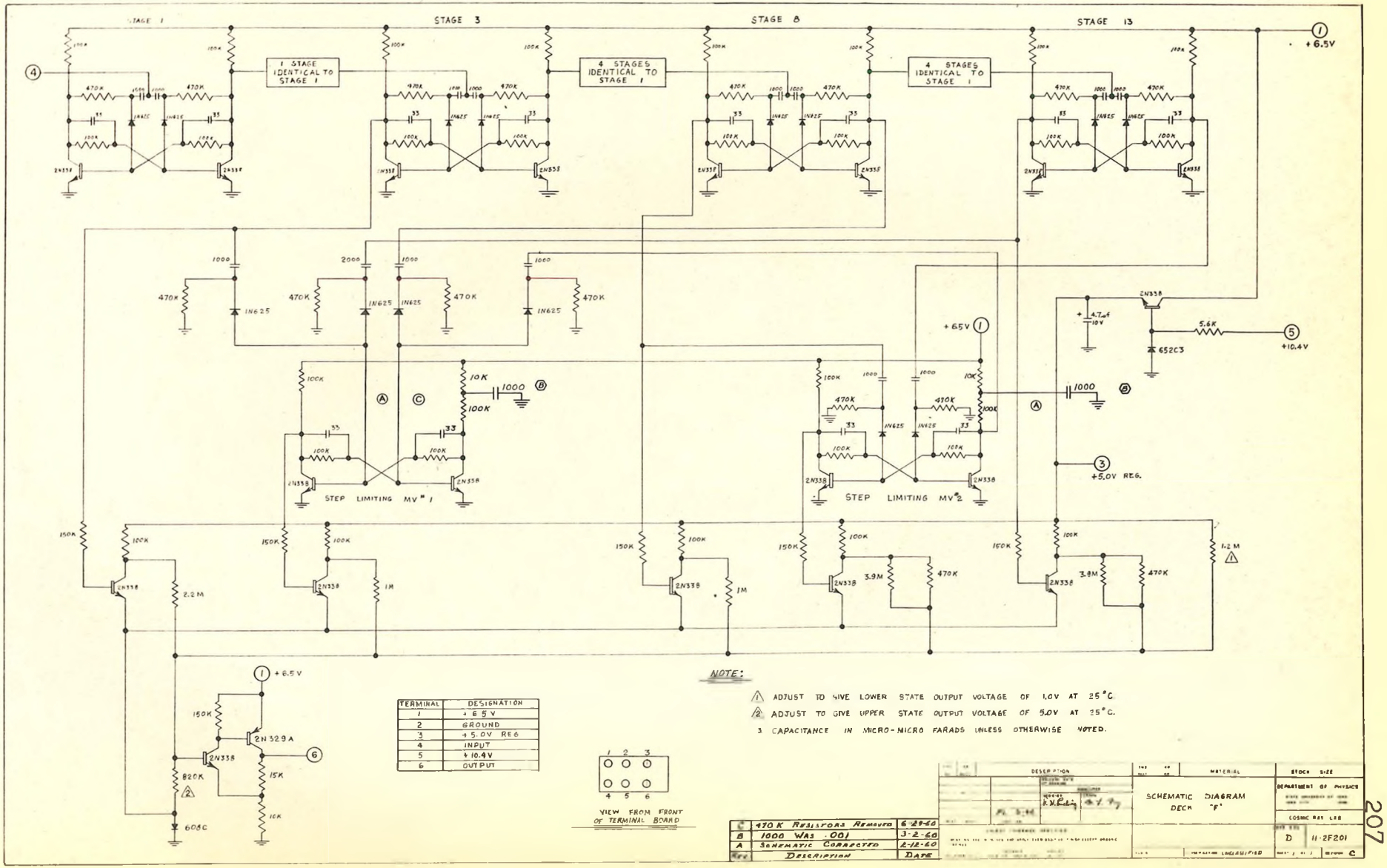

TERMINAL	DESIGNATION
1	+6.5V
2	GROUND
3	+5.0V REG
4	INPUT
5	+10.4V
6	OUTPUT

VIEW FROM FRONT OF TERMINAL BOARD

REV	DESCRIPTION	DATE
C	470K RESISTORS REMOVED	6-29-60
B	1000 WAS .001	3-2-60
A	SCHEMATIC CORRECTED	2-12-60

Fig. 41

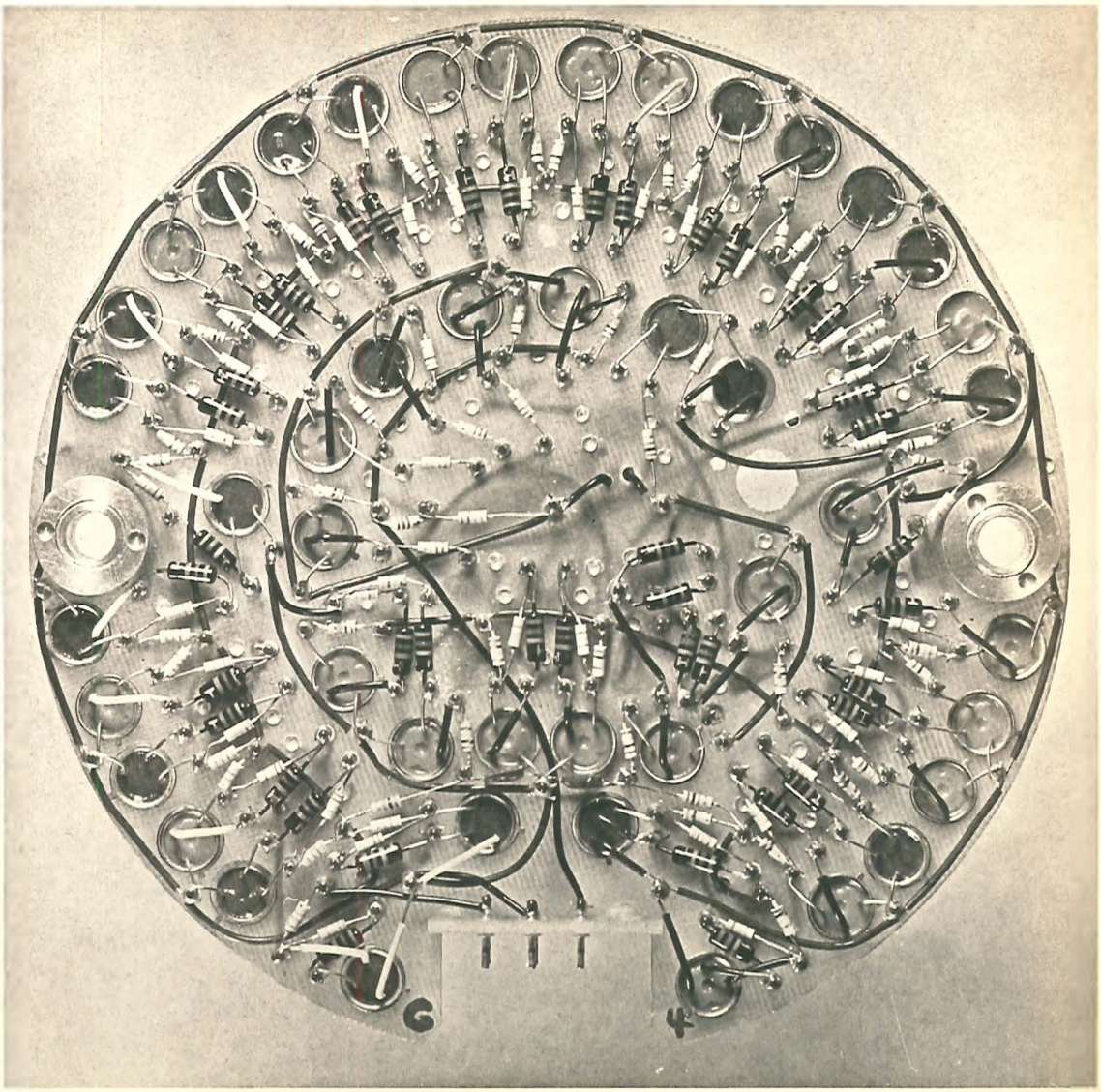

Fig. 42

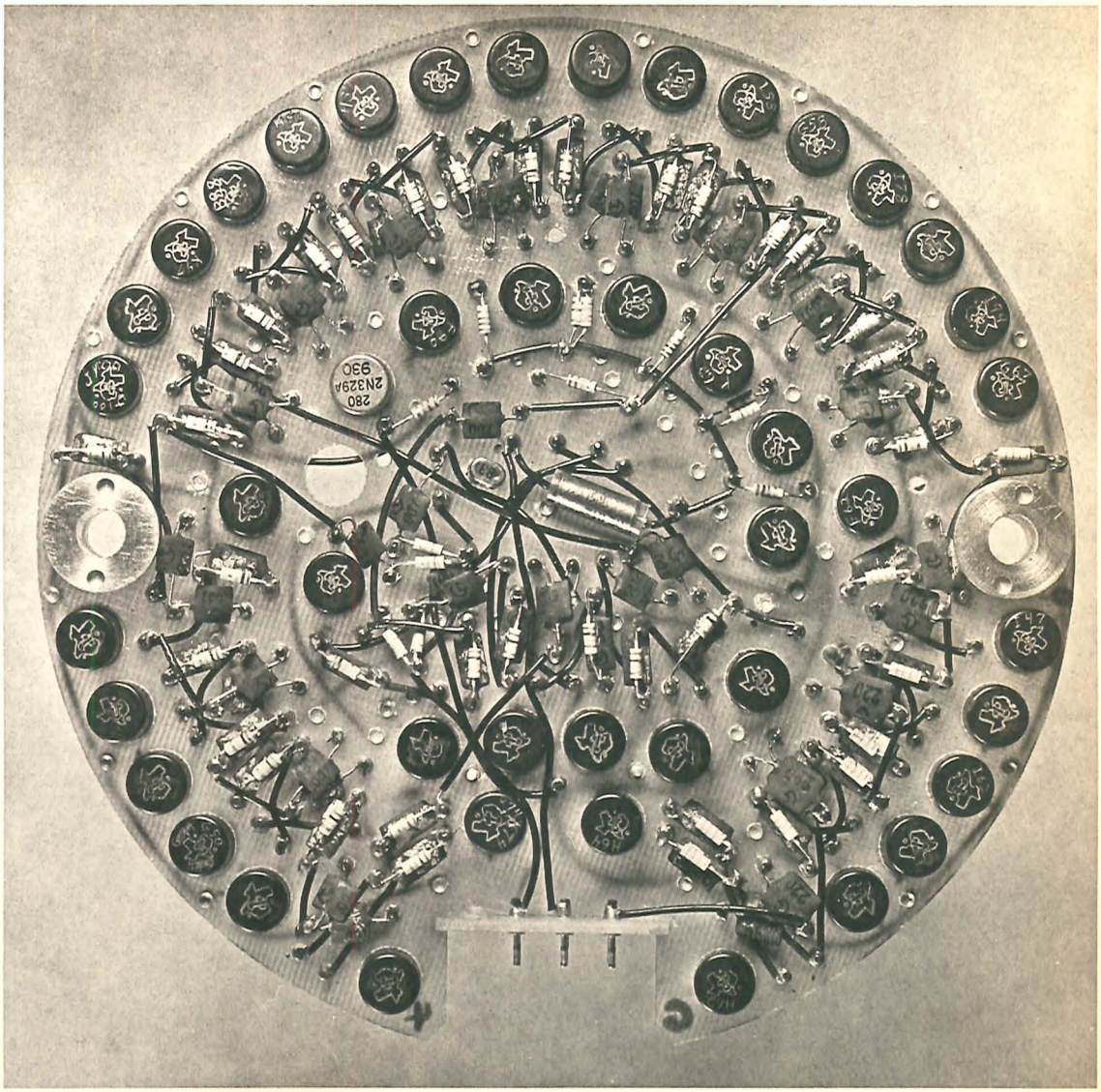

Fig. 43

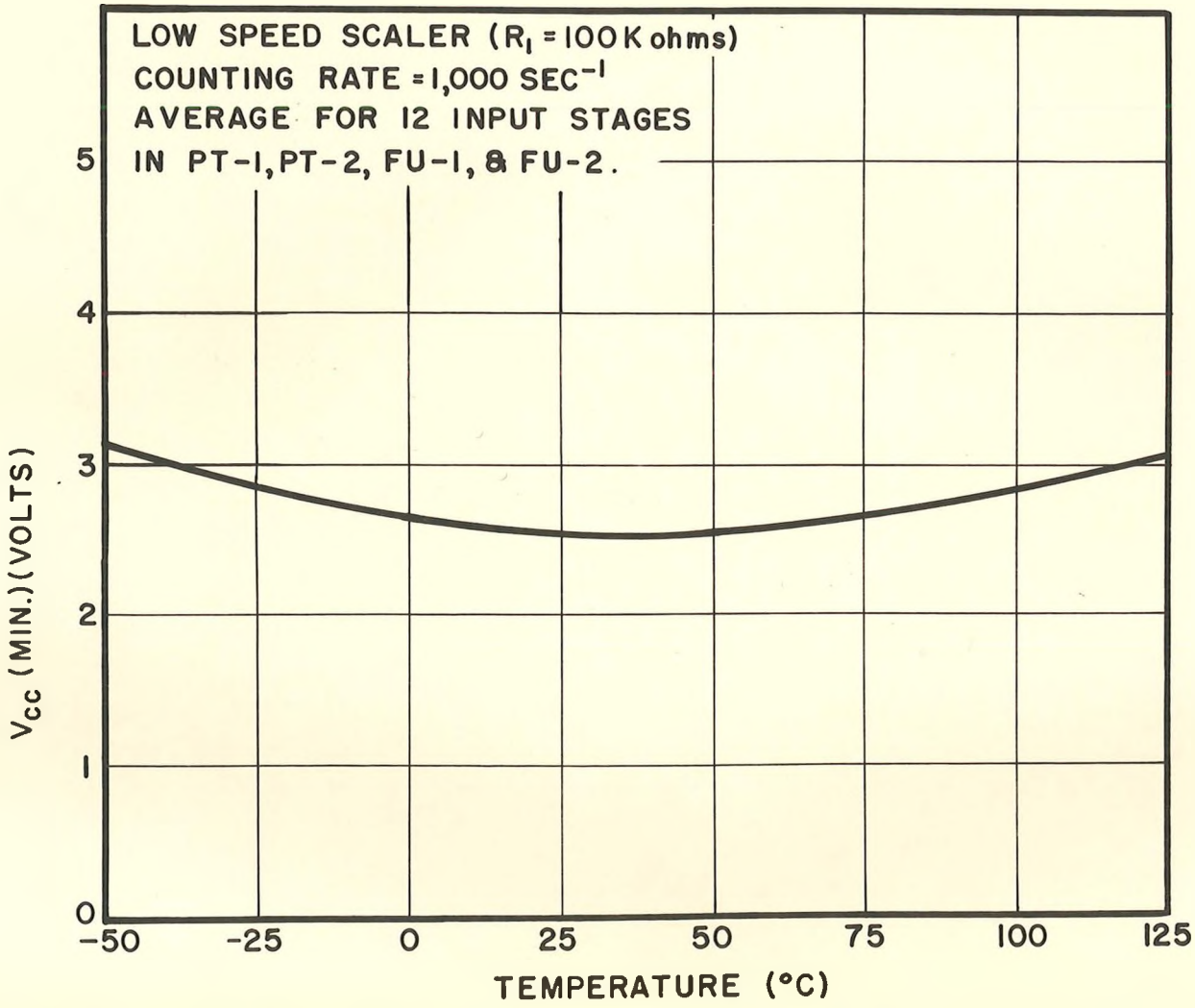

MINIMUM SUPPLY VOLTAGE V_{cc} FOR SCALER OPERATION

Fig. 44

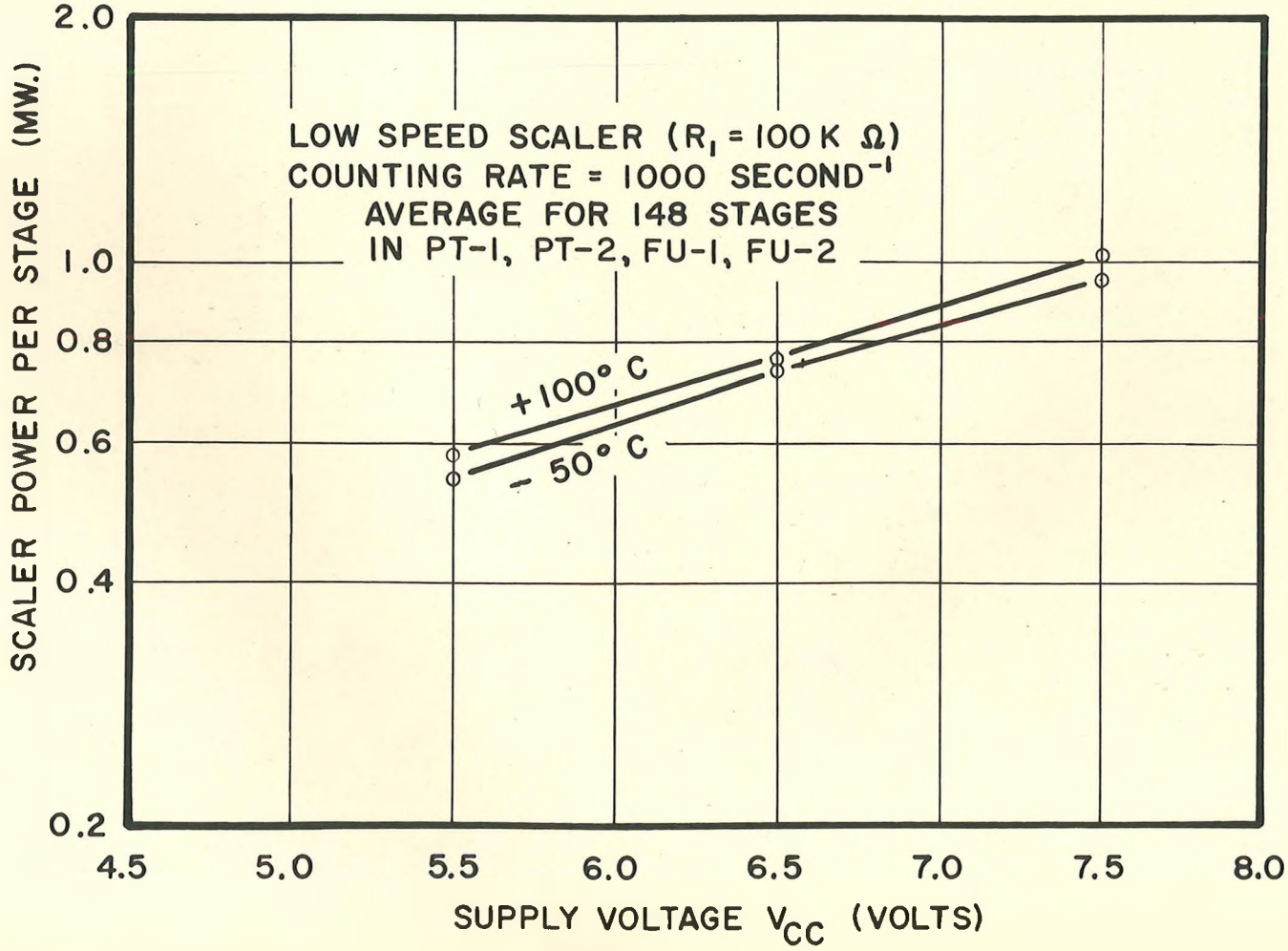

SCALER POWER REQUIREMENTS
Fig. 45

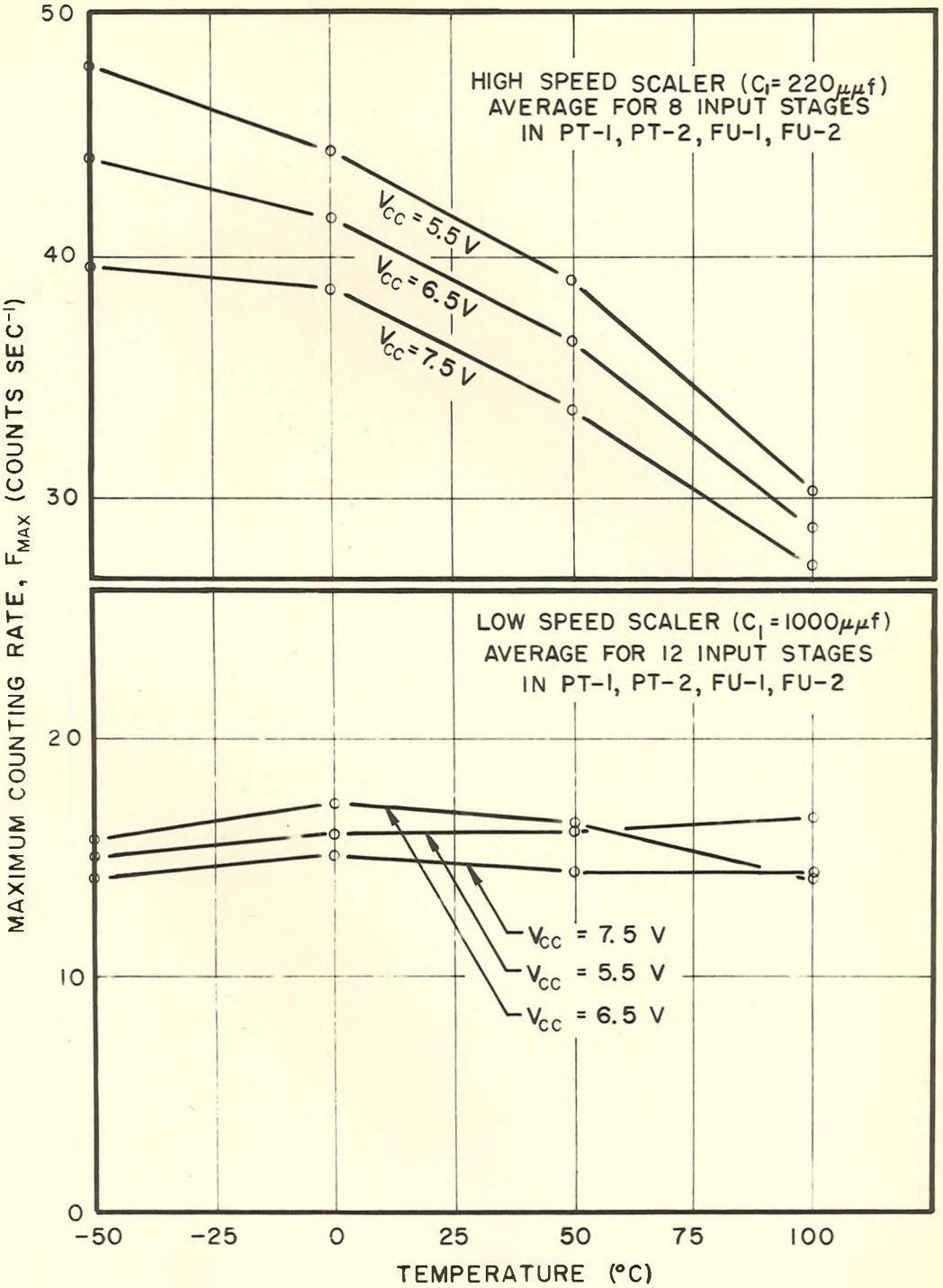

SCALER MAXIMUM COUNTING RATE

Fig. 46

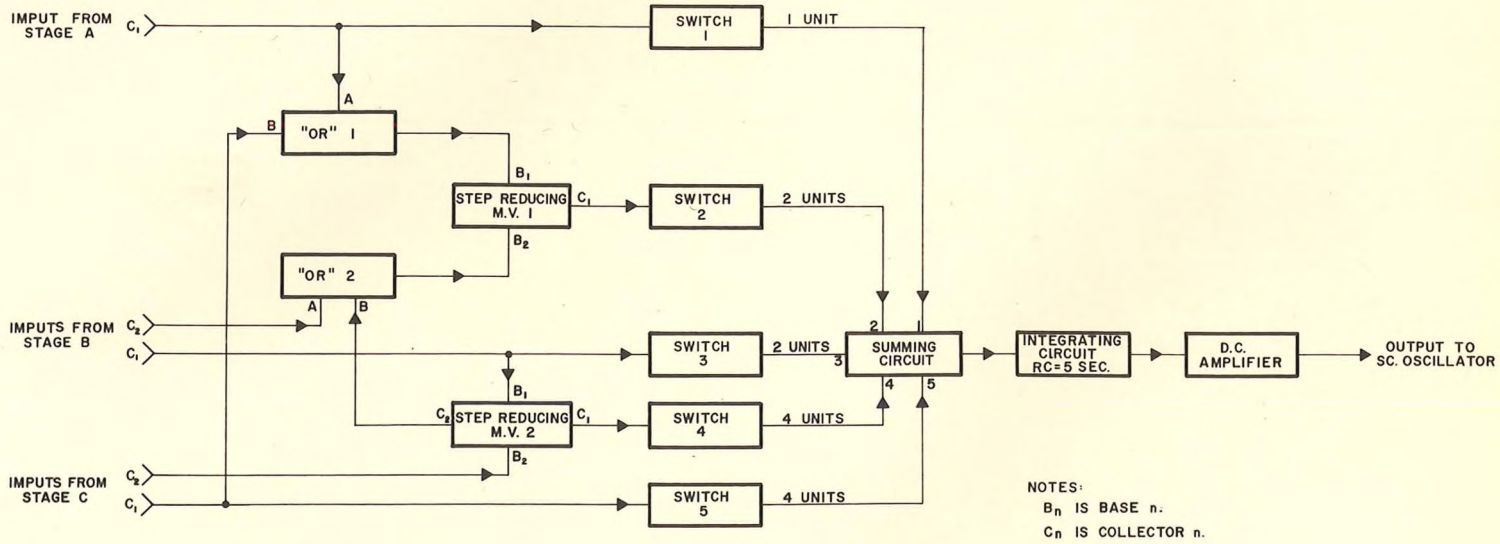

BLOCK DIAGRAM OF LOGIC & OUTPUT AMPLIFIER CIRCUITS

Fig. 47

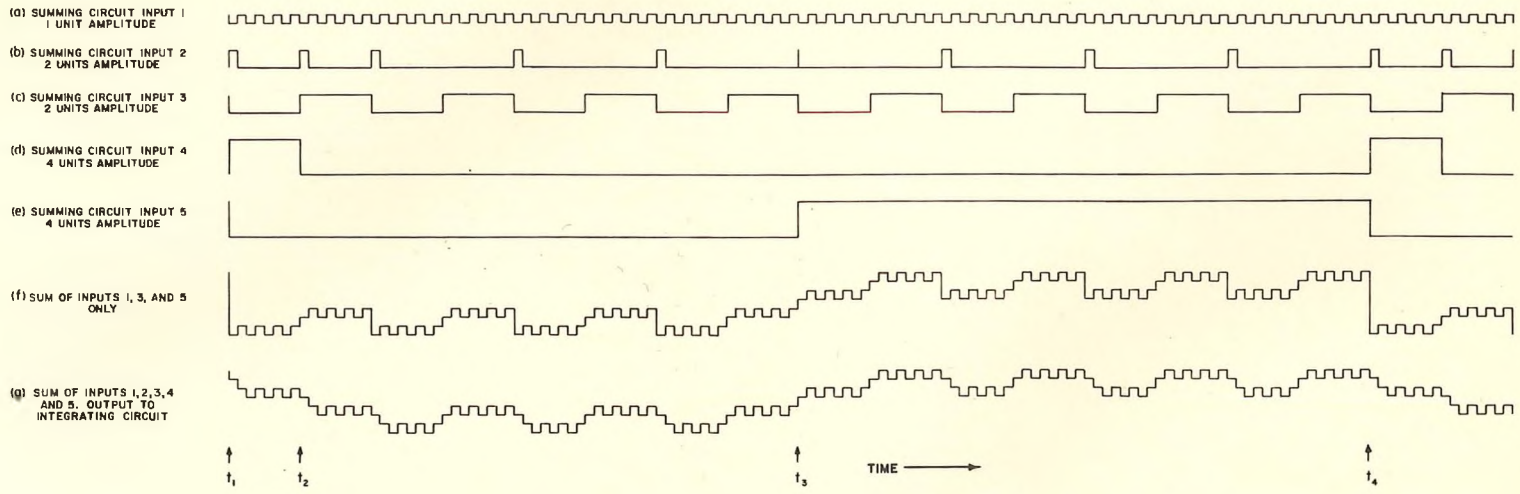

NOTE: RATE, SCALER STAGE A = 8 X RATE, STAGE B = 64 X RATE, STAGE C

LOGIC CIRCUIT WAVEFORMS

Fig. 48

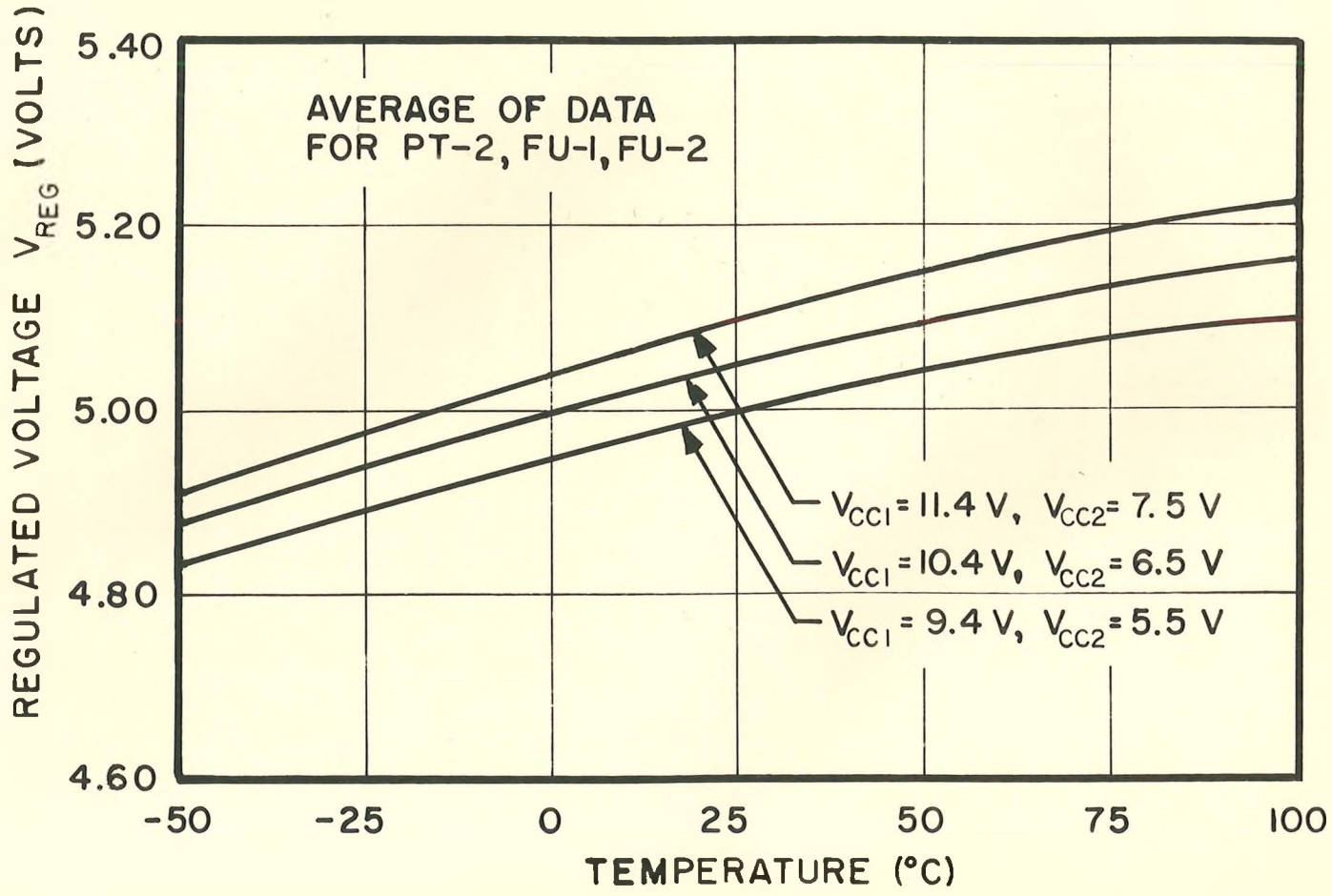

VOLTAGE REGULATOR CHARACTERISTICS

Fig. 49

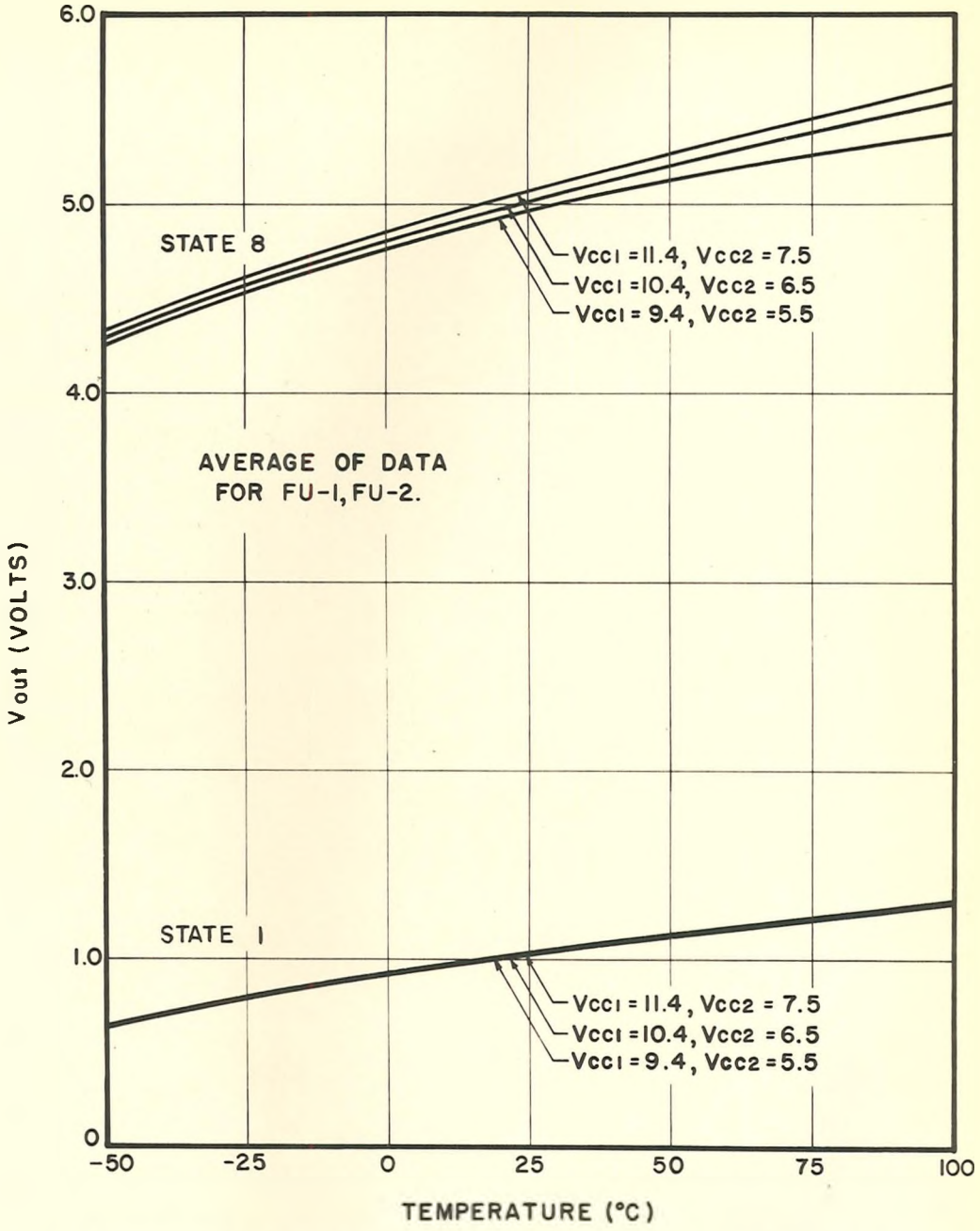

OUTPUT VOLTAGE FOR STATES ONE AND EIGHT

Fig. 50

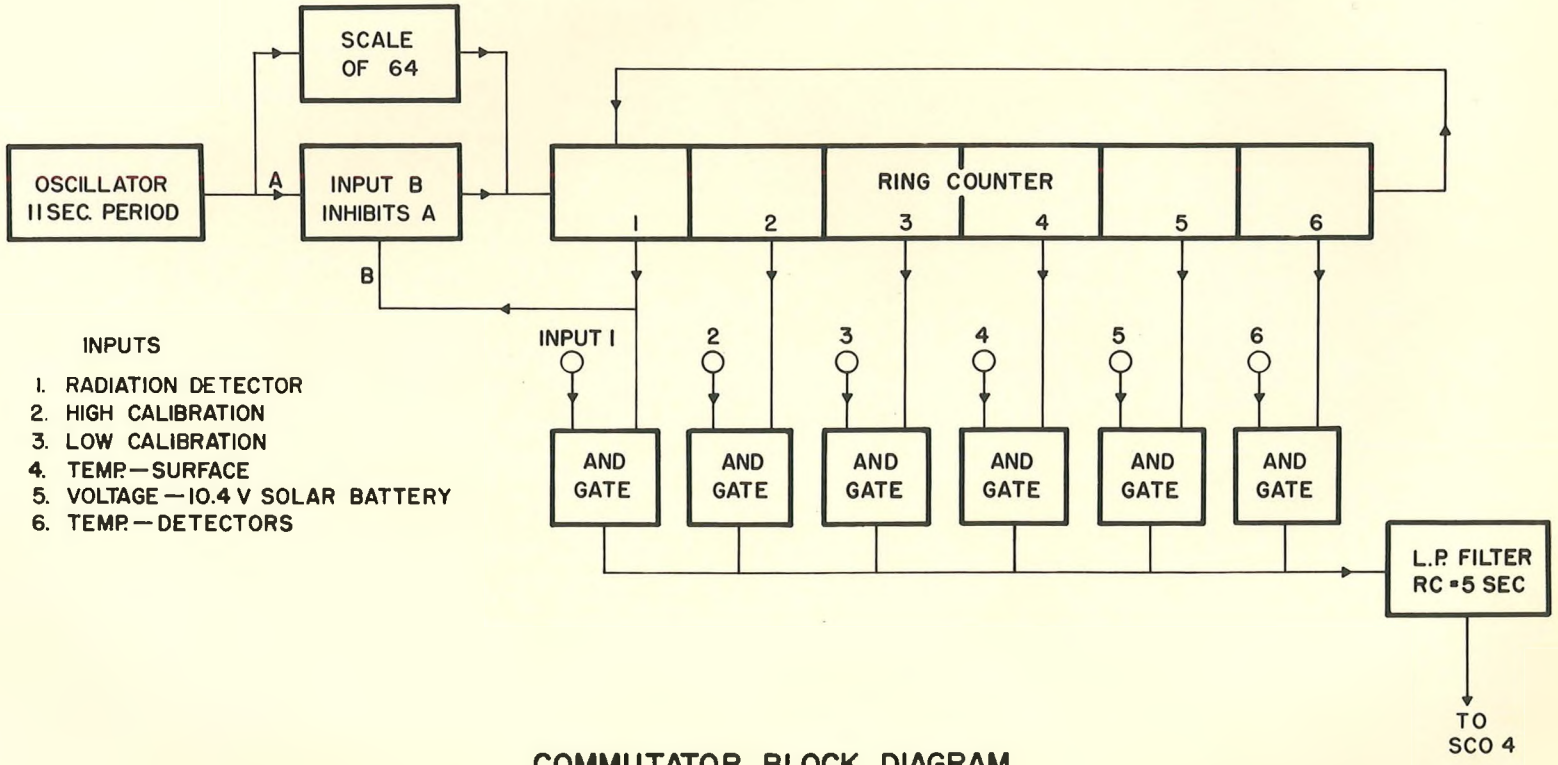

COMMUTATOR BLOCK DIAGRAM

Fig. 51

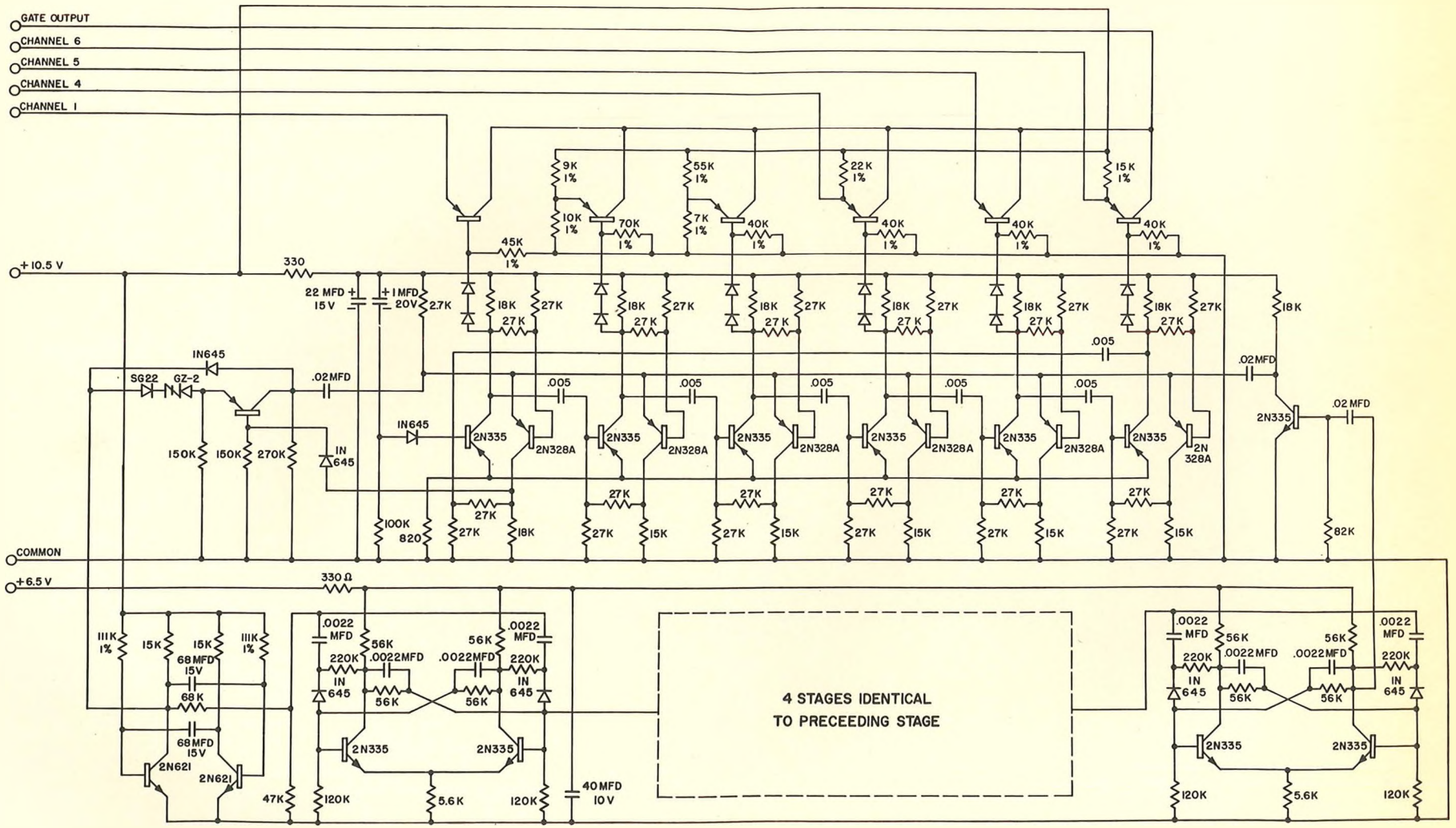

CHANNEL ALLOCATION CHART

CHAN. 1 – SUI RADIATION DATA
CHAN. 2 – HIGH CALIBRATION
CHAN. 3 – LOW CALIBRATION
CHAN. 4 – TEMP, SKIN
CHAN. 5 – SOLAR CELL VOLTAGE (10.4V SYSTEM)
CHAN. 6 – TEMP, SUI PACKAGE

NOTES:
1. ALL TRANSISTORS TI367 UNLESS OTHERWISE NOTED.
2. ALL DIODES IN482B UNLESS OTHERWISE NOTED.
3. ALL RESISTORS 10% UNLESS OTHERWISE NOTED.
4. ALL CAPACITORS 50V UNLESS OTHERWISE NOTED.
5. OUTPUT TO BE TERMINATED IN 68K.
6. SUPPLY VOLTAGE ±10%.
7. CIRCUIT DESIGNED BY ARMY BALLISTIC MISSILE AGENCY

SCHEMATIC DIAGRAM — COMMUTATOR
Fig. 52

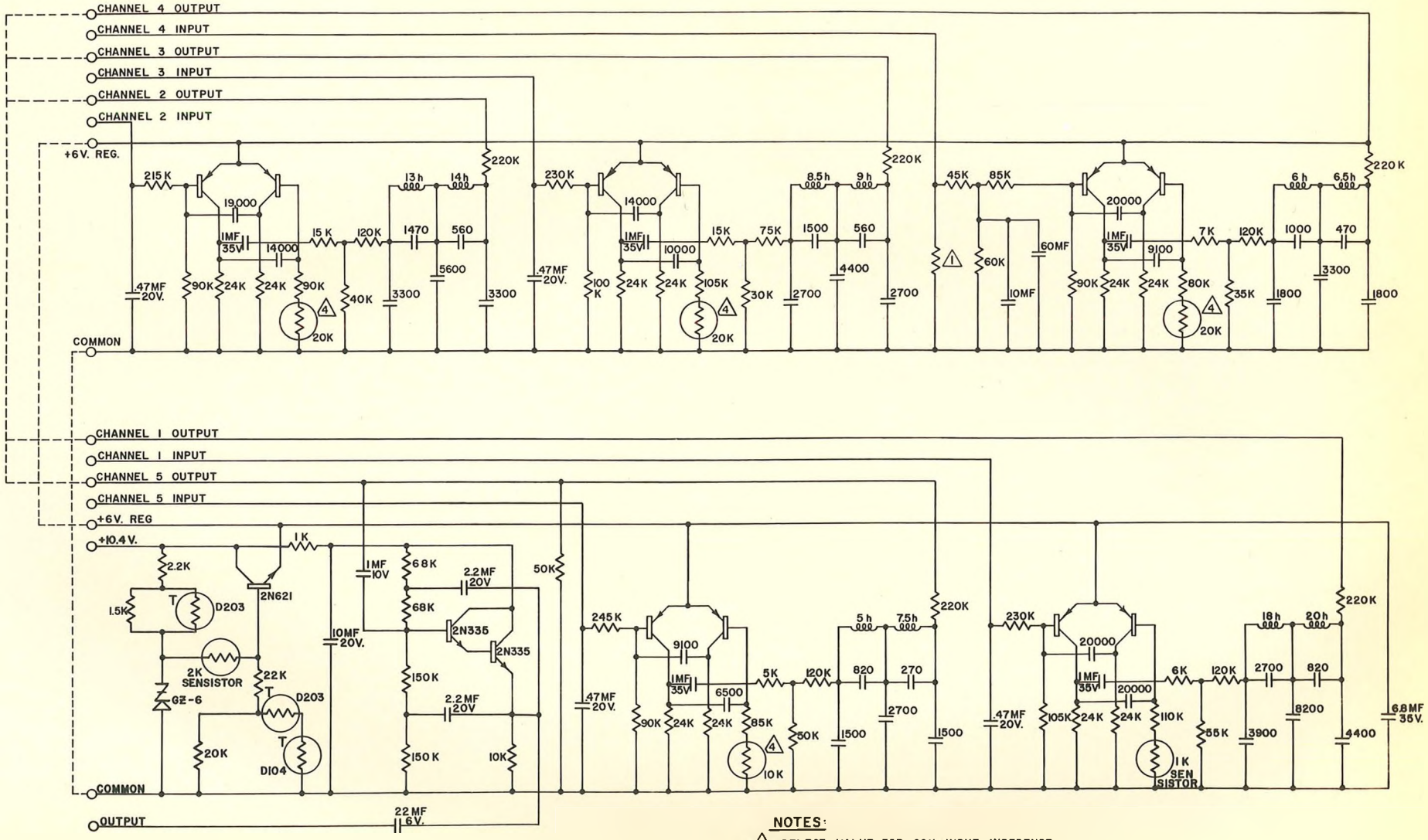

Fig. 53. SCHEMATIC DIAGRAM — SUBCARRIER OSCILLATORS

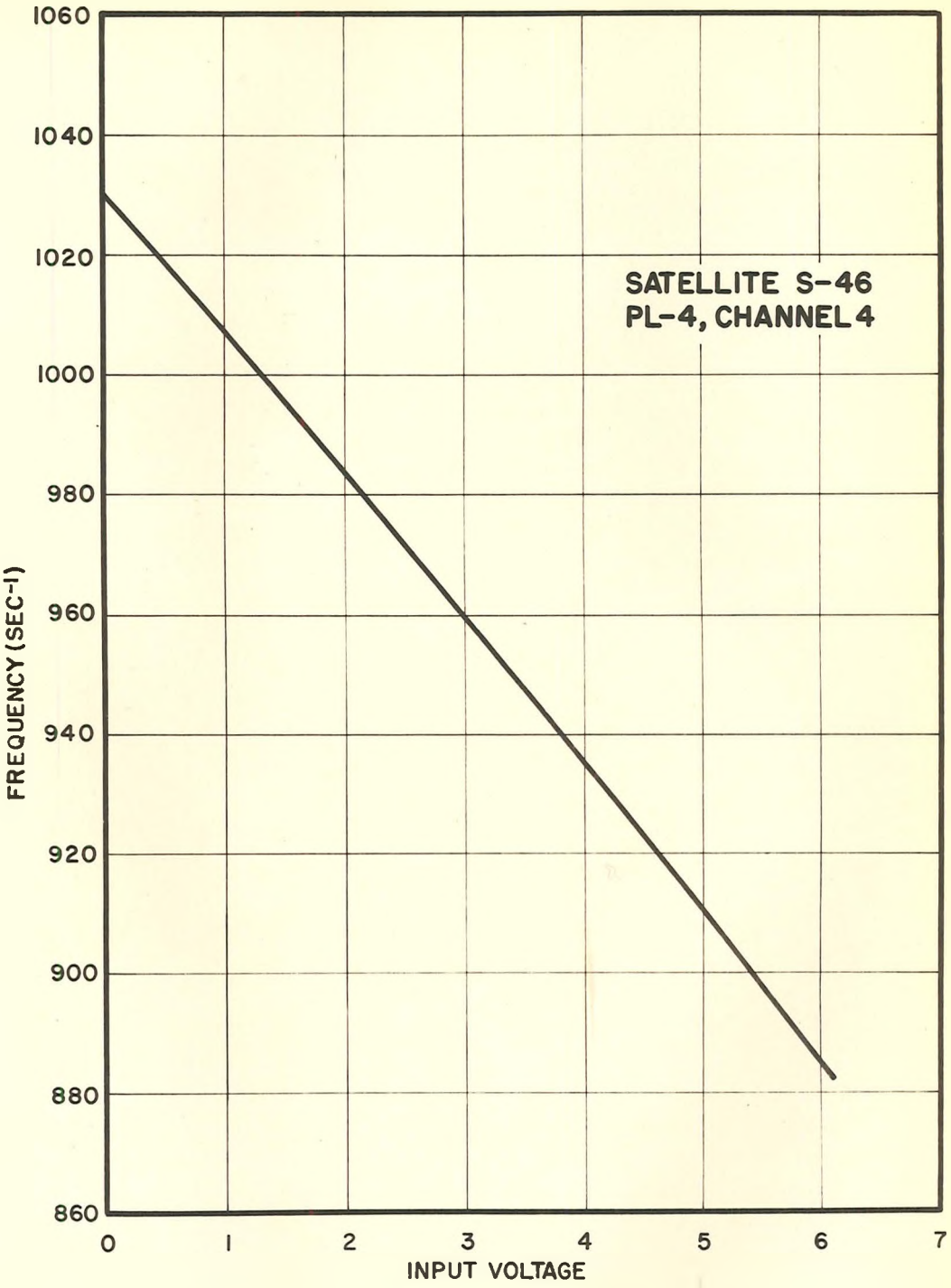

SUBCARRIER OSCILLATOR FREQUENCY CALIBRATION

Fig. 54

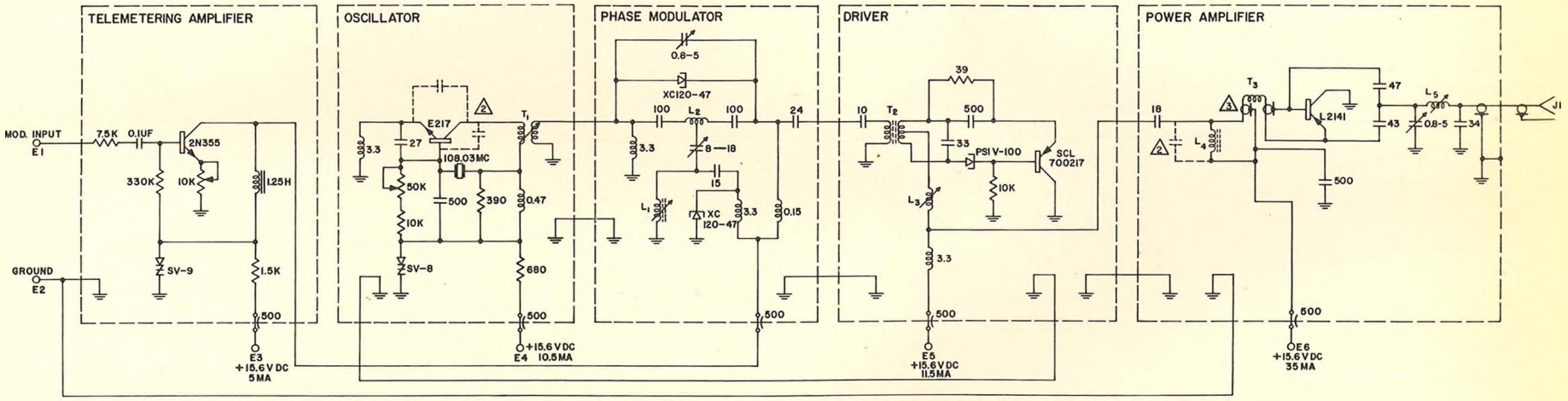

NOTES:

1. UNLESS OTHERWISE NOTED:
   ALL RESISTORS ARE IN OHMS 1/2W ±5%
   ALL CAPACITORS ARE IN MMF
   ALL INDUCTORS ARE IN UH

2 – INDICATES DISTRIBUTED CAPACITANCE

3 – BALUN TRANSFORMER

4. CIRCUIT DESIGNED BY ARMY BALLISTIC MISSILE AGENCY

SCHEMATIC DIAGRAM – TELEMETRY TRANSMITTER

Fig. 55

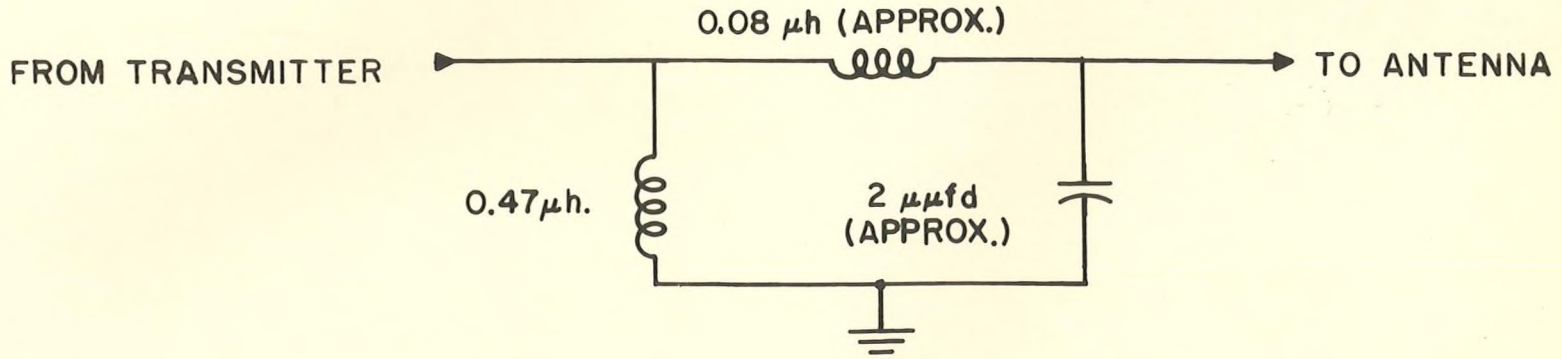

ANTENNA MATCHING NETWORK

Fig. 56

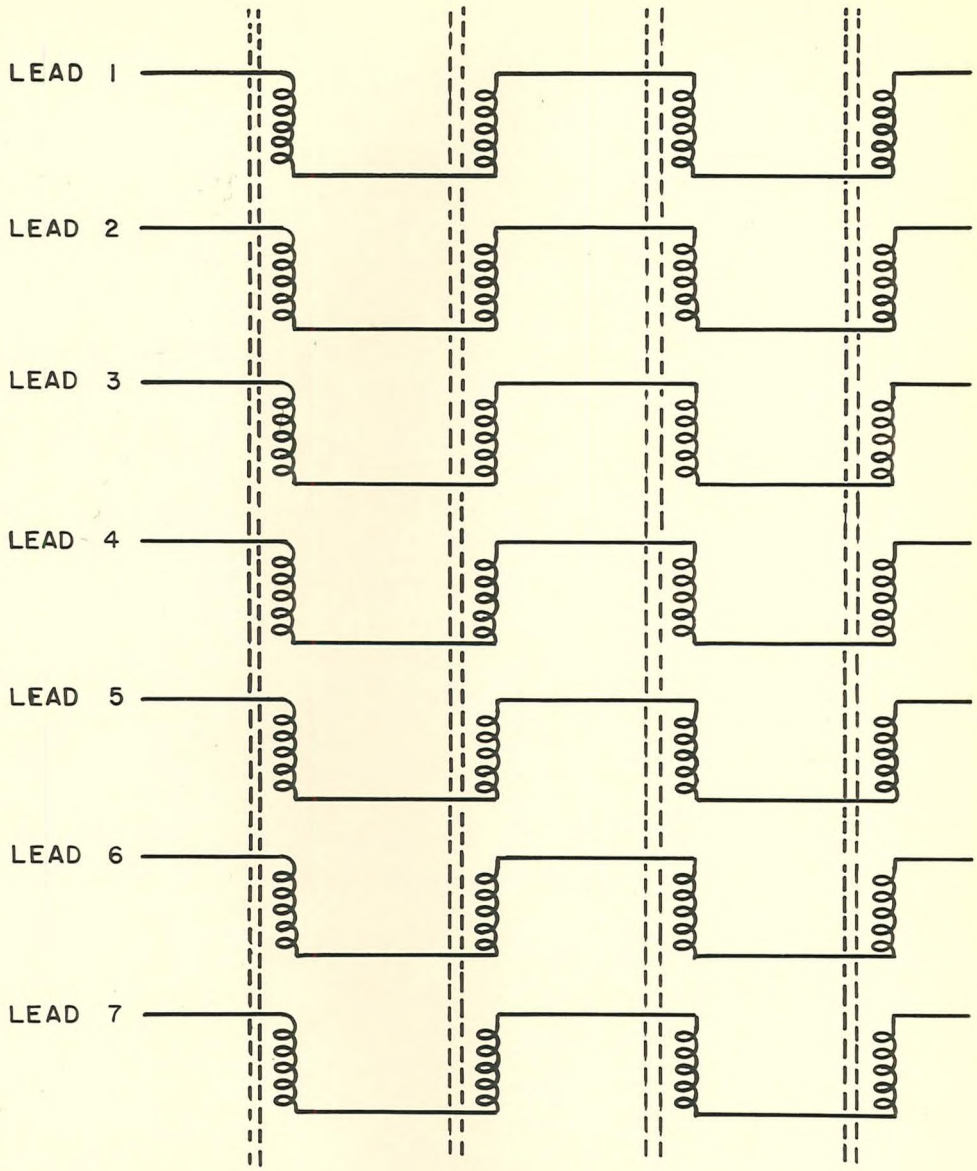

NOTES:

1. ALL COILS 5 TURNS
2. ALL FERRITE CORES GENERAL CERAMICS CORP. TYPE Q-2

EXTERNAL LEAD ISOLATING FILTERS

Fig. 57

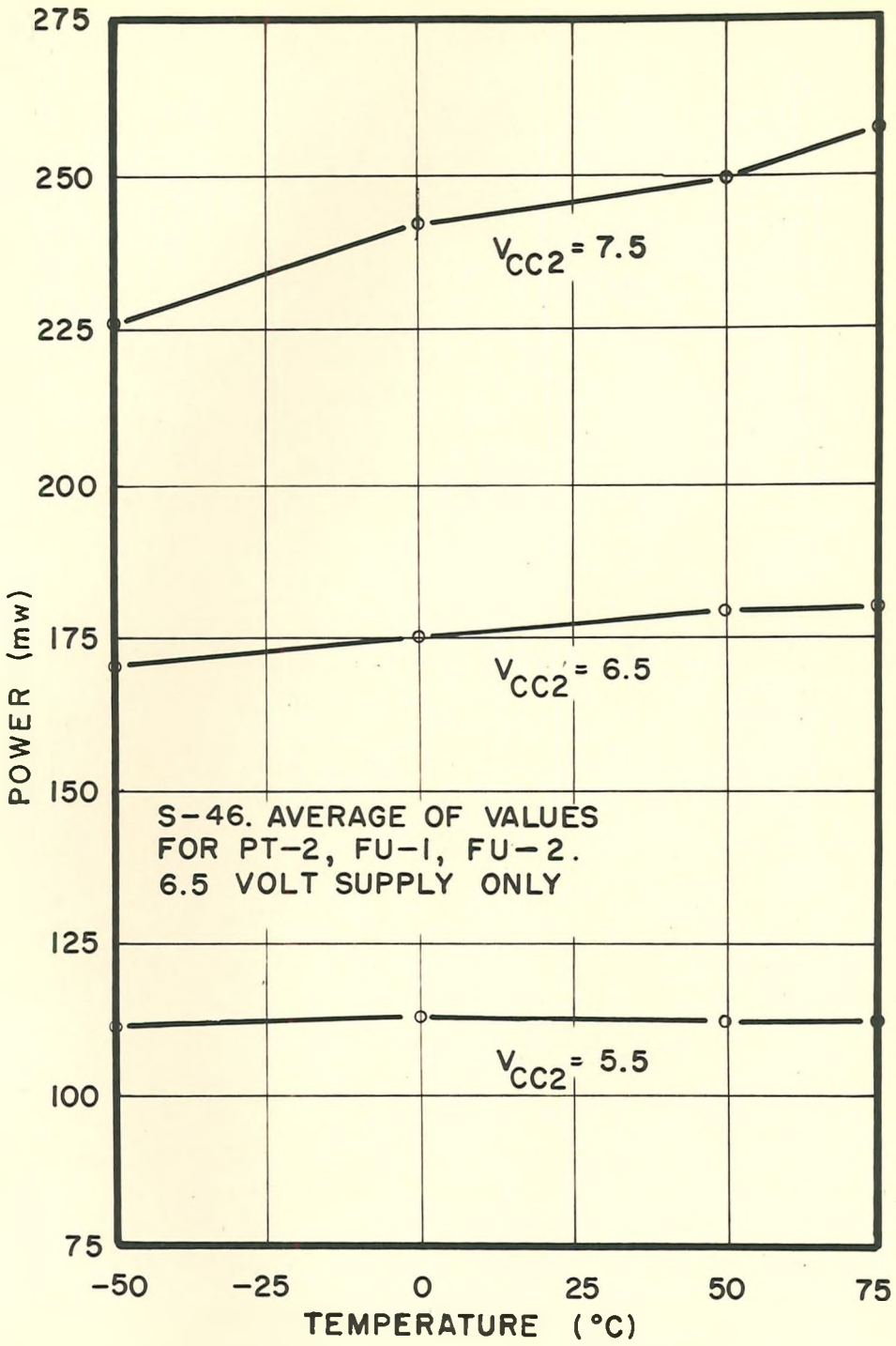

POWER REQUIREMENTS OF SUI INSTRUMENTS

Fig. 58

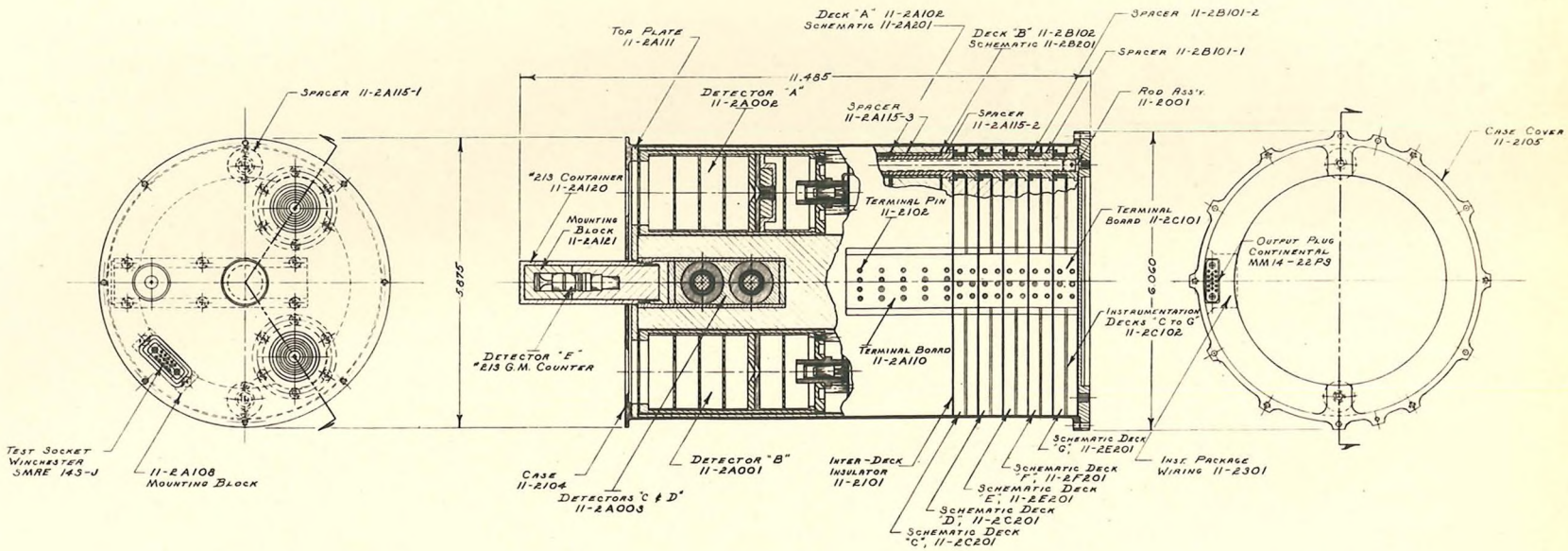
Top Plate 11-2A111
Deck "A" 11-2A102 Schematic 11-2A201
Deck "B" 11-2B102 Schematic 11-2B201
Spacer 11-2B101-2
Spacer 11-2B101-1
11.485
Spacer 11-2A115-1
Detector "A" 11-2A002
Spacer 11-2A115-3
Spacer 11-2A115-2
Rod Ass'y. 11-2001
Case Cover 11-2105
"213 Container 11-2A120
Mounting Block 11-2A121
Terminal Pin 11-2102
Terminal Board 11-2C101
Output Plug Continental MM14-22P3
3.875
6.000
Instrumentation Decks "C to G" 11-2C102
Detector "E" "213 G.M. Counter
Terminal Board 11-2A110
Test Socket Winchester SMRE 143-J
11-2A108 Mounting Block
Case 11-2104
Detectors "C & D" 11-2A003
Detector "B" 11-2A001
Inter-Deck Insulator 11-2101
Schematic Deck "G", 11-2E201
Inst. Package Wiring 11-2301
Schematic Deck "F", 11-2F201
Schematic Deck "E", 11-2E201
Schematic Deck "D", 11-2C201
Schematic Deck "C", 11-2C201

Fig. 59

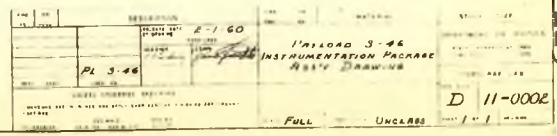
E-1 60
PL 3-46
1'Nload 3-46
Instrumentation Package
Assy Drawing
D 11-0002
Full
Unclass

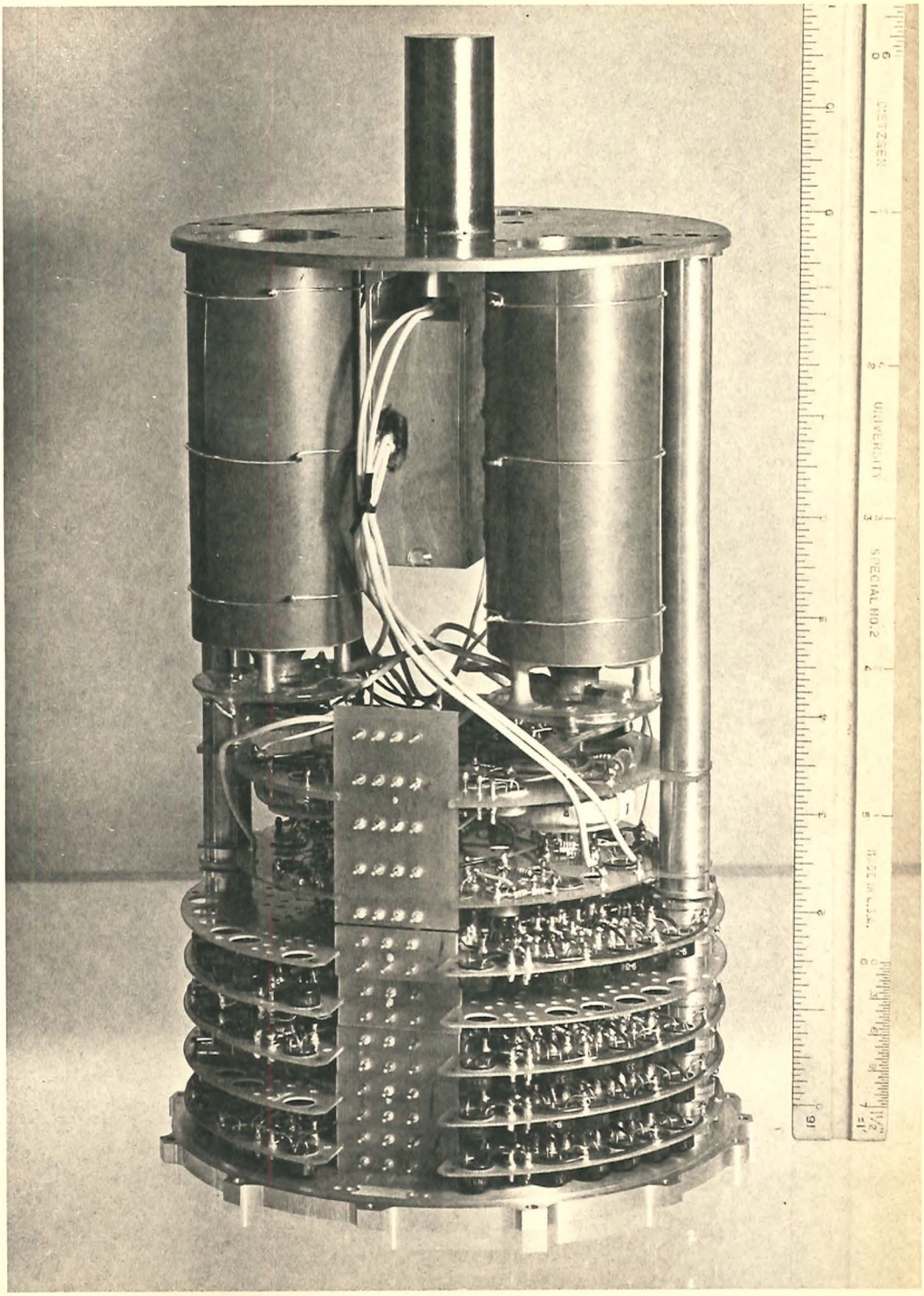

Fig. 60

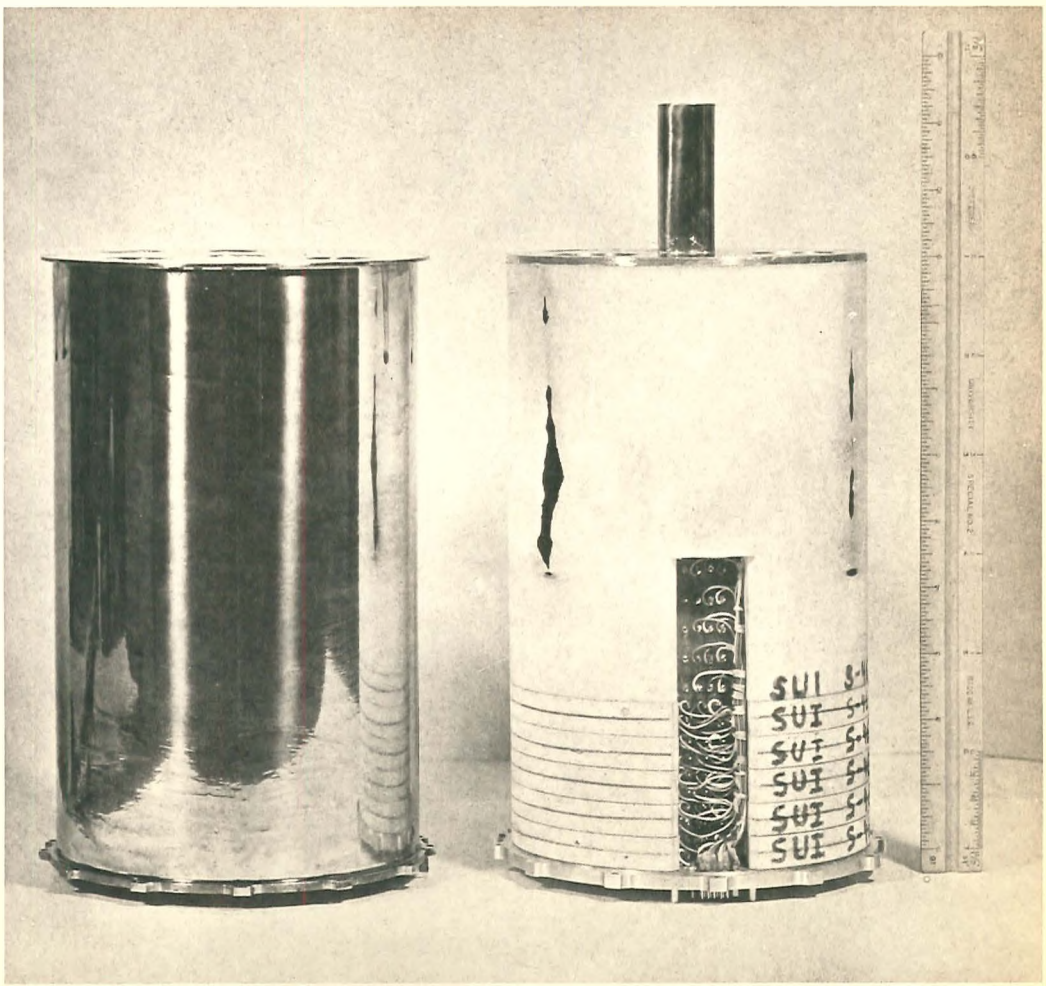

Fig. 61

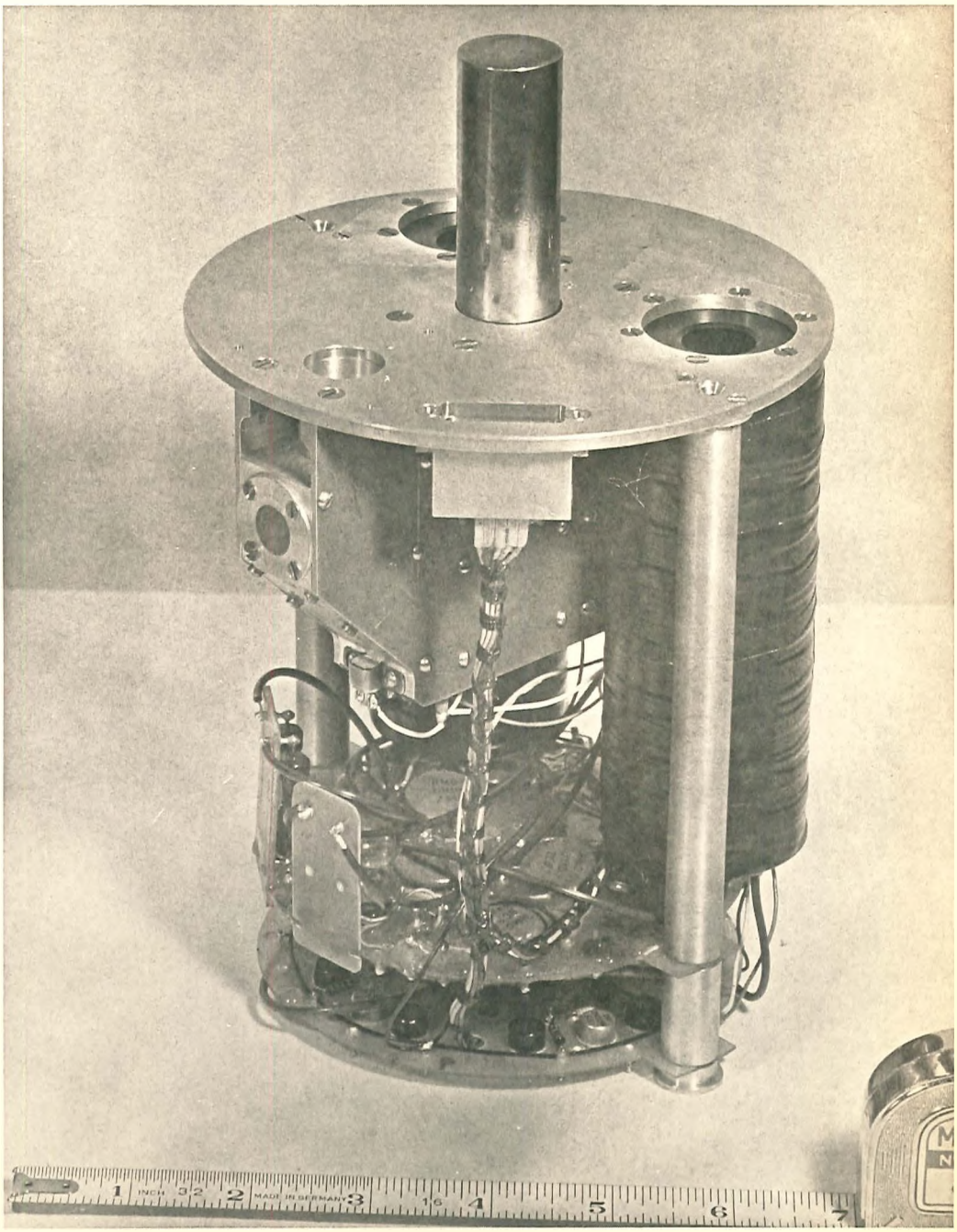

Fig. 62

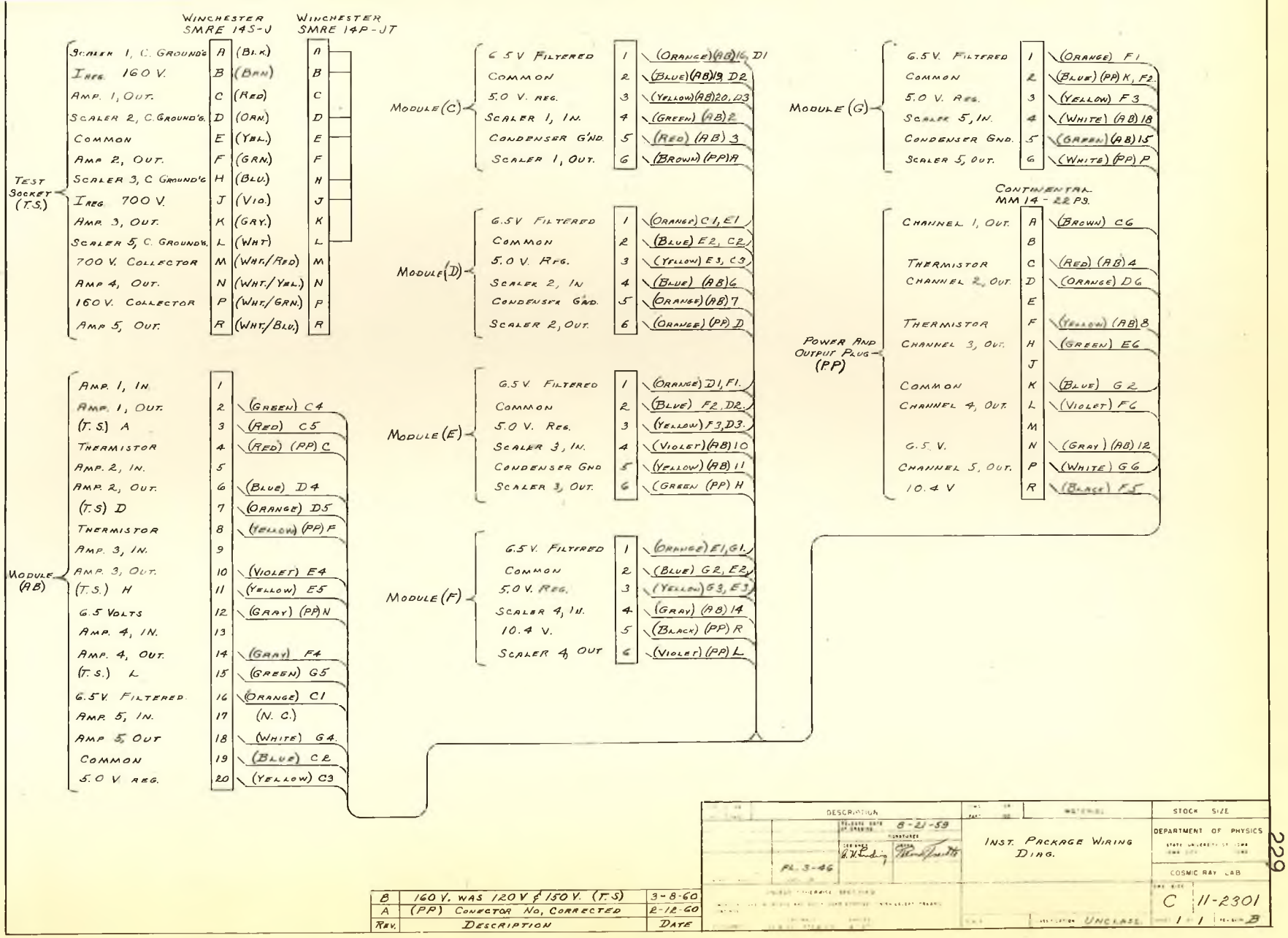

Rev.	Description	Date
B	160 V. WAS 120 V & 150 V. (T.S)	3-8-60
A	(PP) Conector No, Corrected	2-12-60

DESCRIPTION — 8-21-59 — INST. PACKAGE WIRING DIAG. — STOCK SIZE — DEPARTMENT OF PHYSICS — COSMIC RAY LAB — FL. 3-46 — C 11-2301 — UNCLASS

229

Fig. 63

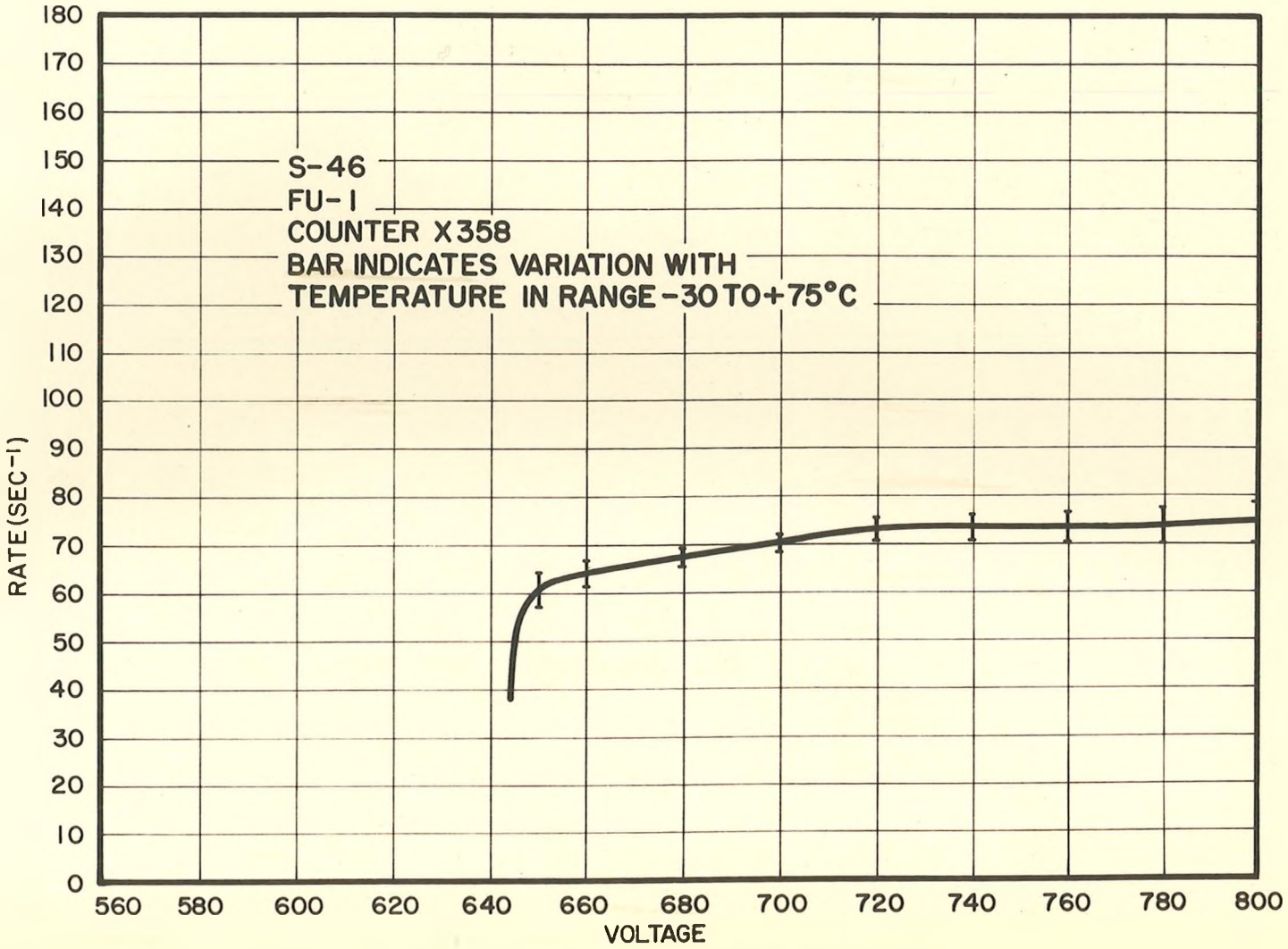

Fig. 64 TYPE 302 G.M. COUNTER PLATEAU

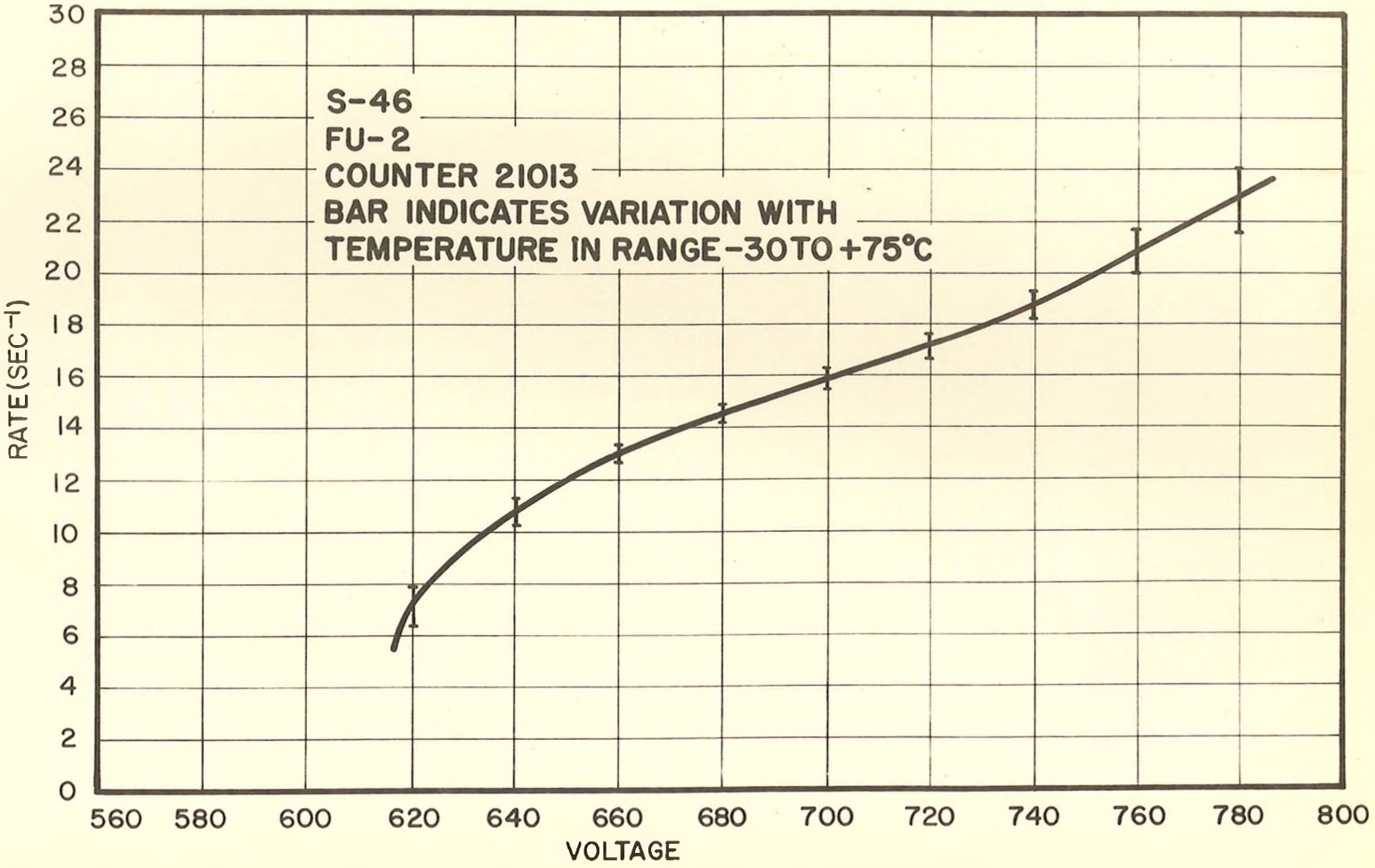

Fig. 65 TYPE 213 G.M. COUNTER PLATEAU

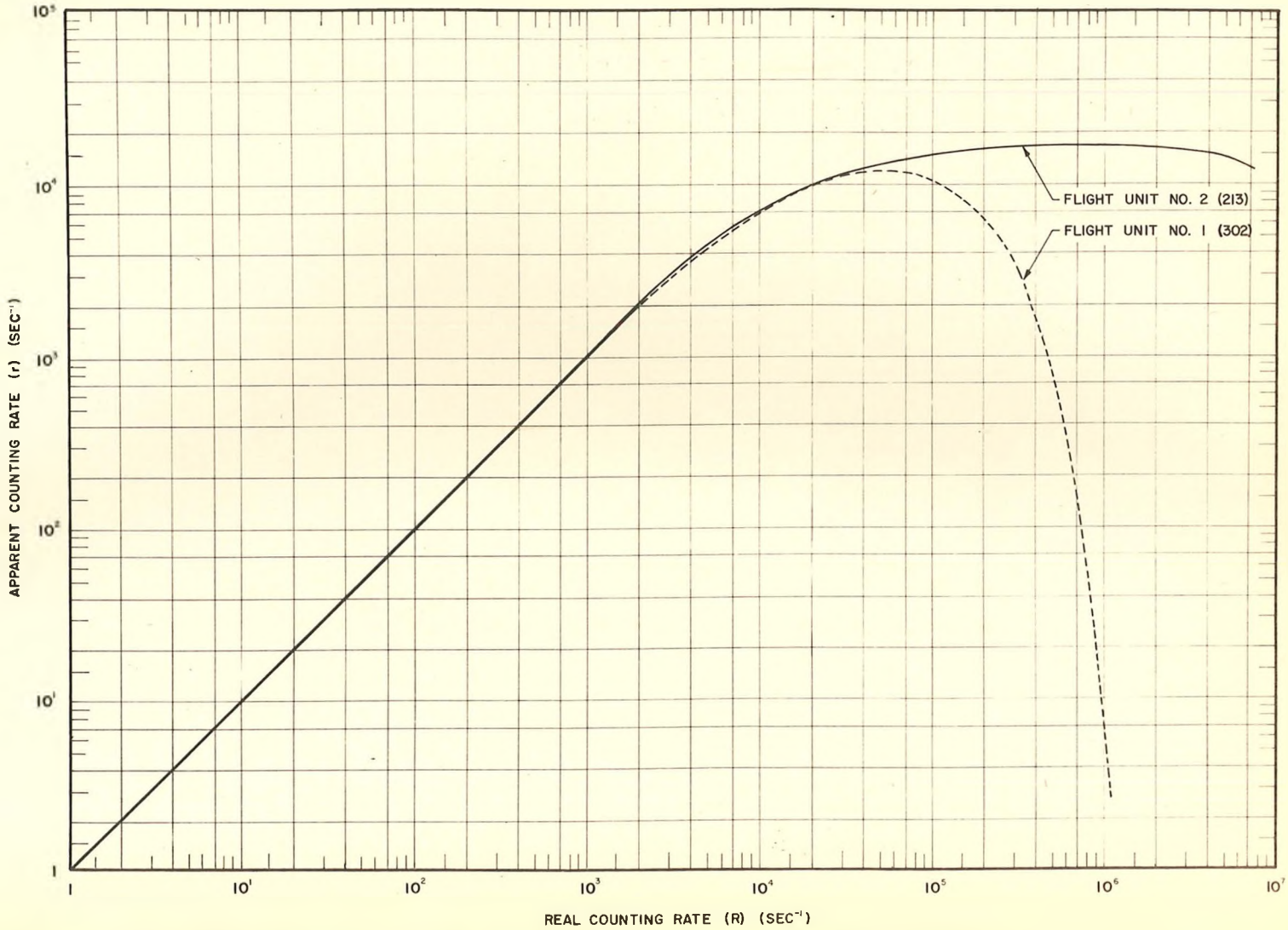

Fig. 66 G.M. COUNTER APPARENT VS. TRUE COUNTING RATE

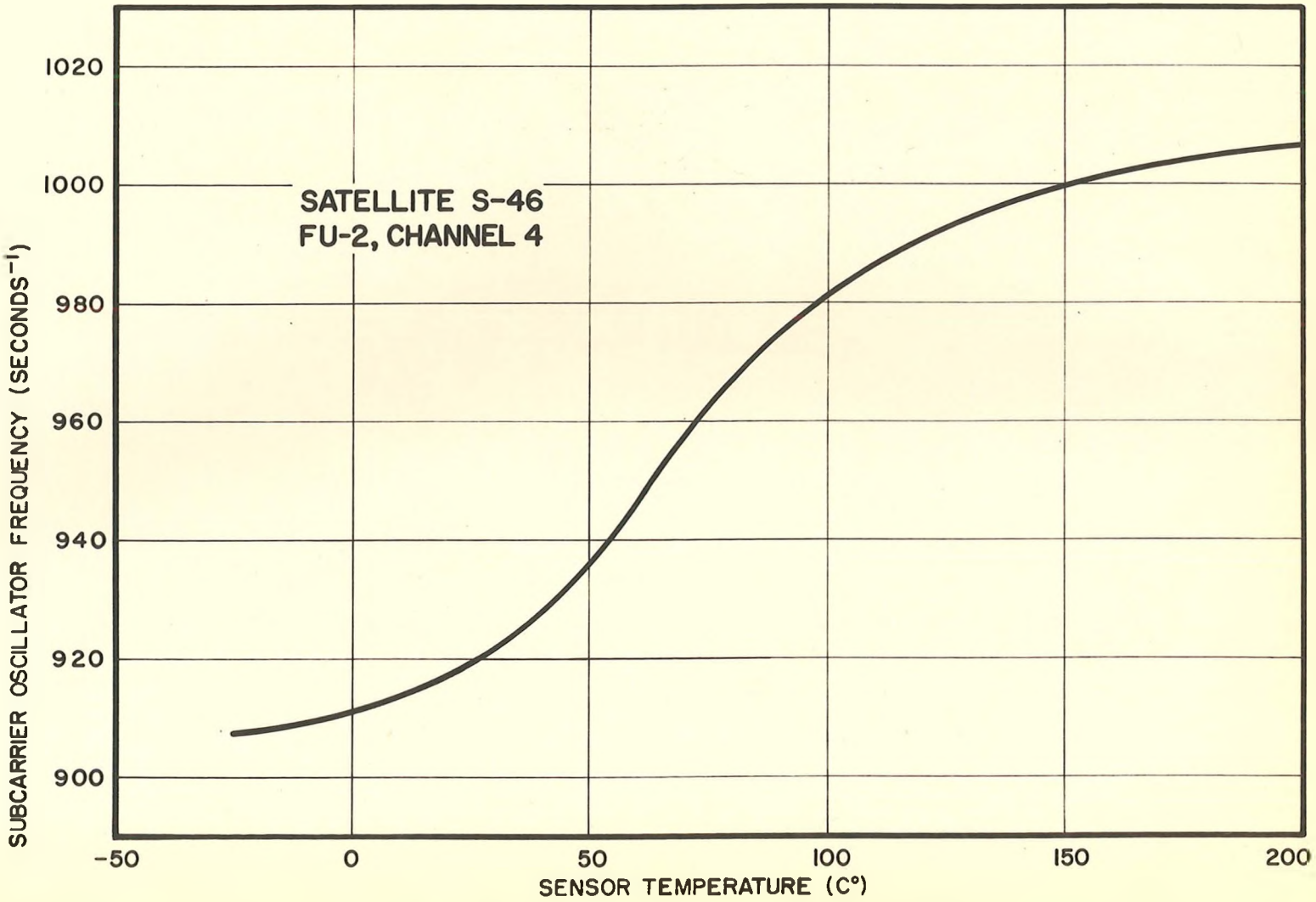

Fig. 67 TABOR SURFACE TEMPERATURE CALIBRATION

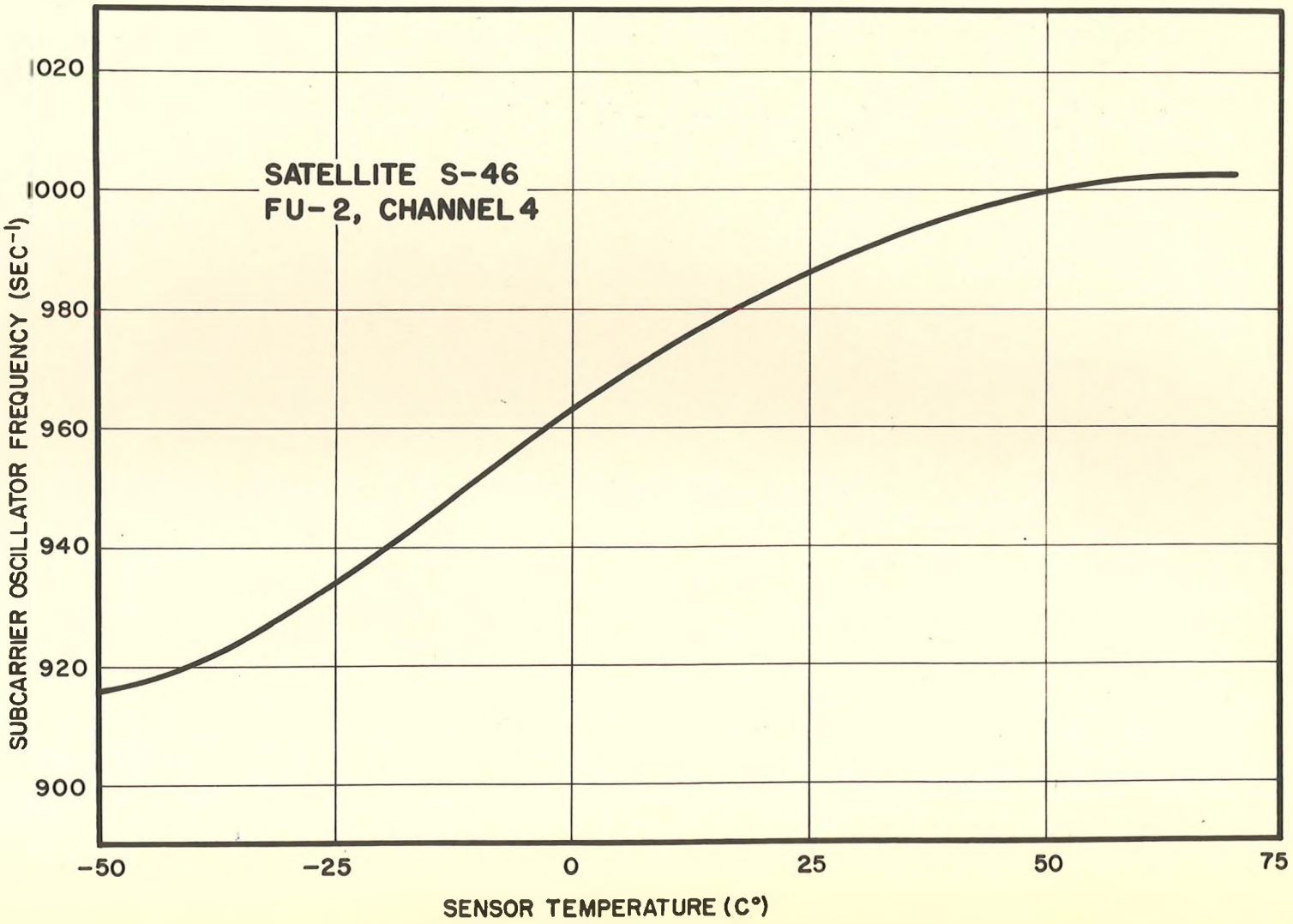

Fig. 68 SUI PACKAGE TEMPERATURE CALIBRATION

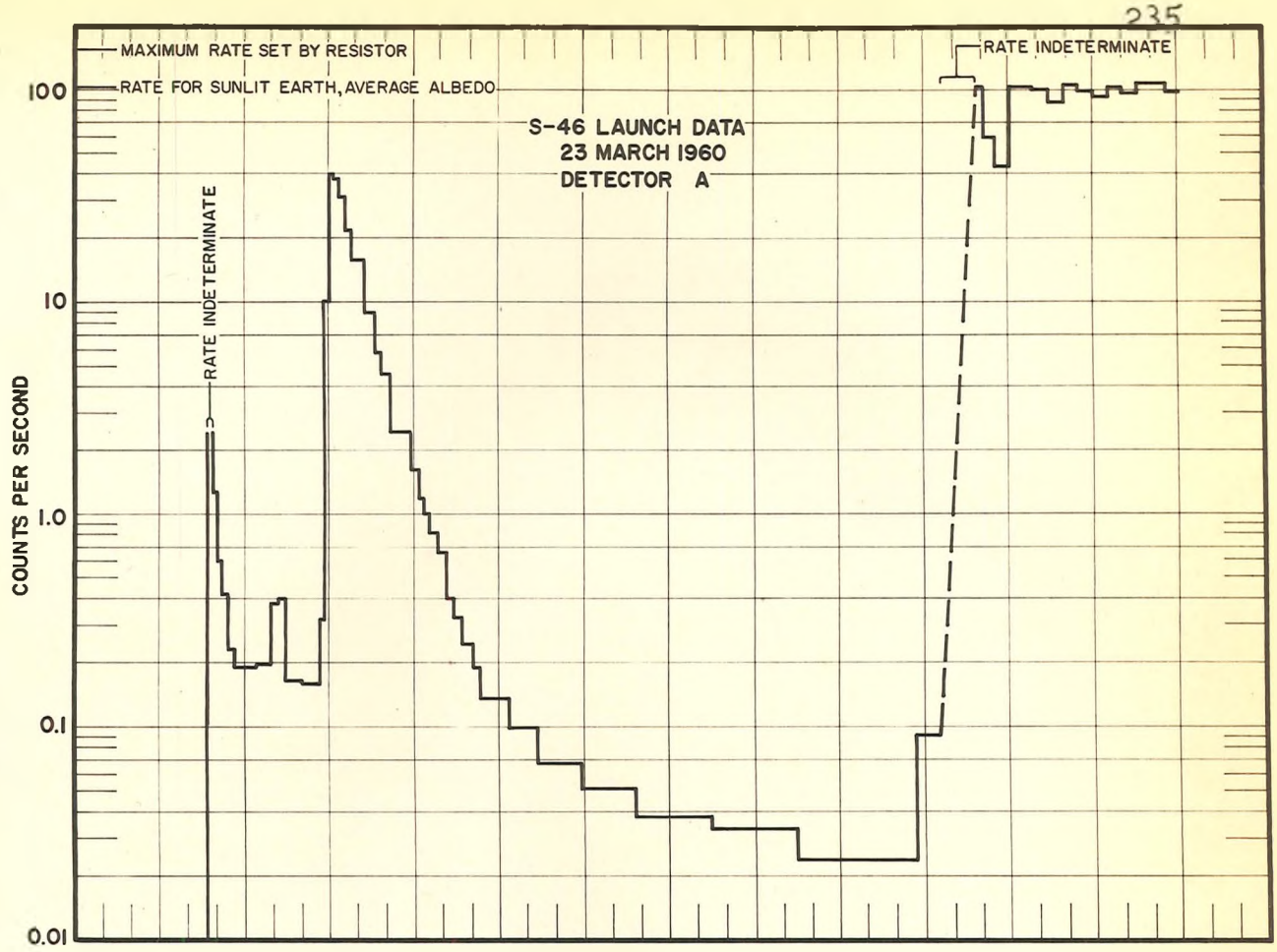
MAXIMUM RATE SET BY RESISTOR
RATE FOR SUNLIT EARTH, AVERAGE ALBEDO
RATE INDETERMINATE
S-46 LAUNCH DATA
23 MARCH 1960
DETECTOR A
RATE INDETERMINATE
100
10
1.0
0.1
0.01
COUNTS PER SECOND

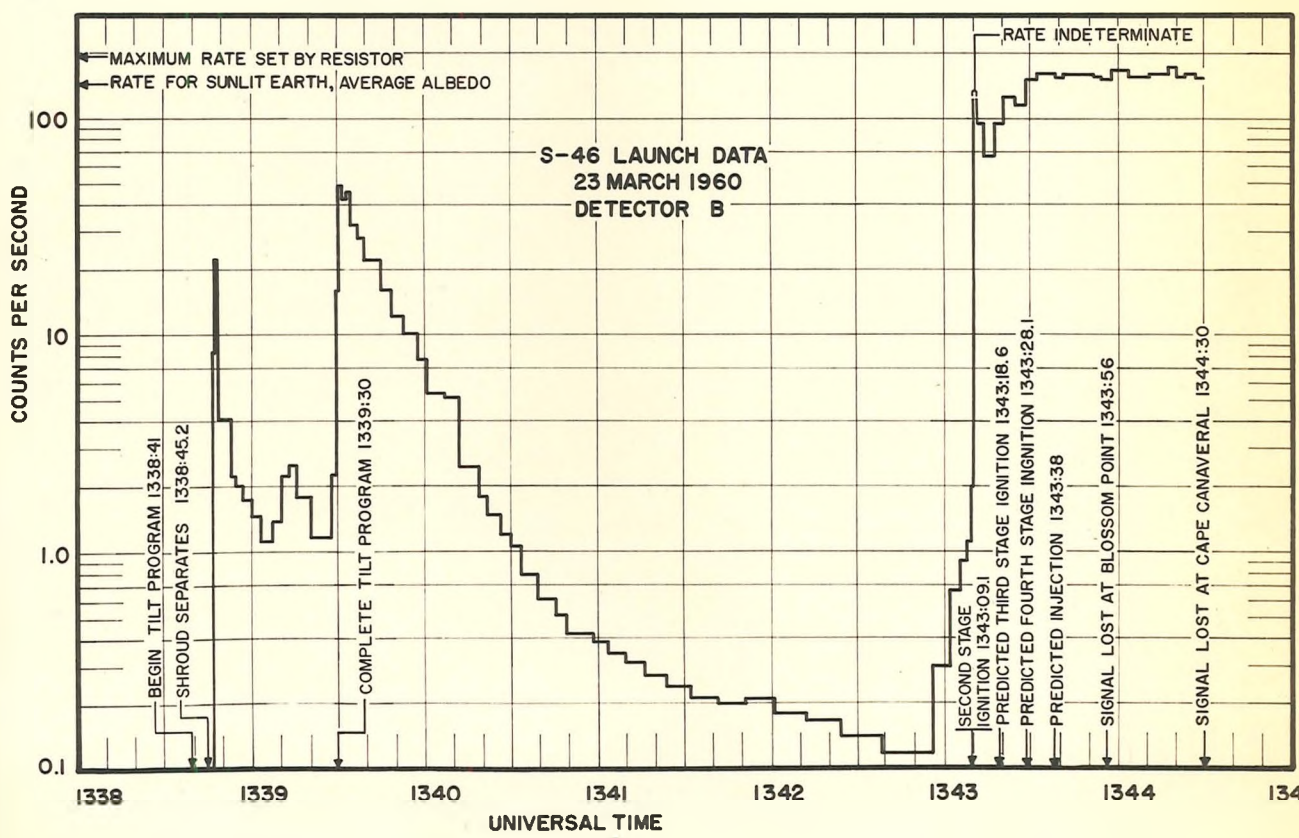
MAXIMUM RATE SET BY RESISTOR
RATE FOR SUNLIT EARTH, AVERAGE ALBEDO
RATE INDETERMINATE
S-46 LAUNCH DATA
23 MARCH 1960
DETECTOR B
BEGIN TILT PROGRAM 1338:41
SHROUD SEPARATES 1338:45.2
COMPLETE TILT PROGRAM 1339:30
SECOND STAGE IGNITION 1343:09.1
PREDICTED THIRD STAGE IGNITION 1343:18.6
PREDICTED FOURTH STAGE INGNITION 1343:28.1
PREDICTED INJECTION 1343:38
SIGNAL LOST AT BLOSSOM POINT 1343:56
SIGNAL LOST AT CAPE CANAVERAL 1344:30
100
10
1.0
0.1
COUNTS PER SECOND
1338
1339
1340
1341
1342
1343
1344
1345
UNIVERSAL TIME

Fig. 69

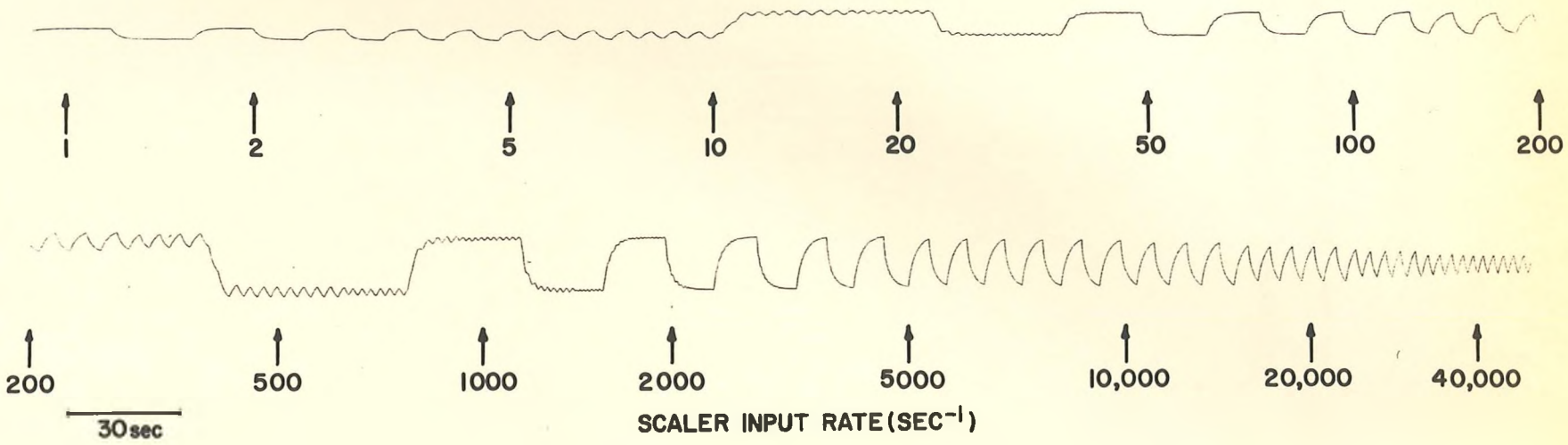

SUBCARRIER OSCILLATOR INPUT WAVEFORM

Fig. 70

APPENDIX I

MECHANICAL DRAWINGS FOR THE DETECTOR INSTRUMENTATION ASSEMBLY.

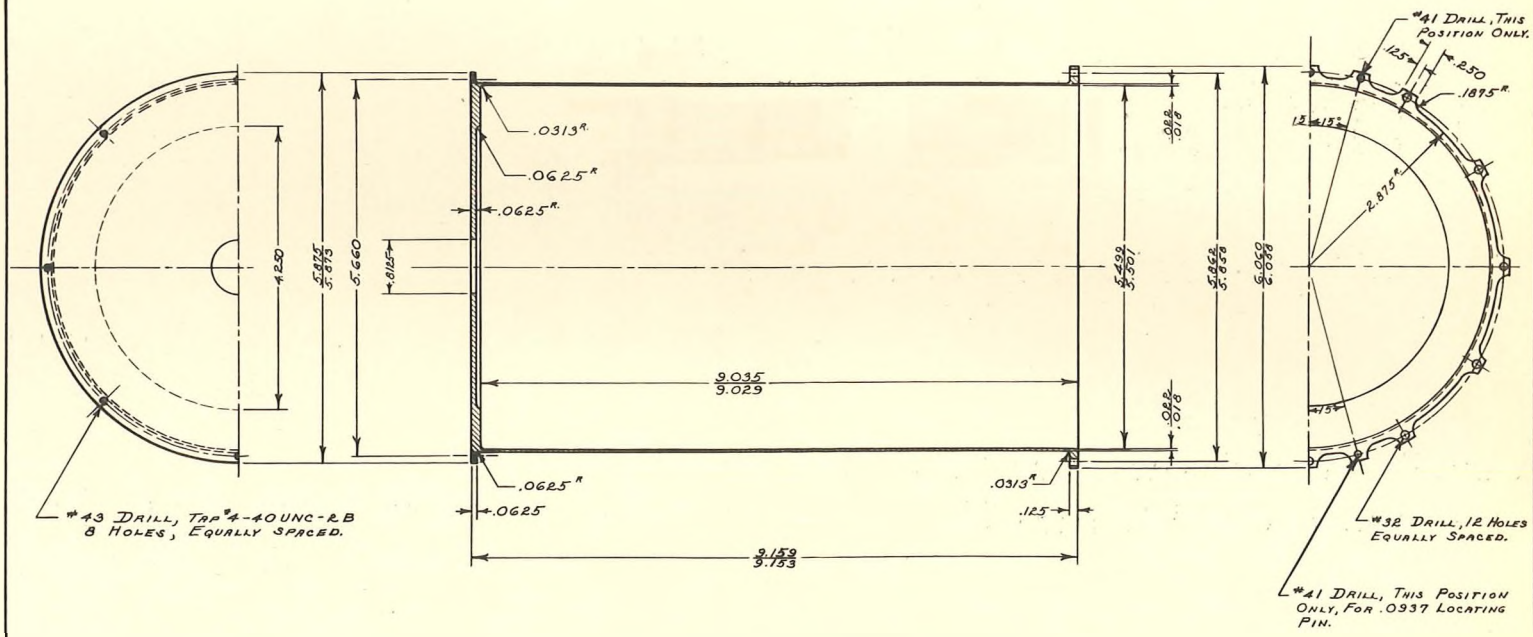

NOTE:
OUTSIDE OF CASE TO BE POLISHED AND BUFFED. ALSO SPRAYED W/ STRIPABLE COATING.

NOTE:
SEE DRAW'G. No. 11-2107 FOR ADDITIONAL HOLE IN CAN.

REV.	DESCRIPTION	DATE
C	8, #4-40 UNC-2 HOLES ADD.	9-10-59
B	NOTE ADDED.	8-29-59
A	4.250 DIA. RECESS ADDED.	8-7-59

1 / 1	CASE	AL.	6½ DIA. x 9⅛ LG.
	DESCRIPTION	MATERIAL	STOCK SIZE
RELEASE DATE BY DRAWING	7-22-59	CASE, INSTRUMENTATION	DEPARTMENT OF PHYSICS
DRAWN	J.H.L.		
	FL. S-46		COSMIC RAY LAB
SCALE FULL	CLASSIFICATION UNCLASS.	C	11-2104
		SHEET 1 OF 1	REVISION C

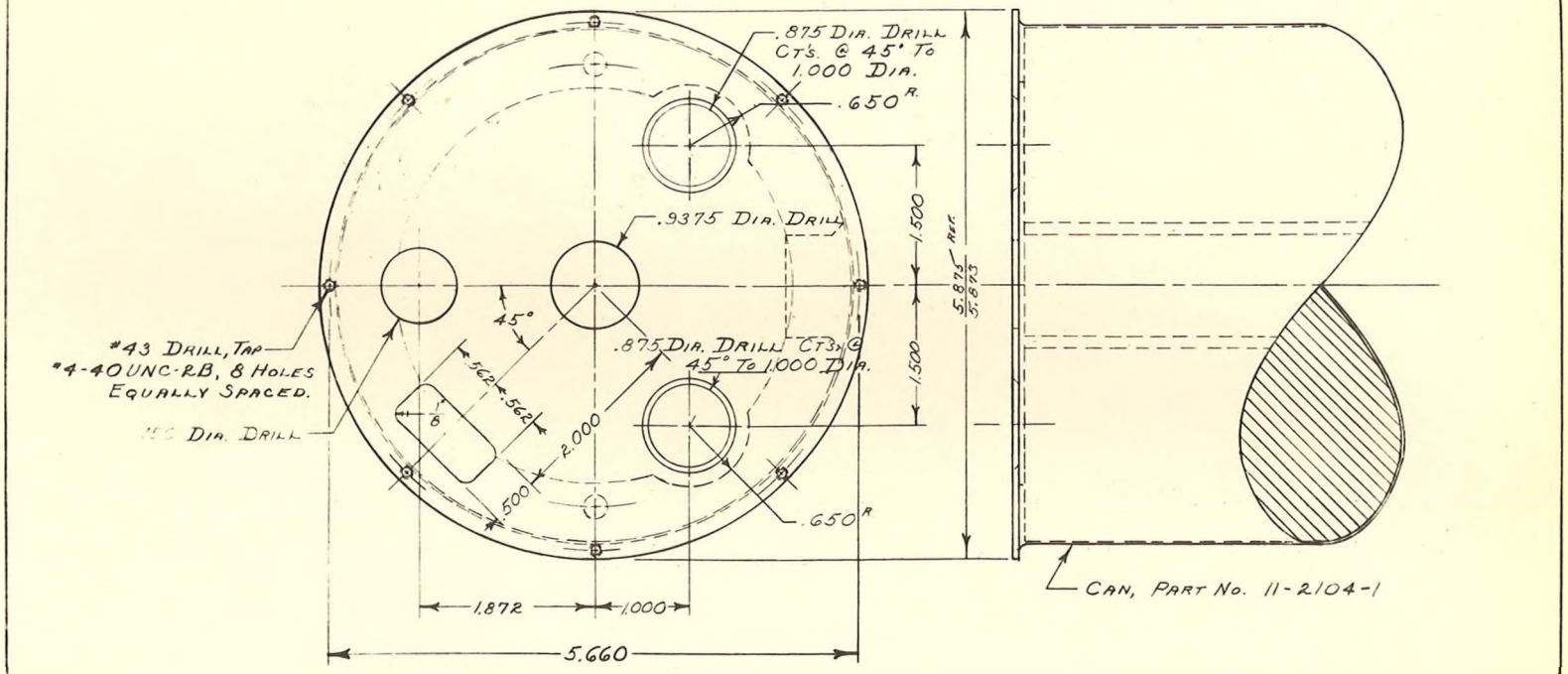

DESCRIPTION	MATERIAL	STOCK SIZE
RELEASE DATE OF DRAWING 8-27-59	HOLE LOCATIONS IN CAN PART NO. 11-2104-1	DEPARTMENT OF PHYSICS, STATE UNIVERSITY OF IOWA, IOWA CITY, IOWA
DESIGNED [signature] DRAWN [signature]		COSMIC RAY LAB
PL. S-46 USED ON		SIZE B, 11-2107
UNLESS OTHERWISE SPECIFIED: DIMENSIONS ARE IN INCHES AND APPLY OVER ADDITIVE FINISH EXCEPT ORGANIC COATINGS; TOLERANCES: DECIMALS, ANGLES	SCALE FULL, CLASSIFICATION UNCLASS.	SHEET 1 OF 1, REVISION A

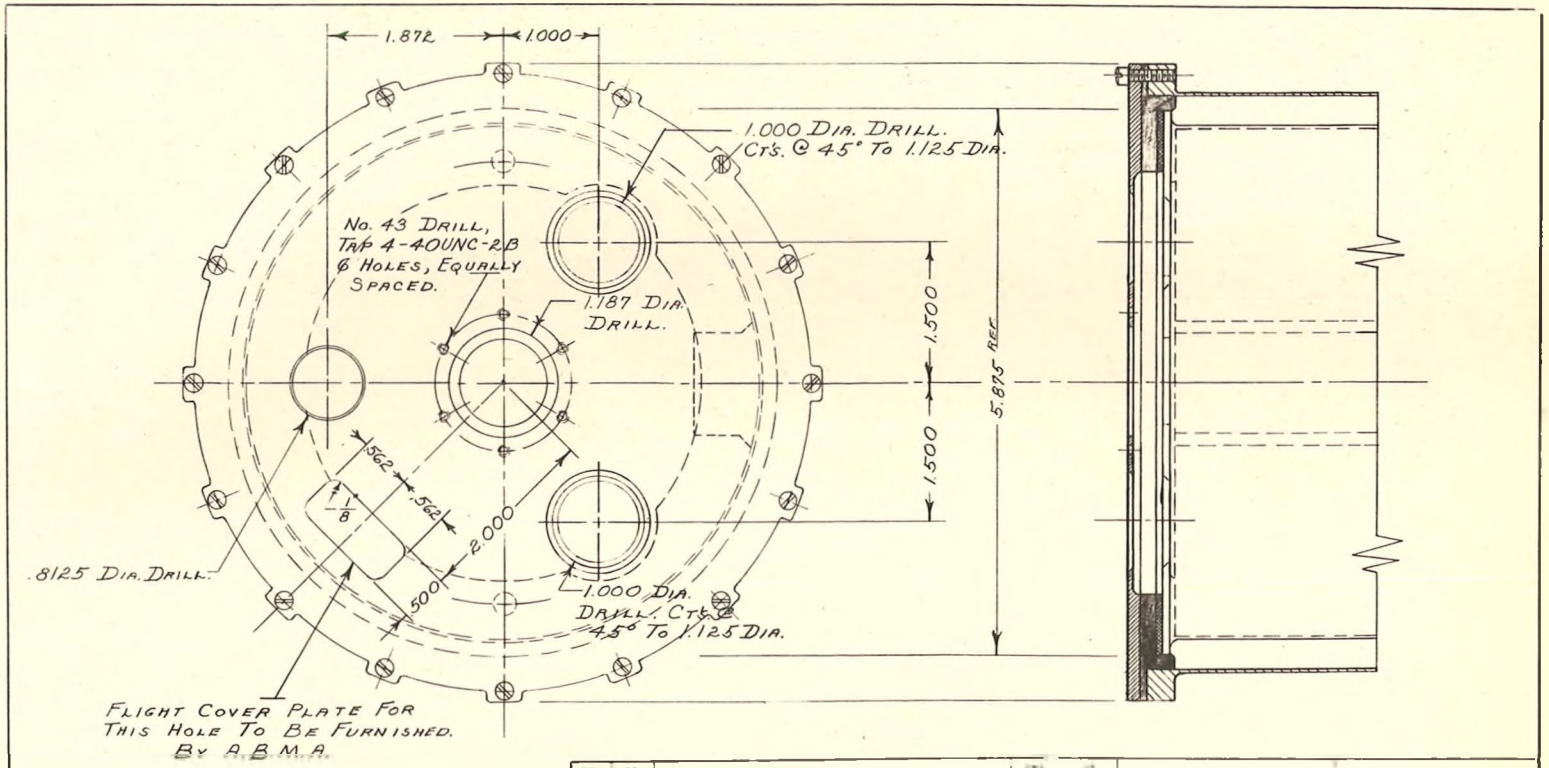

NOTE:
A.B.M.A. TO FURNISH COVERS FOR THE 2, 1.000 DIA. HOLES, TO BE USED DURING TEST & HANDLING ONLY.
A.B.M.A. TO FURNISH COVER FOR 1 8125 DIA. HOLE, TO BE USED DURING TEST & HANDLING ONLY.

DESCRIPTION	MATERIAL	STOCK SIZE
RELEASE DATE OF DRAWING 8-28-59	HOLE SIZE & LOCATION IN OUTSIDE SHELL OF PL. S-46.	DEPARTMENT OF PHYSICS
DESIGNED T. Fuding		
PL S-46		COSMIC RAY LAB
UNLESS OTHERWISE SPECIFIED	SCALE FULL	B 11-2108
	UNCLASS.	SHEET 1 / 1 SIZE A

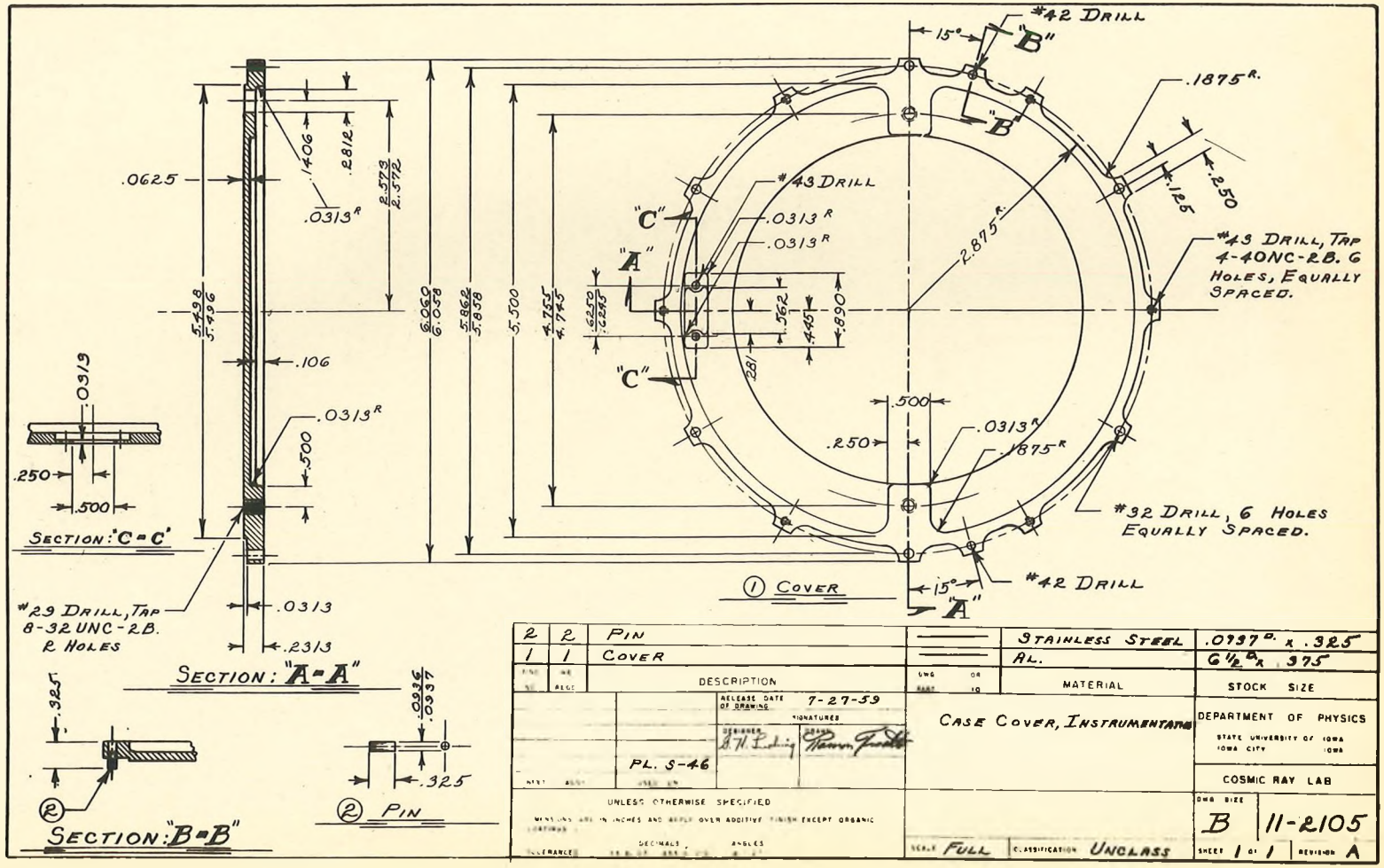

2	2	PIN		STAINLESS STEEL	.0937 D. x .325
1	1	COVER		AL.	6 1/2 D. x .375
PIECE NO.	NO. REQ'D	DESCRIPTION	UNG OR BART ID	MATERIAL	STOCK SIZE
		RELEASE DATE OF DRAWING 7-27-59		CASE COVER, INSTRUMENTATION	DEPARTMENT OF PHYSICS
		SIGNATURES			STATE UNIVERSITY OF IOWA IOWA CITY IOWA
		DESIGNED B.H. Ludwig DRAWN Warren Gentle			COSMIC RAY LAB
NEXT ASSY		PL. S-46			DWG SIZE B 11-2105
UNLESS OTHERWISE SPECIFIED DIMENSIONS ARE IN INCHES AND REFER OVER ADDITIVE FINISH EXCEPT ORGANIC COATINGS					
TOLERANCE DECIMALS ANGLES			SCALE FULL	CLASSIFICATION UNCLASS	SHEET 1 OF 1 REVISION A

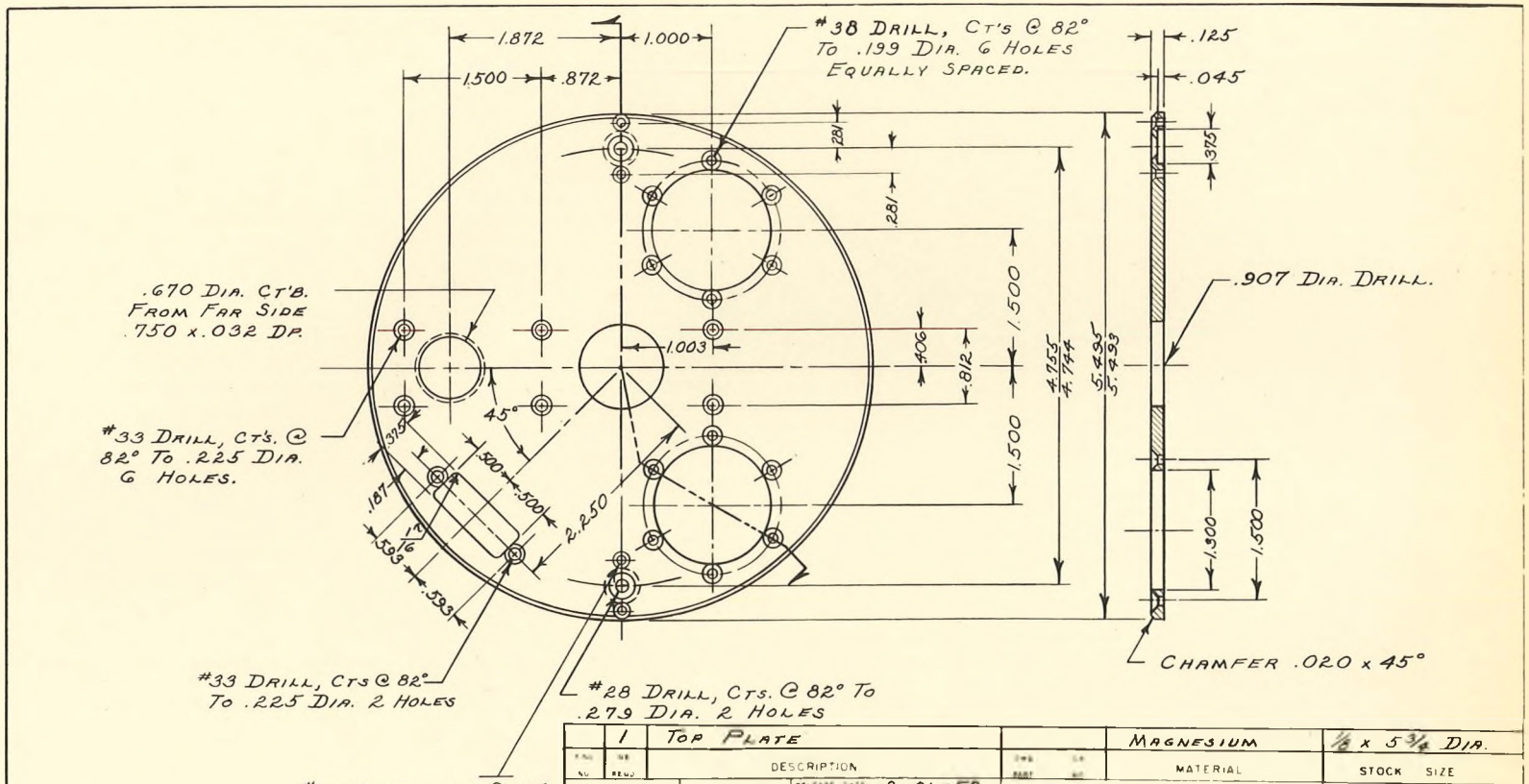

	1	TOP PLATE	MAGNESIUM — 1/8 x 5 3/4 DIA.
	NO. REQ'D	DESCRIPTION	MATERIAL — STOCK SIZE
		RELEASE DATE OF DRAWING 8-31-59	DEPARTMENT OF PHYSICS, STATE UNIVERSITY OF IOWA, IOWA CITY, IOWA
		SIGNATURES: DESIGNER E.H. Ludwig; DRAWN Thomas Tracht	DETECTOR ASS'Y. TOP PLATE.
		NEXT ASSY. PL 5-46	COSMIC RAY LAB
		UNLESS OTHERWISE SPECIFIED: DIMENSIONS ARE IN INCHES AND APPLY OVER ADDITIVE FINISH EXCEPT ORGANIC COATINGS; TOLERANCES: DECIMALS, ANGLES	SCALE FULL; CLASSIFICATION UNCLASS; SIZE B; 11-2A111; SHEET 1 OF 1; REVISION A

REV.	DESCRIPTION	DATE
A	.907 DRILL WAS 7/8-14 UNF-2B TAP	9-10-59

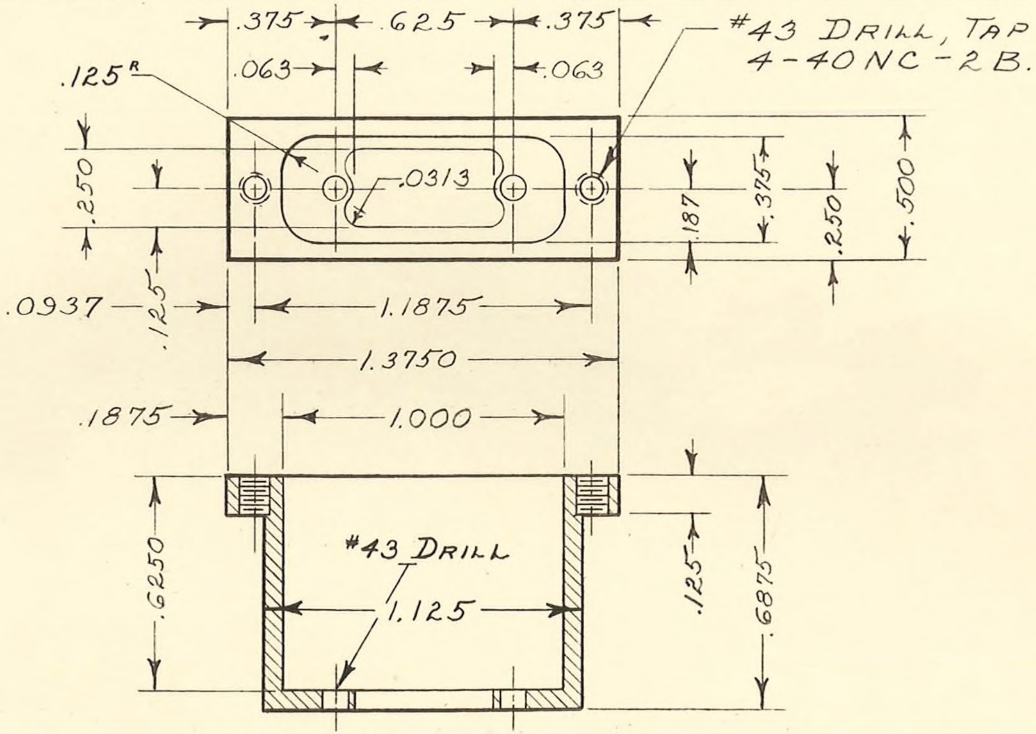

—	1	HOUSING	——	MAGNESIUM	7/8" x 1 1/2" x 5/8"	
		DESCRIPTION	DWG / PART	MATERIAL	STOCK SIZE	

PL S-46	RELEASE DATE OF DRAWING 8-21-59; SIGNATURES: DESIGNER, DRAWN	SOCKET, MOUNTING BLOCK	DEPARTMENT OF PHYSICS, STATE UNIVERSITY OF IOWA, IOWA CITY, IOWA; COSMIC RAY LAB
UNLESS OTHERWISE SPECIFIED			DWG SIZE A 11-2A108
	SCALE 2/1	CLASSIFICATION UNCLASS	SHEET 1 OF 1 REVISION A

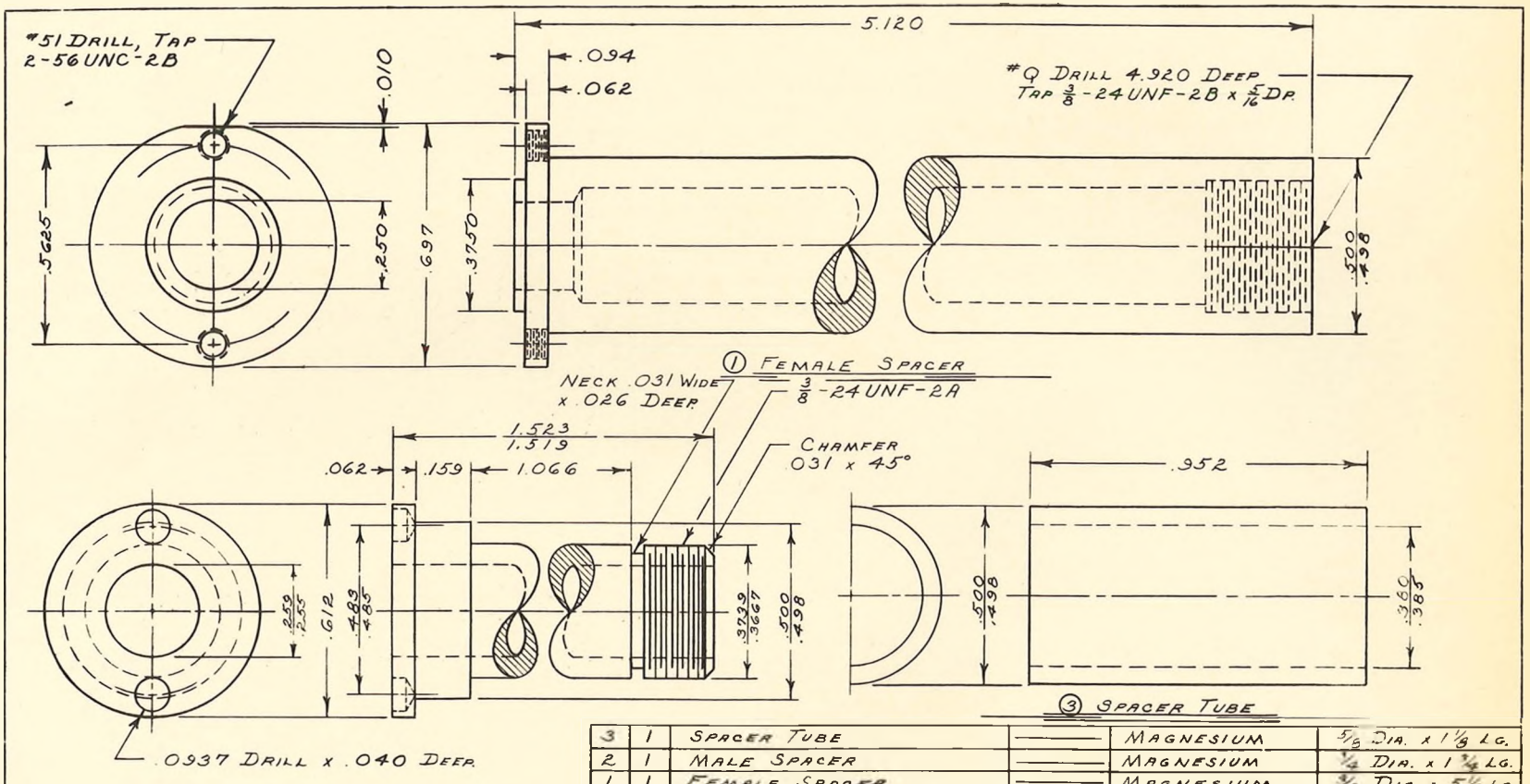

FIND NO	REQ'D	DESCRIPTION	DWG OR PART NO.	MATERIAL	STOCK SIZE
3	1	SPACER TUBE	———	MAGNESIUM	5/8 DIA. x 1 1/8 LG.
2	1	MALE SPACER	———	MAGNESIUM	3/4 DIA. x 1 3/4 LG.
1	1	FEMALE SPACER	———	MAGNESIUM	3/4 DIA. x 5 1/4 LG.

RELEASE DATE OF DRAWING: 10-5-59
SIGNATURES: DESIGNER [illegible] CHECKED [illegible]
NEXT ASSY: PL. 5-46 USED ON

SPACER, MODULE STACKING DECKS, A, B, AND DETECTOR ASS'Y.

DEPARTMENT OF PHYSICS
STATE UNIVERSITY OF IOWA
IOWA CITY IOWA
COSMIC RAY LAB

UNLESS OTHERWISE SPECIFIED
DIMENSIONS ARE IN INCHES AND APPLY OVER ADDITIVE FINISH EXCEPT ORGANIC COATINGS
TOLERANCES: DECIMALS ANGLES

SCALE 4/1 | CLASSIFICATION UNCLASS | DWG SIZE B | 11-2-2115 | SHEET 1 OF 1 | REVISION

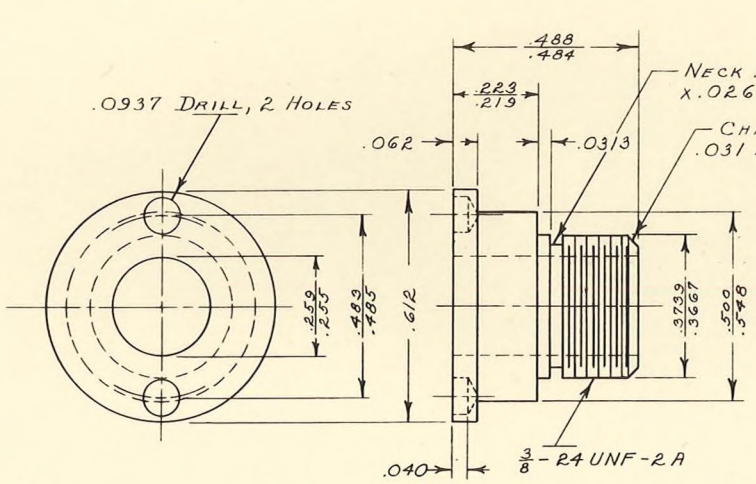

① MALE SPACER

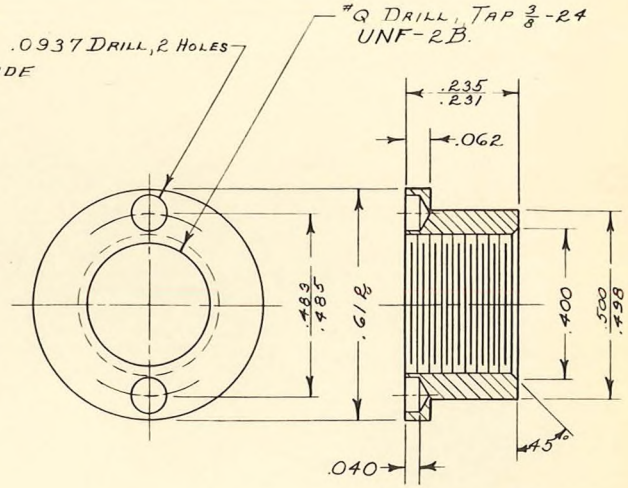

② FEMALE SPACER

2	1	FEMALE SPACER		ALUMINUM	
1	1	MALE SPACER		ALUMINUM	
		DESCRIPTION		MATERIAL	STOCK SIZE

7-1-59

SPACER, MODULE STACKING DECKS — C, D, E, F & G.

DEPARTMENT OF PHYSICS

COSMIC RAY LAB

PL S-46

UNLESS OTHERWISE SPECIFIED

4/1 UNCLASS

B 11-2B101

1 OF 1

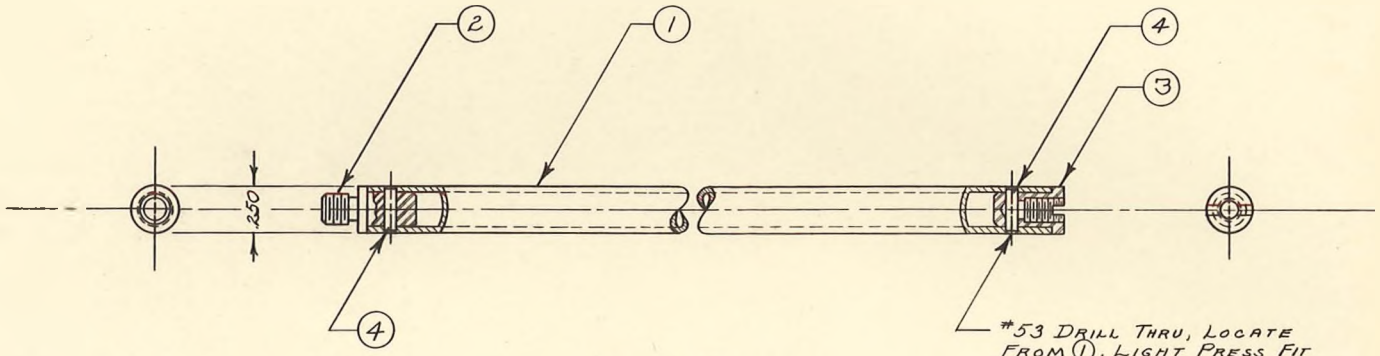

ROD ASSEMBLY

NO.	REQ'D	DESCRIPTION	PART NO.	MATERIAL	STOCK SIZE
4	2	PIN	11-2107-4		
3	1	NUT	11-2106-3		
2	1	SCREW	11-2106-2		
1	1	TUBE	11-2106-1		

RELEASE DATE OF DRAWING 7-30-59

SIGNATURES

DRAWN G. N. Ludwig

CHKD Thomas Gold

PL. S-46

ROD ASSEMBLY

DEPARTMENT OF PHYSICS
STATE UNIVERSITY OF IOWA
IOWA CITY, IOWA

COSMIC RAY LAB

UNLESS OTHERWISE SPECIFIED

SIZE B

DWG. NO. 11-2001

SCALE 2/1

CLASSIFICATION UNCLASS

REV. 1

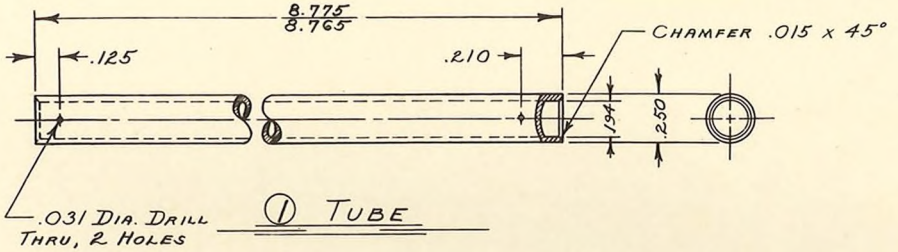

① TUBE

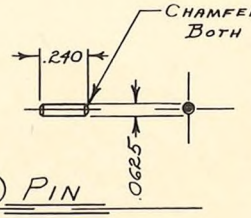

④ PIN

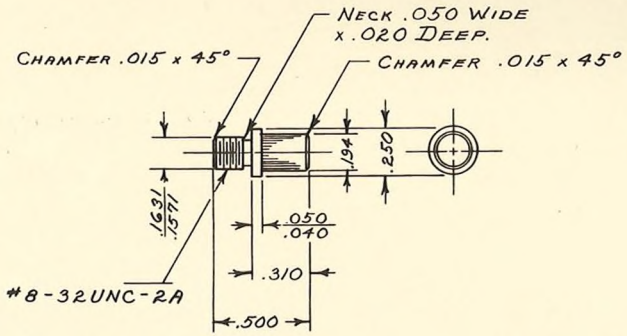

② SCREW

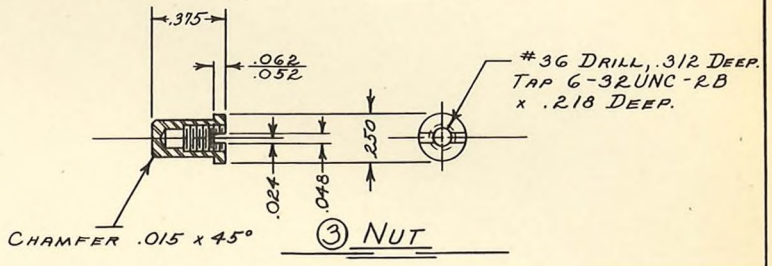

③ NUT

DWG NO	PART NO	DESCRIPTION	DWG OR PART NO	MATERIAL	STOCK SIZE
4	2	PIN		STAINLESS STEEL	.0625 ϕ x .250" LG.
3	1	NUT		STAINLESS STEEL	.250 ϕ x 1/2" LG.
2	1	SCREW		STAINLESS STEEL	.250 ϕ x 5/8" LG.
1	1	TUBE		MAGNESIUM ALY-MIN.	.250 ϕ x .028 WALL x 9"

RELEASE DATE OF DRAWING: 7-31-59

SIGNATURES

DESIGNED: A.H. Lindsay

CHK'D: Thomas Gaisser

PL. 8-46

DETAILS ROD ASSEMBLY

DEPARTMENT OF PHYSICS
STATE UNIVERSITY OF IOWA
IOWA CITY, IOWA

COSMIC RAY LAB

UNLESS OTHERWISE SPECIFIED
DIMENSIONS ARE IN INCHES AND APPLY OVER ADDITIVE FINISH EXCEPT ORGANIC COATINGS
TOLERANCES: DECIMALS ± .01, .03, .005; ANGLES ± 1/2°

SCALE 2/1

CLASSIFICATION UNCLASS

DWG SIZE B

11-2106

SHEET 1 OF 1

REVISION

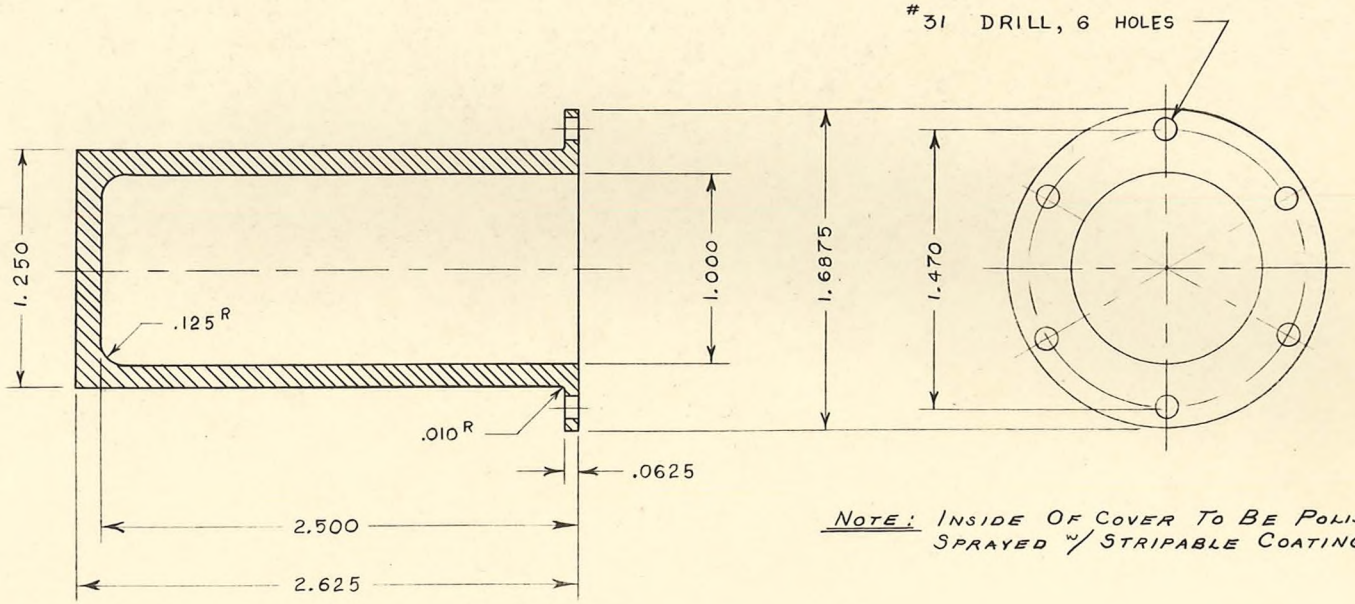

NOTE: INSIDE OF COVER TO BE POLISHED & SPRAYED W/ STRIPABLE COATING.

—	1	302 G.M. TUBE COVER
		DESCRIPTION

AL.	1 3/4 x 2 3/4 Lg.
MATERIAL	STOCK SIZE

RELEASE DATE OF DRAWING | SIGNATURES
DESIGNER: A.Y. Ludwig | DRAWN: W. L. Fraser
PL. S-46

#302 G.M.
TUBE THICK COVER

DEPARTMENT OF PHYSICS
STATE UNIVERSITY OF IOWA
IOWA CITY IOWA

COSMIC RAY LAB

UNLESS OTHERWISE SPECIFIED

SCALE 2/1 | CLASSIFICATION UNCLASSIFIED | B | 11-1101 | REVISION A

Rev	Description	Date
A	Added Note & New Title	2-11-60

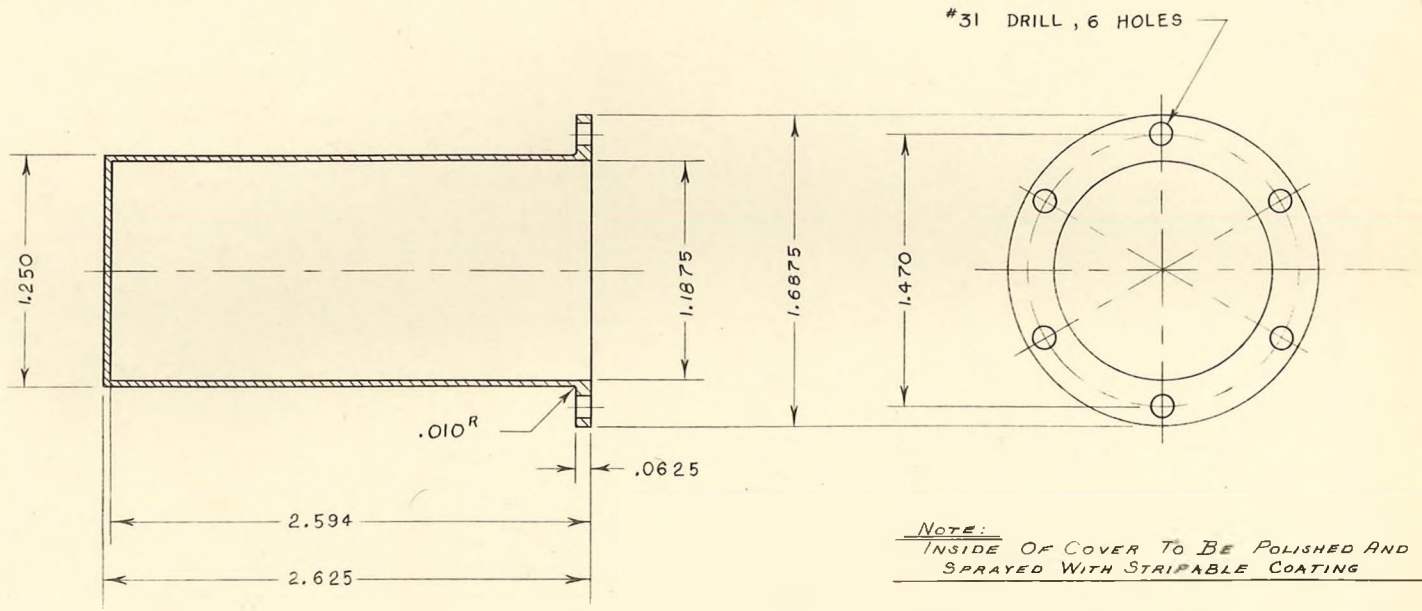

NOTE:
INSIDE OF COVER TO BE POLISHED AND SPRAYED WITH STRIPABLE COATING

—	1	TUBE FLIGHT COVER
		DESCRIPTION
		AL.
		MATERIAL
		1 3/4 x 2 3/4 Lc
		STOCK SIZE
	PL. S-46	#213 G.M. TUBE THIN COVER
		DEPARTMENT OF PHYSICS
		STATE UNIVERSITY OF IOWA IOWA CITY IOWA
		COSMIC RAY LAB
		B 11-1102
		2/1 UNCLASSIFIED SHEET 1 OF 1 REVISION B

UNLESS OTHERWISE SPECIFIED

Rev.	Description	Date
B	NOTE & TITLE CORRECTED	2-12-60
A	NOTE ADDED	11-17-59

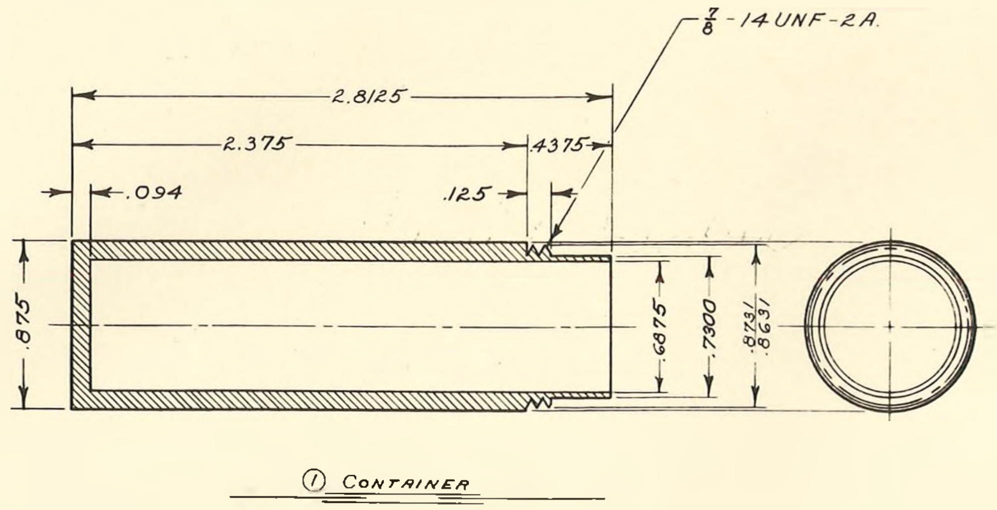

NOTE:
POLISH OUTSIDE OF CONTAINER
& SPRAY WITH STRIPABLE COATING.

1 | 1 | CONTAINER | AL

DESCRIPTION | MATERIAL | STOCK SIZE

RELEASE DATE OF DRAWING: 1-25-60

USED ON: PL S-46

CONTAINER, #213
G.M. COUNTER

DEPARTMENT OF PHYSICS

COSMIC RAY LAB

UNLESS OTHERWISE SPECIFIED

SCALE 2/1

B 11-2A120

SHEET 1 OF 1

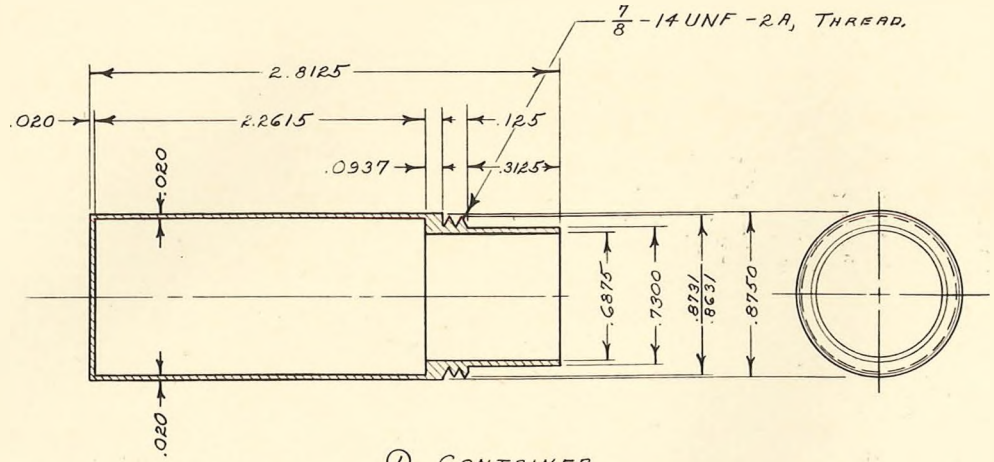

① CONTAINER

NOTE:
POLISH OUTSIDE OF CONTAINER.
OUTSIDE TO BE SPRAYED WITH STRIPABLE COATING.

1	1	CONTAINER		AL.	1" DIA. x 3 1/4" LG.
		DESCRIPTION		MATERIAL	STOCK SIZE
		RELEASE DATE OF DRAWING 8-24-59		302 G.M. COUNTER CONTAINER	DEPARTMENT OF PHYSICS STATE UNIVERSITY OF IOWA IOWA CITY IOWA
		SIGNATURES DESIGNED A.W. Ludwig CHKD Norman Franklin			COSMIC RAY LAB
		PL. S-76			DWG SIZE B 11-2A105
		UNLESS OTHERWISE SPECIFIED		SCALE R/1 CLASSIFICATION UNCLASS	SHEET 1 OF 1 REVISION B

REV.	DESCRIPTION	DATE
B	R. 8125 WAS 3.000, .9125 WAS .500	9-9-59

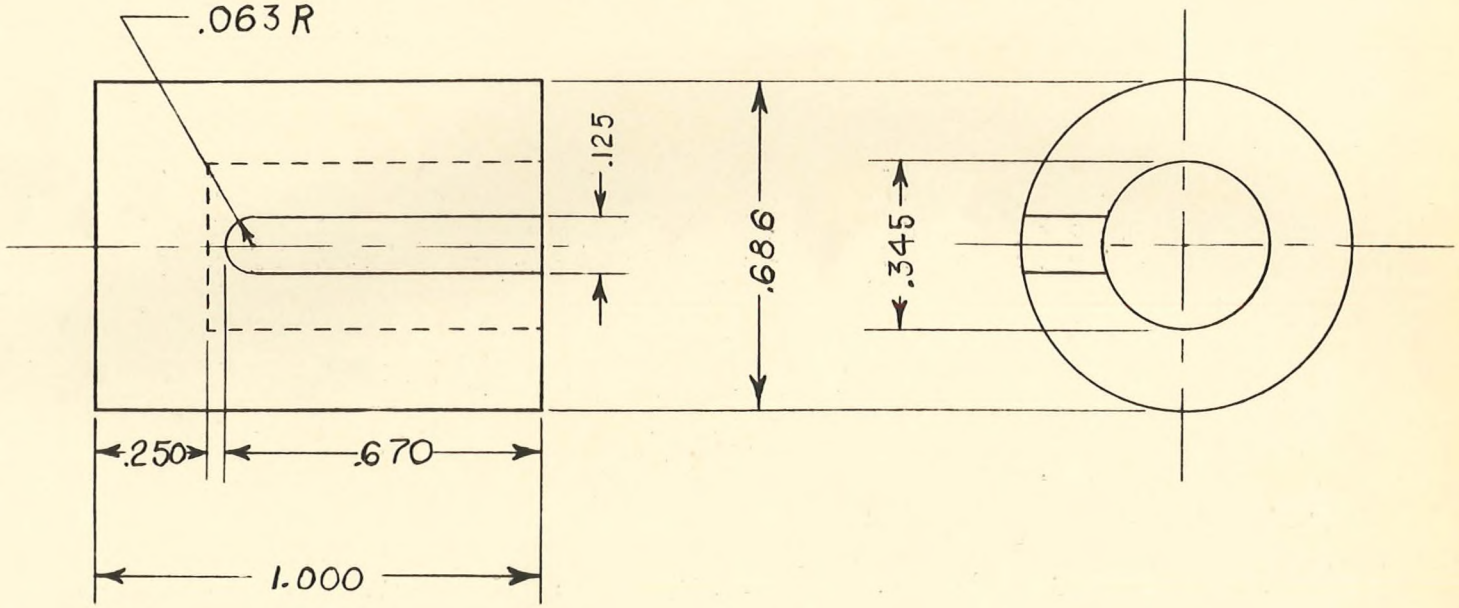

—	1	ALLIGNMENT BLOCK	———	FOAM	3/4 ϕ x 1
FIND NO	REQD NO	DESCRIPTION	DWG OR PART NO	MATERIAL	STOCK SIZE
		RELEASE DATE OF DRAWING FEB. 11, 1960		ALLIGNMENT BLOCK FOR 213 COUNTER	DEPARTMENT OF PHYSICS STATE UNIVERSITY OF IOWA IOWA CITY IOWA
		SIGNATURES			
		DESIGNER [signature]	DRAWN William Fry		
	P.L. S-46				COSMIC RAY LAB
NEXT ASSY	USED ON				

UNLESS OTHERWISE SPECIFIED

DIMENSIONS ARE IN INCHES AND APPLY OVER ADDITIVE FINISH EXCEPT ORGANIC COATINGS

TOLERANCES — DECIMALS: XX ± .03, XXX ± 010 — ANGLES: ± 1/2°

			DWG SIZE A	11-2A121
SCALE 3/1	CLASSIFICATION UNCLASS.	SHEET 1 OF 1	REVISION	

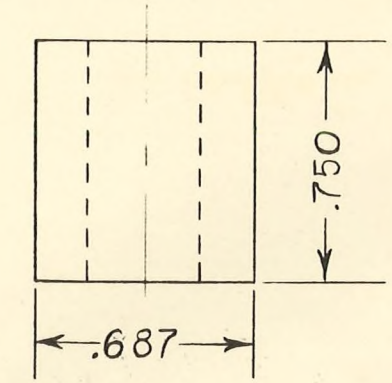

①

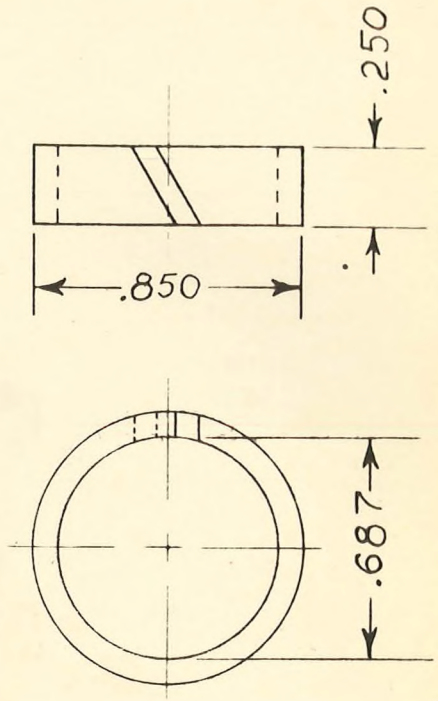

②

FIND NO	NO REQD	DESCRIPTION	DWG OR PART NO	MATERIAL	STOCK SIZE
②	1	ALLIGNMENT RING	——	FOAM	1$^{\phi}$ x 1/4
①	1	BLOCK	——	FOAM	3/4$^{\phi}$ x 3/4

RELEASE DATE OF DRAWING

SIGNATURES

DESIGNER Warren Travis

DRAWN William Fry

NEXT ASSY

USED ON P.L. S-46

ALLIGNMENT BLOCK FOR #302 G.M. COUNTER

DEPARTMENT OF PHYSICS
STATE UNIVERSITY OF IOWA
IOWA CITY IOWA

COSMIC RAY LAB

UNLESS OTHERWISE SPECIFIED

DIMENSIONS ARE IN INCHES AND APPLY OVER ADDITIVE FINISH EXCEPT ORGANIC COATINGS

TOLERANCES DECIMALS XX ± .03 XXX ± 010 ANGLES ± 1/2°

SCALE 2/1

CLASSIFICATION UNCLASS.

DWG SIZE A

11-2A122

SHEET 1 OF 1

REVISION

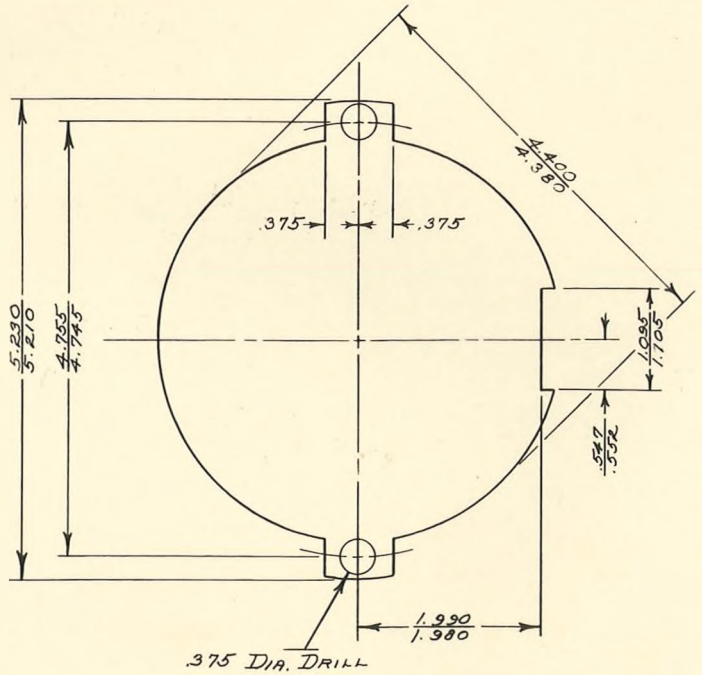

1	CARD		1/16" TH. FORMICA FF-91	5 1/2" DIA.
		8-13-59	POWER SUPPLY, CARD DECK "A."	
	PL S-46			
			FULL	UNCLASS

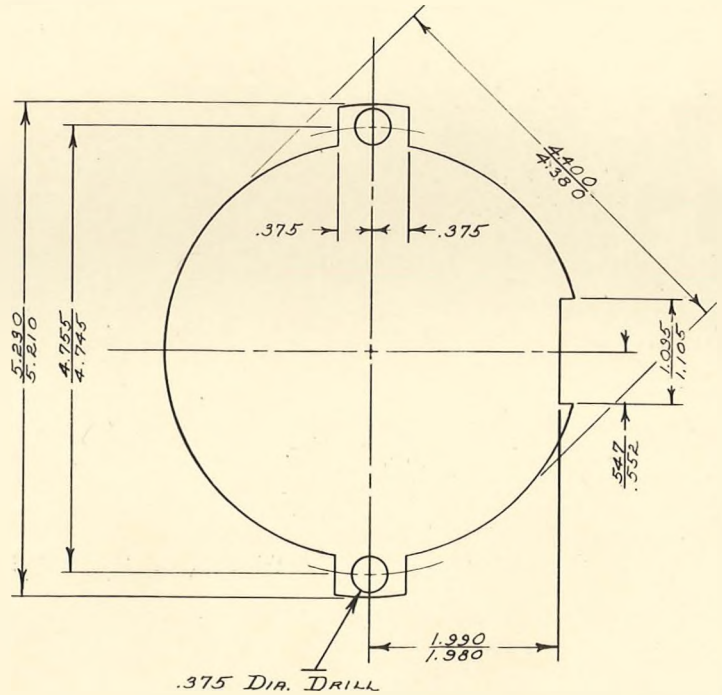

1	CARD		1/32" TH. FORMICA FF-91	5 1/2" DIA.
NO.	DESCRIPTION		MATERIAL	STOCK SIZE
	RELEASE DATE OF DRAWING 8-13-59	AMPLIFIER CARD DECK "B"		DEPARTMENT OF PHYSICS
	DESIGNED [signature] DRAWN [signature]			
	PL S-46			COSMIC RAY LAB
UNLESS OTHERWISE SPECIFIED				B 11-2B102
		SCALE FULL	CLASSIFICATION UNCLASS	SHEET 1 OF 1 REVISION

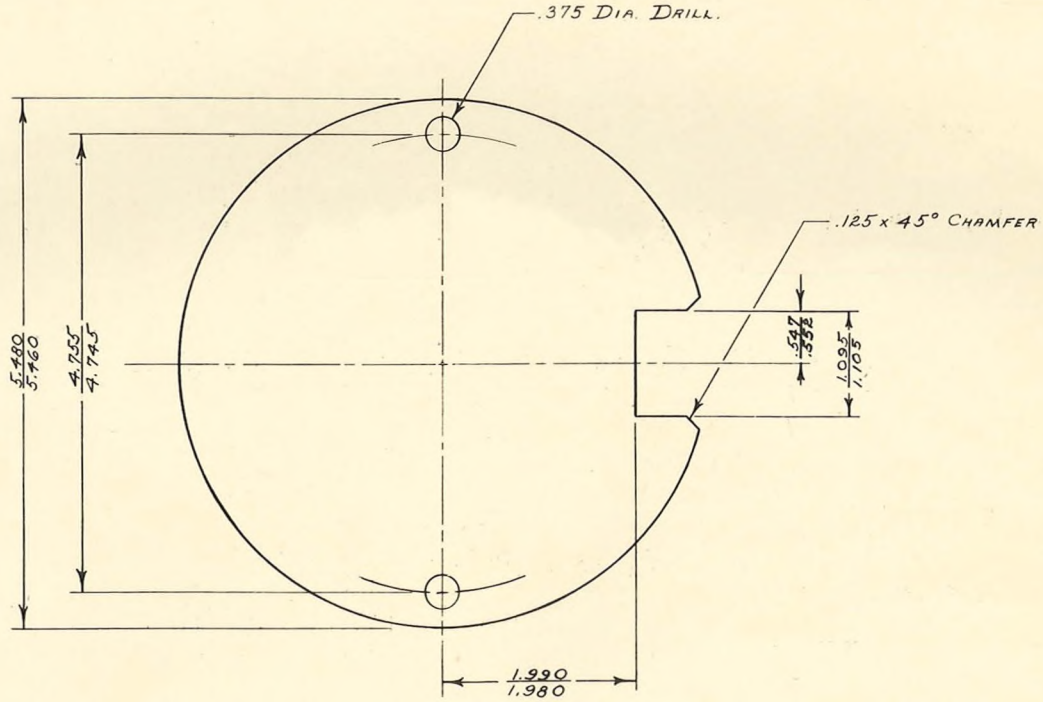

1	CARD	1/32 TH. FORMICA FF-91	5 3/4 DIA.
	DESCRIPTION	MATERIAL	STOCK SIZE
	PL S-46	INSTRUMENTATION CARD DECKS "C TO G"	DEPARTMENT OF PHYSICS COSMIC RAY LAB
		WAS DWG NO 11-2101 REV "A"	B 11-2C102
		1/1 UNCLASS	1 1 A

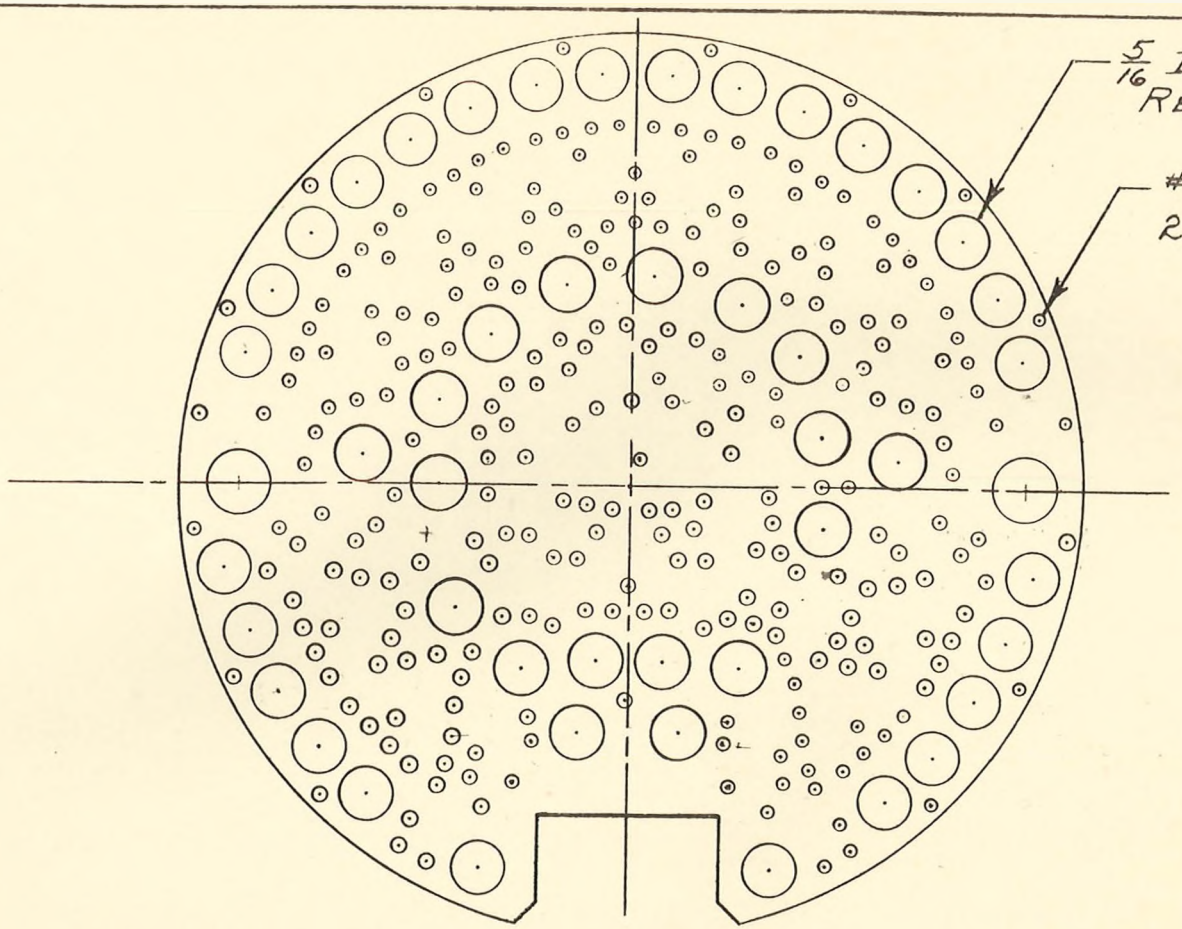

FIND NO	NO REQD	DESCRIPTION	DWG OR PART NO	MATERIAL	STOCK SIZE
		RELEASE DATE OF DRAWING 7-7-59			
		SIGNATURES			
		DESIGNER H-K. McCann	DRAWN Thomas Truett	HOLE LOCATION INSTRUMENT DECKS C, D, E, F, & G.	DEPARTMENT OF PHYSICS STATE UNIVERSITY OF IOWA IOWA CITY IOWA
	PL-19A	S.N. Lindsay			COSMIC RAY LAB
NEXT ASSY	USED ON				

UNLESS OTHERWISE SPECIFIED

DIMENSIONS ARE IN INCHES AND APPLY OVER ADDITIVE FINISH EXCEPT ORGANIC COATINGS

TOLERANCES DECIMALS .XX ± .01 .XXX ± .005 ANGLES ± 1/2°

SCALE FULL | CLASSIFICATION UNCLASS | DWG SIZE A | 11-2C103 | SHEET 1 OF 1 | REVISION

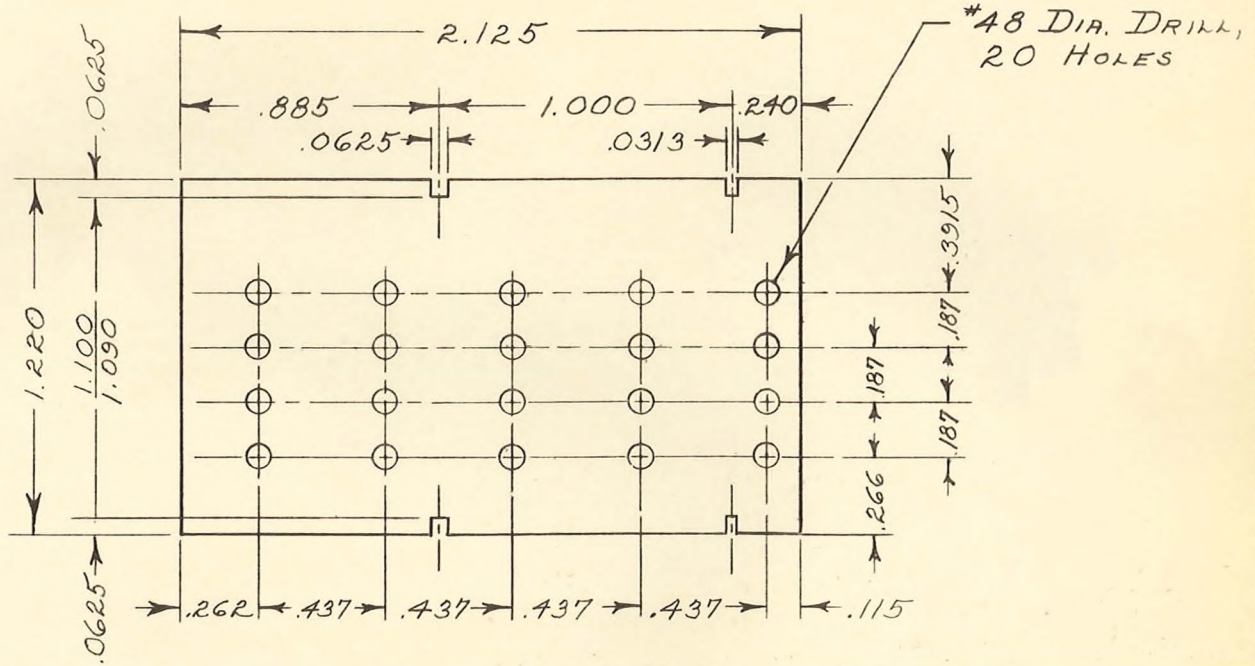

	1	TERMINAL BOARD	FORMICA FF-91	1/16 TH. x 1 1/4 x 2 1/4
	NO. REQ.	DESCRIPTION	DWG OR PART NO.	MATERIAL	STOCK SIZE

RELEASE DATE OF DRAWING 8-28-59

SIGNATURES

DESIGNER W. H. Lansing

DRAWN Thomas Smith

PL S-46

USED ON

TERMINAL BOARD
DECK "A & B."

DEPARTMENT OF PHYSICS
STATE UNIVERSITY OF IOWA
IOWA CITY IOWA

COSMIC RAY LAB

UNLESS OTHERWISE SPECIFIED

DWG SIZE A

11-2A110

SCALE 2/1

CLASSIFICATION UNCLASS.

SHEET 1 OF 1

REVISION

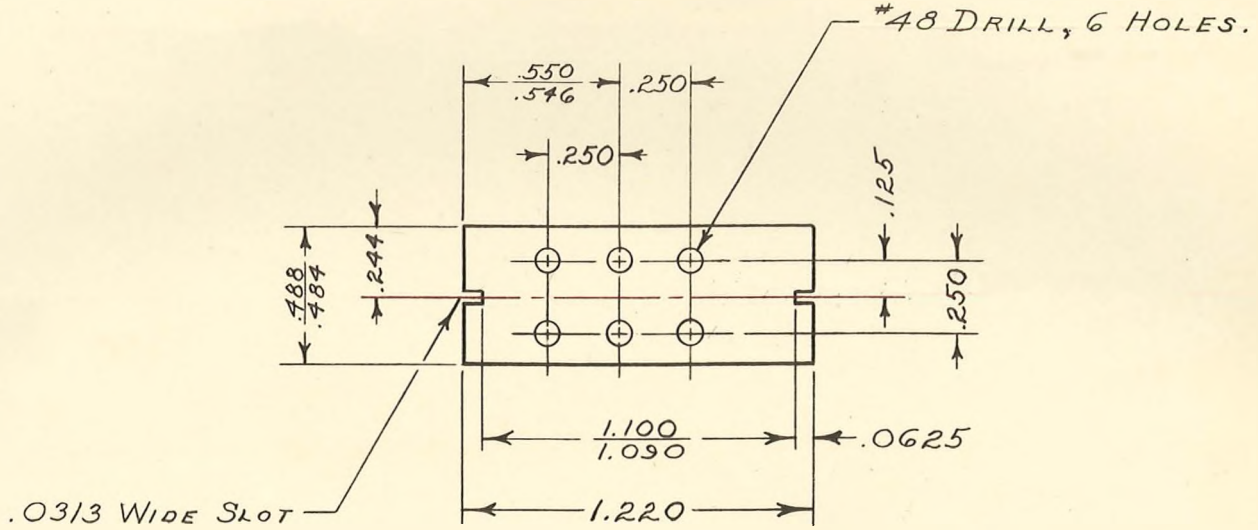

	1	TERMINAL BOARD.		FORMICA FF-91	1/16 THICK, 1/2 x 1 1/4
CND	NO REQ	DESCRIPTION	DWG OR PART NO	MATERIAL	STOCK SIZE

RELEASE DATE OF DRAWING 6-30-59

SIGNATURES

DESIGNER S. H. Ludwig DRAWN Randy Fratt

PL. 3-46

TERMINAL BOARD
DECK C, D, E, F, & G

DEPARTMENT OF PHYSICS
STATE UNIVERSITY OF IOWA
IOWA CITY IOWA

COSMIC RAY LAB

UNLESS OTHERWISE SPECIFIED

DWG SIZE A 11-2C101

SCALE 2/1 CLASSIFICATION UNCLASS SHEET 1 OF 1 REVISION

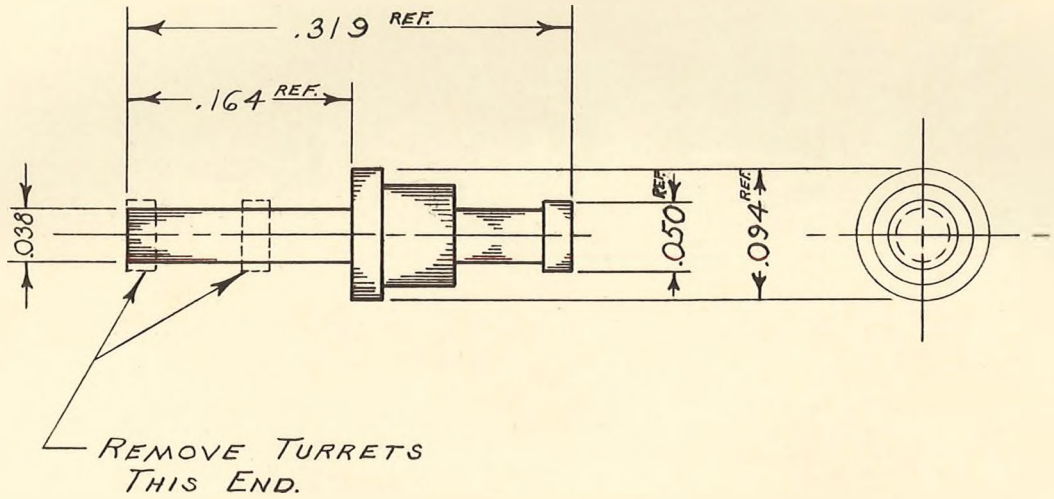

	1	TERMINAL	X2044B	PURCHASED.	CAMBRIDGE CORP.
		DESCRIPTION	PART NO.	MATERIAL	STOCK SIZE
		RELEASE DATE OF DRAWING 6-29-59			DEPARTMENT OF PHYSICS
		SIGNATURES			STATE UNIVERSITY OF IOWA
		DESIGNER Mc CUNE	DRAWN	TERMINAL PIN FOR CHANNEL WIRING.	IOWA CITY IOWA
	P.L. S-46				COSMIC RAY LAB
UNLESS OTHERWISE SPECIFIED					DWG SIZE A 11-2102
			SCALE 10/1	CLASSIFICATION UNCLASS.	SHEET 1 OF 1 REVISION A

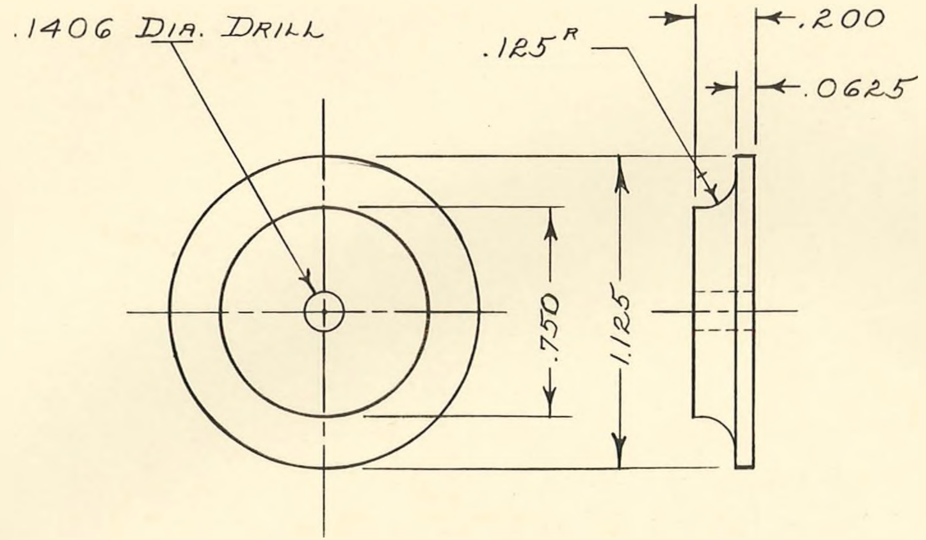

	1	WASHER	———	TEFLON	1 3/16 x 1/4"
ITEM NO.	NO. REQ'D	DESCRIPTION	DWG OR PART NO.	MATERIAL	STOCK SIZE

NEXT ASSY | PL 9-46 USED ON

RELEASE DATE OF DRAWING 8-28-59

SIGNATURES

DESIGNED G. H. Ludwig | DRAWN [signature]

150 V. TRANSFORMER MOUNTING WASHER.

DEPARTMENT OF PHYSICS
STATE UNIVERSITY OF IOWA
IOWA CITY IOWA

COSMIC RAY LAB

UNLESS OTHERWISE SPECIFIED

DIMENSIONS ARE IN INCHES AND APPLY OVER ADDITIVE FINISH EXCEPT ORGANIC COATINGS

TOLERANCES DECIMALS ANGLES ± 2°

DWG SIZE A | 11-2A109

SCALE 2/1 | CLASSIFICATION UNCLASS. | SHEET 1 OF 1 | REVISION

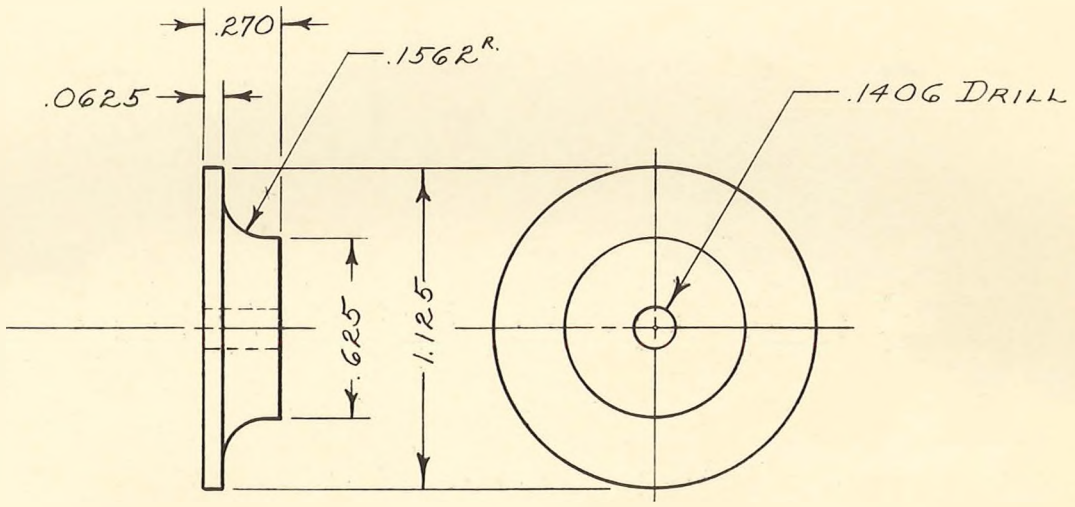

	1	WASHER		TEFLON	$1\frac{3}{16}$ x $\frac{3}{8}$
	QTY REQ'D	DESCRIPTION	DWG OR PART NO	MATERIAL	STOCK SIZE

RELEASE DATE OF DRAWING 7-28-59

SIGNATURES

DESIGNED H. N. Ludwig

CHECKED Norman Tractt

P.L. S-46

700 V. TRANSFORMER MOUNTING WASHER

DEPARTMENT OF PHYSICS

STATE UNIVERSITY OF IOWA IOWA CITY IOWA

COSMIC RAY LAB

UNLESS OTHERWISE SPECIFIED

DWG SIZE A 11-2A101

SCALE 2/1 CLASSIFICATION UNCLASS

SHEET 1 OF 1 REVISION

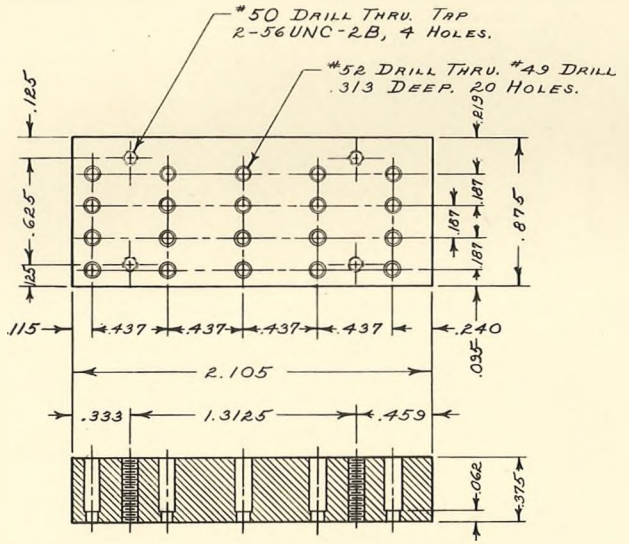

① TEST PLUG

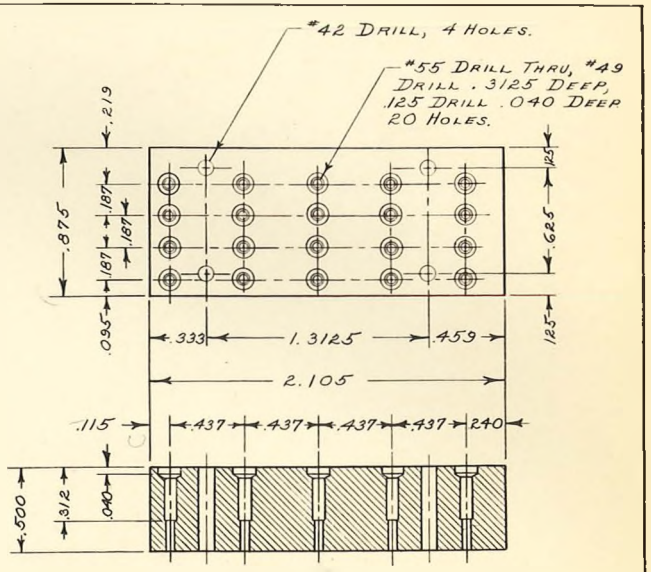

② TEST PLUG

2	1	TEST PLUG		FORMICA GRADE "C"	5/8 x 1" x 2 1/4"
1	1	TEST PLUG		FORMICA GRADE "C"	1/2" x 1" x 2 1/4"
		DESCRIPTION		MATERIAL	STOCK SIZE

9-16-59

PL. S-46

TEST PLUG.
DETECTOR ASS'Y.

DEPARTMENT OF PHYSICS
COSMIC RAY LAB

B 11-2A401

2/1 UNCLASS. 1 1

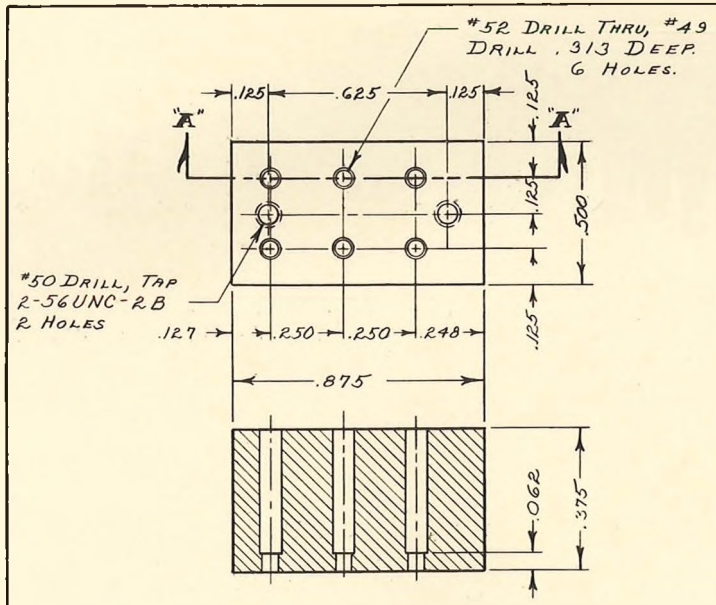

① TEST PLUG

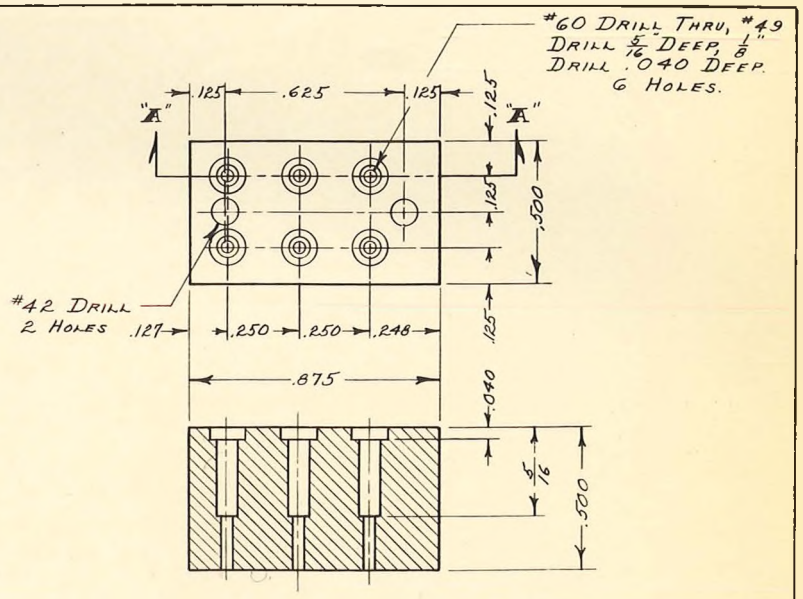

② TEST PLUG

2	1	TEST PLUG		FORMICA GRADE C.	3/8 x 1/2 x 1/2
1	1	TEST PLUG		FORMICA GRADE C	1/2 x 1/2 x 1/2
		DESCRIPTION		MATERIAL	STOCK SIZE

TEST PLUG - SCALER MODULE

DEPARTMENT OF PHYSICS
STATE UNIVERSITY OF IOWA

COSMIC RAY LAB

PL S-46

B 11-2C401

3/1 UNCLASS

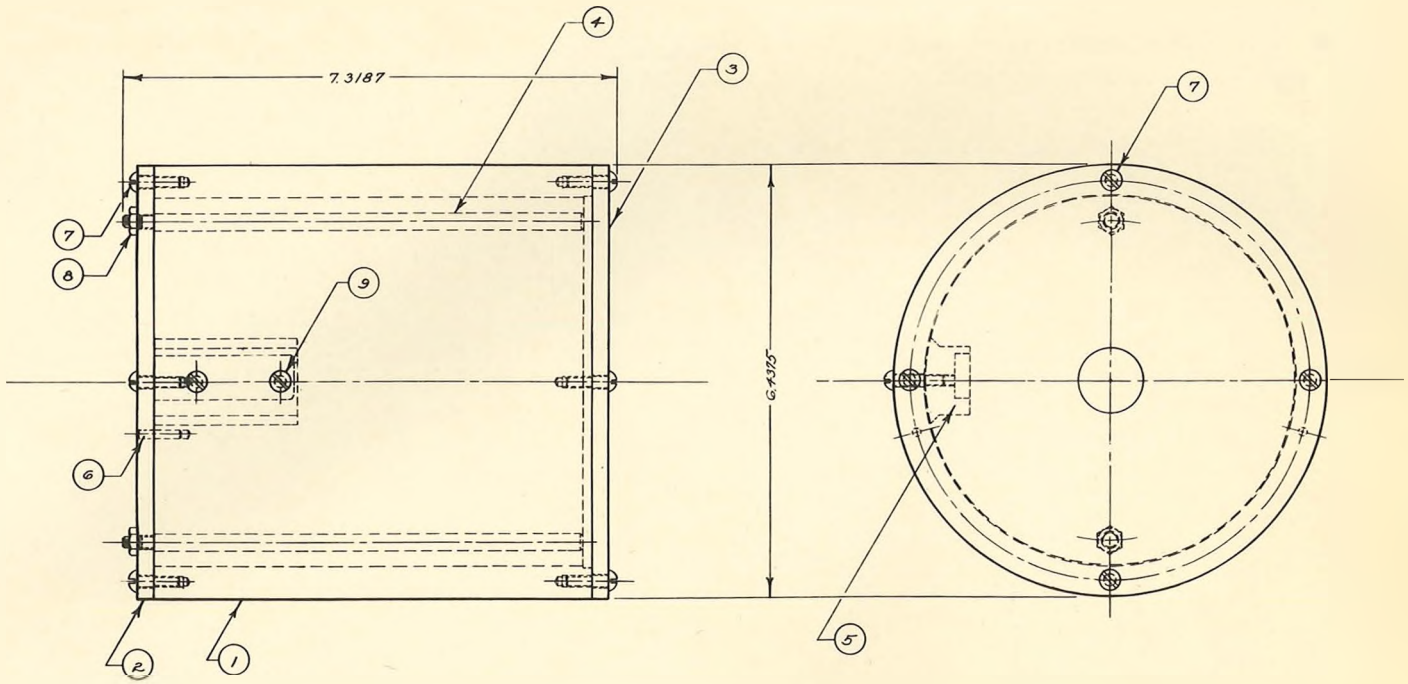

ENCAPSULATION MOLD ASS'Y.

9	2	#8-32 UNC-2 RD. HD MACH SC			3/8" Lg.
8	2	#8-32 UNC-2 HEX. NUT			
7	8	#8-32 UNC-2 RD. HD. MACH SC.			5/8" Lg.
6	2	LOCATING PIN	11-2A116-6		
5	1	CHANNEL INSERT	11-2A116-5		
4	2	ALIGNMENT RODS	11-2A116-4		
3	1	TOP PLATE	11-2A116-3		
2	1	BOTTOM PLATE	11-2A116-2		
1	1	HOUSING	11-2A116-1		
NO.	REQ.	DESCRIPTION	DWG. NO.	MATERIAL	STOCK SIZE

RELEASED DATE OF DRAWING 10-7-59

SIGNATURES

DESIGNED J.A.W.

CHECKED

APP'D

PL 5-96

UNLESS OTHERWISE SPECIFIED

DIMENSIONS ARE IN INCHES AND APPLY EVEN AFTER FINISH EXCEPT GROUND EDGES

DECIMALS ±.01 ±.005 ±.002

ANGLES ±1/2°

TOLERANCES

DETECTOR ASS'Y ENCAPSULATION MOLD ASS'Y

DEPARTMENT OF PHYSICS

STATE UNIVERSITY OF IOWA IOWA CITY IOWA

COSMIC RAY LAB

DWG SIZE C 11-2A004

SCALE FULL CLASSIFICATION UNCLASS

SHEET 1 OF 1 REVISION

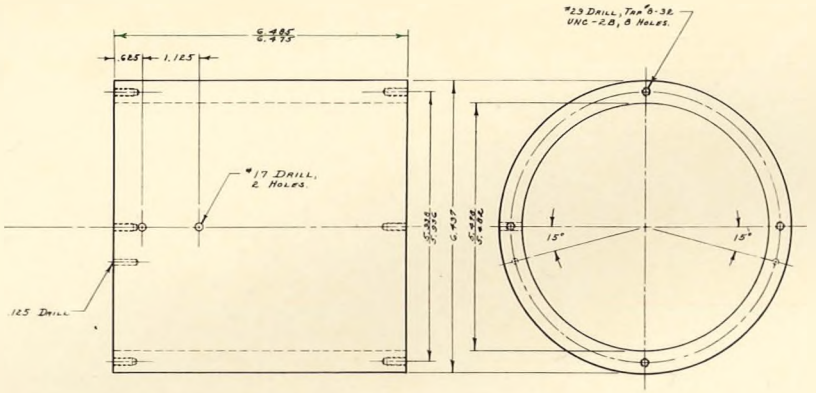

① HOUSING

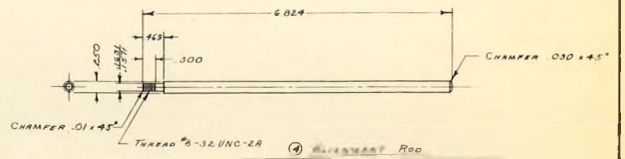

④ ALIGNMENT ROD

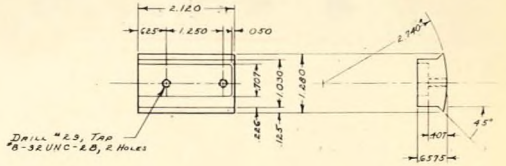

⑤ CHANNEL INSERT

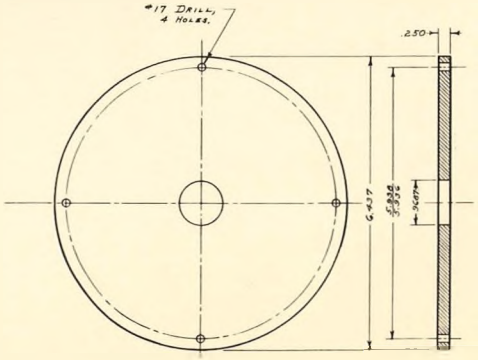

③ TOP PLATE

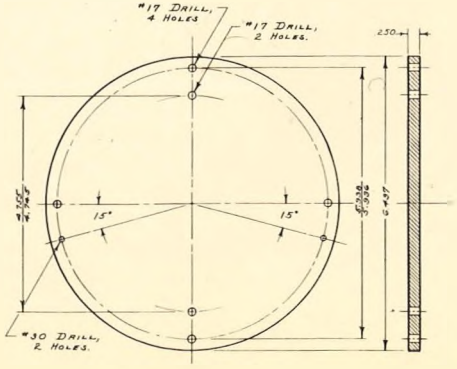

② BOTTOM PLATE

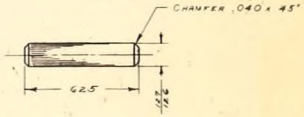

⑥ LOCATING PIN

6	1	LOCATING PIN	STAINLESS STEEL	.125 x .75 Lg.
5	1	CHANNEL INSERT	AL	.125 x .125 x 1.75
4	2	ALIGNMENT ROD	AL	.125 x 7.25
3	1	TOP PLATE	AL	6.437 Dia. x .250
2	1	BOTTOM PLATE	AL	6.437 Dia. x .250
1	1	HOUSING	AL	6.495 x 6.495 x .625

DETAILS OF 48 DIP ENCAPSULATION MOLD

D 11-2A116

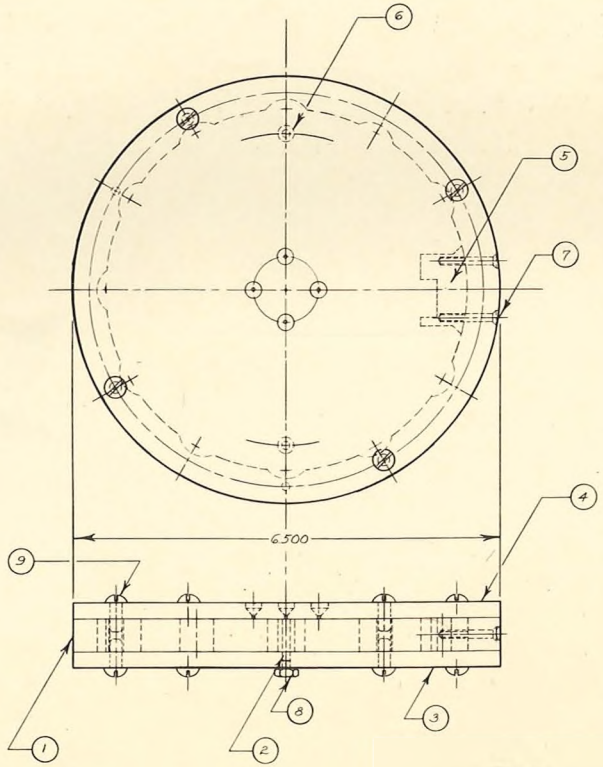

ENCAPSULATION MOLD

9	8	#8-32 UNC SCREW x 5/16 LG			STOCK
8	2	#6-32 UNC-2B NUTS.			STOCK
7	2	#4-40 UNC FT. HD. SCREW x 1/4 LG			STOCK
6	2	LOCATING PIN	6-2B402-9		
5	1	CHANEL INSERT	11-2C104-3		
4	1	TOP PLATE	11-2C104-2		
3	1	BOTTOM PLATE	6-2B402-2		
2	2	PIN	11-2C104-4		
1	1	CENTER RING	11-2C104-1		
		DESCRIPTION		MATERIAL	STOCK SIZE

PROJECT DATE 8-11-53
PL 5-46

ENCAPSULATION MOLD ASS'Y

DEPARTMENT OF PHYSICS
COSMIC RAY LAB

C 11-2C001

FULL | UNCLASS | A

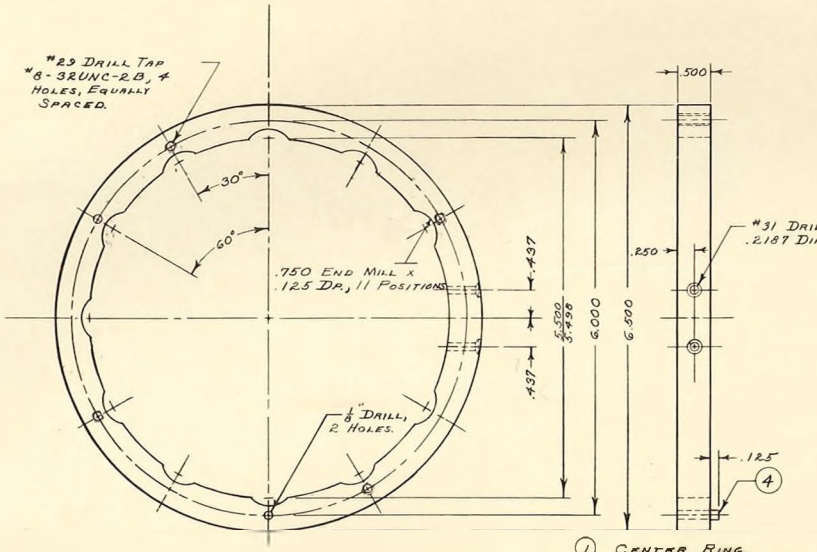

① CENTER RING

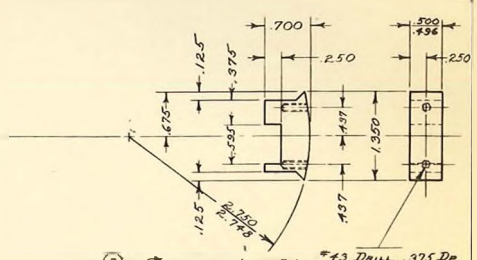

③ CHANEL INSERT

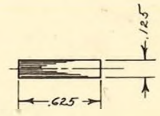

④ LOCATING PIN

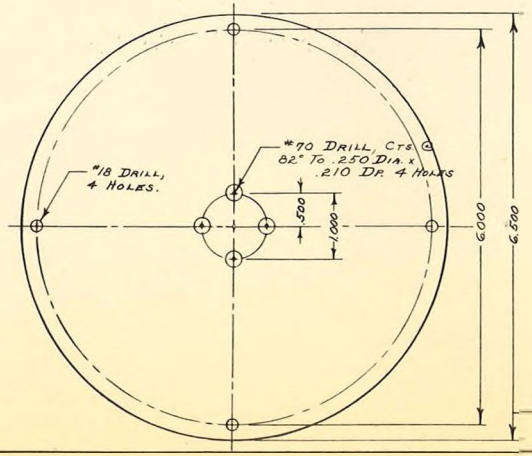

② TOP PLATE

4	2	PIN		STAINLESS STEEL	1/8 x .625
3	1	INSERT		TEFLON	1/8 x 3/8 x 1 1/2
2	1	TOP PLATE		AL.	1/4 x 6 5/8 DIA.
1	1			AL	1/8 x 6 5/8 DIA.
NO.	REQ'D	DESCRIPTION	DWG NO	MATERIAL	STOCK SIZE

8-7-59
PL. 3-46

DETAILS, ENCAPSULATION MOLD.

DEPARTMENT OF PHYSICS
COSMIC RAY LAB

SCALE FULL | UNLESS OTHERWISE SPECIFIED UNCLASS

C | 11-2C104
SHEET 1 / 1 | REVISION A

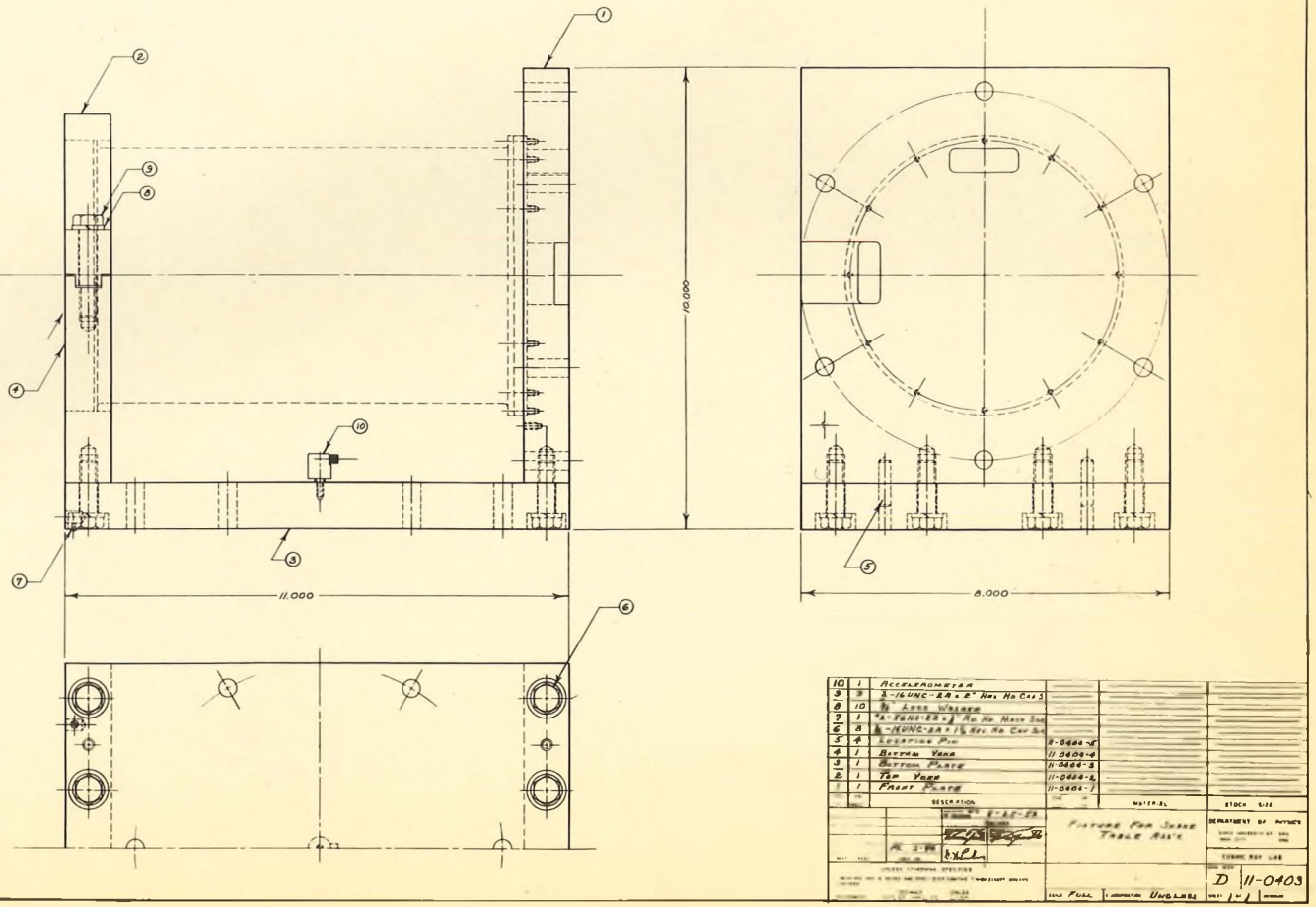

10	1	ACCELEROMETER		
9	2	3-16UNC-2A x 2" Nor. Ht. Cap S.		
8	10	#8 LOCK WASHER		
7	1	#4-40UNC-2A x Nor. Ht. Hex Soc.		
6	8	1/4-20UNC-2A x 1/2 Nor. Ht. Cap Soc.		
5	4	LOCATING PIN	D-0404-5	
4	1	BOTTOM VANE	D-0404-4	
3	1	BOTTOM PLATE	D-0404-3	
2	1	TOP VANE	D-0404-2	
1	1	FRONT PLATE	D-0404-1	

DESCRIPTION — MATERIAL — STOCK SIZE

E-AE-59

FIXTURE FOR SHAKE TABLE ASS'Y

DEPARTMENT OF PHYSICS — CYCLOTRON LAB

UNLESS OTHERWISE SPECIFIED — SCALE FULL — DIMENSIONS IN INCHES — UNCLASS

D 11-0403

SHEET 1 OF 1

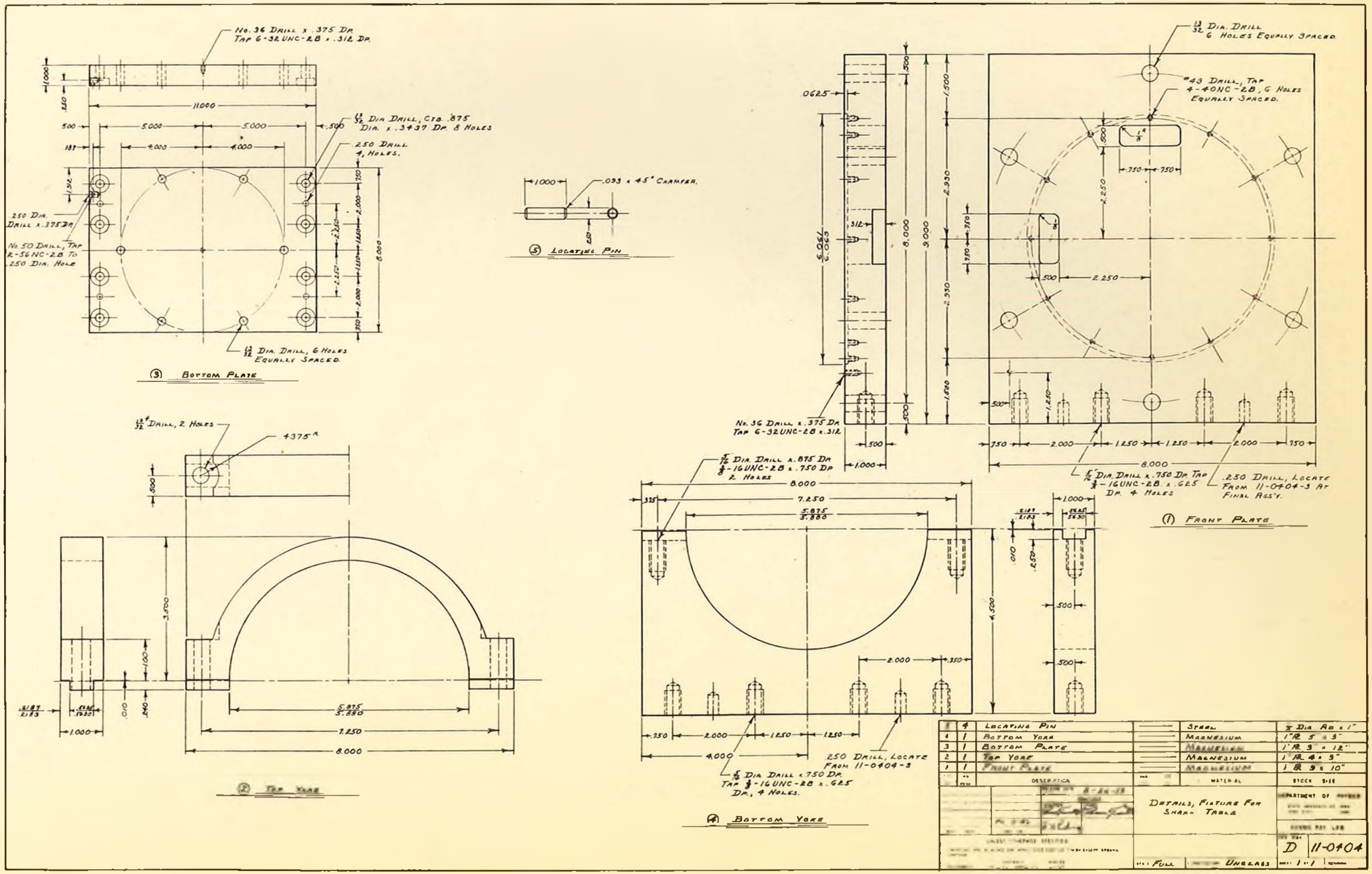

No. 36 Drill x .375 Dp. Tap 6-32 UNC-2B x .312 Dp.
13/32 Dia. Drill, Ctd. .875 Dia. x .3437 Dp. 8 Holes
.250 Drill 4, Holes.
.250 Dia. Drill x .375 Dp.
No. 50 Drill, Tap 2-56NC-2B To .250 Dia. Hole
13/32 Dia. Drill, 6 Holes Equally Spaced.
(3) Bottom Plate
.093 x 45° Chamfer.
(5) Locating Pin
13/32 Dia. Drill 6 Holes Equally Spaced.
#43 Drill, Tap 4-40NC-2B, 6 Holes Equally Spaced.
No. 36 Drill x .375 Dp. Tap 6-32UNC-2B x .312
5/16 Dia. Drill x .750 Dp. Tap 3/8-16UNC-2B x .625 Dp. 4 Holes
.250 Drill, Locate From 11-0404-3 At Final Ass'y.
(1) Front Plate
13/32 Drill, 2 Holes
(2) Top Yoke
5/16 Dia. Drill x .875 Dp. 3/8-16UNC-2B x .750 Dp. 2 Holes
.250 Drill, Locate From 11-0404-3
5/16 Dia. Drill x .750 Dp. Tap 3/8-16UNC-2B x .625 Dp., 4 Holes.
(4) Bottom Yoke
5 | 4 | Locating Pin | Steel | 1/2 Dia. Rd. x 1"
4 | 1 | Bottom Yoke | Magnesium | 1" Pl. 5 x 3"
3 | 1 | Bottom Plate | Magnesium | 1" Pl. 9 x 12"
2 | 1 | Top Yoke | Magnesium | 1" Pl. 4 x 9"
1 | 1 | Front Plate | Magnesium | 1" Pl. 9 x 10"
Description
Material
Stock Size
Details, Fixture For Shake Table
D
11-0404
Full
Unglass

APPENDIX II

TEST PROCEDURES AND SPECIFICATIONS.

A. Testing of Individual Components at SUI Before Assembly.

Individual components were mechanically and electrically inspected upon receipt from the manufacturers. They were then aged at a temperature of 120° C for approximately two weeks and retested. Parameter change patterns were determined, and components whose changes differed appreciably from the normal patterns were discarded.

Several critical components, such as G.M. counters, were tested much more extensively following aging, in order to determine their operating characteristics and to facilitate selection of the best units.

Following is a listing of the tests and the criteria for rejection of abnormal components.

1. Transistors.
    a. Check beta before and after aging.
        (1) Beta to be within manufacturer's tolerance before and after aging.

(2) Change in beta to be less than ± 5 per cent.

b. Check switching time before and after aging in a grounded emitter amplifier circuit with V_{cc} = 6.5 volts, R_L = 47 K ohms, and a 47 K ohm resistor between base and the low impedance output of a square wave generator adjusted to switch between zero and ± 3 volts.

(1) Rise time (to within e^{-1} of final value) to be less than five microseconds before and after aging.

(2) Change in risetime to be less than ± 10 per cent.

2. Diodes, 1N625.

a. Back resistance as measured with a Simpson model 260 meter to be greater than 20 M ohms before and after aging.

b. Forward resistance as measured with a Simpson model 260 meter to be 1 K ohm ± 30 per cent before and after aging. Change in forward resistance to be less than + 5 per cent.

3. Diodes, 608C.

   Same as 1N625 except back resistance to be greater than 5 M ohms and forward resistance to be between 20 and 35 ohms.

4. Diodes, zener, 650C0 and 652C3.

   Zener voltage to be within manufacturer's tolerance before and after aging.

5. Diodes, zener, 1N1327.

   a. Zener voltage to be within manufacturer's tolerance before and after aging.

   b. Flight unit diodes to be selected on the basis of zener voltage dependence on diode current and temperature.

6. Diodes, high Voltage. HR10318.

   a. Forward resistance as measured with a Simpson model 269 meter to be between 18 and 24 ohms before and after aging.

   b. Back resistance as measured with a Simpson model 269 meter (10^5 scale) to be greater than 200 M ohms before and after aging.

c. Read reverse current with the diode, a 135 volt battery and a Keithley electrometer in series, with the diode at 75° C.

(1) Reverse current to be below 0.2μA before and after aging.

(2) Change in reverse current to be less than 0.1μA.

7. Resistors, Allen Bradley type TR

a. Resistor value to be within manufacturer's tolerance before and after aging.

b. Change in resistance to be less than minus 5 per cent, plus zero.

8. Resistors, Dale Products type DC (used in series with 700 volt regulator).

a. Resistor value to be within manufacturer's tolerance before and after aging.

b. Change in resistance to be less than minus zero, plus one per cent.

9. Capacitors, RMC for high voltage power supplies.

Read leakage current with the capacitor, a 700 volt battery, a 10 M ohm resistor,

and a Keithley electrometer in series before and after aging. Leakage current to be less than 10^{-9} amp. before and after aging.

10. Capacitors, Glenco ceramic.

    Check before and after aging for abnormally high leakage current at 67 1/2 volts.

11. Capacitors, Sprague type 150D tantalum.

    Check before and after aging for abnormally high leakage current at rated voltage.

12. Transformers, Rayco type 0-3767A.

    Check in test circuit before and after aging.

    a. Overall circuit power efficiency to be 42 $\pm$ 3 per cent.

    b. Change in efficiency to be less than $\pm$ 1 per cent.

    c. Transformers having the highest efficiencies to be set aside as flight components.

13. Transformers, Rayco type 0-3753.
    Check in test circuit before and after aging.
    a. Overall circuit power efficiency to be 51 ± 3 per cent.
    b. Change in efficiency to be less than ± 1 per cent.
    c. Transformers having the highest efficiencies to be set aside as flight components.

14. Voltage regulator tubes, Victoreen, 700 volt. Note: Aging temperature for regulator tubes 100° C.
    a. Check regulator voltage as a function of regulator current at room temperature before aging in test circuit (with tube paralleled by a series connected 0.01μfd capacitor and 100 K ohm resistor). Voltage and regulation to be within manufacturer's tolerance.
    b. Stabilize regulator tube operation after aging by running at about 20μA. for 12 hours at room temperature.

c. After aging check regulator voltage as a function of regulator current in test circuit at 75, 50, 25, 0, -25, and -50° C.

(1) Room temperature characteristics to be essentially the same as those before aging.

(2) Tubes having the best regulation characteristics to be set aside as flight components.

15. Neon bulbs.

To be selected on the basis of firing voltage stability as a function of temperature, and leakage resistance.

16. Cadmium sulfide detectors.

To be selected on the basis of dark current, response time, physical size, physical structure, electron sensitivity, and X-ray sensitivity.

17. G. M. Counters.

To be selected on the basis of threshold voltage, constancy of threshold voltage, shape of the counting rate vs. voltage and temperature curves, and effectiveness of quenching (absence of double pulses and continuous discharge).

B. Inspection and Testing of SUI Modules Before Stacking.

Following assembly of the components on the deck cards the modules were subjected to a series of inspections and tests to make sure that they would operate according to specifications.

1. Preliminary inspection of scaler decks.
   a. Check alignment of interdeck spacers and terminal boards.
   b. Inspect each solder joint under a binocular microscope (10X).
   c. Visually check wire clearances and security of parts.
2. Preliminary inspection of detector assembly.
   a. Inspect each solder joint under a microscope.

b. Visually check wire clearances and security of parts.

3. Preliminary electrical check of scaler decks (room temperature).

a. Connect decks to test panel. Apply power (6.50 and 10.40 volts) to deck F and check the regulator voltage (5.0 $\pm$ 0.2 volts) and the input currents. Deck F must remain on during all other tests.

b. Turn on the other scaler decks in turn and check the input currents.

c. With the test panel time constant switch on "fast" (capacitors ungrounded) feed a test signal to one deck at a time and check the scaling factors. Input pulse requirements are width = 5μsec, amplitude = 3.1 volts, polarity = negative, rise time $<$ 0.1μsec, source impedance = 50 ohms.

d. Check scaler operation, one deck at a time, as a function of input pulse rate.

Decks E and G should count to at least 30,000 sec^{-1} and decks C, D and F to at least 10,000 sec^{-1}.

e. Adjust the 820 K ohm and 1.2 M ohm nominal value resistors in the logic summing circuits so that the maximum and minimum output voltages are 5.0 $\pm$ 0.2 and 1.0 $\pm$ 0.1.

f. Ground the logic circuit RC capacitors and check that the time constants are 5 $\pm$ 1 sec.

g. Repeat steps B3a through B3d with the supply voltages equal to 5.50 and 9.40, and 7.50 and 11.40 volts.

4. Preliminary electrical check on detector assembly (room temperature).

a. Connect assembly to test panel with AB and TS cables (with all scaler decks also connected). Apply power and check currents.

b. Adjust the two power supply bias resistors separately. The 160 volt supply should draw 6.0 $\pm$ 0.1 ma. at

V_{cc2} = 6.50 volts (R ≈47 K ohm), producing 125 ± 7μA. regulator diode current. The 700 volt supply should draw 11.0 ± 0.2 ma. at V_{cc2} = 6.50 volts (R ≈ 22 K ohm), producing 45 ± 5μA. regulator tube current. These resistors should be deposited carbon.

c. With the appropriate detectors connected to the inputs, check the pulse shaping amplifier output pulse heights (3.2 ± 0.1 volt), rise times (less than one microsecond), widths at half amplitude (22 ± 2μsec for detectors A and B, 9 ± 3μsec for detectors C and D, and 13 ± 3μsec for detector E), and widths at full height (about 2μsec less than at half height).

d. Check that the current (regulated 5.0 volts) to the pulse shaping amplifiers is less than 15μA. total (no sources near detectors).

e. Repeat steps B4a, c, and d with the supply voltages equal to 5.50 and 9.40, and to 7.50 and 11.40 volts.

5. Temperature cycle test of scaler decks.
   a. Locate modules in temperature chamber and connect to test panel. Provide a pulse source to all five scalers and monitor the outputs continuously.
   b. Temperature cycle between 100° and -50° C. Check operation after stabilization following each temperature change.
   c. Continue the test for at least one complete cycle after repairing the last difficulty, but in any event for at least three full cycles.
6. Temperature cycle test of detector assembly.
   a. Locate assembly in temperature chamber and connect through AB and TS cables to test panel. Connect all scaler modules to test panel. Provide appropriate radioactive and light sources to stimulate the detectors.
   b. Temperature cycle between 75° and -50° C. Do not exceed 75° C. Check operation after stabilization following each temperature change.

c. Same as B5c above.

7. Temperature-voltage test of scaler decks.

a. Connect the modules as in B5 above. Use the following test conditions.

(1) Temperature = 25, 100, 50, 0, and -50° C (in that order).

(2) V_{cc1} = 9.40, 10.40, and 11.40 when V_{cc2} = 5.50, 6.50, and 7.50 volts respectively.

b. Check and record:

(1) Minimum supply voltage V_{cc2} (min) for proper operation (voltage at which scaling factor changes) with V_{cc1} = 9.40, pulse rate = 1000 sec^{-1} for decks C, D, and F, pulse rate = 10,000 sec^{-1} for decks E and G.

(2) Same as B7 b(1) above except determine the supply voltage at which the output amplifier state 8 output voltage begins to decrease appreciably.

(3) Power supply current to each module from each supply.

(4) Maximum counting rate for each scaler.

(5) Output amplifier minimum and maximum voltages.

(6) Voltage from the nominal 5.0 volt regulator.

c. Upon completion of test elevate package temperature before opening chamber to prevent condensation of moisture on instruments.

8. Temperature-voltage test of detector assembly.

a. Connect the modules as in B6a above. Use the same test conditions as in B7a above. Locate sources at appropriate fixed distances for the duration of the complete test.

b. Check and record:

(1) Power supply current from the nominal 6.5 volt supply.

(2) 700 volt supply regulator tube current.

(3) 160 volt supply regulator diode current.

(4) 700 volt supply voltage. Measure with electrostatic voltmeter, with V_{cc2} adjusted for regulator currents of 5, 10, 30, 50, and 70μA.

(5) 160 volt supply voltage. Measure with Simpson type 269 100,000 ohm/volt meter on 400 volt scale, with V_{cc2} adjusted for regulator diode currents of 20, 40, 60, 80, 100, 120, and 140μA. Disconnect voltmeter for all other tests.

(6) Pulse shaping amplifier pulse amplitudes, rise times, widths at half amplitude, and widths at full amplitude.

(7) Counting rates of the five detectors with the sources located in their standard positions.

9. Test of modules after encapsulation.

a. Inspect for voids and trim.

b. Connect to test panel. Check currents, regulated voltage, scaling factors and

logic circuit operation, maximum scaling rates, output voltages, pulse shaping amplifier output waveforms, and high voltage power supply regulator currents at room temperature.

c. Mark modules with deck identification and serial number.

C. Testing of the Completely Assembled Instrumentation Package at SUI.

1. Inspection following final assembly and channel wiring.

a. Before applying power check all wiring with a terminal-to-terminal continuity check.

b. Connect to the test panel with the PP and TS cables.

c. Apply power and measure currents.

d. Check high voltage power supply regulator currents.

e. Check power supply collector waveforms.

f. Check pulse shaping amplifier output waveforms.

g. With sources in their standard positions read counting rates and compare with earlier readings.

h. Check scaling factors and operation of the logic circuits and output amplifiers.

i. Ground the integrating capacitors in the logic circuits and check the time constants.

2. Vibration test.

a. Mount package on the table in the proper position. Vibrate along the thrust axis, transverse to the thrust axis and along the spectrometer axis, and transverse to the thrust and spectrometer axes. Connect to test panel through PP and TS cables. Connect output signal to data recording system.

b. Locate sources to give appropriate counting rates.

c. Before each run equalize the shake system with the instrument assembly in place. Do not exceed 1 g vibration level during equalization.

d. Before and after each test check and compare with previous readings:
   (1) Supply currents.
   (2) Regulator currents.
   (3) Pulse shaping amplifier output waveforms.
   (4) Scaling factors and logic circuit operation.

e. Before, during, and after each test record the outputs of all five channels simultaneously and continuously to check for faulty operation. Record the counting rates.

f. Vibrate according to the following schedule. All tests are random noise, uniform spectral density over range 20-1500 cycles per second.
   (1) Direction of thrust.
   Prototype units - 25 g. RMS for 2 minutes.
   Flight units - 20 g. RMS for 30 seconds.

(2) Both transverse axes.

Prototype units - 15 g. RMS for 2 minutes.

Flight units - 12 g. RMS for 30 seconds.

3. Vacuum Test.

a. Install instrumentation package in vacuum chamber. Connect to test panel through PP and TS cables. Record both high voltage power supply currents continuously throughout duration of test on a moving chart recorder.

b. Reduce pressure to less than 100 microns Hg (preferably to less than 10 microns Hg) and monitor for at least one hour. Power supply arcover is indicated by downward deflections of the current readings.

c. Remove power from package and allow it to remain overnight at a pressure of less than 100 microns.

d. Apply power, run for at least one hour, checking continuously for arcover.

e. Increase pressure to atmospheric and check continuously for arcover for at least one hour.

4. Temperature test and calibration.

a. Locate instrumentation package in temperature chamber and connect to test panel through PP and TS cables. Connect output signal to data recording system.

b. Locate sources in standard positions.

c. Use the following test conditions:

(1) Temperature = 25, 75, 50, 0, -50°C (in that order).

(2) V_{cc1} = 9.40, 10.40, and 11.40 when V_{cc2} = 5.50, 6.50, and 7.50 volts respectively.

d. Allow package to stabilize at each new temperature as determined by monitoring the rate of change of the SUI thermistor resistance. At least three hours is required for stabilization after a 50° C change.

e. Check and record:

(1) Power supply current to the package from each supply.

(2) Both high voltage power supply currents.

(3) Pulse shaping amplifier output pulse amplitude and width at half height.

(4) Counting rates of all five detectors.

(5) Steady-state resistance of the SUI thermistor.

f. Upon completion of the test elevate package temperature before opening chamber to prevent condensation of moisture on instruments.

5. Temperature soak.

a. Connect package as in C4a and b above. Place silica gel in chamber during the low temperature soak.

b. Allow the package to remain for twelve hours at 65° and -25° C.

c. Using the test conditions outlined in section C4c(2) above, check and record the data outlined in section C4e above

before each temperature change and two hours after each temperature change.

d. Upon completion of the test elevate the package temperature before opening chamber to prevent condensation of moisture on instruments.

D. Testing of the Completely Assembled Payload at ABMA.

A complete set of electrical, mechanical, and rf tests was made following final assembly of the payloads at ABMA.

1. Payload checkout procedure. Before and after each phase of the testing program perform an operational check to determine whether a malfunction results from the test. During the environmental tests make those operational checks which are possible in view of the limited access to the payload during the test, and which are necessary to determine the occurrence of a malfunction.

a. Connecting the payload.

(1) Connect the external power supply to the payload.

(2) Connect the SUI package TS cable to the SUI test panel. Note: Whenever power is applied to the SUI package either the test panel must be connected to the TS socket or a shorting plug must be in place.

(3) Connect the transmitter output cable to an rf wattmeter through a 2 db attenuator. Note: The transmitter must always be terminated in a proper load whenever input power is supplied.

(4) Provide standard radioactive and light sources for the detectors. Note: The source strength and position must be the same for all tests in order that changes in detector sensitivity and scaling factors can be easily discovered.

b. Activation of the payload.

(1) Allow all test equipment to warm up.

(2) Apply the 15.6, 10.4, and 6.5 volt power, either from the external or internal supply as necessary.

(3) Read and record the supply voltages and currents.

(4) Read and record the SUI high voltage power supply regulator currents.

c. Transmitter measurements.

(1) Read and record the power output. This should be 300 ± 30 mw.

(2) Connect the transmitter output to the AM and PM detectors. Note: Always turn the 15.6 volt power off when disconnecting the transmitter load. Read and record the relative amplitudes of the outputs of the AM and PM detectors.

(3) Connect the transmitter output to the frequency counter. Read and record the transmitter center frequency. This should be 108.0300 ± 0.0015 mc/sec.

d. Subcarrier oscillator measurements.

(1) Connect the transmitter output to the modified Clarke receiver, and

the receiver output to the subcarrier discriminators, Sanborn recorder, and, if necessary, to the tape recorders. Calibrate the equipment.

(2) Obtain a Sanborn record of the telemetered data.

(3) Observe from the calibrated Sanborn record that the subcarrier oscillators are operating properly.

e. Electronic commutator check. Obtain at least one full cycle of the commutator and ascertain that all channels are operating properly.

f. SUI package measurements.

(1) Read and record the counting rates of all five detectors from the Sanborn record.

(2) Read and record the pulse shaping amplifier output pulse heights and widths from the SUI test panel.

Note: It is necessary to perform this test only every few days during the testing program.

(3) Ground the integrating capacitors at the SUI test panel and check the time constants as observed on the Sanborn record.

g. Deactivation of payload.

(1) Turn the power supplies off.

(2) Remove the external cables and radioactive and light sources.

2. Dynamic balance.

a. Applicability: PL-2, 3, 4 and 5.

b. Operational checks: None required.

c. Specifications:

(1) Spin rate during balancing not to exceed 600 RPM.

(2) Final balance to be such that the perpendicular distance from the center of gravity to the nominal axis of rotation does not exceed 0.51 mm.

3. Spin.

   a. Applicability:

      (1) Prototype approval test to PL-3.

      (2) Flight acceptance test to PL-4 and 5.

   b. Operational checks:

      (1) Before and after test. See section 1.

      (2) During test. Monitor demodulated signals on Sanborn recorder.

   c. Specifications:

      (1) Prototype approval test.

         (a) Spin rate: 750 RPM.

         (b) Duration: 20 minutes.

      (2) Flight acceptance test.

         (a) Spin rate: 600 RPM

         (b) Duration: 3 minutes.

4. Shock.

   a. Applicability: PL-3

   b. Operational checks: See section 1.

   c. Specifications:

      (1) Number of shocks: 45.

      (2) Linear acceleration: 25 g near shock.

(3) Impulse rise time: about 90 msec.

5. Vibration.

a. Applicability:

(1) Prototype approval test to PL-3.

(2) Flight acceptance test to PL-2, 4, and 5.

b. Operational checks:

(1) Before and after each phase. See section 1. In addition solar batteries to be carefully checked.

(2) During tests. Monitor demodulated signals on Sanborn recorder.

c. Method of application: Tests to be performed along three axes: the thrust axis and two mutually perpendicular transverse axes.

(1) Thrust axis. Payload to be mounted vertically on the horizontal vibration table.

(2) Transverse to thrust axis. Payload to be mounted to table with L-shaped fixture. Table vibrating surface to

be vertical. Payload to be vertical. Payload and fixture weight to be supported by two elastic supports fastened to ceiling.

d. Specifications: All tests to be random noise, uniform spectral density in frequency range 20 to 1500 cycles per second.

(1) Prototype approval test.

Direction	RMS g Level	Duration (sec)
Thrust	25	0.2
	15	7.8
	25	0.2
	15	7.8
	25	0.2
	15	7.8
	25	0.2
	15	7.8
	20	120.0
Trans. to Thrust	20	0.2
	12	7.8
	15	120.0

(2) Flight acceptance test.

Direction	RMS g Level	Duration (sec)
Thrust	20	0.2
	12	7.8
	20	0.2
	12	7.8
Trans. to Thrust	12.5	0.2
	7.5	7.8

6. Linear acceleration and spin combined.

a. Applicability:

(1) Prototype approval test to PL-3.

(2) Flight approval test to PL-4 and 5.

b. Operational checks:

(1) Before and after test. See section 1.

(2) During test. Monitor demodulated signals on Sanborn recorder.

c. Method of application: Payload to be mounted with nose toward centrifuge axis. Base of payload to be 2.285 meters from centrifuge center.

d. Specifications:

(1) Prototype approval test. Radial acceleration of 99 g corresponds to centrifuge speed of 148 RPM.

Accumulative time (min)	Payload spin rate (RPM)	Radial acceleration (g)
0-15	735	0
15-17	735	0-99
17-18	735	99
18-20	735	99-0
20-25	735	0

(2) Flight acceptance test. Radial acceleration of 35 g corresponds to centrifuge speed of 88 RPM.

Accumulative time (min)	Payload spin rate (RPM)	Radial acceleration (g)
0-5	437	0
5-7	437	0-35
7-8	437	35-0
8-10	437	0

7. Solar cell continuity during spin.

a. Applicability:

(1) Prototype approval test to PL-3.

(2) Flight acceptance test to PL-4 and 5.

b. Operational checks:

During test check continuity of all solar cells.

c. Specifications:

(1) Prototype approval test. Spin rate to be 750 RPM for as long as necessary to conduct continuity check.

(2) Flight acceptance test. Spin rate to be 500 RPM for as long as necessary to conduct continuity check.

8. Temperature-vacuum soak.

a. Applicability: PL-2.

b. Operational checks: Satellite instrumentation to be operated continuously throughout test, and demodulated signal to be recorded and checked on Sanborn recorder continuously throughout test. External power to be used except as specified below.

c. Specifications:

(1) Vacuum of 5×10^{-4} mm Hg. or better to be maintained throughout test.

(2) Total duration of test to be 14 days.

(3) No part of the payload is to be permitted to fall below -20° C or to rise above 75° D during the test.

(4) Temperatures to be maintained within $\pm 5^{\circ}$ C of specifications and to be read with an accuracy of $\pm 1^{\circ}$ C.

(5) Test to begin with the establishment of vacuum at room temperature.

(6) Heat and stabilize payload temperature at 50° C. Stabilization will require about six hours. Maintain at 50° C for 12 hours after stabilization.

(7) Cool and stabilize payload temperature at 0° C and maintain at that temperature for 12 hours after stabilization.

(8) Heat and stabilize payload temperature at 25° C. Calibrate payload temperature measurements and read counting rates.

(9) Heat and stabilize payload temperature at 50° C. Maintain at that temperature for half of the remainder of the 14 day period. Calibrate payload temperature measurements and read counting rates near beginning and end of this period. Operate instrumentation on internal power for the last 40 minutes.

(10) Cool and stabilize payload temperature at 0° C. Maintain at that temperature for all but six hours of the remainder of the 14 day period. Calibrate payload temperature measurements and read counting rates near beginning and end of this period. Operate instrumentation on internal power for the last 40 minutes.

(11) Heat payload to room temperature and terminate test.

(12) Chemical batteries to be subjected to a discharge-charge cycle at ambient pressure following termination of test.

9. Temperature calibration and vacuum test.

a. Applicability:

(1) See section 8 for calibration and vacuum test of PL-2.

(2) This section applies to PL-3, 4, and 5.

b. Specifications:

(1) Vacuum of 0.1 mm Hg. or better to be maintained throughout test.

(2) SUI high voltage power supply regulator currents to be monitored and recorded continuously throughout test.

(3) No part of the payload is to be permitted to fall below -20° C or to rise above 75° C during the calibration and test.

(4) Calibrations to be made at 0^{o}, 25^{o}, and 50^{o} C. Payload temperature is to be completely stabilized before making readings.

(5) Calibration is to include calibration of the payload temperature measurements and reading of the detector counting rates.

(6) The occurrence of any rapid downward deflections of the high voltage power supply regulator currents is to be interpreted as failure of the payload to pass the vacuum test and will require resealing of the high voltage power supply.

10. Determination of thermal characteristics.

a. Applicability: PL-1.

b. Instrumentation is not to be operated during the test. Operational checks are not required.

c. Thermistors are to be located in the payload in such a manner that the tempera-

tures of all sections of the payload can be measured.

d. Vacuum of 5×10^{-4} mm Hg or better to be maintained throughout tests.

e. Test 1 (perform twice) to determine thermal time constant. Stabilize temperature at -20° C. Heat all external surfaces rapidly to 70° C and hold constant until internal payload temperature is nearly stabilized. Step-change in temperature to be accomplished in such a manner that the external surfaces rise from -20° C to 60° C in less than 3 minutes.

f. Test 2 (perform twice) to determine thermal characteristics when illuminated by the sun from a direction normal to one side of satellite. Stabilize temperature at -20° C. Heat external surfaces on one side of payload. Heat input to be known and variable over range 0 to at least 1 watt per square inch. Heat input to be

varied as determined from consideration of detailed thermal design. Unheated surfaces to exchange radiant energy with either highly reflective surfaces or surfaces at the temperature of liquid nitrogen. Test to end when payload temperatures stabilize.